

**ANALYTICAL STUDY OF
HEAT TRANSFER ENHANCEMENT
DUE TO INTERNAL OSCILLATING FLOW
AT CONSTANT HEAT FLUX**

**A THESIS
SUBMITTED TO
THE COLLEGE OF ENGINEERING
UNIVERSITY OF BASRAH
IN PARTIAL FULFILLMENT OF
THE REQUIREMENTS FOR THE DEGREE OF
DOCTR OF PHILOSOPHY
IN MECHANICAL ENGINEERING**

BY

**AHMED KADHUM MOHAMMED AL-SHARA
(M.Sc. Mech. Eng.)**

DECEMBER -2006

بِسْمِ اللَّهِ الرَّحْمَنِ الرَّحِيمِ

الرَّحْمَنُ (١) عَلَّمَ الْقُرْآنَ (٢) خَلَقَ

الْإِنْسَانَ (٣) عَلَّمَهُ الْبَيَانَ (٤)

صدق الله العلي العظيم

سورة الرحمن الآية ١-٤

الإهداء

إلى نبي الرحمة محمد صلى

الله عليه وآله وسلم

وأهل بيته الذين أذهب الله

عنهم الرجس وطهرهم

تطهيراً

CERTIFICATION

I certify that this thesis was prepared under my supervision at the University of Basrah, as a partial requirement for the degree of Doctor of Philosophy in Mechanical Engineering.

Signature:

Advisor Name: **Prof. Dr. Abdul-Muhsin A. Rageb**

Date:

In view of the available recommendations, I forward this thesis for debate by the Examining Committee.

Signature: 

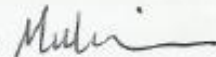
Name: **Dr. Qais A. Rishak**

Head of Mech. Eng. Department

Date: **28/12/2006**

EXAMINING COMMITTEE REPORT

We certify that we have read this thesis entitled " **Analytical Study of Heat Transfer Enhancement Due to Internal Oscillating Flow at Constant Heat Flux**" as Examining committee, and have examined the student (**Ahmed Kadhum Mohammed Al-Shara**) in its contents. In our opinion it is adequate, as a thesis for the degree of **Doctor of Philosophy in Mechanical Engineering**.

Signature: 

Name: **Dr. Abdul-Muhsin A. Rageb**

(Professor)

(Member & Supervisor)

Date: / /2007

Signature: 

Name: **Dr. Ayad A. Al-Chalaby**

(Advisor)

(Member)

Date: / /2007

Signature: 

Name: **Dr. Abdul-Wadood S. Shaab**

(Ass. Professor)

(Member)

Date: / /2007


Signature: 

Name: **Dr. Ameen A. Nassar**

(Ass. Professor)

(Member)

Date: 4/ 4/2007

Signature: 

Name: **Dr. Majid H. Majeed**

(Ass. Professor)

(Member)

Date: / /2007

Signature: 

Name: **Dr. Dr. Saleh E. Najim**

(Professor)

(Chairman)

Date: 4/ 4/2007

APPROVED FOR THE UNIVERSITY

Signature:

Name: **Prof. Dr. Saleh E. Najim**
(The Dean of the College of Engineering)

Date: / /2007

ACKNOWLEDGEMENT

Thanks God for completion of this work. I wish to express my sincere gratitude and his appreciation to Prof. Dr. Abdul-Muhsin A. Rageb for his encouragement and guidance during his supervision.

The author is grateful to Dean of Engineering College, Prof. Dr. Saleh E. Najim and Dr. Qais A. Rashid Head of Mechanical Engineering Department for their continuous helps and encouragements.

Special thanks and appreciation to the author's colleagues and staff of College Library for helping whenever.

Particular heartfelt thanks and appreciation to the author's family for their continuous help and support, which without the work could not be completed.

ABSTRACT

Hydrodynamics and heat transfer study in a fully developed, laminar, 2D, incompressible, no viscous dissipation, reciprocating and pulsating pressure driven flow in horizontal channel and pipe subjected to a constant heat flux has been investigated. New theoretical model is obtained by solving analytically the momentum and energy equations for both reciprocating and pulsating flow in the channel and the pipe using similarity transformation solutions. The main controlling parameters obtained in the reciprocating flow are: Womersly number λ , dimensionless amplitude of fluid displacement A_o , Prandtl number Pr and the ratio of distance to hydraulic diameter x/D_h , while the controlling parameters of pulsating flow are: Womersly number λ , mean Reynolds number Re_m , the ratio of amplitude to steady pressure gradient γ' , Prandtl number Pr and the ratio of distance to hydraulic diameter x/D_h .

The results of reciprocating flow showed that both velocity and temperature distributions are affected by the oscillation, and Richardson's annular effect is appeared in the velocity and temperature distributions. The instantaneous-local Nusselt number Nu_x is varied periodically with time and its enhanced by the order of magnitude with increasing Womersly number or the frequency of oscillation.

Further, the results of pulsating flow showed that an imposed flow pulsation causes both the temperature and Nusselt number fluctuate periodically about the solution for steady laminar flow. The time average-local Nusselt number $\overline{Nu_x}$ is constant and equal to 8.235 for channel and 4.364 for pipe with variation of all controlling parameters.

The results were found in very good agreement with that obtained numerically using finite volume method. The comparison between experimental results of other authors available in literature and present analytical model gave a reasonable identification.

CONTENTS

Titles	Page
ACKNOWLEDGEMENTS	i
ABSTRACT	ii
CONTENTS	iv
NOMENCLATURE	viii
CHAPTER ONE: INTRODUCTION	1
1.1 General	1
1.2 Characteristics of the Oscillatory Flow	2
1.2.1 The Flow Near an Oscillating Flat Plate	2
1.2.2 Reciprocating Flow	2
1.2.3 Pulsating Flow	3
1.3 Characteristics of Heat Transfer	4
1.3.1 Heat Diffusion in Oscillatory Flow	4
1.3.2 Heat Transfer in Reciprocating Flow	5
1.3.3 Heat Transfer in a Pulsating Flow	6
1.4 Hydrodynamics and Thermal Considerations of Oscillating Flow	7
1.5 The Aim of the Present Work	8
CHAPTER TWO: LITERATURE REVIEW	11
2.1 Preface	11
2.2 The General Unsteady Flow	11
2.3 Hydrodynamics of Oscillatory Flow	16
2.3.1 Hydrodynamics the Reciprocating Flow	16
2.3.2 Hydrodynamics of the Pulsating Flow	20
2.3.3 The Turbulence Considerations in the Oscillatory Flow	24
2.4 Heat Transfer in the Oscillatory Flow	25

2.4.1 Enhanced Axial Heat Diffusion by Oscillatory Flow	25
2.4.2 Heat Transfer in Internal Reciprocating Flow	30
2.4.3 Heat Transfer in Internal Pulsating Flow	34
2.5 Summary	41
CHAPTER THREE: THEORETICAL ANALYSIS	45
3.1 Analytical Model of Reciprocating Flow and Heat Transfer in the Channel	46
3.1.1 Hydrodynamics Analysis	46
3.1.2 Heat Transfer Analysis	49
3.2 Analytical Model of Reciprocating Flow and Heat Transfer in the Pipe	52
3.2.1 Hydrodynamics Analysis	52
3.2.2 Heat Transfer Analysis	55
3.3 Analytical Model of Pulsating Flow and Heat Transfer in the Channel	59
3.3.1 Hydrodynamics Analysis	59
3.3.2 Heat Transfer Analysis	62
3.4 Analytical Model of Pulsating Flow and Heat Transfer in the Pipe	67
3.4.1 Hydrodynamics Analysis	67
3.4.2 Heat Transfer Analysis	71
3.5 Numerical Model for Oscillatory Flow	77
3.5.1 Numerical Model of Reciprocating Flow in the Channel	77
3.5.2 Numerical Model of Reciprocating Flow in the Pipe	79
3.5.3 Numerical Model of Pulsating Flow in the Channel	83
3.5.4 Numerical Model of Pulsating Flow in the Pipe	86

CHAPTER FOUR: RESULTS AND DISCUSSION	91
4.1 Analytical Solution of the New Model	91
4.1.1 Analytical Results of Reciprocating Flow and Heat Transfer in the Channel	92
4.1.2 Analytical Results of Reciprocating Flow and Heat Transfer in the Pipe	97
4.1.3 Analytical Results of Pulsating Flow and Heat Transfer in the Channel	101
4.1.4 Analytical Results of Pulsating Flow and Heat Transfer in the Pipe	106
4.2 Numerical Solution for Checking the Analytical Model	110
4.2.1 Numerical Results of the Reciprocating Flow in the Channel	111
4.2.2 Numerical Results of the Reciprocating Flow in the Pipe	111
4.2.3 Numerical Results of the Pulsating Flow in the Channel	112
4.2.4 Numerical Results of the Pulsating Flow in the Pipe	112
4.3 Comparison of the New Model with Experimental Results of Other Authors	113
CHAPTER FIVE: CONCLUSIONS & RECOMMENDATIONS	148
5.1 Conclusions	148
5.2 Recommendations	149
REFERENCES	151
Appendices	158
Appendix A	158

Appendix B	159
Appendix C	160
Appendix D	161
Appendix E	163
Appendix F	164
Appendix G	165
Appendix H	166
Appendix I	167
Appendix J	168

NOMENCLATURE

List of Symbols

Symbol	Definition	SI Units
a	Radius of the pipe, Constant	m
A	Area, Parameter defined be Eq.3.10a	m^2
A_c	Flow area	m^2
A_o	Dimensionless amplitude of the fluid displacement, X_{\max} / D_h	
B	Parameter defined by Eq.3.10b	
Bei_n	Imaginary part of complex Bessel function defined in Appendix B	
Ber_n	Real part of complex Bessel function defined in Appendix B	
$\overline{C}_{f,\infty}$	Time-averaged friction coefficient of a fully developed flow	
c_v	Specific heat at constant volume	J/kg.K
c_p	Specific heat at constant pressure	J/kg.K
C	Parameter defined by Eq.3.10c Parameter defined in Appendix A&F	
C_1	Constant	
C_2	Constant, Function defined in Appendix G	
C_3	Constant, Function defined in Appendix A&F	
C_4	Constant	
D	Diameter, Parameter defined by Eq.3.10d, Parameter defined in Appendix A&F	m
D_h	Hydraulic diameter	m
E	Parameter defined in Appendix A & F	
E_1	Parameter defined in Appendix A & F	
f	Similarity transformation function for velocity, Frequency	Hz
F	Parameters defined in Appendix A & F	

F_1	Parameters defined in Appendix A & F	
g	Similarity transformation function for temperature	
Gz	Gratez number, $x/Re Pr$	
h	Half height of the channel	m
h_x	Instantaneous-local heat transfer coefficient	W/m^2 .K
\bar{h}_x	Time averaged-local heat transfer coefficient	W/m^2 .K
H	Height of the channel	m
IM_1	Parameters defined in Appendix C	
IM_2	Parameters defined in Appendix C	
IM_3	Parameters defined in Appendix C	
J_n	Bessel function of order n, n=0, 1, 2, 3	
k	Thermal conductivity of the fluid, Constant	W/m.K
L	Length of pipe	m
\overline{Nu}	Space-cycle average Nusselt number	
Nu_x	Instantaneous-local Nusselt number	
\overline{Nu}_x	Time averaged-local Nusselt number	
p	Pressure	N/m^2
P	Wetted perimeter, Parameter defined in Appendix A & F	m
$P(\alpha)$	Parameter defined by Eqs.2.25a & 2.25b	
$P1$	Parameter defined in Appendix A & F	
Pe	Peclet number, $Re Pr$	
P_o	Amplitude of pressure gradient $-\frac{1}{\rho} \frac{\partial p}{\partial x}$	m/s^2
Pr	Prandtl number	
q''	Heat flux	W/m^2
Q	Parameter defined in Appendix A & F	
$Q1$	Parameter defined in Appendix A & F	
Q_{conv}	Convective energy transfer in one cycle	W/m^2
r	Radial coordinate	m
R	Radius of pipe, Function defined by Eq.3.112	m
RE_1	Parameter defined in Appendix C	

RE_2	Parameter defined in Appendix C	
RE_3	Parameter defined in Appendix C	
Re	Reynolds number, $\frac{uD}{\nu}$	
Re_{cri}	Critical Reynolds number, 2300 for pipe	
Re_m	Mean Reynolds number, $\frac{u_m D}{\nu}$	
Re_δ	Reynolds number based on the Stokes's layer, $\frac{u_{max} \cdot \delta}{\nu}$	
Re_ω	Kinetic Reynolds number, $\frac{D^2 \cdot \omega}{\nu}$	
Str_x	Strouhal number, $\frac{\omega \cdot x}{u_\infty}$	
t	Time	s
T	Temperature	K
T_t	Fluctuation temperature	K
T_s	Steady temperature	K
u	Axial velocity in x-direction	m/s
u_m	Mean velocity	m/s
u_{max}	Maximum velocity	m/s
u_t	Fluctuation axial velocity	m/s
u_s	Steady axial velocity	m/s
u_∞	Free stream velocity	m/s
U	Dimensionless axial velocity in x-direction, Parameter defined in Appendix A&F	
U_1	Parameter defined in Appendix A & F	
U_2	Parameter defined in Appendix A & F	
v	Velocity in the y-direction	m/s
V	Volume	m^3
\vec{V}	Velocity vector	m/s
W	Parameter defined in Appendix A&F	
x	Axial coordinate	m
X	Function defined by Eq.3.112, Dimensionless axial distance	

X_1, X_2	Functions defined in Eq.3.76	
X_{\max}	Maximum displacement of the fluid	m
y	Normal coordinate	m
Y	Parameter defined in Appendix A & F	
Y_1	Parameter defined in Appendix A & F Function defined in Eq.3.76	
Y_2	Function defined in Eq.3.76	
z	Complex variable.	
Z	Parameter defined in Appendix A & F	
Z_1	Parameter defined in Appendix A & F	

Greek symbols

symbol	Definition	SI Units
α	Thermal diffusivity of fluid	m^2 / s
α_{eff}	Effective thermal diffusivity due to flow oscillation	m^2 / s
β	Parameter defined by Eq3.49	
β_{cri}	Critical value of reciprocating pipe flow, $(A_o \sqrt{Re_\omega})_{cri}$	
γ	Time average axial dimensionless temperature gradient, $\frac{d\bar{T}_b^+}{dT^+}$	
γ'	The ratio of the amplitude to the steady value of the pressure gradient	
δ	Oscillatory boundary-layer thickness, $\sqrt{2\nu/\omega}$	
δ_x^+	Axial distance between the nodes	
δ_y^+	Normal distance between the nodes	
Δx	Tidal displacement.	m
ε	velocity ratio, $\frac{u_{\max}}{u_\infty}$	
η	Dimensionless distance, $y\sqrt{\omega/2\nu}$	
θ	Weighting parameter, Concentration of the contaminant, Dimensionless temperature, $\frac{T - T_i}{T_w - T_i}$	mole

κ	Diffusivity of the contaminant	m^2 / s
κ_{eff}	Effective diffusivity of contaminant	m^2 / s
λ	Womersly number, $h\sqrt{\omega/\nu}$ or $\frac{D}{2}\sqrt{\omega/\nu}$	
μ	Dynamic viscosity	kg/m.s
ν	Kinematics viscosity	m^2 / s
ρ	Density	kg/m ³
τ	Time of period.	s
φ	Angle of radial coordinate (crank angles).	rad
ψ	Intermittency of flow turbulence.	
ω	Angular frequency.	rad/s
Ω	Stokes number, $\frac{D}{2}\sqrt{\omega/2\nu}$.	

Subscripts

b	Bulk
c	Center
cri	Critical
e	East
eff	Effective
f	Fluid
h	Hydraulic
i	Inlet
m	Mean
max	Maximum
min	Minimum
n	North
r	Relative
p	Pulsating
t	Time, fluctuation
s	Steady or mean flow, south
w	Wall, west
∞	Fully developed flow or at free surface.

Superscripts

-	Average, mean.
+	Dimensionless.
o	Lag time.

CHAPTER ONE

INTRODUCTION

1.1 General

The modern life progress and its increased requirements lead to thinking about the several phenomena that surround us. Out of these phenomena, unsteady of the flow and the heat transfer (oscillatory flow), which have a rich interest from researchers to enhance the performance of this operation.

Generally, the oscillatory flow can be classified as either a reciprocating flow where the mass flow rate and the pressure gradient of reciprocating flow fluctuate about a zero mean value, therefore, a zero net flow of fluid along the duct, or a pulsating flow where the mass flow rate and the pressure gradient of pulsating flow fluctuate about a mean value of nonzero and there is, therefore, a net flow of fluid along the duct (Fig.1.1). These two types of the flow occurred in numerous fields such as: oscenilological, medical or biological (human respiratory and vascular systems), and industrial applications such as

- 1-The intake or the exhaust manifold of internal combustion engines and a Stirling-cycle machines.
- 2-The electronic cooling and the space-base technology.
- 3-The flow in the hydraulic or the pneumatic lines and control systems.
- 4-The heat exchangers (heaters, regenerators and coolers) and pulse combustor.
- 5-The chemical and the food technology.
- 6-The pumping systems and the cavitations and hydraulic pipe lines.
- 7- The continuous casting and metallurgical processes.

For more clarity, this introduction will be divided into a number of sections and it will be discussed separately as bellow:

1.2 Characteristics of the Oscillatory Flow

There are several motions that depend on the time (unsteady flow), a simple example of unsteady boundary layer is the oscillatory boundary layer, the motion that starts from the rest (accelerated film by gravity), or when it is driven by periodically flow. The oscillatory flows are classified as:

1.2.1 The Flow Near an Oscillating Flat Plate

This type of flow is called Stokes's second problem which discuss the flow about an infinite flat wall, that execute linear harmonic oscillations parallel to itself and which was first treated by Stokes^[1]. Because of: no slip condition at the wall the velocity of the particles of the fluid at the wall is considered as a part of the wall, and must be equal to that of the wall (the wall moves harmonically). It was found the layer which is carried by the wall has a thickness of order $\delta \propto \sqrt{\nu / \omega}$ (Stokes layer), and it decreases for decreasing kinematics viscosity and increasing frequency^[1].

Recently, there are more extended researches (similar to Stokes's second problem) to study the effects of a periodically changed conditions at the wall, such as a oscillatory temperature or oscillatory heat flux at the wall or surface^[2]. In the special design for heat exchangers (for examples plate heat exchangers), the plate are made periodic wavy to improve the heat transfer^[3,4].

1.2.2 Reciprocating Flow

The necessity to improve the thermal and hydrodynamic performance of Stirling machine, crycoolers, internal combustion engines, etc., have

prompted researchers to pay increasing attention to the study of heat transfer and fluid flow characteristics in the reciprocating flow. In the reciprocating flow the fluid displacement is obtained by displacer such as piston and by periodical motion of displacer, the harmonic motion is made. The reciprocating flow requires to interchange between the inflow and outflow boundaries during a cycle. For most application, it is a difficult to determine the inflow/outflow boundary conditions, since the fluid particles exiting the flow domain during a part of cycle are fed back into the domain later in the cycle.

The main parameters in the reciprocating flow are depending on frequency and amplitude of the harmonic motion which called: Womersly number λ or kinetic Reynolds number Re_w and dimensionless amplitude of the fluid displacement A_o . It is agreed in general, that a reciprocating flow becomes unstable with increasing either the dimensionless amplitude of the fluid displacement A_o , or the kinetic Reynolds number Re_w or Womersly number. The critical dimensionless parameters for which the transition from laminar to turbulent occurs is $\beta_{cri} = (A_o \sqrt{Re_w})_{cri}$.

1.2.2 Pulsating Flow

The pulsating flow has a several practical applications for examples: rocket engine, heat exchangers (heaters and crycoolers), cavitations in hydraulic pipelines, refrigerating systems, pressure surges and circulation flow of blood and pumping systems, etc.. Pulsating flow can be produced by reciprocating pump or by steady flow pumps together with some mechanical pulsating device. The principle difference between the pulsating flow and reciprocating flow are: The pulsating flow rate has a time-mean

value and do not reverse to another direction. These differences make a new controlling parameters for this type of flow, represented by the mean –flow Reynolds number behind the frequency and amplitude parameters. Thus, the transition criteria for a pulsating flow becomes more complicated than in a reciprocating flow because of the intersection between the mean flow and oscillating effects. The criteria of transition from laminar to turbulent depends on the Reynolds number of mean flow Re_{cri} and on oscillating parameters A_o and λ .

1.3 Characteristics of Heat Transfer

There are many efforts done to improve the rate of heat transfer. The improvements of the heat transfer depends on two method , the first is by increasing the area of heat transfer such as extended surface (it is limited by the design of device and the cost), the second depends on affecting the boundary layer (thermally and hydrodynamically) such as varying the flow from laminar to turbulent or changing the nature of flow from the steady to unsteady by pulsating or reciprocating flow. The enhancement of heat transfer in the oscillatory flow can be classified as

1.3.1 Heat Diffusion in Oscillatory Flow

The heat or mass diffusion can be improved by oscillating flow. The reciprocating flow can enhanced the diffusion rate by several order of magnitude greater than that possible by molecular diffusion alone. The rate of mass transfer of a diffusing substance may be increased by an oscillatory motion and affecting with oscillatory parameters such as low and high frequency^[5]. These types of studies are concerned with the comparing the effective axial diffusion coefficient for oscillatory flow with molecular

diffusion in steady flow. The ratio of effective diffusivity of the contaminant for unsteady and steady fluid flow (κ_{eff} / κ) is represented as a function to a two oscillating parameters: Womersly number and tidal displacement. The most of previous works in this field are shown a considerable increase in axial diffusion heat transfer between two different temperature reservoirs without a net transfer of mass due to a large time dependent radial temperature gradient produced by the fluid oscillations. The temperature distribution in many cases were obtained by assuming similarity transformation solution and solving the conjugate energy equations.

1.3.2 Heat Transfer in Reciprocating Flow

Reciprocating motions are found in many applications such as heat exchangers, internal combustion engines and electronic cooling. It is found that from the numerical investigations that annular effects (similar to annular effects in velocity) also exists in the temperature profile of a laminar reciprocating flow. The axial and radial diffusion of heat transfer under reciprocating flow conditions is considerably larger than in the absence of the reciprocating flow. This enhancement is produced by the interaction between the radially varying of velocity and temperature profiles that it can be given a heat transfer coefficients of orders of magnitude larger than without oscillating flow. The main parameters that effect of heat transfer in the reciprocating flow are: Womersly number λ or kinetic Reynolds number Re_{ω} , dimensionless amplitude of the fluid displacement A_{ω} , Prandtl number Pr and the ratio of length to diameter x/D .

Reciprocating flow is used to enhance conduction heat transfer between two reservoirs maintained at different temperature to increase efficiency of fins^[6] by improving the diffusivity of the fluid.

The careful observations of the literature for reciprocating flow heat transfer shows two different kinds of investigations associated with this type of flow. The first one is focused on heat transfer by conduction enhancement with high frequency and low amplitude oscillations, while the second is focused on forced convection with low frequency, large amplitude of oscillation.

There are a survey correlations for \overline{Nu} of experimental works of the reciprocating flow depending on parameters A_o and Re_ω ^[7], and a few theoretical researches are made in this field.

1.3.3 Heat Transfer in a Pulsating Flow

The enhancement and investigation of convective heat transfer of pulsating flow characteristic have been of most important engineering space of heat transfer researches. Heat transfer for pulsating flow is obtained as either on flat plate or in internal flow. The external oscillatory flow over a flat plate with a stream velocity depends on a frequency parameter and Strouhal number Str_x , gives not much difference from that of the mean flow (steady flow) in the ranges of smaller and larger Strouhal number Str_x , while it becomes more significant near the region^[7] $Str_x=1$.

For internal pulsating flow the effective parameters are λ , Re_m , Pr , A_o and x/D_h . It may normally be expected that the heat transfer to or from the flow would be changed because the pulsation would alter the thickness of the boundary layer and hence the thermal resistance. The main exerted efforts in the study of heat transfer in the pulsating are concerned with a pulsating flow enhances heat transfer comparing to steady flow. The results obtained from these studies can be classified into a four cases such as:

1-The pulsating flow enhances the heat transfer.

2-It either enhances or decreases the heat transfer depending on the controlling parameters.

3-The pulsating flow decreases the heat transfer .

4-It has no effects on heat transfer.

These conflicting results showed that the heat transfer phenomenon in pulsating flow is still not clearly understood.

1.4 Hydrodynamics and Thermal Considerations of Oscillating Flow

The considerations that were taken into account during the study of oscillatory flow takes a wide area in the analysis. From these: studies concerns the developing of the flow or the entrance region, where at the entrance region the analysis is more difficulties and gives greater change in all dependent variables such as friction factor and Nusselt number^[8]. Number of authors made a simplifications for solving momentum and energy equations theoretically in the developing region, and in most of their analysis they assumed

1-Existence of a boundary layer.

2-The velocity in the inertia terms of boundary layer equation being the same as at the entrance velocity given at the inlet.

Usually, the systems of reciprocating flow have a developing flow more probably than a fully developing flow, owing to reverse flow, for which a little length is not enough to complete the development, while the pulsating flow systems usually reach the fully developing flow.

The conditions of fully developed in both hydrodynamics and thermal boundary layer for oscillatory flow are similar to the conditions of steady flow^[9].

The criteria of transition from laminar to turbulent have new conditions represented by oscillating parameters. The oscillations makes the velocity fluctuations near the wall are much stronger than at center line of duct, i.e. the fluid flow near the wall may be first become unstable and eddies occur near the wall, this is because high kinetic Reynolds number. Furthermore, there are another criteria for turbulent flow represent by the intermittency of turbulence of the flow, which is defined as the percentage of the time to detect the critical values (transition from laminar to turbulent region)^[7].

1.5 The Aim of the Present Work

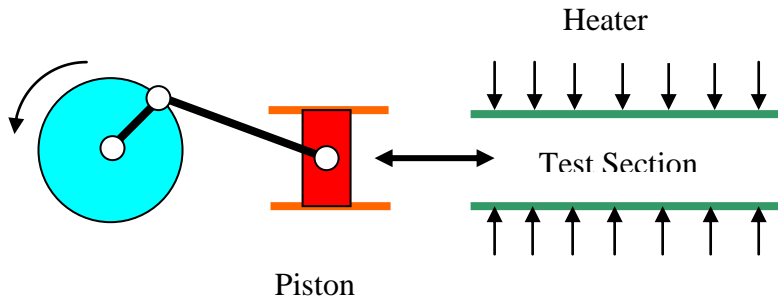
There are nearly scarce analytical researches concern heat transfer in oscillatory flow. On other hand, the available results about heat transfer enhancement in the pulsating flow is not cleared, therefore the present study is aimed to investigate the main points below:

- 1- Obtain an analytical model for hydrodynamics and heat transfer in both reciprocating and pulsating flows by solving the momentum and energy equation and overcome the complexity due to the unsteady flow.
- 2- Study the ability of enhancement the heat transfer by oscillating flow and obtaining the controlling parameters of the process and detecting the improvement caused by the unsteady flow over the steady flow.
- 3- Support the numerical and experimental researches in this field with analytical model .

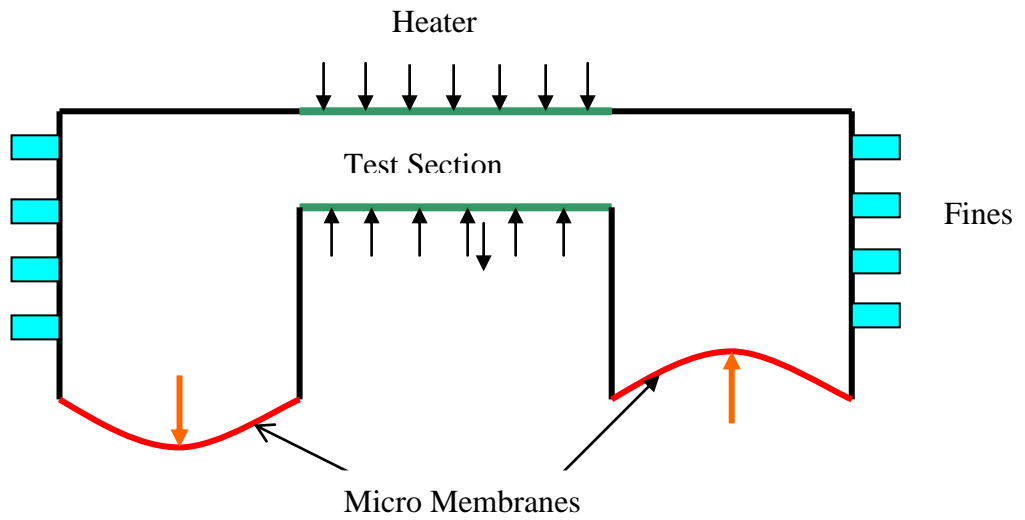
In this study, an analytical simulation based on similarity transformation solution for momentum and energy equations are to be obtained. The considered flow is to be oscillatory flow in the internal horizontal duct (channel and pipe) subjected to a constant heat flux, for

laminar, 2D, incompressible and fully developed flow. Both kinds of oscillatory flow the reciprocating and pulsating flow were to be considered.

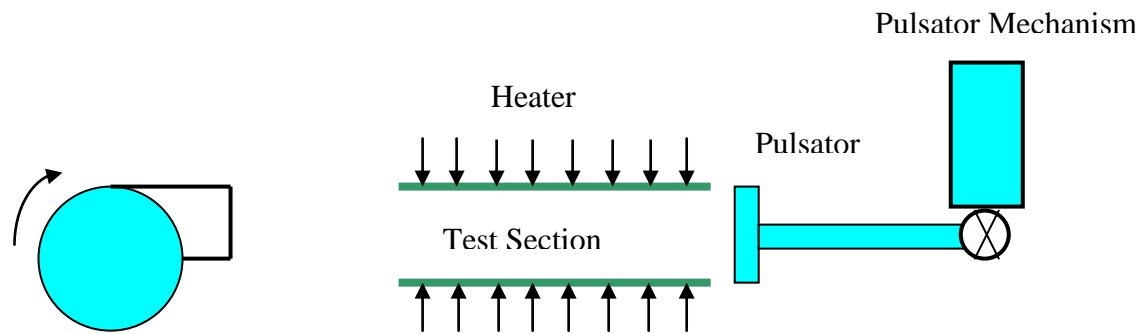
Numerical simulation is to be performed using finite volume approach, and the difference between the analytical and numerical solution for dimensionless velocity and temperature distributions is to be illustrated. Also, the results of analytical solution for Nusselt number were to be compared with experimental data or experimental correlations of other authors.



a- Reciprocating flow



b- Reciprocating flow



c- Pulsating flow

Fig.1.1 A Simple sketches for oscillatory flows.

CHAPTER TWO

LITERATURE REVIEW

2.1 Preface

A considerable amount of theoretical and experimental works have been devoted to the study of oscillatory flow owing to its importance in real life. Therefore, the oscillatory flow were extensively studied by a several investigators in wide fields like: human, engineering and nature. The oscillatory flow and heat transfer review is performed for all faces that has some effects on the hydrodynamics and thermal behaviors. A large number of articles illustrate all considerations, types and controlling parameters of oscillatory flow and heat transfer to obtain the conditions for enhancement of heat transfer. Literatures have been categorized according to the following fields:

- 1- A general study for unsteady flow (human and nature phenomenon).
- 2- Hydrodynamics considerations of the oscillatory flow.
- 3- Heat transfer considerations in oscillatory flow.

2.2 The General Unsteady Flow

The phenomenon of unsteady propagate in the wide fields because of a several of these phenomena are repeated with time periodically, which represent a common factor between them. The unsteady flow is started from the heart of human and a specific type of unsteady flows include oscillatory flow and pulsatile flow which occurs in the nature phenomena and the biological systems such as the human respiratory and the vascular systems.

The unsteady flow is simply occurred when the motion of the fluid is started suddenly from rest. The flow near a flat plate which are impulsively accelerated from the rest was solved firstly by stokes as cited by Schlichting^[1]. The Navier-Stokes equation

$$\frac{\partial u}{\partial t} = \nu \frac{\partial^2 u}{\partial y^2} \quad (2.1)$$

is reduced to an ordinary differential equation by using similarity parameter as $\xi = y / 2\sqrt{\nu t}$.

The similar case for suddenly accelerated flow from rest is the flow about an infinite flat wall which executes linear harmonic oscillations parallel to itself and which was first treated by Stokes and later by Rayleigh as cited by^[1]. They supposed that this motion is given

$$u(0, t) = \frac{X_{\max} \cdot \omega}{2} \cos \omega t = u_{\max} \cos \omega t \quad (2.2)$$

where X_{\max}, u_{\max} being the amplitude of the velocity and displacement of the oscillating plate respectively. The velocity distribution above the oscillating plate is given as

$$U(y, \tau) = \frac{u(y, t)}{u_{\max}} = e^{-\eta} \cos(\tau - \eta) \quad (2.3)$$

where $\eta = y \sqrt{\frac{\omega}{2\nu}}$

They found that the oscillatory boundary layer or the so called ‘Stokes layer’ has thickness of $\delta = \sqrt{2\nu/\omega}$ which increased with increasing the kinematics viscosity and decreasing with increasing the angular frequency. This showed that the thickness of boundary layer became thinner with increasing the frequency, which lead to enhance the characteristics of oscillatory flow.

Evans^[10] 1973, considered a semi-infinite plate moving with a velocity $u_w(t)$ into a stagnant fluid and he obtained a solution of heat transfer with constant surface enthalpy corrected to second order. The second order results were obtained by numerical integration for Prandtl number of 0.72.

Peattie^[11] 1989, carried out experimental work to establish, a piston-driven pipe flow (flow is driven at frequencies characteristic of human breathing), in order to assess the effect of frequency on the transport of a passive scalar contaminant in an oscillating flow. In the test section he used in one a straight, round and uniform pipe and in other a uniformly tapering pipe (i.e. conical). As a results he found that: (i) The convective transport is increasing with frequency at constant amplitude (ii) The effective diffusivity increase with flow amplitude, more strongly at $\lambda=5.7$ than at $\lambda=16$, but does not increase by a constant scale factor as λ varies from 5.7 to 16. He defined the effective mean axial diffusivity for thermal energy transfer in a tube, as

$$\alpha_{eff} = \frac{Q_{con}}{\pi a^2 \rho c_v \tau \frac{dT_b}{dx}} \quad (2.4)$$

where a: radius of the pipe, τ : time of period.

The oscillatory or periodic heat transfer in extended surface was studied by Aziz and Lanardini^[12] 1994. They obtained analytical and numerical approaches for periodic or oscillating heat transfer processes occurring in extended surface. For liner problems the techniques include complex combination, Laplace transforms, finite differences and boundary elements. They discussed the applications of each approach in detail. Both straight and annular fin configuration are covered for

different profile shapes include rectangular, trapezoidal and convex parabolic. The periodic conditions involve oscillatory base temperature, oscillating base heat flux, oscillating environment temperature, convection at the fin's base through a fluid with oscillating temperature and some combination of these conditions. In this work the various combinations of analytical and numerical methods had been found to be effective in dealing with nonlinear problems.

Flow in the elliptical blood vessels calculated for a physiological waveform by Robertson et al.^[13] 2000. They idealized the geometry of a non-circular vessel to an elliptical cross section and the dynamic properties were calculated for a physiological waveform. The Fourier harmonics for a common carotid waveform were determined and the velocity profile and wall shear stress were calculated from the superposition of the individual contributions from each harmonic. They concluded that in pulsative flow, the frequency perform a strong role in determining the motion of the fluid and the resultant velocity profile. They also concluded if the frequency is reduced, the relative viscous drag between the central core and the lamina near the vessel wall is decreased until the response of the different lamina to the applied pressure gradient is equivalent.

Concerning, the heat transfer considerations of the unsteady flow (oscillatory flow) a number of studies were carried out for the heat transfer in a porous medium. Hassain et al.^[2] 2000, considered the unsteady free convection boundary layer flow which induced by time-periodic variations in the surface temperature of a vertical surface embedded in a porous medium. Both the low and high frequency limits are considered separately and they observed:

1- At intermediate value of frequency parameter the amplitude of the local Nusselt number increase as the surface temperature exponent increase, but the phase of Nusselt number decrease.

2- There is always a phase lead increment as frequency parameter increase and approaches the common asymptotic value $\pi/4$.

Al-Salman^[14] 2002, investigated experimentally and theoretically the direct contact condensation process of saturated vapor on fully developed subcooled laminar wavy falling liquid film flowing over an adiabatic vertical wall. The results of the model illustrated that the main parameters affecting the condensation process are the wave amplitude, wave length, Peclet number and subcooling number. He showed that the waviness of liquid film increases the heat transfer rate up to several tenths of a percent, mainly due to the effective thinning of the film, increasing convection along the film and circulation of the flow.

The streaming and oscillating flow fields and heat transfer efficiency across channel between two long parallel beams was investigated by Wan and Kuznestov^[15] 2003. One of these beams is stationary and the other is oscillating in standing waveform. The temperature field was computed for two cases: both beams are kept at constant but different temperature or the oscillating beam is kept at constant temperature and the stationary beam is prescribed a constant heat flux. It is found that the streaming fields shows that the streaming velocities approach constant values at the edge of the boundary layers and provide slip velocities for the streaming field in the core region. The results reveal a jump of Nusselt number and heat transfer coefficient when the bifurcation occurs, and Nusselt number increases before the jump and decreases after it. Khalid and Vafai^[16] 2003, analyzed the flow

and heat transfer inside oscillatory squeezed thin films subject to a varying clearance of the films. They assumed the velocity of the fluid at the squeezing plate as

$$V = h_o \omega \gamma \beta \sin(\gamma \omega t) \quad (2.5)$$

where h_o : reference thin film thickness, γ : is the dimensionless frequency, β : is the dimensionless amplitude of the upper plate's motion, and ω : is the reference frequency. Nusselt number and their amplitudes are decreasing with increasing the dimensionless slop of upper plate.

Recently, Khalid and Vafai^[17] 2004, analyzed the stokes and Couette flow produced by an oscillating motion of a wall under conditions where the no-slip assumption between the wall and the fluid is no longer valid. It is found that wall slip reduces the transient velocity for Stokes flow while minimum transient effects for Couette flow is achieved only for large and small values of the wall slip coefficient and the gap thickness respectively. The time needed to reach to steady periodic Stokes flow due to sine oscillations is greater than that for cosine oscillations with both wall slip and no-slip conditions.

2.3 Hydrodynamics Considerations in Oscillatory Flow

There are many works done in hydrodynamic of oscillatory flow, which deals with all kinds of oscillatory flow and take into account the effect of the variety of conditions acting on the flow. These works can be classified into the following

2.3.1 Hydrodynamics of Reciprocating Flow

In the earlier time, the reciprocating flow taken a wide space of investigations of oscillatory flow. The reciprocating motion of the fluid

driven either by sinusoidal displacer has a fluid displacement X_m is explained as

$$X_m = \frac{X_{\max}}{2} (1 - \cos \omega t) \quad (2.6)$$

or by a sinusoidal variation of pressure gradient as

$$-\frac{1}{\rho} \frac{\partial p}{\partial x} = P_o \cos \omega t \quad (2.7)$$

where P_o : the oscillation amplitude of externally imposed pressure gradient.

Uchida^[7] 1956, obtained an exact solution for axial velocity profile of a fully developed laminar reciprocating flow in a circular pipe (with diameter of $D=2a$). This solution was simplified to give the velocity distribution for small values of the Womersly number (very low oscillation) and large values of Womersly number (very high oscillation)^[1].

Zhao and Cheng^[18] 1995, presented a numerical solution for laminar forced convection of an incompressible periodically reversing flow in a pipe of finite length at constant wall temperature. They illustrated that is typical phase shifts between temperature and axial velocity at selected locations.

Zhao and Cheng^[19] 1996, carried out analytical and experimental work for reciprocating flow. They obtained an exact solution for the axial velocity profile of a fully developed reciprocating pipe flow from modification of Uchida's analytical solution. Algebraic expression for the time averaged friction coefficient of a fully developed reciprocating flow was obtained as

$$\bar{C}_{f,\infty} = \frac{3.272}{A_o(\text{Re}_\omega^{0.548} - 2.039)} \quad (2.8)$$

where $A_o = \frac{X_{\max}}{D}$ dimensionless amplitude and $\text{Re}_\omega = \frac{\omega D^2}{\nu}$ kinetic Reynolds number.

They found that, although the dimensionless axial velocity profile of a fully developed flow depends only on the kinetic Reynolds number, while the friction coefficients depend not only on the kinetic Reynolds number but also on the dimensionless oscillation amplitude. Comparison were made for the time resolved and the cycle-averaged friction coefficients between the analytical solution and the experimental data which gives a good agreement.

Reciprocating flow in the channel differs from the reciprocating flow in the pipe by (i) The hydraulic diameter may be partly wetted the perimeter ($D_h = \frac{4A_c}{P}$, where A_c : flow area and P : wetted perimeter)^[20]. (ii) Womersly number for channel is defined as $h\sqrt{\omega/\nu}$ where h: the half height of channel, while in the pipe $D/2\sqrt{\omega/\nu}$.

Kurzweg^[6] 1985, found analytical solution for sinusoidally oscillatory viscous fluid in an array of parallel-plate channels. He found the axial velocity profile existing in the channel which is represented by the real part of

$$U(\eta, t) = U_o f(\eta) e^{i\omega t} = \frac{iU_o \lambda}{\alpha^2} \left[1 - \frac{\cosh \sqrt{i\alpha} \eta}{\cosh \sqrt{i\alpha}} \right] e^{i\omega t} \quad (2.9)$$

where $\eta = y/a$, U_o representative axial velocity, $\alpha = a\sqrt{\omega/\nu}$ the Womersly number and $\lambda = \left| \frac{\partial p}{\partial x} \right| a^2 / \rho U_o \nu$.

Yakhot et al.^[21] 1999, studied numerically oscillating laminar flow of a viscous, incompressible liquid in a rectangular duct. The influence of the aspect ratio of the rectangular duct and the pulsating pressure gradient frequency on the phase lag, the amplitude of the induced oscillating velocity, and the wall shear were analyzed. They found the induced velocity has a phase lag (shift) with respect to the imposed pressure oscillation, which varies from zero at very slow oscillations, to 90° at fast oscillations.

Karagoz^[22] 2002, introduced analytical solution based on similarity transformation for oscillatory pressure driven, fully developed flow in a channel. Variations of the velocity profile and skin friction coefficient over a cycle had been obtained together with behavior of the flow for various oscillation frequencies. He concluded that, when the frequency is low, velocity profiles resemble much of the quasi steady solution. An increase of α leads to a wider core region where the fluid moves as if it were frictionless slug flow. The effects of oscillation become dominant in a narrow zone adjacent to the walls in the case of high α . Phase lag occurs between pressure and velocity variations so that it is higher in the core region than in the boundary layers, due to variation of the inertial forces across the flow section. Skin friction coefficient was also affected by oscillation frequency of which high values give rise to the amplitude of skin friction coefficient.

Sert and Beskok^[23] 2002, introduced a new micro heat spreader (MHS) concept for efficient transport of large concentrated heat load. The (MHS) is a single phase closed micro fluidic system, which utilize reciprocating flow forced convection. They solved numerically the momentum and energy equations by applying the spectral element

algorithm. Fluid flow and thermal transport equations are solved in moving domains (the domain is divided into 68 quadrilateral and triangular elements) using a recently developed arbitrary Lagrangian Eulerian algorithm.

Sert and Beskok^[24] 2003, performed a numerical simulation for reciprocating flow in two-dimensional channels. The flow between two parallel plates drive harmonically in time with a pressure gradient was considered. They observed the quasi-steady flow behavior for $\alpha=1$ (where $\alpha = H\sqrt{\omega/\nu}$) (low frequency), and Richardson's effect for $\alpha=10$ (high frequency). The numerical algorithm based on a spectral element formulation, which enable high order spatial resolution with exponential decay of discretization errors, and second order time accuracy.

Finally, Cosgrove^[25] 2003, studied the applicability of the Lattice Boltzman method to oscillatory channel flow with a zero mean velocity. The model has been compared to exact analytical solutions in the laminar oscillatory channel flow case ($Re_\delta < 100$, where Re_δ the Reynolds number based on the Stokes layer), for the Womersly parameter $1 < \alpha < 31$. They defined analytical expression for the velocity for large α as

$$u \cong \frac{P}{\omega\rho} \sin \omega t \quad (2.10)$$

where P: amplitude of pressure gradient $-\partial p / \partial x$

2.3.2 Hydrodynamics of Pulsating Flow

In the preceding section two types of the harmonic pulsation flow were mentioned: internal and external pulsation flow. The external free stream flow represented by^[7]

$$u(t) = u_{\infty} (1 + \varepsilon e^{i\omega t}) \quad (2.11)$$

where $\varepsilon = \frac{u_{\max}}{u_{\infty}}$ being the dimensionless oscillating velocity amplitude

which assumed to be small.

The internal pulsation flow was studied by Christian and Kerczek^[26] 1982. They investigated the instability of oscillatory plane Poiseuille flow, in which the pressure gradient is time-periodically modulated by a perturbation technique. They showed that the sinusoidally oscillating plane Poiseuille flow for a wide range of frequencies of the imposed oscillation and for substantial values of oscillation amplitude.

Turbulent and laminar pulsating flow were measured experimentally by Shemer et al.^[27] 1985, in a straight smooth pipe and compared at identical frequencies and Reynolds numbers. Most measurements were made at mean Reynolds numbers of 400 but the influence of the mean Reynolds number was checked for $2900 < Re < 7500$ and the nondimensional frequency parameter, $\alpha = R\sqrt{\omega/\nu}$ from 4.5 to 15. The amplitude of imposed oscillation did not exceed 35% of the mean, in order to avoid flow reversal or relaminarization. The velocity at the exit plane of the pipe and pressure drop along the pipe were measured simultaneously. The velocity measurements were made with arrays of normal hot wires. They concluded that:

i- Mean properties of the flow are not affected by pulsations in both laminar and turbulent flow regimes, provided the amplitude is not excessively high.

ii- The radial distributions of amplitudes and phases of velocity oscillation are strongly dependent on the flow regime in the pipe (i.e. whether is laminar or turbulent).

Valencia and Hinojosa^[28] 1997, studied numerically the incompressible laminar flow of air and heat transfer in a channel with a back ward-facing step, for steady cases and for pulsatile inlet conditions. They used parabolic entrance profile for numerical solutions of pulsatile flow. It was found at the amplitude of oscillation which is represented by Reynolds number equal to 100, the primary vortex break down through one pulsatile cycle. The wall shear rate in separation zone was varied markedly with pulsatile flow.

Ju et al.^[29] 1998, developed an improved numerical modeling for simulating the oscillating fluid flow and detail dynamic performance of the orifice and double-inlet pulse tube refrigerator. They assumed a simple sinusoidal oscillations for the compressor volume change with crank angles as

$$V = V_d + \frac{1}{2} V_s (1 + \cos \omega t) \quad (2.12)$$

where V_d is the dead volume, and V_s is the swept volume.

They proposed a numerical simulation and experimental verification of the oscillatory flow in pulse tube refrigerator. The discretization of governing equations based on full implicit time dependent and upwind second order finite difference scheme. They found a good agreement between the numerical simulation and experimental verification. Also Ju et al.^[30] 1998, studied experimentally the oscillating flow characteristics

for a regenerator in a pulse tube cryocooler. They determined a correlation for a cycle-averaged friction factors at the frequency 50Hz.

José et al.^[31] 2002, carried out both experimental and numerical studies for unsteady pressure field inside a centrifugal pump. The measurement were carried out with pressure transducers installed on the volute shroud. The unsteady pressure field inside volute of centrifugal pump has been numerically modeled using a finite volume code. The numerical code used (FLUENT) solved the fully 3D, incompressible Navier-Stokes equations, including the centrifugal force source in the impeller and the unsteady terms and turbulence was simulated with the standard $\kappa-\varepsilon$ model. The results of the numerical simulation were focused on the blade passing frequency to study two effective phenomena occurring at that frequency for a given position: the blade passing in front of the tongue and the wakes of the blades.

Yakhot and Grinberg^[32] 2003, studied a pulsating laminar flow of a viscous, incompressible fluid through a pipe with an orifice at relatively low Reynolds numbers. The phase instantaneous state was found as an ellipse. The ellipses of the instantaneous states (volumetric flow rate vs pressure difference) during a cycle allow readily computing the phase shift between them.

Baranyi^[33] 2003, computed Strouhal number, time-mean drag and base pressure coefficient as well as the average Nusselt numbers by solving the governing equations (continuity, Navier-Stokes equations, Poisson equation for pressure and energy equation) for 2D, low Reynolds number unsteady flow around and heat transfer from a stationary circular cylinder placed in a uniform flow.

2.3.3 The Turbulence Considerations in the Oscillatory Flow

The considerations of transition flow from laminar to turbulent in the oscillatory flow differ from that taken in the steady flow. The condition of transition the laminar to turbulent flow in steady flow depends on Reynolds number only, while in oscillatory flow it is affected by frequency and amplitude of oscillation.

There are many researches concerned the criteria of oscillatory flow to detect the conditions of transition from laminar to turbulent flow.

The transition behavior of pulsating flow is characterized by a new parameter in addition to frequency and amplitude of oscillation represented by the mean-flow Reynolds number Re_m . If Reynolds number is lower than critical value^[9], the onset of turbulence depends on A_o and λ or Re_ω .

Calmen and Minton^[7] 1977, found the velocity disturbances by measuring intermittency of turbulence ψ of the flow (ψ : defined as the percentage of the time of flow was disturbed during a 5 minutes measuring period). The intermittency of turbulence depend on three parameters: λ , A_o and Re_m . They found that (i) the intermittency ψ rises from zero with the increase of the Womersly number λ at a given value of dimensionless amplitude of oscillation A_o (5.8, 2.9, or 1.45); (ii) for a given value of frequency of oscillation, an increase in A_o produces an increase in the intermittency; (iii) the intermittency ψ increase as Re increased from 1275 to 1535 at fixed values of λ and A_o ; (iv) as the mean-flow Reynolds number Re approaches the critical value of a steady pipe flow, the minimum value of intermittency ψ becomes much

greater than zero. This implied that the pulsating flow becomes turbulent when the mean-flow Reynolds number approaches the critical value of steady pipe flow, or λ and A_o approach from critical values (β_{cri}).

Zhao and Cheng^[34] 1996, carried out an experimental numerical study for laminar forced convection in along pipe heated by uniform heat flux and subjected to reciprocating flow of air. They used the range of $A_o = 8.5-34.9$ and $Re_{\omega} = 23-464$.

2.4 Heat Transfer in the Oscillatory Flow

Research works dealing with heat transfer in oscillatory flow can be categorized into the following

- 1- Enhanced axial heat diffusion by oscillating flow.
- 2- Heat transfer in internal reciprocating flow.
- 3- Heat transfer in internal pulsating flow.

2.4.1 Enhanced Axial Heat Diffusion by Oscillatory Flow

The oscillatory flow was not used in enhancement heat transfer only, but it is also used for enhancement the rate of mass transfer of diffusing substance. The dispersion in oscillatory flow is important in many practical cases varying from tidal flow in estuaries to respiratory flow in the air ways of lungs. Watson^[5] 1983, studied the diffusion of substance along a pipe and a two dimensional channel driven by an oscillatory motion of ambient fluid in the pipe. He assumed the concentration of the contaminant $\theta(x,y,z,t)$ as

$$\theta(x, y, z) = -\gamma z + \text{Re}\{\gamma g(x, y) e^{i\omega t}\} \quad (2.13)$$

where θ satisfies the concentration equation

$$\frac{\partial \theta}{\partial t} + w \frac{\partial \theta}{\partial z} = \kappa \nabla^2 \theta \quad (2.14)$$

where κ : diffusivity of the contaminant.

He found that the effective diffusivity of the contaminant in the oscillating flow using Green's theorem as

$$\kappa_{eff} = \kappa (1 + R) \quad (2.15)$$

where

$$R = f \left(\frac{D^2 \omega}{\nu}, \frac{\nu}{\kappa} \right) \left(\frac{V}{AD} \right)^2 \quad (2.16)$$

where V is tidal volume.

He concluded that the flux of contaminant can be increased significantly, for given tidal volume, by using of a high frequency of oscillation.

Joshi et al.^[35] 1983, studied experimentally the gas exchange in laminar oscillatory flow to determine the diffusivity of axial transport through a tube of circular cross-section of a contaminant gas in oscillatory flow and compared the results with results of Watson^[5], which gives an excellent agreement. For $\sigma = 1$ (where $\sigma = \frac{V}{\kappa}$). They

found that the effective diffusivity at high and low frequency as

$$\kappa_{eff} = \kappa \left(1 + \frac{1}{192} . Pe^2 \right) \quad \alpha \leq 1 \quad (2.17a)$$

$$\kappa_{eff} = \kappa \left(1 + \frac{\alpha + 3\sqrt{1/2}}{8\sqrt{2}\alpha^4} Pe^2 \right) \quad \alpha > 1 \quad (2.17b)$$

where Pe : Peclet number, α : dimensionless frequency parameters.

Kurzweg^[6] 1985, examined analytically enhanced heat conduction in oscillatory viscous flow within parallel plate channels. The widths of the fluid layers and the solid walls in this configuration were taken as $2a$ and $2b$ respectively. He showed that for fixed frequency the corresponding effective thermal diffusivity reaches a maximum when the product of the Prandtl number and the square of the Womersly number is approximately equal to $\lambda^2 \text{Pr} = \pi$ and the axial heat transfer achievable can be exceed that possible with heat pipes by several orders of magnitude. He also found the temperature distribution between two reservoirs at different temperature by suggesting a try locally valid solution to solve the augmented problem as

$$T(x, \eta, t) = \gamma (x + a g(\eta)e^{i\omega t}) \quad (2.18)$$

where $\eta=y/a$ and γ : time-averaged axial temperature gradient.

The above analysis was based on an important assumption that the time-averaged axial temperature gradient of the fluid is constant along the pipes. He defined the effective averaged thermal diffusivity as

$$-\alpha_{eff}\gamma = \frac{\omega}{2\pi} \int_0^{2\pi/\omega} dt \int_0^1 \text{Re}[T(x, \eta, t)] \cdot \text{Re}[V(x, \eta, t)] d\eta \quad (2.19)$$

for very high frequencies the α_{eff} is

$$\frac{\alpha_{eff}}{\omega \Delta x^2} = \frac{1}{8\sqrt{2\alpha}} \left[\frac{\text{Pr}(\text{Pr}+1) * (\mu + \sqrt{\sigma})}{\text{Pr}(\text{Pr}^2-1)(\mu + \sqrt{\sigma})} - \frac{\sqrt{\text{Pr}}(1 + \sqrt{\text{Pr}})(\mu\sqrt{\text{Pr}} + \sqrt{\sigma})}{\text{Pr}(\text{Pr}^2-1)(\mu + \sqrt{\sigma})} \right] \quad (2.20)$$

where Δx is tidal displacement, $\sigma = \frac{\alpha_f}{\alpha_s}$ and $\mu = \frac{k_f}{k_s}$.

For low-oscillation frequency α_{eff} is

$$\frac{\alpha_{eff}}{\omega \Delta x^2} = \frac{\alpha^2 \text{Pr}}{8} \left[\frac{17}{35} - \frac{4\mu}{5(\mu + \sigma(\varepsilon - 1))} + \frac{\mu}{3} \frac{\mu + \sigma^2(\varepsilon - 1)^3}{3(\mu + \sigma(\varepsilon - 1)^2)} \right] \quad (2.21)$$

where $\varepsilon = b/a$

Kurzweg^[36] 1985, examined the enhancement of conduction heat transfer for sinusoidal oscillatory flow through circular tube connecting two fluid reservoirs maintained at different temperatures. He solved the governing heat conduction equation using the multiple time scale expansion technique, the temperature variation expanding in the perturbation series is

$$T = T_o + \varepsilon T_1 + \varepsilon^2 T_2 \quad (2.22)$$

where ε : small parameter used in multi scale expansion and T_o , T_1 and T_2 : temperature expansion terms, °C.

He obtained a relation for effective diffusivity as

$$\frac{\alpha_{eff}}{\alpha} = 1 + \frac{(\text{Pr} \Delta z)^2}{16 a^2} P(\lambda) \quad (2.23)$$

where

$$P(\lambda) = \frac{1}{24} \quad \text{for } \lambda \ll 1 \quad (2.24a)$$

$$P(\lambda) = \lambda^2 \left(1 - \frac{1}{\sqrt{2}\lambda} \right) \quad \text{for } \lambda \gg 1 \quad (2.24b)$$

where Δz : tidal displacement of fluid, λ is Womersly number.

He concluded that the values of effective conductivity in liquid metals is three orders of magnitude grater than the normal thermal conductivity

under typical experimental conditions without a net transfer of mass. This was explained due to a large time dependent of radial temperature gradient produced by the fluid oscillations at region near the wall. The results was merged at approximately $\lambda^2 \text{Pr} = \pi$, which is the point where the used multiple time scale expansion technique becomes invalid.

Performance of heat exchangers occupied a part of the studies of enhanced heat diffusions in fluids by oscillation. Kaviany^[37] 1990, analyzed fluid flow and heat transfer in capillary tubes (Stokes's boundary layer thickness nearly equal to the tube radius), subjected to oscillatory flow between two reservoirs maintained at different temperature. He defined the effective thermal diffusivity as

$$\frac{\alpha_{eff}}{R^2 \omega} = -\frac{1}{\pi} \int_0^{2\pi} \int_0^1 \text{Re}(u) \text{Re}(T) r dr dt \quad (2.25)$$

and assumed temperature field as

$$T_f = \frac{\partial \bar{T}}{\partial x} x + \frac{\partial \bar{T}}{\partial x} \theta(r, t) \quad (2.26)$$

where θ : fluctuating component, m.

He concluded that (i) the performance of heat exchanger deteriorate as thermal boundary layer becomes smaller than the tube radius (ii) the viscous dissipation is generally negligible for water.

Kaviany and Rekker^[38] 1990, presented experimental study for the performance of a heat exchanger that takes advantage of enhanced heat diffusion in oscillated fluids. Good agreement had been found between the actual performance of the heat exchanger and the idealized analysis for low and high frequencies. The measurements showed that there is a temperature variation across the bundle and that the fluid entering the

tubes has a nonsteady temperature due to weak, non uniform mixing within the reservoirs therefore, a spatial/temporal average was taken.

Further more, Khaled and Vafai^[39] 2002, studied the effects of both external squeezing inside non-isothermal and incompressible thin films supported by soft seals. The main controlling parameters were: squeezing number, squeezing frequency, frequency of pulsations, fixation number (for the seal) and the thermal squeezing parameters. They found that the fluctuations in the heat transfer and the fluid temperature can be maximized at relatively lower frequency of internal pressure pulsations.

2.4.2 Heat Transfer in Internal Reciprocating Flow

Generally, heat transfer in the reciprocating flow depends on oscillatory frequency and tidal displacement of the fluid. The following works to be presented includes some studies on forced convection in laminar and turbulent reciprocating flow in a pipe and a duct that show the effect of controlling parameters on heat transfer characteristics i.e. Nusselt number and bulk temperature.

Cooper et al.^[7] 1994, investigated experimentally the convective heat transfer in rectangular duct. The duct was heated from below and subjected to a periodically reciprocating flow. The frequency and stroke of oscillations were varied such that the range of Re_{ω} was from 43 to 684 while the range of dimensionless oscillation amplitude of fluid A_o was from 23 to 600, such that the parameter $(A_o \sqrt{Re_{\omega}})$ ranging from 603 to 5568 (typical values of critical parameter β_{cri} ranging from 400 to 800). The experimental data were arranged to obtain a correlation of

space-cycle averaged Nusselt number \overline{Nu} for reciprocating turbulent flow of air in a rectangular duct with one-side heated

$$\overline{Nu} = \frac{q'' 2a}{k_f (\overline{T_w} - T_f)} = 0.548 A_o^{0.3} \text{Re}_\omega^{0.536} \quad (2.27)$$

where $\overline{T_w}$ being the space-cycle averaged temperature measured at the outer surface of heated floor, and T_f being the ambient temperature.

A numerical solution was presented by Zhao and Cheng ^[18] 1995, for laminar forced convection of incompressible periodically reversing flow in a pipe of finite length at constant wall temperature. They found that four parameters govern the heat transfer characteristics for the problem. These parameters are: the kinetic Reynolds number Re_ω , the dimensionless oscillation amplitude A_o , the length to diameter ratio L/D and Prandtl number Pr of the fluid. They solved numerically the dimensionless energy equation given below.

$$\frac{\partial \theta}{\partial \tau} + \frac{A_o}{2} (\vec{V} \cdot \nabla) \theta = \frac{1}{\text{Re}_\omega \text{Pr}} (\nabla^2 \theta) \quad (2.28)$$

where θ : is dimensionless temperature $\left(\frac{T - T_i}{T_w - T_i} \right)$, τ : is dimensionless

time. They used a highly nonuniform grid because of the extremely thin thermal boundary layer at a high kinetic Reynolds number. The time-space averaged Nusselt number \overline{Nu} was correlated by the following expression

$$\overline{Nu} = 0.00495 A_o^{0.9} \text{Re}_\omega^{0.656} \quad (2.29)$$

for $A_o=10$ to 35 and $\text{Re}_\omega=10$ to 400 and L/D=40.

For other values of A_o , Re_ω and L/D , Nusselt number was correlated as

$$\overline{Nu} = 0.00495 A_o^{0.9} Re_\omega^{0.656} [43.74(D/L)^{1.18} + 0.06] \quad (2.30)$$

The numerical results showed that annular effects also exist in the temperature profiles near the entrance and the exit of the pipe during each half cycle at high kinetic Reynolds numbers. The averaged heat transfer rate was found to increase with both kinetic Reynolds number and dimensionless oscillation amplitude but decrease with length to diameter ratio.

Zhao and Cheng^[34] 1996, carried out an experimental and numerical study for laminar forced convection in along pipe heated by uniform heat flux and subjected to reciprocating flow of air. The test section was made of a copper tube, with length $L=60.5$ cm, inside diameter $D_i=1.35$ cm, and outside diameter $D_o=1.57$ cm. They correlated the experimental results of \overline{Nu} based on conjugate heat transfer problem. It followed that \overline{Nu} was a function of Re_ω , A_o , Pr and L/D_i . The following correlation was obtained based on a least squares fit of 53 experimental runs for laminar reciprocating flow of air in along tube with constant heat flux:

$$\overline{Nu} = 0.02 A_o^{0.85} Re_\omega^{0.58} \quad (2.31)$$

where $A_o=8.54$ to 34.9 and $Re_\omega=23$ to 464 at $L/D_i=44.8$ and $Pr=0.71$.

They found a good agreement between numerical and experimental results for space-averaged Nusselt number \overline{Nu} , time-resolved centerline fluid temperature T_c and cycle-averaged wall temperature $\overline{T_w}$.

The reciprocating flow in a channel was analyzed by Karagoz^[40] 2001. He solved numerically two-dimensional time dependent

governing equations (continuity, momentum and energy) using control volume based on pressure correlation procedure. The flow has zero mean oscillatory flow over a heated plate mounted on the bottom wall of a channel. They found that the thickness of Stokes boundary layer decreases and the core region of the flow exhibits more uniform velocity profiles as the Womersly number increases. They compared the numerical solutions with experimental values and the effects of Reynolds number and Womersly number on the velocity and temperature profiles were presented for the same Prandtl number.

Chang^[41] 2002, investigated experimentally the heat transfer of forced convection in a reciprocating square duct fitted with 45° cross ribs on two opposite walls. The parametric conditions involved several Reynolds, pulsating and buoyancy numbers, in the ranges of 600-10000, 0-10 and 0-0.14, respectively with five different reciprocating frequencies, namely, 0.67, 1, 1.33, 1.67 and 2 Hz. The rib-induced flows in static duct produced an augmentation of heat transfer in the range of 260-300 % compared to the smooth-walled situation. They observed that when the Reynolds and pulsating numbers were relatively low, a range of heat transfer impediments, could lead the spatial-time averaged heat transfer to levels about 71% of non reciprocating values. A further increase of pulsating number resulted in a subsequent heat transfer recovery, which leads to heat transfer improvement relative to the non reciprocating level.

A new micro heat spreader (MHS) concept for efficient transport of large concentrated loads was introduced by Sert and Beskok^[23] 2002. The channel was insulated from bottom and subjected to constant heat flux at the upper wall and Nusselt number defined as

$$Nu(x,t) = \frac{q''}{T_w(x,t) - T_b(x,t)} \cdot \frac{2H}{k} \quad (2.32)$$

where H: the channel height.

The results of minimum, maximum and time-averaged Nusselt number at mid-cross section of the channel were shown in table(2.2), which illustrated that the time-averaged Nusselt number increased with increasing kinetic Reynolds number and Prandtl number.

Finally, Sert and Beskok^[24] 2003, proposed a numerical simulation of laminar forced convection heat transfer for reciprocating, 2D, channel flow as a function of the penetration length (amplitude of displacement), Womersly number (α) and Prandtl number (Pr). Uniform heat flux and constant temperature boundary conditions were imposed on certain regions of the top surface, while the bottom surface was kept insulated (these sets of boundary condition enable time-periodic solution of the problem). They illustrated at high Womersly number, the temperature field is significantly affected by the Richardson's annular and heat transfer was increased with increasing the penetration length, α and Pr. They showed the results for eight cases as in table(2.3).

2.4.3 Heat Transfer in Internal Pulsating Flow

The principle aim of studying the pulsating convection heat transfer in an internal flow is whether a superposed flow pulsation enhances heat transfer compared to the original steady flow. The following review of works deals with this part of oscillatory flow.

Valencia and Hinojosa^[28] 1997, found a numerical solutions for pulsating flow and heat transfer characteristics in a channel with a backward-facing step. They showed that the wall heat transfer in the

separation zone was remained relatively constant and the time-average pulsatile heat transfer at the walls was greater than in steady flow with the same mean Reynolds number.

From review of Zhao and Cheng^[7] 1998, the variation of $(Nu_p - Nu_s)$ (where Nu_p : Nusselt number of the pulsating flow, Nu_s : Nusselt number of mean flow) due to pulsating was pronounced in the regions along a two-dimensional channel near the inlet of the heated channel (small Graetz number $Gz = \frac{x}{Re Pr}$), and the influence of pulsating becomes less significant with the increase of the axial distance (nearly zero, i.e. the Nusselt number of the pulsating flow equal the Nusselt number of mean flow). They found when the pulsation amplitude Δ is small, the temporal behavior of $(Nu_p - Nu_s)$ is fairly symmetric about the half-period point while when Δ is larger, the profiles of $(Nu_p - Nu_s)$ are non-symmetric about the half-period point.

Experimental and numerical study was performed by Ju et al.^[29] 1998. They improved a numerical modeling for simulating the oscillating fluid flow and detail dynamic performance of the orifice and double-inlet pulse refrigerator. The simulation model is useful for understanding the physical process occurring in the pulse tube refrigerator. They obtained the time-dependent axial wall temperature distribution, transient gas temperature variations, mean mass flow rate and dynamic pressure distribution of the oscillation flow in the pulse tube refrigerator.

Habib et al.^[42] 1999, experimentally investigated heat transfer characteristics of pulsated turbulent pipe flow under different conditions

of pulsation frequency, amplitude and Reynolds number. The pipe wall was kept at uniform heat flux and Reynolds number was varied from 5000 to 29000, while the used frequency of pulsation varied from 1 to 8 Hz. They showed an enhancement in the local Nusselt number at the entrance region and the rate of enhancement decreased as Re increased. This work included a total of 90 tests for different cases of Reynolds number, frequency and amplitude. They found a correlation in a good agreement with experimental data as (for fully developed region)

$$\overline{Nu} = 0.022 \text{ Re}^{0.8} \text{ Pr}^{0.5} \quad (2.33)$$

They concluded (i) The heat transfer coefficient enhancement was more pronounced in the entrance region than in the fully developed region (ii) Negligible effect of pulsation frequency on the mean Nusselt numbers at low Reynolds numbers (iii) A reduction of up to 13% in \overline{Nu} occurs at higher Reynolds number and the reduction was shown to depends on pulsation frequency.

The experimental study of heat transfer enhancement in oscillatory flow in grooved channel was carried out by Herman and Kang^[43] 2001. They used holographic interferometry combined with high speed cinematography to visualize the unsteady temperature fields in self-sustained oscillatory flow of incompressible flow air over heated rectangular blocks in a two dimensional horizontal channel. Experiments were conducted in the laminar, transitional and turbulent flow regimes for Reynolds number in the range from 520 to 6600 and interferometric measurements were obtained for thermally and dynamically periodically fully developed flow region on the ninth heated block. The results presented for the heat transfer and pressure

drop, as function of the Reynolds number, in term of the block-average Nusselt number and the local Nusselt number as well as friction factor. They concluded that at Reynolds number beyond the onset of oscillations the heat transfer in the grooved channel exceeds the performance of the reference geometry, the asymmetrically heated parallel channel.

Valencia et al.^[44] 2001, investigated numerically the unsteady laminar flow and heat transfer in a channel of height H with periodically mounted square bars of height $0.2H$ arranged side by side to the approaching flow, for different transverse separation distance of bars. They solved the unsteady Navier-Stokes equations and energy equation by finite volume code with staggered grids combined with the SIMPLIC algorithm and a fine grid resolution. They showed as consequence of the self-sustained oscillations, there was an important heat transfer enhancement on the channel wall.

Habib et al.^[45] 2002, investigated experimentally heat transfer characteristics of laminar pulsating flow under different conditions of Reynolds number and pulsation frequency. The tube wall was subjected to a uniform heat flux condition and Reynolds number was varied from 780 to 1987 while the frequency of pulsation ranged from 1 to 29.5 Hz. They showed that the relative mean Nusselt number was strongly affected by pulsation frequency while it was slightly affected by Reynolds number. They correlated the experimental data by the following general dimensionless equations:

1- For frequency range 1-14 Hz ($3 < \Omega \leq 12$) and Reynolds number ($780 \leq Re \leq 1987$) is

$$Nu_r = 5.2087 Re^{-0.1285} \Omega^{-1.9423 Re^{-0.2216}} \quad (2.34a)$$

2- For frequency range 14-29.5 Hz ($12 < \Omega \leq 17.5$) and Reynolds number ($780 \leq Re \leq 1366$) is

$$Nu_r = 0.0084\Omega^3 - 0.4111\Omega^2 + 6.6024\Omega - 33.789 \quad (2.34b)$$

3- For frequency range 14-29.5 Hz ($12 < \Omega \leq 17.5$) and Reynolds number (1643 and 1987) is

$$Nu_r = 0.0168\Omega^3 - 0.7646\Omega^2 + 11.487\Omega - 55.923 \quad (2.34c)$$

where Ω is Stokes number, defined as $\Omega = \frac{D}{2} \sqrt{\frac{\omega}{2\nu}}$, Nu_r is relative mean Nusselt number defined as Nu_p / Nu_s .

They showed in the frequency range of 1-4 Hz, an enhancement up to 30% at Reynolds number of 1366 and pulsation frequency of 1.4 Hz and in the frequency range of 1-25 Hz, an enhancement up to 9% at Reynolds number of 1366 and pulsation frequency of 1.75 Hz. The rate of enhancement of the relative mean Nusselt number decreased as pulsation frequency increased or as Reynolds number increased. They indicated a reduction in relative mean Nusselt number up to 40% for pulsation frequency range of 4.1-17 Hz and a reduction up to 20% for pulsation frequency range of 25-29.5 Hz for Reynolds number range of 780-1987.

Bouhadji and Djilali^[46] 2003, presented a simulations for the unsteady separated-reattaching flow and associated heat transfer along rectangular plate subjected to an oscillatory inlet velocity, $U = 1 + A_p \sin 2\pi f_p t$. The simulations were worked by solving Navier-Stokes and energy equation using a finite volume method at Reynolds

number of 1000 and the response of the flow over a range of frequencies up to 60th harmonic of the natural vortex shedding frequencies and velocity perturbation amplitude up to 20% of the free stream. They concluded that the highest forcing amplitudes ($A_p=0.2$) yields the shortest as well as the largest reattachment lengths depending on the forcing frequency. A significant enhancement in the local Nusselt number was accompanied the effect of forcing on the flow, and the effect was localized to a small region near the leading edge for high amplitude forcing, and in fact the overall average heat transfer rate was reduced in this case.

Computation of unsteady momentum and heat transfer from a fixed cylinder in laminar flow studied by Baranyi^[33] 2003. The fluid was assumed to be 2D, low Reynolds number, uniform flow and constant properties. He solved Navier-Stokes equation, the continuity equation, a Poisson equation for pressure and the energy equation at constant temperature of the cylinder wall using finite difference solution. The computed Strouhal number, time-mean drag and pressure coefficients as well as the average Nusselt number compared well with existing experimental results.

Yu et al.^[47] 2004, investigated analytically the pulsating laminar and fully developed convection heat transfer in a circular tube with constant heat flux. The pulsating flow was driven by a pressure gradient that varies sinusoidally with time as

$$\frac{\partial p}{\partial x} = \left(\frac{\partial p}{\partial x} \right)_s (1 + \gamma' \cos \omega t) \quad (2.35)$$

where γ' is a constant that controls the amplitude of the pressure fluctuation. They showed that both the temperature profile and Nusselt

number fluctuate periodically about the solution for steady laminar convection, with the fluctuation amplitude depending on the dimensionless pulsation frequency ω^* , the amplitude γ' and Prandtl number, Pr. It was also shown that the pulsation has no effect on time-average Nusselt number for pulsating convection heat transfer and the fluctuation in the Nusselt number was negligibly small for $\gamma'=0.5$ and $\omega^*>50$.

Moon et al.^[48] 2005, investigated experimentally the effect of pulsating flow on convective heat transfer from periodically spaced blocks in tandem on a channel wall. The spacing between repeated blocks is varied from 0.3 to 0.6 of the Block pitch. The experiments were carried out in the ranges of forcing frequency of pulsating flow higher than 10 Hz and less 100 Hz and the oscillating amplitude of axial velocity is between (0.2-0.3). The experimental results showed that thermal transport from the block is greatly affected by frequency, the amplitude of the flow pulsation, the inter-block spacing and the Reynolds number. Also, they found (i) A noticeable enhancement in heat transfer when the pulsating flow was imposed, depending on the inter-block spacing as well as the pulsation frequency. (ii) Heat transfer enhancement at the most upstream block showed a peak at around frequency=40 Hz irrespective of the variation of inter-block spacing.

Finally, Zohir et al.^[49] 2006, investigated experimentally the heat transfer characteristics to both laminar and turbulent pulsating pipe flows under different conditions of Reynolds number, pulsation frequency, pulsator location and tube diameter. The tube wall of uniform heat flux condition was considered for both cases. Reynolds

number was varied from 750 to 12320 while the frequency of pulsation ranged from 1 to 10 Hz. The results showed an increase in heat transfer rate due to pulsation by as much as 30% with flow Reynolds number of 1643 and pulsation frequency of 1 Hz, for the pulsater located upstream of the inlet of the test section. Comparing the heat transfer results of the two studied test sections tubes for Reynolds number range from 8000 to 12000 and pulsation frequency range from 1.0 to 10 Hz showed that more improvement in heat transfer rate was observed with a larger tube diameter. For Reynolds number ranging from 8000 to 12000 and pulsating frequency of 10 Hz, an improvement in the relative mean Nusselt number of about 50% was obtained for test section diameter of 50mm. While, for the same test section diameter of 15mm at same conditions of Reynolds number and frequency, a reduction in the relative mean Nusselt number of up to 10% was obtained. They concluded (i) that the behavior of the local Nusselt number under the influence of pulsation revealed that the improvement in the heat transfer coefficient is more pronounced in the entrance region. (ii) comparing the heat transfer results of the upstream and the downstream pulsation, at Reynolds number of 1366 and 1643, low values of the relative mean Nusselt number were obtained with the upstream pulsation.

2.5 Summery

This literature review has brought together a variety of analytical, numerical and experimental findings and conclusions of fluid mechanics and heat transfer characteristics of oscillatory flow. The main points that concluded are summarized below:

- 1-The amplitude and frequency of oscillating flow have a greater effect on the characteristics of flow and heat transfer.
- 2-The oscillating flow becomes unstable with increasing either the dimensionless fluid displacement A_o or kinetic Reynolds number Re_ω .
- 3- The variation of the boundary conditions with time or the periodic change in the surface of heat transfer conditions give a similar effect that produce by the oscillatory flow.
- 4- The effective thermal diffusivity is proportional to the kinetic Reynolds number Re_ω and dimensionless displacement of fluid A_o , and also it depends on the thermophysical properties of fluid and solid.
- 5- The numerical results reveal that the annular effects exist in the hydrodynamic is also acts similarly in temperature profiles for reciprocating flow in a pipe at high kinetic Reynolds number.
- 6-There are a survey correlations for \overline{Nu} of experimental works of the reciprocating flow depending on parameters A_o and Re_ω , and a few theoretical researches are made in this field.
- 7-The cycle averaged Nusselt number obtained for laminar pulsating internal flow is either higher or lower than that for steady-flow value, depending on the frequency.

Table(2.1) Critical values of β_{cri} for the reciprocating pipe flow^[7].

Authors	Year	β_{cri}
Li	1954	800
Collins	1963	230
Sergeev	1966	700
Vincent	1967	160
Pelissier	1973	150-420
Daneshvar	1973	730
Merkli & Tomann	1975	400
Hino, Sawamoto & Takasu	1975	780
Ohmi, Lguchi & Urahata	1982	800
Kurzweg, Lindgren & Lorthron	1989	700
Zhao & Cheng	1996	761

Table(2.2) The minimum, maximum and time-averaged Nusselt numbers at mid-cross section of the channel^[23].

Re	Pr	Min. Nu	Max. Nu	Ave. Nu
2π	1	3.62	5.92	5.50
2π	10	5.34	9.88	8.42
2π	25	6.96	11.82	10.20
4π	1	2.30	6.96	5.92
8π	1	0.66	8.00	6.31

Table(2.3) Non-dimensional parameters used in the simulations of Sert and Beskok^[24].

Case no.	L	L_h	L_p	α	Pr	Re'
1	20	12	5	1	1	$5/\pi$
2	20	12	5	1	10	$5/\pi$
3	20	12	5	10	1	$500/\pi$
4	20	12	5	10	10	$500/\pi$
5	20	12	10	1	1	$10/\pi$
6	20	12	10	1	10	$10/\pi$
7	20	12	10	10	1	$1000/\pi$
8	20	12	10	10	10	$1000/\pi$

Where

L : The ratio of total channel length to channel height.

L_h : The ratio of length of the heated portion of the channel to channel height.

L_p : The ratio of tidal displacement to the channel height.

Re': Reynolds number based on volumetric flow rate per unit channel width ($\frac{u.H}{\nu}$).

CHAPTER THREE

THEORETICAL ANALYSIS

Theoretical model for study of heat transfer enhancement due to internal oscillatory flow in a duct is developed to obtain a complete description for enhancement of heat transfer in the oscillatory flow. The exact analytical solution is found base on using the similarity transformations for solving the Navier-Stokes and energy equations, while the numerical solution is based on the applying the finite volume technique.

This model needs evaluation of the characteristics of hydrodynamics of the oscillatory flow, therefore hydrodynamics investigation will be made for both types of oscillatory flow (pulsating and reciprocating), in addition to the heat transfer investigation. The duct is considered to be of a uniform diameter (pipe) or two dimensional channel. The frequency and amplitude of oscillatory flow and other dimensionless numbers are studied aiming to investigate the effect of parameters that controlling this phenomenon.

The governing equations, for the present model of reciprocating and pulsating flow are based on the following physical and geometrical assumptions:

- 1- The flow is unsteady.
- 2- The oscillating flow (reciprocating or pulsating) is driven by a sinusoidally varying pressure gradient.
- 3- The internal flow is laminar.

- 4- The flow is fully developed hydrodynamically and thermally.
- 5- The fluid is flowing in the closed duct (pipe or channel).
- 6- The properties of the fluid are constant.
- 7- The viscous dissipation within the fluid is negligible ($\Phi=0$).
- 8- The fluid is incompressible.
- 9- The duct is horizontal and thin thickness.
- 10- Two dimensional flow of the fluid for the pipe or channel.

The theoretical analysis in this work will be classified into four parts depending on the type of the oscillatory flow (reciprocating or pulsating) and on the geometry of the duct (pipe or channel).

3.1 Analytical Model of Reciprocating Flow and Heat Transfer in the Channel

3.1.1 Hydrodynamics Analysis

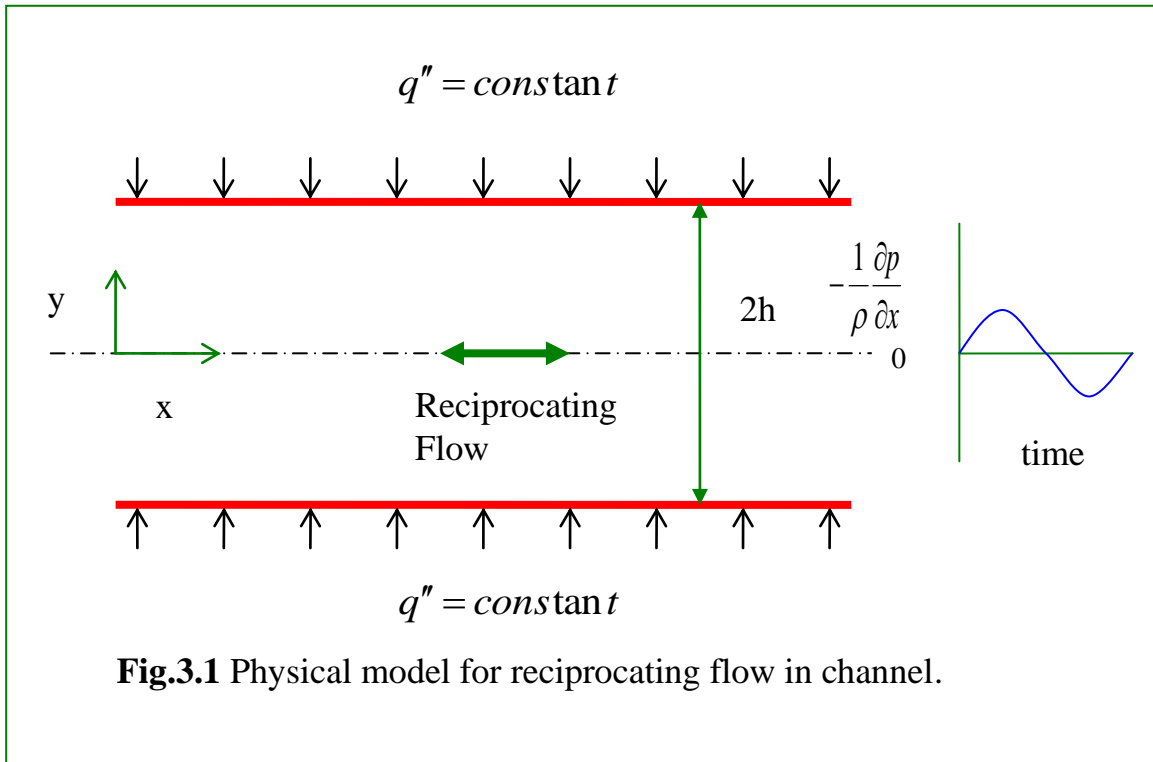
The reciprocating flow in the 2D channel Fig.3.1, is analyzed hydrodynamically. The Navier-Stokes equations for fully developed flow, constant properties, reciprocating pressure driven and laminar flow through a horizontal channel can be written as

$$-\frac{1}{\rho} \frac{\partial p}{\partial y} = 0 \quad (3.1)$$

$$\frac{\partial u}{\partial t} = -\frac{1}{\rho} \frac{\partial p}{\partial x} + \nu \frac{\partial^2 u}{\partial y^2} \quad (3.2)$$

where

$$-\frac{1}{\rho} \frac{\partial p}{\partial x} = P_o \cos \omega t \approx \text{Re}(P_o e^{i\omega t}) \quad (3.3)$$



with boundary and initial conditions

$$1. \quad u = 0 \quad \text{at} \quad y = \pm h \quad \text{for} \quad t > 0 \quad \text{no slip at th wall} \quad (3.4a)$$

$$2. \quad \frac{\partial u}{\partial y} = 0 \quad \text{at} \quad y = 0 \quad \text{for} \quad t > 0 \quad \text{axisymetric} \quad (3.4b)$$

$$3. \quad u = f(y) \quad \text{at} \quad t = 0 \quad \text{initial condition} \quad (3.4c)$$

or in dimensionless form Eq.3.2 can be written as

$$\frac{\partial u^+}{\partial t^+} = e^{it^+} + \frac{1}{\lambda^2} \frac{\partial^2 u^+}{\partial y^{+2}} \quad (3.5)$$

where

$$u^+ = \frac{u}{u_{\max}}, \quad u_{\max} = \frac{X_{\max} \cdot \omega}{2} = \frac{P_o}{\omega}, \quad \lambda = h\sqrt{\omega/\nu} = \frac{1}{4}\sqrt{\text{Re}_\omega}, \quad \text{Re}_\omega = \frac{D_h^2 \cdot \omega}{\nu},$$

$$y^+ = \frac{y}{h}, \quad t^+ = \omega t \quad \text{and} \quad D_h = 4h \quad (\text{for the channel with width} \gg \text{height})$$

The boundary and initial conditions in dimensionless form becomes

$$1. u^+ = 0 \quad \text{at } y^+ = \bar{y}1 \quad t^+ > 0 \quad (3.6a)$$

$$2. \frac{\partial u^+}{\partial y^+} = 0 \quad \text{at } y^+ = 0 \quad t^+ > 0 \quad (3.6b)$$

$$3. u^+ = f(y^+) \quad \text{at } t^+ = 0 \quad \text{initial condition} \quad (3.6c)$$

Applying similarity transformation of the form^[22] $u^+ = f(y^+)e^{it^+}$ in Eq.3.5 gives

$$f'' - i\lambda^2 f = -\lambda^2 \quad (3.7)$$

Solving the ordinary differential equation Eq.3.7 yields

$$f = i \left[\frac{\cosh \sqrt{i}\lambda y^+}{\cosh \sqrt{i}\lambda} - 1 \right] \quad (3.8a)$$

and

$$u^+ = i \left[\frac{\cosh \sqrt{i}\lambda y^+}{\cosh \sqrt{i}\lambda} - 1 \right] e^{it^+} \quad (3.8b)$$

Applying the identify $\sqrt{i} = \frac{1+i}{\sqrt{2}}$, the real part of u^+ can be written as

$$u^+ = \frac{(C^2 + D^2 - AC - BD)\sin t^+ - (BC - AD)\cos t^+}{C^2 + D^2} \quad (3.9)$$

where

$$A = \cosh(\lambda y^+ / \sqrt{2}) \cos(\lambda y^+ / \sqrt{2}) \quad (3.10a)$$

$$B = \sinh(\lambda y^+ / \sqrt{2}) \sin(\lambda y^+ / \sqrt{2}) \quad (3.10b)$$

$$C = \cosh(\lambda / \sqrt{2}) \cos(\lambda / \sqrt{2}) \quad (3.10c)$$

$$D = \sinh(\lambda / \sqrt{2}) \sin(\lambda / \sqrt{2}) \quad (3.10d)$$

3.1.2 Heat Transfer Analysis

Taking into account the previous assumptions the energy equation without viscous dissipation ($\Phi=0$) could be reduced to

$$\frac{\partial T}{\partial t} + u \frac{\partial T}{\partial x} = \alpha \frac{\partial^2 T}{\partial y^2} \quad (3.11)$$

with the boundary and initial conditions as

$$1. \frac{\partial T}{\partial y} = 0 \quad \text{at } y = 0 \quad \text{for } t > 0 \quad \text{axisymmetric} \quad (3.12a)$$

$$2. q'' = k \frac{\partial T}{\partial y} \quad \text{at } y = \pm h \quad \text{for } t > 0, \quad \text{const. heat flux at the wall} \quad (3.12b)$$

$$3. T = f(y) \quad \text{at } t = 0 \quad \text{initial condition} \quad (3.12c)$$

Eq.3.11 in the dimensionless form becomes

$$\text{Pr} \lambda^2 \frac{\partial T^+}{\partial t^+} + \frac{1}{2} A_o \text{Pr} \lambda^2 u^+ \frac{\partial T^+}{\partial x^+} = \frac{\partial^2 T^+}{\partial y^{+2}} \quad (3.13)$$

where

$$\text{Pr} = \frac{\mu c_p}{k}, \quad T^+ = \frac{kT / D_h}{q''}, \quad x^+ = \frac{x}{D_h} \quad \text{and} \quad A_o = \frac{X_{\max}}{D_h}$$

and $D_h = 4h$ (for the channel with width \gg height)

with boundary conditions becomes

$$1. \frac{\partial T^+}{\partial y^+} = 0 \quad \text{at } y^+ = 0 \quad \text{for } t^+ > 0 \quad \text{axisymmetric} \quad (3.14a)$$

$$2. \frac{\partial T^+}{\partial y^+} = 1 \quad \text{at } y^+ = \pm 1 \quad \text{for } t^+ > 0 \quad \text{const. heat flux at the wall} \quad (3.14b)$$

$$3. T^+ = \gamma(x^+ + g(y^+)) \quad \text{at } t^+ = 0 \quad \text{initial condition} \quad (3.14c)$$

Assuming similarity transformation of the form^[6]

$$T = \frac{d\bar{T}_b}{dx} (x + D_h g(y) e^{i\omega t}) \quad (3.15)$$

or in dimensionless form yields

$$T^+ = \frac{d\bar{T}_b^+}{dx^+} (x^+ + g(y^+) e^{it^+}) = \gamma (x^+ + g(y^+) e^{it^+}) \quad (3.16)$$

where: $\frac{d\bar{T}_b^+}{dx^+}$ is a time-average axial dimensionless temperature gradient.

and

$$\bar{T}_b^+ = \frac{1}{\pi} \int_0^\pi T_b^+ dt^+ \quad (3.17a)$$

where

$$T_b^+ = \frac{\int_0^1 T^+ u^+ dy^+}{\int_0^1 u^+ dy^+} \quad (3.17b)$$

substituting of the similarity transformation of T^+ Eq.3.16, and the solution of u^+ Eq.3.8b in Eq.3.13, the energy equation described by Eq.3.13 can be reduced to ordinary differential equation as

$$g'' - i \text{Pr} \lambda^2 g = \frac{iA_o}{2} \text{Pr} \lambda^2 \left[\frac{\cosh \sqrt{i\lambda} y^+}{\cosh \sqrt{i\lambda}} - 1 \right] \quad (3.18)$$

The solution of Eq.3.18 can be written as

$$g = C_1 \cosh \sqrt{i \text{Pr} \lambda} y^+ + C_2 \sinh \sqrt{i \text{Pr} \lambda} y^+ + \frac{A_o \text{Pr}}{2(1 - \text{Pr})} \frac{\cosh \sqrt{i\lambda} y^+}{\cosh \sqrt{i\lambda}} + \frac{A_o}{2} \quad (3.19)$$

where C_1 and C_2 are constants.

Using the boundary conditions described by equations Eqs.3.14a and 3.14b yield the temperature distribution

$$T^+ = \gamma \left[x^+ + \frac{E_1 + F_1}{U_2 \sqrt{2 \text{Pr} \lambda \gamma}} - \frac{A_o \text{Pr}}{2 \sqrt{\text{Pr} (1 - \text{Pr})}} * \left(\frac{(E_1 Y_1 - F_1 Z_1) \text{cost}^+}{U_2 C_3} - \frac{(E_1 Z_1 + F_1 Y_1) \text{sin} t^+}{U_2 C_3} \right) + \frac{A_o \text{Pr}}{2} \left(\frac{Q_1 \text{cost}^+ - P_1 \text{sin} t^+}{C_3 (1 - \text{Pr})} + \frac{\text{cost}^+}{\text{Pr}} \right) \right] \quad (3.20)$$

where $E_1, F_1, U_2, Y_1, Z_1, C_3, Q_1$ and P_1 are functions obtained during derivation and given in the Appendix A.

The gradient of dimensionless time-average bulk temperature γ used in the previous derivation can be obtained from the energy balance for control volume of the fluid in the channel as

$$2q'' \cdot 1 \cdot dx = \rho c_p (2h \cdot 1) \bar{u}_m d\bar{T}_b \quad (3.21)$$

or in dimensionless form

$$\frac{d\bar{T}_b^+}{dx^+} = \frac{4\nu}{\text{Pr} h \bar{u}_m} \quad (3.22)$$

where \bar{u}_m is obtained from the following relation

$$\bar{u}_m = \frac{1}{\pi} \int_0^\pi u_{\max} \sin \phi d\phi = \frac{2u_{\max}}{\pi} \quad (3.23)$$

thus Eq.3.22 can be written as

$$\frac{d\bar{T}_b^+}{dx^+} = \gamma = \frac{\pi}{4\text{Pr} A_o \lambda^2} \quad (3.24)$$

The instantaneous-local Nusselt number is defined as

$$Nu_x = \frac{h_x \cdot D_h}{k} = \frac{1}{T_w^+ - T_b^+} \quad (3.25)$$

while the time averaged -local Nusselt number is defined as

$$\overline{Nu}_x = \frac{\bar{h}_x \cdot D_h}{k} = \frac{1}{\bar{T}_w^+ - \bar{T}_b^+} \quad (3.26)$$

where

$$\bar{T}_w^+ = \frac{1}{\pi} \int_0^\pi T_w^+ dt^+ \quad (3.27)$$

3.2 Analytical Model of Reciprocating Flow and Heat Transfer in the Pipe

3.2.1 Hydrodynamics Analysis

The Navier-Stokes equations for a fully developed, 2D, constant properties, reciprocating pressure driven and laminar flow in a horizontal pipe Fig.3.2 , are written as

$$-\frac{1}{\rho} \frac{\partial p}{\partial r} = 0 \quad (3.28)$$

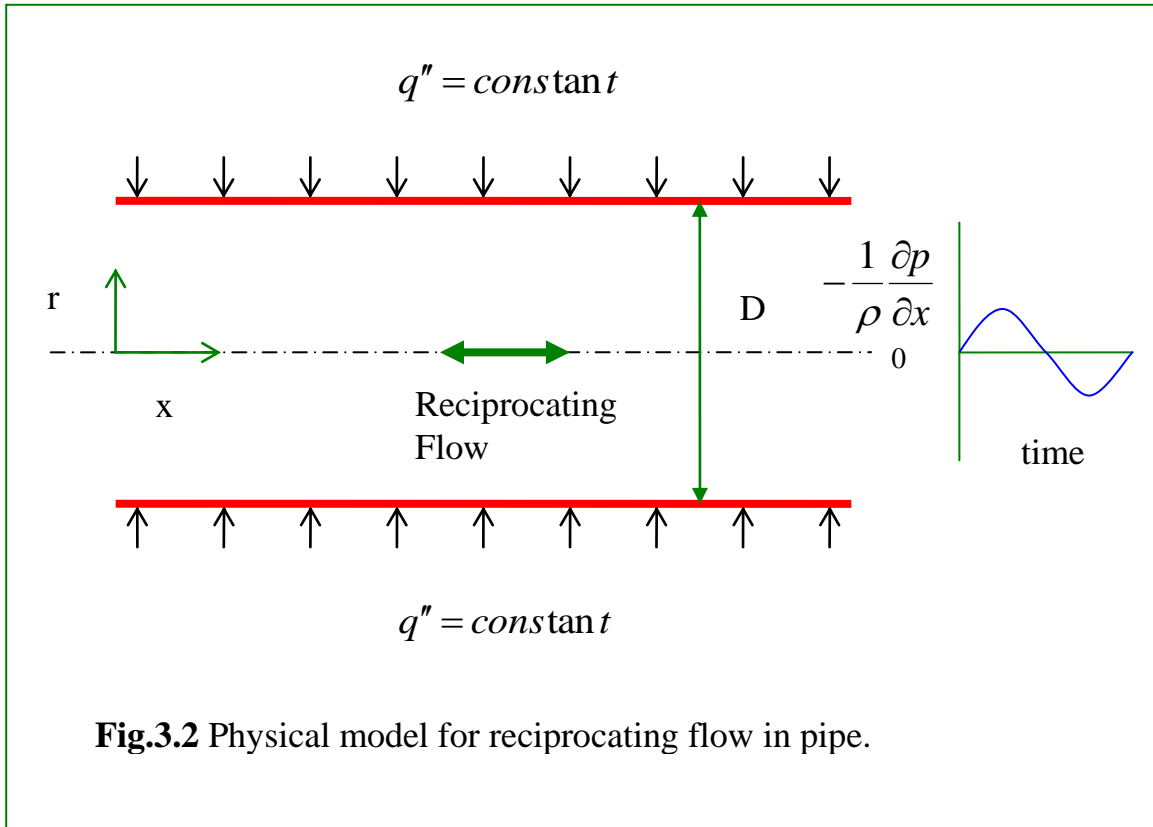
$$\frac{\partial u}{\partial t} = -\frac{1}{\rho} \frac{\partial p}{\partial x} + \nu \left(\frac{\partial^2 u}{\partial r^2} + \frac{1}{r} \frac{\partial u}{\partial r} \right) \quad (3.29)$$

with boundary and initial conditions

$$1. \frac{\partial u}{\partial r} = 0 \text{ or } u \text{ is finite at } r=0 \text{ for } t > 0 \text{ axisymmetric} \quad (3.30a)$$

$$2. u = 0 \text{ at } r = D/2 \text{ for } t > 0 \text{ no slip at th wall} \quad (3.30b)$$

$$3. u = f(r) \text{ at } t = 0 \text{ initial condition} \quad (3.30c)$$



where

$$-\frac{1}{\rho} \frac{\partial p}{\partial x} = P_o \cos \omega t \approx \text{Re}(P_o e^{i\omega t}) \quad (3.31)$$

or in dimensionless form Eq.3.29 yields

$$4\lambda^2 \frac{\partial u^+}{\partial t^+} = 4\lambda^2 e^{it^+} + \frac{\partial^2 u^+}{\partial r^{+2}} + \frac{1}{r^+} \frac{\partial u^+}{\partial r^+} \quad (3.32)$$

where

$$u^+ = \frac{u}{u_{\max}}, \quad u_{\max} = \frac{X_{\max} \cdot \omega}{2} = \frac{P_o}{\omega}, \quad \lambda = \frac{D}{2} \sqrt{\omega/\nu} = \frac{1}{2} \sqrt{\text{Re}_\omega}, \quad \text{Re}_\omega = \frac{D^2 \cdot \omega}{\nu},$$

$$r^+ = \frac{r}{D} \quad \text{and} \quad t^+ = \omega t$$

Eq.3.32 is subjected to the boundary conditions

$$1. \quad \frac{\partial u^+}{\partial r^+} = 0 \quad \text{or} \quad u^+ \text{ is finite} \quad \text{at} \quad r^+ = 0 \quad \text{for} \quad t^+ > 0 \quad (3.33a)$$

$$2. u^+ = 0 \quad \text{at} \quad r^+ = 1/2 \quad \text{for} \quad t^+ > 0 \quad \text{no slip at th wall} \quad (3.33b)$$

$$3. u^+ = f(r^+) \quad \text{at} \quad t^+ = 0 \quad \text{initial condition} \quad (3.33c)$$

Assuming similarity transformation solution for Eq.3.32 of the form

$$u^+ = f(r^+)e^{it^+}$$

gives

$$f'' + \frac{1}{r^+} f' + i^3 4\lambda^2 f = -4\lambda^2 \quad (3.34)$$

Using the general form of Bessel function^[50], Eq.3.34 can be solved and gives

$$f = i \left[\frac{J_0(2i^{3/2}\lambda r^+)}{J_0(i^{3/2}\lambda)} - 1 \right] \quad (3.35)$$

and

$$u^+ = i \left[\frac{J_0(2i^{3/2}\lambda r^+)}{J_0(i^{3/2}\lambda)} - 1 \right] e^{it^+} \quad (3.36)$$

After simplifying Eq.3.36 (see Appendix B), the real part of u^+ can be written as

$$u^+ = \sin t^+ - \left\{ \frac{(Ber_0(2\lambda r^+)Ber_0(\lambda) + Bei_0(2\lambda r^+)Bei_0(\lambda))\sin t^+}{Ber_0^2(\lambda) + Bei_0^2(\lambda)} + \frac{(Bei_0(2\lambda r^+)Ber_0(\lambda) - Ber_0(2\lambda r^+)Bei_0(\lambda))\cos t^+}{Ber_0^2(\lambda) + Bei_0^2(\lambda)} \right\} \quad (3.37)$$

For large value of λ , the asymptotic of Bessel function could be used^[50] as

$$J_n(z) \approx \sqrt{\frac{2}{\pi}} e^{iz} (iz)^{-1/2} (i)^{-n} \quad (3.38)$$

where: n is order of Bessel function and z : is complex variable.

Applying the asymptotic of Bessel function and identify $i^{3/2} = \frac{1-i}{\sqrt{2}}$,

Eq.3.36 becomes

$$u^+ = i \left[\frac{1}{\sqrt{2r^+}} e^{\lambda/\sqrt{2}(2r^+-1)} e^{i\lambda/\sqrt{2}(2r^+-1)} - 1 \right] e^{it^+} \quad (3.39)$$

The real part of u^+ (Eq.3.39) is

$$u^+ = \sin t^+ - \left[\frac{1}{\sqrt{2r^+}} e^{\lambda/\sqrt{2}(2r^+-1)} \sin(t^+ + \lambda/\sqrt{2}(2r^+-1)) \right] \quad (3.40)$$

3.2.2 Heat Transfer Analysis

The energy equation for thermally fully developed reciprocating flow in the pipe, without viscous dissipation ($\Phi=0$) is

$$\frac{\partial T}{\partial t} + u \frac{\partial T}{\partial x} = \alpha \left(\frac{\partial^2 T}{\partial r^2} + \frac{1}{r} \frac{\partial T}{\partial r} \right) \quad (3.41)$$

with the boundary and initial conditions

$$1. T = T_i \quad \text{at } x = 0 \quad \text{inlet condition} \quad (3.42a)$$

$$2. q'' = k \frac{\partial T}{\partial r} \quad \text{at } r = D/2 \quad \text{for } t > 0 \quad \text{const. heat flux at the wall} \quad (3.42b)$$

$$3. \frac{\partial T}{\partial r} = 0 \quad \text{at } r = 0 \quad \text{for } t > 0 \quad \text{axisymmetric} \quad (3.42c)$$

$$4. T = f(r) \quad \text{at } t = 0 \quad \text{initial condition} \quad (3.42c)$$

Using the dimensionless form

$$\text{Pr} = \frac{\nu}{\alpha}, \quad T^+ = \frac{kT/D}{q''}, \quad x^+ = \frac{x}{D} \quad \text{and} \quad A_o = \frac{X_{\max}}{D}$$

Eq.3.41 can be transformed to

$$4 \text{ Pr } \lambda^2 \frac{\partial T^+}{\partial t^+} + 2 A_o \text{ Pr } \lambda^2 u^+ \frac{\partial T^+}{\partial x^+} = \frac{\partial^2 T^+}{\partial r^{+2}} + \frac{1}{r^+} \frac{\partial T^+}{\partial r^+} \quad (3.43)$$

The boundary and initial condition in the dimensionless form becomes

$$1. T^+ = T_i^+ \quad \text{at } x^+ = 0 \quad \text{inlet condition} \quad (3.44a)$$

$$2. \frac{\partial T^+}{\partial r^+} = 1 \quad \text{at } r^+ = 1/2 \quad \text{for } t^+ > 0 \quad \text{const. heat flux at the wall} \quad (3.44b)$$

$$3. \frac{\partial T^+}{\partial r^+} = 0 \quad \text{at } r^+ = 0 \quad \text{for } t^+ > 0 \quad \text{axisymmetric} \quad (3.44c)$$

$$4. T^+ = f(r^+) \quad \text{at } t^+ = 0 \quad \text{initial condition} \quad (3.44c)$$

Assuming a similarity transformation solution for Eq.3.43 of the form

$$T = \frac{d\bar{T}_b}{dx} (x + D g(r) e^{i\omega t}) \quad (3.45)$$

or in dimensionless form as

$$T^+ = \gamma (x^+ + g(r^+) e^{it^+}) \quad (3.46)$$

where $\gamma = \frac{d\bar{T}_b^+}{dx^+}$

and

$$\bar{T}_b^+ = \frac{1}{\pi} \int_0^\pi \left[\frac{\int_0^{1/2} T^+ u^+ r^+ dr^+}{\int_0^{1/2} u^+ r^+ dr^+} \right] dt^+ \quad (3.47)$$

Substituting Eq.3.46 and u^+ (Eq.3.36) into Eq.3.43, an ordinary differential equation can be obtained

$$g'' + \frac{1}{r^+} g' + i^3 4 \text{Pr} \lambda^2 g = i 2 \text{Pr} A_o \lambda^2 \left[\frac{J_0(2i^{3/2} \lambda r^+)}{J_0(i^{3/2} \lambda)} - 1 \right] \quad (3.48)$$

Using the rule^[50]

$$g'' + \frac{1}{r} g' = -\beta^2 g \quad (3.49)$$

where

$$g = J_0(\beta r^+)$$

and applying the boundary conditions (Eqs.3.44b and 3.44c). The solution of homogeneous and nonhomogeneous parts of Eq.3.48 will be

$$T^+ = \gamma \left\{ x^+ + e^{it^+} \left[\frac{-J_0(2i^{3/2} \lambda \sqrt{\text{Pr}} r^+)}{\sqrt{\text{Pr}} J_1(i^{3/2} \lambda \sqrt{\text{Pr}})} \left(\frac{\sqrt{2}(1+i)}{4\gamma \lambda e^{it^+}} + \frac{A_o}{2} * \frac{\text{Pr}}{(1-\text{Pr})} \frac{J_1(i^{3/2} \lambda)}{J_0(i^{3/2} \lambda)} \right) + \frac{A_o}{2} \left(\frac{\text{Pr}}{(1-\text{Pr})} \frac{J_0(2i^{3/2} \lambda r^+)}{J_0(i^{3/2} \lambda)} + 1 \right) \right] \right\} \quad (3.50)$$

The functions $J_0(2i^{3/2} \lambda \sqrt{\text{Pr}} r^+)$, $J_1(i^{3/2} \lambda \sqrt{\text{Pr}})$, $J_1(i^{3/2} \lambda)$, $J_0(i^{3/2} \lambda)$ and $J_0(2i^{3/2} \lambda r^+)$ are simplified to real and imaginary parts (see Appendix C). The final real relation for temperature distribution of Eq.3.50 is

$$T^+ = \gamma x^+ - \left\{ \frac{\sqrt{2}}{4\lambda \sqrt{\text{Pr}}} (RE_1 - IM_1) - \frac{A_o \text{Pr} \gamma}{2\sqrt{\text{Pr}}(1-\text{Pr})} * \left((RE_1 RE_2 - IM_1 IM_2) * \cos t^+ - (RE_1 IM_2 + IM_1 RE_2) * \sin t^+ \right) + \frac{A_o \gamma \text{Pr}}{2(1-\text{Pr})} (RE_3 \cos t^+ - IM_3 \sin t^+) + \frac{A_o \gamma}{2} \cos t^+ \right\} \quad (3.51)$$

where: $RE_1, IM_1, RE_2, IM_2, RE_3$ and IM_3 are functions defined in Appendix C.

For large value of λ or Pr , the asymptotic Bessel function should be used for complex variable (Eq.3.38), simplification of Eq.3.50 (see Appendix D) gives

$$\begin{aligned}
T^+ = \gamma x^+ + & \left\{ \frac{\sqrt{2} e^{\lambda \sqrt{Pr/2}(2r^+ - 1)}}{4\lambda \sqrt{Pr} \sqrt{2r^+}} \left(\cos(\sqrt{Pr/2} \lambda (2r^+ - 1)) \right. \right. \\
& + \left. \left. \sin(\sqrt{Pr/2} \lambda (2r^+ - 1)) \right) \right. \\
& - \frac{\gamma A_o Pr e^{\lambda \sqrt{Pr/2}(2r^+ - 1)}}{2(1 - Pr) \sqrt{Pr} \sqrt{2r^+}} \left(\cos(t^+ + \sqrt{Pr/2} \lambda (2r^+ - 1)) \right) \\
& + \frac{\gamma A_o Pr e^{\lambda / \sqrt{2}(2r^+ - 1)}}{2(1 - Pr) \sqrt{2r^+}} \left(\cos(t^+ + \lambda / \sqrt{2} (2r^+ - 1)) \right) \\
& \left. + \frac{A_o \gamma}{2} \cos t^+ \right\} \quad (3.52)
\end{aligned}$$

where the value of time-averaged dimensionless bulk temperature gradient γ is obtained from heat balance for a control volume from the pipe, in a similar manner as that done for rectangular channel. The dimensionless value of temperature gradient has the form

$$\frac{d\bar{T}_b^+}{dx^+} = \gamma = \frac{\pi}{Pr A_o \lambda^2} \quad (3.53)$$

The instantaneous-local Nusselt number is defined as

$$Nu_x = \frac{h_x \cdot D}{k} = \frac{1}{T_w^+ - T_b^+} \quad (3.54)$$

and the time averaged -local Nusselt number is defined as

$$\overline{Nu}_x = \frac{\bar{h}_x \cdot D}{k} = \frac{1}{\bar{T}_w^+ - \bar{T}_b^+} \quad (3.55)$$

where

$$\bar{T}_w^+ = \frac{1}{\pi} \int_0^\pi T_w^+ dt^+ \quad (3.56)$$

3.3 Analytical Model of Pulsating Flow and Heat Transfer in the Channel

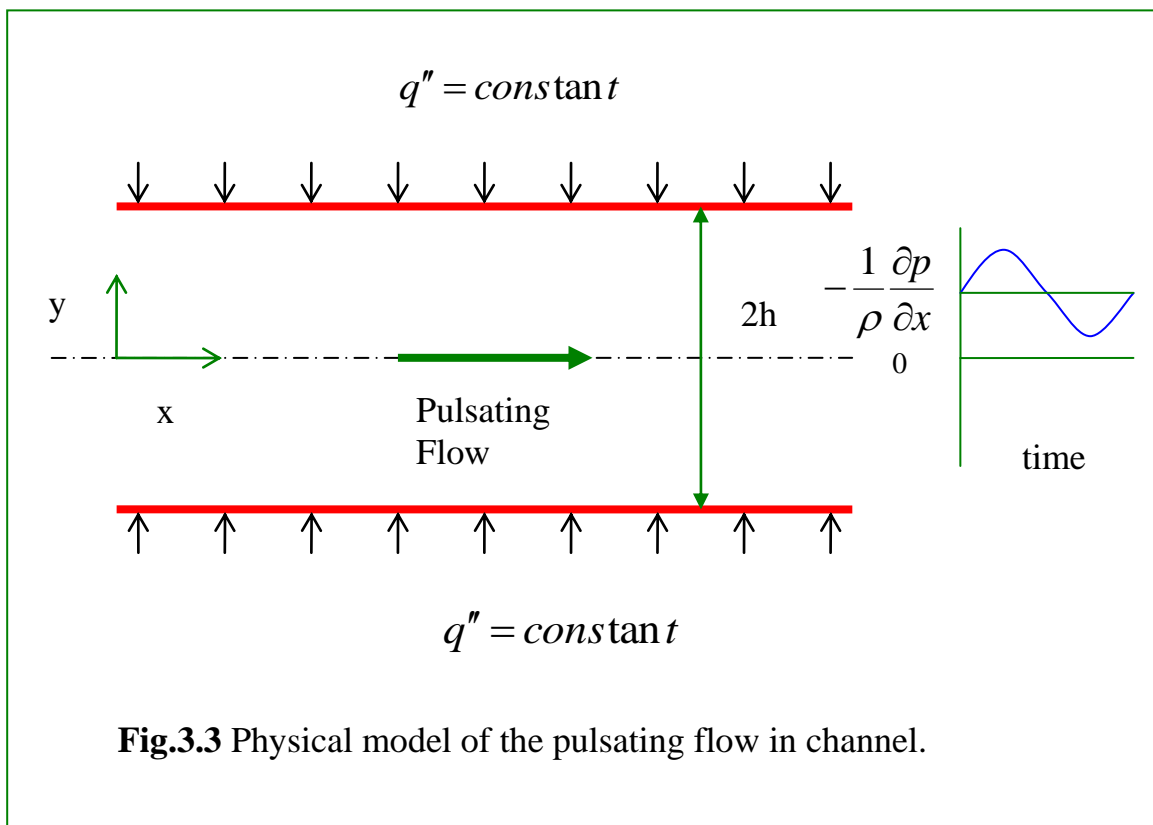
3.3.1 Hydrodynamics Analysis

The momentum equations for fully developed flow, laminar, 2D, constant properties, pulsating pressure driven flow in a horizontal channel Fig.3.3, could be described by Eqs.3.1&3.2, with boundary conditions as

$$1. u = 0 \quad \text{at } y = \pm h \quad \text{no slip at the wall} \quad (3.57a)$$

$$2. \frac{\partial u}{\partial y} = 0 \quad \text{at } y = 0 \quad \text{axisymmetric} \quad (3.57b)$$

$$3. u = f(y) \quad \text{at } t = 0 \quad \text{initial condition} \quad (3.57c)$$



The pressure gradient of pulsating flow is written as

$$-\frac{1}{\rho} \frac{\partial p}{\partial x} = \left(-\frac{1}{\rho} \frac{\partial p}{\partial x} \right)_s (1 + \gamma' \cos \omega t) = P_o (1 + \gamma' \cos \omega t) \quad (3.58)$$

where

$$\left(-\frac{1}{\rho} \frac{\partial p}{\partial x} \right)_s = P_o : \text{is pressure gradient of steady flow (mean flow).}$$

and γ' : the ratio of amplitude of pressure gradient to that steady flow at value ($0 < \gamma' < 1$), and has values less than 0.5 to avoid reversion flow and relaminarization.

Using dimensionless form

$$u^+ = \frac{u}{u_{\max}}, \quad u_{\max} = \frac{P_o h^2}{2\nu}, \quad \lambda = h\sqrt{\omega/\nu}, \quad y^+ = \frac{y}{h} \quad \text{and} \quad t^+ = \omega t$$

Eq.3.2 can be written as

$$\lambda^2 \frac{\partial u^+}{\partial t^+} = 2(1 + \gamma' \cos t^+) + \frac{\partial^2 u^+}{\partial y^{+2}} \quad (3.59)$$

For pulsating flow the velocity distribution form is assumed as

$$u^+(y^+, t^+) = u_s^+(y^+) + u_t^+(y^+, t^+) \quad (3.60)$$

where

u_s^+ : steady dimensionless axial velocity.

and

u_t^+ : fluctuation dimensionless axial velocity.

Substituting Eq.3.60 in Eq.3.59 gives

$$\lambda^2 \left(\frac{\partial u_s^+}{\partial t^+} + \frac{\partial u_t^+}{\partial t^+} \right) = 2(1 + \gamma' \cos t^+) + \left(\frac{\partial^2 u_s^+}{\partial y^{+2}} + \frac{\partial^2 u_t^+}{\partial y^{+2}} \right) \quad (3.61)$$

Using superposition method the following equation can be obtained

$$\frac{\partial^2 u_s^+}{\partial y^{+2}} + 2 = 0 \quad (3.62a)$$

$$\lambda^2 \frac{\partial u_t^+}{\partial t^+} = 2\gamma' \cos t^+ + \frac{\partial^2 u_s^+}{\partial y^{+2}} \quad (3.62b)$$

and the boundary conditions becomes

$$1. u^+ = 0 \text{ at } y^+ = \pm 1 \Rightarrow u_s^+ = 0 \text{ and } u_t^+ = 0 \text{ no slip at the wall} \quad (3.63a)$$

$$2. \frac{\partial u^+}{\partial y^+} = 0 \text{ at } y^+ = 0 \Rightarrow \frac{\partial u_s^+}{\partial y^+} = 0 \text{ and } \frac{\partial u_t^+}{\partial y^+} = 0 \text{ axisymmetric} \quad (3.63b)$$

$$3. u^+ = f(y^+) \text{ at } t^+ = 0 \quad \text{initial condition} \quad (3.63c)$$

For steady part the integration of Eq.3.62a with boundary conditions Eqs.3.63a & 3.63b gives

$$u_s^+ = (1 - y^+) \quad (3.64)$$

For unsteady part, applying similarity transformation form

$$u_t^+ = f(y^+) e^{it^+} \quad (3.65)$$

Eq.3.62b can be transformed to

$$f'' - i\lambda^2 f = -2\gamma' \quad (3.66)$$

Solving Eq.3.66 for homogeneous and nonhomogeneous parts with boundary conditions Eq.3.63a & 3.63b yields

$$f = \frac{2i\gamma'}{\lambda^2} \left[\frac{\cosh \sqrt{i}\lambda y^+}{\cosh \sqrt{i}\lambda} - 1 \right] \quad (3.67a)$$

and

$$u_t^+ = \frac{2i\gamma'}{\lambda^2} \left[\frac{\cosh \sqrt{i}\lambda y^+}{\cosh \sqrt{i}\lambda} - 1 \right] e^{it^+} \quad (3.67b)$$

Using the identify $\sqrt{i} = \frac{1+i}{\sqrt{2}}$, trigonometric relations and complex relations (such as $\cosh ix = \cos x$ and $\sinh ix = i \sin x$), the real part of u_t^+ can be obtained as

$$u_t^+ = \frac{2\gamma'}{\lambda^2} \left[\frac{(C^2 + D^2 - AC - BD)\sin t^+ - (BC - AD)\cos t^+}{C^2 + D^2} \right] \quad (3.68)$$

where A, B, C, and D defined in Eq.3.10.

Then the total velocity ($u_s^+ + u_t^+$) could be written as

$$u^+ = (1 - y^+) + \frac{2\gamma'}{\lambda^2} \left[\frac{\left(\frac{C^2 + D^2 - AC - BD}{AC - BD} \right) \sin t^+ - (BC - AD)\cos t^+}{C^2 + D^2} \right] \quad (3.69)$$

3.3.2 Heat Transfer Analysis

The energy equation defined by Eq.3.11 also can be used for this case and could be transformed to dimensionless form

$$\text{Pr} \lambda^2 \frac{\partial T^+}{\partial t^+} + \frac{3}{32} \text{Re}_m \text{Pr} u^+ \frac{\partial T^+}{\partial x^+} = \frac{\partial^2 T^+}{\partial y^{+2}} \quad (3.70)$$

with boundary conditions

$$1. \frac{\partial T^+}{\partial y^+} = 0 \quad \text{at } y^+ = 0 \quad (3.71a)$$

$$2. \frac{\partial T^+}{\partial y^+} = \frac{1}{4} \quad \text{at } y^+ = \pm 1 \quad (3.71b)$$

$$3. T^+ = 0 \quad \text{at } x^+ = 0 \quad (3.71c)$$

by using the dimensionless form

$$\text{Pr} = \frac{\nu}{\alpha}, T^+ = \frac{k(T - T_i)/D_h}{q''}, x^+ = \frac{x}{D_h}, \lambda = h\sqrt{\omega/\nu}, \text{Re}_m = \frac{u_m \cdot D_h}{\nu}$$

and $y^+ = y/h$

and

$$u_m = \frac{2}{3} u_{\max} \quad (\text{see Appendix E})$$

For pulsating flow the temperature distribution form is assumed as

$$T^+(x^+, y^+, t^+) = T_s^+(x^+, y^+) + T_t^+(y^+, t^+) \quad (3.72)$$

Substituting u^+ defined in Eq.3.60 and T^+ defined in Eq.3.72 into Eq.3.70 and using superposition gives

$$\frac{3}{32} \text{Re}_m \text{Pr} u_s^+ \frac{\partial T_s^+}{\partial x^+} = \frac{\partial^2 T_s^+}{\partial y^{+2}} \quad (3.73)$$

and

$$\text{Pr} \lambda^2 \frac{\partial T_t^+}{\partial t^+} + \frac{3}{32} \text{Re}_m \text{Pr} u_t^+ \frac{\partial T_s^+}{\partial x^+} = \frac{\partial^2 T_t^+}{\partial y^{+2}} \quad (3.74)$$

with boundary conditions

$$1. \frac{\partial T^+}{\partial y^+} = 0 \quad \text{at } y^+ = 0 \Rightarrow \frac{\partial T_s^+}{\partial y^+} = 0 \quad \text{and} \quad \frac{\partial T_t^+}{\partial y^+} = 0 \quad (3.75a)$$

$$2. \frac{\partial T^+}{\partial y^+} = \frac{1}{4} \quad \text{at } y^+ = \pm 1 \Rightarrow \frac{\partial T_s^+}{\partial y^+} = \frac{1}{4} \quad \text{and} \quad \frac{\partial T_t^+}{\partial y^+} = 0 \quad (3.75b)$$

$$3. T^+ = 0 \quad \text{at } x^+ = 0 \quad (3.75c)$$

For steady part the solution of Eq.3.73 is assumed as^[20]

$$T_s^+ = \underbrace{X_1(x^+) Y_1(y^+)} + \underbrace{X_2(x^+)} + \underbrace{Y_2(y^+)} \quad (3.76)$$

↓

↓

↓

decaying initial transient *axial temperaturæ rise due to accumulæd wall flux* *normal temperaturæ variation to let wall flux into fluid*

The initial transients value $(X_1(x^+) Y_1(y^+))$ will be eventually decay to insignificance value, leaving only $T_s^+ = X_2 + Y_2$. Substituting Eq.3.76 and Eq.3.64 into Eq.3.73 and taking into account the above consideration, Eq.3.73 becomes

$$\frac{3}{32} \text{Re}_m \text{Pr}(1 - y^{+2}) X_2' = Y_2' \quad (3.77)$$

The above equation can be solved using the separation of variable method as

$$X_2' = \frac{Y_2''}{\frac{3}{32} \text{Re}_m \text{Pr}(1 - y^{+2})} = k \quad (3.78)$$

then

$$X_2' = k \quad (3.79a)$$

$$Y_2'' = \frac{3}{32} k \text{Re}_m \text{Pr}(1 - y^{+2}) \quad (3.79b)$$

Integrating Eqs.3.79a & 3.79b gives

$$X_2 = k x^+ + C_1 \quad (3.80a)$$

$$Y_2 = \frac{3}{32} k \text{Re}_m \text{Pr} \left(\frac{y^{+2}}{2} - \frac{y^{+4}}{12} \right) + C_2 y^+ + C_3 \quad (3.80b)$$

From boundary condition Eq.3.75a $C_2=0$, and the boundary condition Eq.3.75b gives

$$k = \frac{4}{\text{Re}_m \text{Pr}} \quad (3.81)$$

then

$$T_s^+ = \frac{4x^+}{\text{Re}_m \text{Pr}} + \frac{3}{8} \left(\frac{y^{+2}}{2} - \frac{y^{+4}}{12} \right) + C_4 \quad (3.82)$$

where $C_4 = C_1 + C_3$

Using the definition of bulk temperature (for channel)

$$T_b^+ = \frac{\int_0^1 T_s^+ u_s^+ dy^+}{\int_0^1 u_s^+ dy^+} \quad (3.83)$$

Substituting u_s^+ (Eq.3.64) and T_s^+ (Eq.3.82) into Eq.3.83 and using boundary condition Eq.3.75c gives

$$C_4 = \frac{-39}{1120}$$

Then, the steady dimensionless temperature distribution becomes,

$$T_s^+ = \frac{4x^+}{\text{Re}_m \text{Pr}} + \frac{3}{16} \left(y^{+2} - \frac{y^{+4}}{6} \right) - \frac{39}{1120} \quad (3.84)$$

The unsteady part of temperature distribution defined by Eq.3.74 is simplified by substituting the value of $\frac{\partial T_s^+}{\partial x^+}$ obtained from Eq.3.84,

which is equal to $\frac{16}{\text{Re}_m \text{Pr}}$ and the value of u_t^+ which defined in

Eq.3.67b to get

$$\text{Pr} \lambda^2 \frac{\partial T_t^+}{\partial t^+} + \frac{3}{2} \frac{2i\gamma'}{\lambda^2} \left[\frac{\cosh \sqrt{i}\lambda y^+}{\cosh \sqrt{i}\lambda} - 1 \right] e^{it^+} = \frac{\partial^2 T^+}{\partial y^{+2}} \quad (3.85)$$

Assuming similarity transformation solution as

$$T_t^+ = g(y^+) e^{it^+}$$

and substituting in the above equation the ordinary differential equation can be obtained as

$$g'' - i\text{Pr} \lambda^2 g = \frac{-3i\gamma'}{\lambda^2} \left[\frac{\cosh \sqrt{i}\lambda y^+}{\cosh \sqrt{i}\lambda} - 1 \right] \quad (3.86)$$

Solving above equation with boundary conditions Eqs.3.75a & 3.75b yields

$$T_t^+ = \frac{3\gamma'}{\lambda^4} \cdot e^{it^+} \left[\frac{\cosh(\sqrt{i}\text{Pr}\lambda y^+)}{\sqrt{\text{Pr}} \sinh(\sqrt{i}\text{Pr}\lambda)} \cdot \frac{\sinh(\sqrt{i}\lambda)}{(1-\text{Pr})\cosh(\sqrt{i}\lambda)} - \frac{\cosh(\sqrt{i}\lambda y^+)}{(1-\text{Pr})\cosh(\sqrt{i}\lambda)} - \frac{1}{\text{Pr}} \right] \quad (3.87)$$

Using the identify $\sqrt{i} = \frac{1+i}{\sqrt{2}}$, the real part of T_t^+ is

$$T_t^+ = \frac{3\gamma'}{\lambda^4} \cdot e^{it^+} \left[\frac{(E_1 Y_1 - F_1 Z_1) \text{cost}^+ - (E_1 Z_1 + F_1 Y_1) \text{sin}t^+}{\sqrt{\text{Pr}} (1-\text{Pr}) U_2 C_2} - \frac{Q_1 \text{cost}^+ - P_1 \text{sin}t^+}{(1-\text{Pr}) C_2} - \frac{\text{cost}^+}{\text{Pr}} \right] \quad (3.88)$$

where $E_1, F_1, U_2, Y_1, Z_1, C_2, Q_1$ and P_1 functions defined in the Appendix F.

Then, the total dimensionless temperature distribution ($T_s^+ + T_t^+$) becomes

$$T^+ = \frac{4x^+}{\text{Re}_m \text{Pr}} + \frac{3}{16} \left(y^{+2} - \frac{y^{+4}}{6} \right) - \frac{39}{1120} + \frac{3\gamma'}{\lambda^4} \cdot e^{it^+} \left[\frac{(E_1 Y_1 - F_1 Z_1) \cos t^+ - (E_1 Z_1 + F_1 Y_1) \sin t^+}{\sqrt{\text{Pr}} (1 - \text{Pr}) U_2 C_2} - \frac{Q_1 \cos t^+ - P_1 \sin t^+}{(1 - \text{Pr}) C_2} - \frac{\cos t^+}{\text{Pr}} \right] \quad (3.89)$$

The instantaneous-local Nusselt number is defined as

$$Nu_x = \frac{h_x \cdot D_h}{k} = \frac{1}{T_w^+ - T_b^+} \quad (3.90)$$

and the time averaged-local Nusselt number is defined as

$$\overline{Nu}_x = \frac{\overline{h}_x \cdot D_h}{k} = \frac{1}{\overline{T}_w^+ - \overline{T}_b^+} \quad (3.91)$$

3.4 Analytical Model of Pulsating Flow and Heat Transfer in the Pipe

3.4.1 Hydrodynamics Analysis

The momentum equation for pulsating flow in pipe Fig.3.4, with previous assumptions could be written as

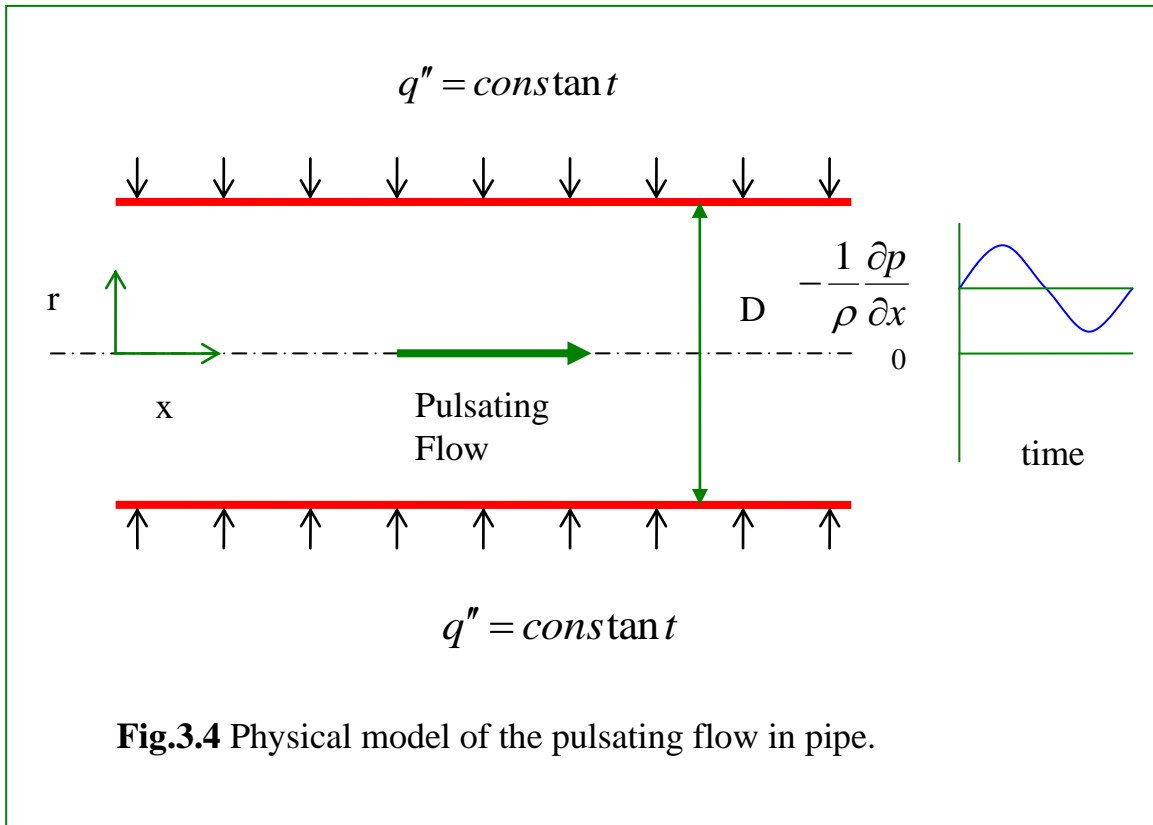
$$\frac{\partial u}{\partial t} = \left(-\frac{1}{\rho} \frac{\partial p}{\partial x} \right)_s (1 + \gamma' \cos \omega t) + \nu \left(\frac{\partial^2 u}{\partial r^2} + \frac{1}{r} \frac{\partial u}{\partial r} \right) \quad (3.92)$$

with boundary and initial conditions

$$1. \quad u = 0 \quad \text{at} \quad r = D/2 \quad \text{for} \quad t > 0 \quad \text{no slip at th wall} \quad (3.93a)$$

$$2. \quad \frac{\partial u}{\partial r} = 0 \quad \text{or} \quad u \text{ is finite} \quad \text{at} \quad r = 0 \quad \text{for} \quad t > 0 \quad \text{axisymmetric} \quad (3.93b)$$

$$3. \quad u = f(r) \quad \text{at} \quad t = 0 \quad \text{initial condition} \quad (3.93c)$$



Using the dimensionless form

$$u^+ = \frac{u}{u_{\max}} = \frac{P_o}{\omega}, \quad \lambda = \frac{D}{2} \sqrt{\omega/\nu}, \quad r^+ = \frac{r}{D} \quad \text{and} \quad t^+ = \omega t$$

Eq.3.42 becomes

$$4\lambda^2 \frac{\partial u^+}{\partial t^+} = 16(1 + \gamma' \cos t^+) + \left(\frac{\partial^2 u^+}{\partial r^{+2}} + \frac{1}{r^+} \frac{\partial u^+}{\partial r^+} \right) \quad (3.94)$$

The velocity of pulsating flow is divided into a two parts: steady part u_s^+ and fluctuation part u_t^+ thus

$$u^+(r^+, t^+) = u_s^+(r^+) + u_t^+(r^+, t^+) \quad (3.95)$$

Substituting of Eq.3.95 into Eq.3.94 , and using superposition, two differential equations are obtained

$$\frac{\partial^2 u_s^+}{\partial r^{+2}} + \frac{1}{r^+} \frac{\partial u_s^+}{\partial r^+} = -16 \quad (3.96a)$$

$$4\lambda^2 \frac{\partial u_t^+}{\partial t^+} = 16\gamma' \cos t^+ + \left(\frac{\partial^2 u_t^+}{\partial r^{+2}} + \frac{1}{r^+} \frac{\partial u_t^+}{\partial r^+} \right) \quad (3.96b)$$

and boundary conditions becomes

$$1. \quad u^+ = 0 \quad \text{at} \quad r^+ = 1/2 \quad \Rightarrow \quad u_s^+ = 0 \quad \text{and} \quad u_t^+ = 0 \quad (3.97a)$$

$$2. \quad \frac{\partial u^+}{\partial r^+} = 0 \quad \text{or} \quad u^+ \text{ is finite} \quad \text{at} \quad r^+ = 0 \quad (3.97b)$$

$$3. \quad u^+ = f(r^+) \quad \text{at} \quad t^+ = 0 \quad \text{initial condition} \quad (3.97c)$$

Integrating Eq.3.96a with boundary conditions Eq.3.97a and Eq.3.97b gives

$$u_s^+ = 1 - 4r^{+2} \quad (3.98)$$

For unsteady part, assuming a similarity transformation solution as

$$u_t^+ = f(y^+) e^{it^+} \quad (3.99)$$

Substituting f Eq.3.99 into Eq.3.96b, the ordinary differential equation can be obtained as

$$f'' + \frac{1}{r^+} f' + i^3 4\lambda^2 f = -16\gamma' \quad (3.100)$$

Using the general form of Bessel function and applying the boundary conditions Eqs.3.97a & 3.97b one can get

$$f = \frac{4i\gamma'}{\lambda^2} \left[\frac{J_0(2i^{3/2}\lambda r^+)}{J_0(i^{3/2}\lambda)} - 1 \right] \quad (3.101)$$

and

$$u_t^+ = \frac{4i\gamma'}{\lambda^2} \left[\frac{J_0(2i^{3/2}\lambda r^+)}{J_0(i^{3/2}\lambda)} - 1 \right] e^{it^+} \quad (3.102)$$

For small value of λ ($\lambda < 2$) the following definition of complex Bessel function can be used

$$J_0(2i^{3/2}\lambda r^+) = Ber_0(2\lambda r^+) + i Bei_0(2\lambda r^+) \quad (3.103a)$$

$$J_0(i^{3/2}\lambda) = Ber_0(\lambda) + i Bei_0(\lambda) \quad (3.103b)$$

Eq.3.102 can be simplified and the real part will be

$$u_t^+ = \frac{4\gamma'}{\lambda^2} \left[\sin t^+ - \left(\frac{(Ber_0(2\lambda r)Ber_0(\lambda) + Bei_0(2\lambda r^+)Bei_0(\lambda))\sin t^+}{Ber_0^2(\lambda) + Bei_0^2(\lambda)} + \frac{(Bei_0(2\lambda r)Ber_0(\lambda) - Ber_0(2\lambda r^+)Bei_0(\lambda))\cos t^+}{Ber_0^2(\lambda) + Bei_0^2(\lambda)} \right) \right] \quad (3.104)$$

The total velocity u^+ , is equal to summation the of the steady part u_s^+ and fluctuation part u_t^+ as

$$u^+ = 1 - 4r^{+2} + \frac{4\gamma'}{\lambda^2} \left[\sin t^+ - \left(\frac{(Ber_0(2\lambda r)Ber_0(\lambda) + Bei_0(2\lambda r^+)Bei_0(\lambda))\sin t^+}{Ber_0^2(\lambda) + Bei_0^2(\lambda)} + \frac{(Bei_0(2\lambda r)Ber_0(\lambda) - Ber_0(2\lambda r^+)Bei_0(\lambda))\cos t^+}{Ber_0^2(\lambda) + Bei_0^2(\lambda)} \right) \right] \quad (3.105)$$

For large value of λ ($\lambda > 2$) asymptotic Bessel function for complex variable Eq.3.38 can be used to simplify Eq.3.102b, the total velocity u^+ can be obtained (see Appendix G)

$$u^+ = 1 - 4r^{+2} + \frac{4\gamma'}{\lambda^2} \left\{ \sin t^+ - \left[\frac{1}{\sqrt{2r^+}} e^{\lambda/\sqrt{2}(2r^+-1)} \sin(t^+ + \lambda/\sqrt{2}(2r^+-1)) \right] \right\} \quad (3.106)$$

4.4.2 Heat Transfer Analysis

Energy Equation for pulsating flow could be described by Eq.3.41 or in dimensionless form as

$$4 \text{Pr} \lambda^2 \frac{\partial T^+}{\partial t^+} + 2 \text{Re}_m \text{Pr} u^+ \frac{\partial T^+}{\partial x^+} = \frac{\partial^2 T^+}{\partial r^{+2}} + \frac{1}{r^+} \frac{\partial T^+}{\partial r^+} \quad (3.107)$$

where

$$\text{Pr} = \frac{\nu}{\alpha}, T^+ = \frac{k(T - T_o)/D}{q''}, x^+ = \frac{x}{D}, \lambda = \frac{D}{2} \sqrt{\omega/\nu}, \text{Re}_m = \frac{u_m \cdot D}{\nu},$$

$$r^+ = r/D \quad \text{and} \quad u_m = \frac{1}{2} u_{\max}^{[9]}$$

Assuming a solution for T^+ compose of two parts: the steady part, and unsteady part as

$$T^+(x^+, r^+, t^+) = T_s^+(x^+, r^+) + T_t^+(r^+, t^+) \quad (3.108)$$

Substituting Eq.3.108 into Eq.3.107 and using the superposition gives

$$2 \operatorname{Re}_m \operatorname{Pr} u_s^+ \frac{\partial T_s^+}{\partial x^+} = \frac{\partial^2 T_s^+}{\partial r^{+2}} + \frac{1}{r^+} \frac{\partial T_s^+}{\partial r^+} \quad (3.109)$$

and

$$4 \operatorname{Pr} \lambda^2 \frac{\partial T_t^+}{\partial t^+} + 2 \operatorname{Re}_m \operatorname{Pr} u_t^+ \frac{\partial T_s^+}{\partial x^+} = \frac{\partial^2 T_t^+}{\partial y^{+2}} + \frac{1}{r^+} \frac{\partial T_t^+}{\partial r^+} \quad (3.110)$$

with boundary conditions

$$1. T^+ \text{ is finite at } r^+ = 0 \Rightarrow T_s^+ \text{ and } T_t^+ \text{ are finite} \quad (3.111a)$$

$$2. \frac{\partial T^+}{\partial r^+} = 1 \quad \text{at } r^+ = 1/2 \Rightarrow \frac{\partial T_s^+}{\partial r^+} = 1 \quad \frac{\partial T_t^+}{\partial r^+} = 0 \quad (3.111b)$$

$$3. T^+ = 0 \quad \text{at } x^+ = 0 \Rightarrow T_s^+ = 0 \quad (3.111c)$$

For steady part Eq.3.109, the following solution is assumed

$$T_s^+(x^+, r^+) = X(x^+) + R(r^+) \quad (3.112)$$

Substituting the above equation and u_s^+ defined by Eq.3.98 into Eq.3.109 gives

$$2 \operatorname{Re}_m \operatorname{Pr} (1 - 4r^{+2}) X' = R'' + \frac{1}{r^+} R' = \frac{1}{r^+} \frac{\partial}{\partial r^+} (r^+ R') \quad (3.113)$$

Using the separation of variables to solve the Eq.3.113 as

$$X' = \frac{R'' + \frac{1}{r^+} R'}{2 \operatorname{Re}_m \operatorname{Pr} (1 - 4r^{+2})} = k \quad (3.114)$$

where k: is constant.

Separating Eq.3.114 yields

$$X' - k = 0 \quad (3.115a)$$

$$R'' + \frac{1}{r^+} R' - 2k \text{Re}_m \text{Pr}(1 - 4r^{+2}) = 0 \quad (3.115b)$$

Integrating both Eqs.3.115a & 3.115b gives

$$X = k x^+ + C_1 \quad (3.116)$$

and

$$R = 2k \text{Re}_m \text{Pr} \left(\frac{r^{+2}}{4} - \frac{r^{+4}}{4} \right) + C_2 \ln r^+ + C_3 \quad (3.117)$$

where C_1 , C_2 and C_3 are constants.

According to Eqs.3.115a & 3.115b the temperature T_s^+ will be

$$T_s^+ = k \left[x^+ + 2\text{Re}_m \text{Pr} \left(\frac{r^{+2}}{4} - \frac{r^{+4}}{4} \right) \right] + C_2 \ln r^+ + C_4 \quad (3.118)$$

where $C_4 = C_1 + C_3$

from boundary condition Eq.3.111a, $C_2=0$, and from boundary condition Eq.3.111b yields

$$k = \frac{4}{\text{Re}_m \text{Pr}}$$

and

$$T_s^+ = \frac{4x^+}{\text{Re}_m \text{Pr}} + 2(r^{+2} - r^{+4}) + C_4 \quad (3.119)$$

Using the definition of bulk temperature for pipe

$$\bar{T}_{s,b}^+ = \frac{\int_0^{1/2} T_s^+ u_s^+ r^+ dr^+}{\int_0^{1/2} u_s^+ r^+ dr^+} \quad (3.120)$$

with the boundary condition Eq.3.111c the constant C_4 is

$$C_4 = \frac{-7}{48}$$

then

$$T_s^+ = \frac{4x^+}{\text{Re}_m \text{Pr}} + 2(r^{+2} - r^{+4}) - \frac{7}{48} \quad (3.121)$$

for unsteady part of T^+ , a similarity transformation solution is assumed as

$$T_t^+(r^+, t^+) = g(r^+) e^{it^+} \quad (3.122)$$

Substituting the similarity transformation solution Eq.3.122 and the value of

$\frac{\partial T_s^+}{\partial x^+}$ obtained from Eq.3.121, which is equal to $\frac{4}{\text{Re}_m \text{Pr}}$, and the

value of u_t^+ from Eq.3.102 into the Eq.3.110 gives

$$g'' + \frac{1}{r^+} + i^3 4\text{Pr} \lambda^2 g = \frac{-32i\gamma'}{\lambda^2} \left[\frac{J_0(2i^{3/2} \lambda r^+)}{J_0(i^{3/2} \lambda)} - 1 \right] \quad (3.123)$$

Solving Eq.3.123 with boundary conditions Eqs.3.111a & 3.111b yields

$$T_t^+ = \frac{8\gamma'}{\lambda^4} \cdot e^{it^+} \left[\frac{J_1(i^{3/2}\lambda)}{(1-\text{Pr})J_0(i^{3/2}\lambda)} \cdot \frac{J_0(2i^{3/2}\lambda\sqrt{\text{Pr}r^+})}{\sqrt{\text{Pr}}J_1(i^{3/2}\lambda\sqrt{\text{Pr}})} - \frac{J_0(2i^{3/2}\lambda r^+)}{(1-\text{Pr})J_0(i^{3/2}\lambda)} - \frac{1}{\text{Pr}} \right] \quad (3.124)$$

and the total dimensionless temperature distribution is

$$T^+ = \frac{4x^+}{\text{Re}_m \text{Pr}} + 2(r^{+2} - r^{+4}) - \frac{7}{48} + \frac{8\gamma'}{\lambda^4} \cdot e^{it^+} \left[\frac{J_1(i^{3/2}\lambda)}{(1-\text{Pr})J_0(i^{3/2}\lambda)} \cdot \frac{J_0(2i^{3/2}\lambda\sqrt{\text{Pr}r^+})}{\sqrt{\text{Pr}}J_1(i^{3/2}\lambda\sqrt{\text{Pr}})} - \frac{J_0(2i^{3/2}\lambda r^+)}{(1-\text{Pr})J_0(i^{3/2}\lambda)} - \frac{1}{\text{Pr}} \right] \quad (3.125)$$

where J_0 and J_1 Bessel function of first and second types (see Appendix C).

The final real value of T^+ is

$$T^+ = \frac{4x^+}{\text{Re}_m \text{Pr}} + 2(r^{+2} - r^{+4}) - \frac{7}{48} + \frac{8\gamma'}{\lambda^4} \left[\frac{((RE_1 RE_2 - IM_1 IM_2) \cos t^+ - (RE_1 IM_2 + IM_1 RE_2) \sin t^+)}{(1-\text{Pr})\sqrt{\text{Pr}}} - \frac{RE_3 \cos t^+ - IM_3 \sin t^+}{(1-\text{Pr})} - \frac{\cos t^+}{\text{Pr}} \right] \quad (3.126)$$

where $RE_1, IM_1, RE_2, IM_2, RE_3$ and IM_3 functions defined in Appendix C.

For large value of $\text{Pr} \lambda$, asymptotic complex Bessel function defined in Eq.3.38 (see Appendix D) could be used to obtain the final relation of T^+ as

$$\begin{aligned}
T^+ = & \frac{4x^+}{\text{Re}_m \text{Pr}} + 2(r^{+2} - r^{+4}) - \frac{7}{48} + \\
& \frac{8\gamma'}{\lambda^4} \left(\frac{e^{\lambda\sqrt{\text{Pr}/2}(2r^+-1)}}{(1-\text{Pr})\sqrt{2\text{Pr}r^+}} \cos(t^+ + \sqrt{\text{Pr}/2}\lambda(2r^+-1)) - \right. \\
& \left. \frac{e^{\lambda/\sqrt{2}(2r^+-1)}}{(1-\text{Pr})\sqrt{2r^+}} \cos(t^+ + \lambda/\sqrt{2}(2r^+-1)) - \frac{\cos t^+}{\text{Pr}} \right) \quad (3.127)
\end{aligned}$$

The instantaneous-local Nusselt number defined as

$$Nu_x = \frac{h_x \cdot D}{k} = \frac{1}{T_w^+ - T_b^+} \quad (3.128)$$

and the time averaged-local Nusselt number defined as

$$\overline{Nu}_x = \frac{\overline{h}_x \cdot D}{k} = \frac{1}{\overline{T}_w^+ - \overline{T}_b^+} \quad (3.129)$$

3.5 Numerical Model for Oscillatory Flow

3.5.1 Numerical Model of Reciprocating Flow in the Channel

Eq.3.5 and Eq.3.13 for reciprocating flow in the channel are solved numerically using the finite volume method^[51], at the same boundary and initial conditions of analytical solutions. In general the, the differences that are used: a forward difference for time, a central difference for dimensions and linear interpolation for medium values. The main steps of the finite volume method are proposed as

Step1 Grid Generation

To start the procedure of finite volume method, the control volume and nodal points are drawn in the Fig.3.5. The first step in the finite volume method is to divide the domain into discrete control volumes.

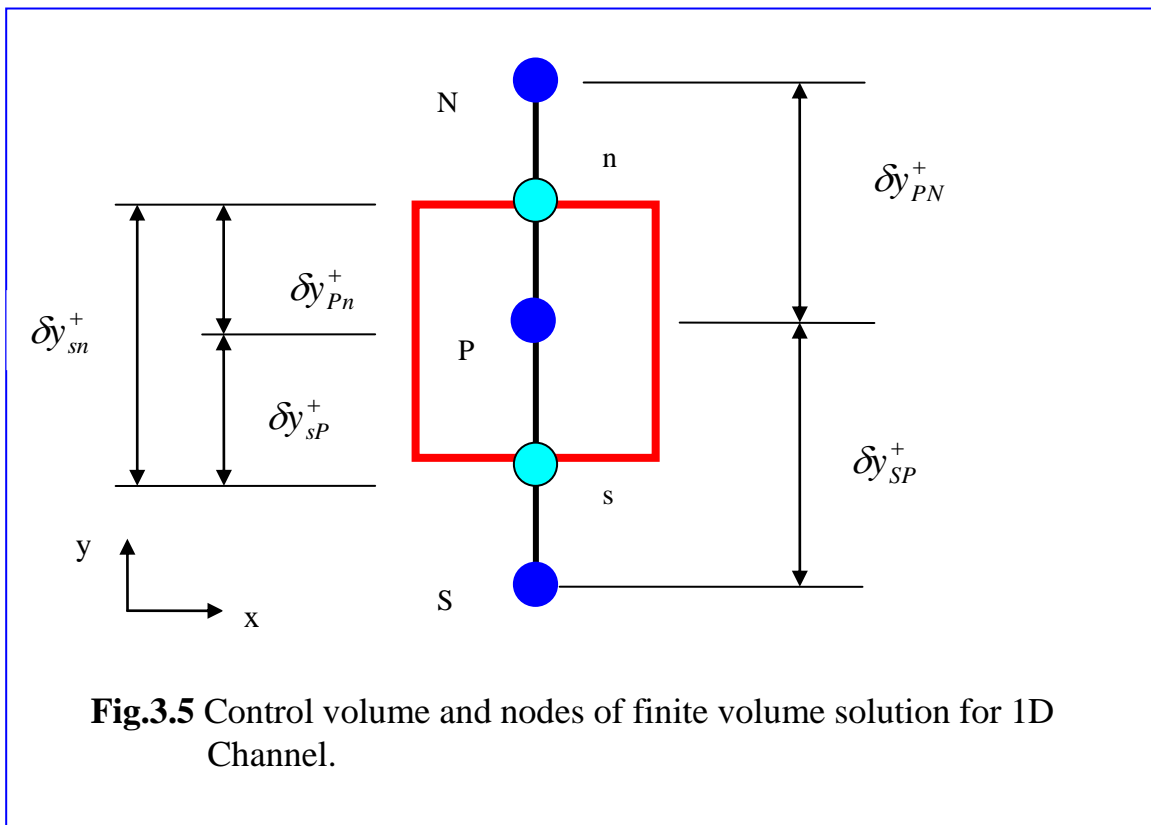


Fig.3.5 Control volume and nodes of finite volume solution for 1D Channel.

Step2 Discretisation

Integrating the governing equation (Eq.3.5) over the control volume and time to obtain a discretised equation at its nodal point P as

$$\int_{t^+}^{t^++\Delta t^+} \left[\int_{C.V} \frac{\partial u^+}{\partial y^+} dV \right] dt^+ = \int_{t^+}^{t^++\Delta t^+} \int_{C.V} \text{cost}^+ dV dt^+ + \int_{t^+}^{t^++\Delta t^+} \int_{C.V} \frac{1}{\lambda^2} \frac{\partial^2 u^+}{\partial y^{+2}} dV dt^+ \quad (3.130)$$

Using the forward difference for the time t^+ and central difference for dimension y^+ , to get a general form as

$$a_P u_P^+ = a_N [\theta u_N^+ + (1-\theta)u_N^{+o}] + a_S [\theta u_S^+ + (1-\theta)u_S^{+o}] + [a_o - (1-\theta)(a_N + a_S)] u_P^+ + b \quad (3.131)$$

where

$$a_o = \frac{\Delta V}{\Delta t^+} \quad (3.132a)$$

$$a_N = \frac{A_N}{\lambda^2} \frac{1}{\delta y_{PN}^+} \quad (3.132b)$$

$$a_S = \frac{A_S}{\lambda^2} \frac{1}{\delta y_{SP}^+} \quad (3.132c)$$

$$a_P = a_o + \theta(a_N + a_S) \quad (3.132d)$$

$$b = \overline{\text{cost}^+} \Delta V = [\theta(\cos(t^+ + \Delta t^+)) + (1-\theta)\text{cost}^+] \Delta V \quad (3.132e)$$

and

θ : weighting parameter between 0 and 1 and has the values

$\theta=0$ for explicit

$\theta=1$ for full implicit

$\theta=1/2$ for Crank-Nicolson

Repeated the above steps for energy equation to obtain

$$a_P T_P^+ = a_N [\theta T_N^+ + (1-\theta)T_N^{+o}] + a_S [\theta T_S^+ + (1-\theta)T_S^{+o}] + [a_o - (1-\theta)(a_N + a_S)]T_P^+ + b \quad (3.133)$$

where

$$a_o = \text{Pr} \lambda^2 \frac{\Delta V}{\Delta t^+} \quad (3.134a)$$

$$a_N = \frac{A_n}{\delta y_{PN}^+} \quad (3.134b)$$

$$a_S = \frac{A_s}{\delta y_{SP}^+} \quad (3.134c)$$

$$a_P = a_o + \theta(a_N + a_S) \quad (3.134d)$$

and

$$b = -\frac{1}{2} A_o \text{Pr} \lambda^2 \Delta V \overline{u_P^+} \quad (3.134e)$$

where

$$\overline{u_P^+} = \theta u_P^+ + (1-\theta)u_P^{+o} \quad (3.134f)$$

3.5.2 Numerical Model of Reciprocating Flow in the Pipe

The steps of section 3.5.1 are repeated, for case of reciprocating flow in the pipe with a control volume as shown in Fig.3.6. The Eq.3.32 is solved numerically using a finite volume method to get a general form as (for $r^+ > 0$)

$$a_P u_P^+ = a_N [\theta u_N^+ + (1-\theta)u_N^{+o}] + a_S [\theta u_S^+ + (1-\theta)u_S^{+o}] + a_P^o u_P^{+o} + b \quad (3.135)$$

where

$$a_o = 4\lambda^2 \Delta V \quad (3.136a)$$

$$a_N = \left[\frac{A_n}{2r_P^+} + \frac{A_n}{\delta r_{PN}^+} \right] \Delta t^+ \quad (3.136b)$$

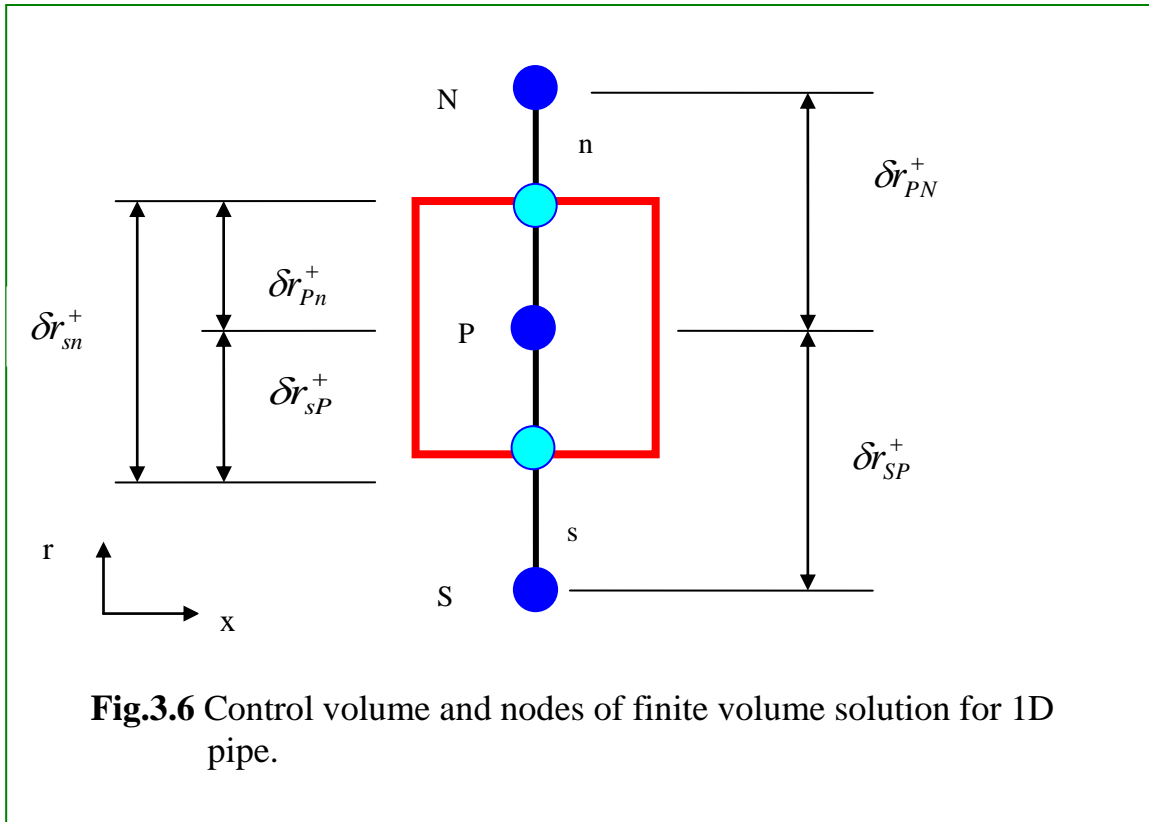
$$a_S = \left[\frac{-A_s}{2r_P^+} + \frac{A_s}{\delta r_{SP}^+} \right] \Delta t^+ \quad (3.136c)$$

$$a_P = a_o - \frac{\theta}{r_P^+} \left[\frac{A_n - A_s}{2} \right] \Delta t^+ + \theta \left[\frac{A_n}{\delta r_{PN}^+} + \frac{A_s}{\delta r_{SP}^+} \right] \Delta t^+ \quad (3.136d)$$

$$a_P^o = a_o + (1-\theta) \left[\left(\frac{A_n}{2r_P^+} - \frac{A_s}{2r_P^+} \right) \Delta t^+ - \left(\frac{A_n}{\delta r_{PN}^+} + \frac{A_s}{\delta r_{SP}^+} \right) \Delta t^+ \right] \quad (3.136e)$$

and

$$b = 4\lambda^2 \Delta V \Delta t^+ \left[\theta \cos(t^+ + \Delta t^+) + (1-\theta) \cos t^+ \right] \quad (3.136f)$$



For $r^+ = 0$, a special form of the equation must be obtained by letting $r^+ \rightarrow 0$ in the Eq.3.32 then becomes

$$4\lambda^2 \left. \frac{\partial u^+}{\partial t^+} \right|_{r^+=0} = 4\lambda^2 \cos t^+ \Big|_{r^+=0} + \left. \frac{\partial^2 u^+}{\partial r^{+2}} \right|_{r^+=0} + \lim_{r^+ \rightarrow 0} \left(\frac{1}{r^+} \frac{\partial u^+}{\partial r^+} \right) \quad (3.137)$$

When L'Hospital rule^[52] is applied to the last term on the right side Eq.3.137 gives

$$4\lambda^2 \left. \frac{\partial u^+}{\partial t^+} \right|_{r^+=0} = 4\lambda^2 \cos t^+ \Big|_{r^+=0} + 2 \left. \frac{\partial^2 u^+}{\partial r^{+2}} \right|_{r^+=0} \quad (3.138)$$

The general form of finite volume method for the above equation can be written as

$$a_p u_1^+ = a_N [\theta u_2^+ + (1-\theta)u_2^{+o}] + a_s [\theta u_0^+ + (1-\theta)u_0^{+o}] + a_p^o u_1^{+o} + b \quad (3.139)$$

where

$$a_o = 4\lambda^2 \Delta V \quad (3.140a)$$

$$a_N = \left[2 \frac{A_n}{\delta r_{PN}^+} \right] \Delta t^+ \quad (3.140b)$$

$$a_s = \left[2 \frac{A_s}{\delta r_{SP}^+} \right] \Delta t^+ \quad (3.140c)$$

$$a_p = a_o + 2\theta \left[\frac{A_n}{\delta r_{PN}^+} + \frac{A_s}{\delta r_{SP}^+} \right] \Delta t^+ \quad (3.140d)$$

$$a_p^o = a_o - 2(1-\theta) \left[\left(\frac{A_n}{\delta r_{PN}^+} + \frac{A_s}{\delta r_{SP}^+} \right) \Delta t^+ \right] \quad (3.140e)$$

and

$$b = 4\lambda^2 \Delta V \Delta t^+ \left[\theta \cos(t^+ + \Delta t^+) + (1-\theta) \cos t^+ \right] \quad (3.140f)$$

The energy equation (Eq.3.43) is solved numerically using the finite volume method to get a general form (*for* $r^+ > 0$)

$$a_p T_p^+ = a_N [\theta T_N^+ + (1-\theta)T_N^{+o}] + a_s [\theta T_s^+ + (1-\theta)T_s^{+o}] + a_p^o T_p^{+o} + b \quad (3.141)$$

where

$$a_o = 4\lambda^2 \text{Pr} \Delta V \quad (3.142a)$$

$$a_N = \left[\frac{A_n}{2r_p^+} + \frac{A_n}{\delta r_{PN}^+} \right] \Delta t^+ \quad (3.142b)$$

$$a_s = \left[\frac{-A_s}{2r_p^+} + \frac{A_s}{\delta r_{SP}^+} \right] \Delta t^+ \quad (3.142c)$$

$$a_p = a_o + \theta \left[\frac{A_n}{\delta r_{PN}^+} + \frac{A_s}{\delta r_{SP}^+} \right] \Delta t^+ - \frac{\theta}{r_p^+} \left[\frac{A_n - A_s}{2} \right] \Delta t^+ \quad (3.142d)$$

$$a_p^o = a_o + (1-\theta) \left[\left(\frac{-A_n}{\delta r_{PN}^+} - \frac{A_s}{\delta r_{SP}^+} \right) \Delta t^+ + \left(\frac{A_n}{2r_p^+} - \frac{A_s}{2r_p^+} \right) \Delta t^+ \right] \quad (3.142e)$$

and

$$b = -2\lambda^2 A_o \text{Pr} \Delta V \Delta t^+ [\theta u_p^+ + (1-\theta)u_p^{+o}] \quad (3.142f)$$

For $r^+ = 0$ applying L'Hospital's rule for energy equation (Eq.3.43) to get

$$4\lambda^2 \text{Pr} \left. \frac{\partial T^+}{\partial t^+} \right|_{r^+=0} + 4\lambda^2 A_o \text{Pr} u^+ \Big|_{r^+=0} = 2 \left. \frac{\partial^2 T^+}{\partial r^{+2}} \right|_{r^+=0} \quad (3.143)$$

The general form of the finite volume expression for the above equation can be written as

$$a_p T_1^+ = a_N [\theta T_2^+ + (1-\theta)T_2^{+o}] + a_s [\theta T_0^+ + (1-\theta)T_0^{+o}] + a_p^o T_1^{+o} + b \quad (3.144)$$

where

$$a_o = 4\lambda^2 \text{Pr} \Delta V \quad (3.145a)$$

$$a_N = 2 \frac{A_n}{\delta r_{PN}^+} \Delta t^+ \quad (3.145b)$$

$$a_S = 2 \frac{A_s}{\delta r_{SP}^+} \Delta t^+ \quad (3.145c)$$

$$a_P = a_o + 2\theta \left[\frac{A_n}{\delta r_{PN}^+} + \frac{A_s}{\delta r_{SP}^+} \right] \Delta t^+ \quad (3.145d)$$

$$a_P^o = a_o + 2(1-\theta) \left(\frac{-A_n}{\delta r_{PN}^+} - \frac{A_s}{\delta r_{SP}^+} \right) \Delta t^+ \quad (3.145e)$$

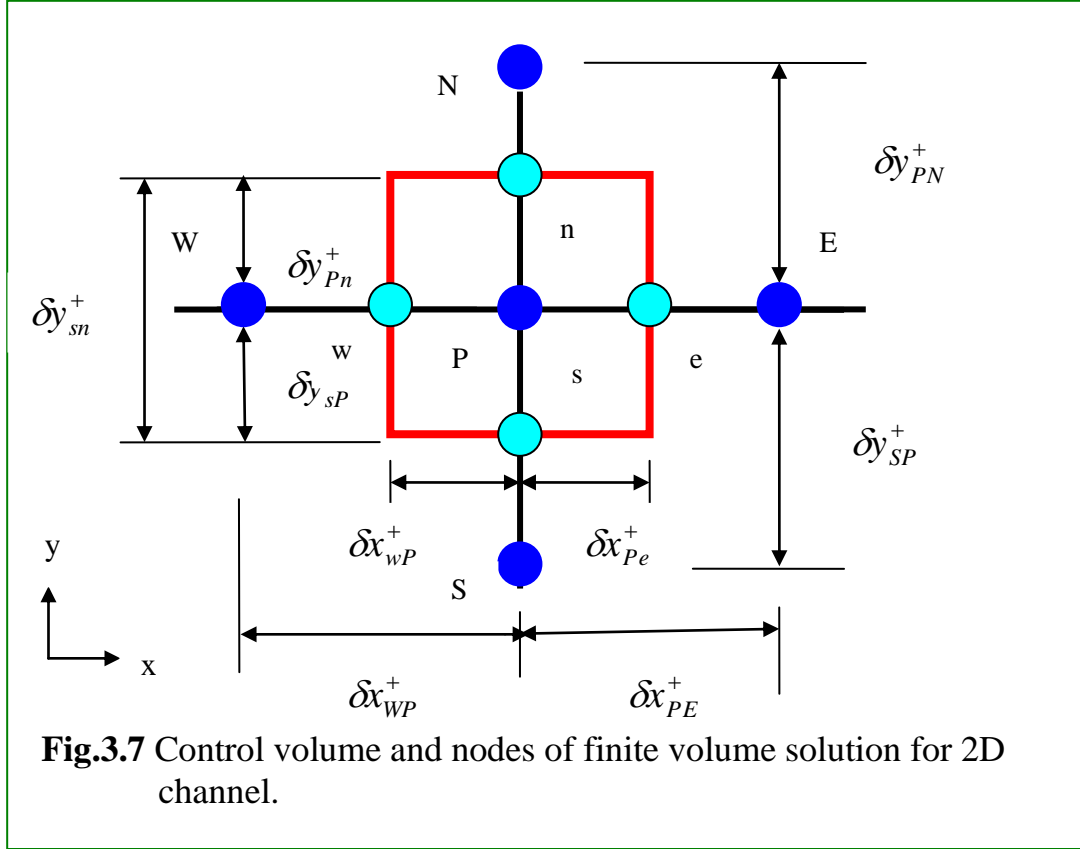
and

$$b = -2\lambda^2 A_o \text{Pr} \gamma \Delta V \Delta t^+ \left[\theta u_1^+ + (1-\theta) u_1^{+o} \right] \quad (3.145f)$$

3.5.3 Numerical Model of Pulsating Flow in the Channel

Momentum equation of pulsating flow (Eq.3.61) in the channel Fig.3.7 is rearranged using finite volume method in the similar maner to get the following general form

$$\begin{aligned} a_P u_P^+ &= a_N \left[\theta u_N^+ + (1-\theta) u_N^{+o} \right] + a_S \left[\theta u_S^+ + (1-\theta) u_S^{+o} \right] \\ &\quad + \left[a_o - (1-\theta)(a_N + a_S) \right] u_P^{+o} + b \quad (3.146) \end{aligned}$$



where

$$a_o = \frac{\Delta V}{\Delta t^+} \quad (3.147a)$$

$$a_N = \frac{A_N}{\lambda^2} \frac{1}{\delta y_{PN}^+} \quad (3.147b)$$

$$a_S = \frac{A_S}{\lambda^2} \frac{1}{\delta y_{SP}^+} \quad (3.147c)$$

$$a_P = a_o + \theta(a_N + a_S) \quad (3.147d)$$

and

$$b = \frac{2}{\lambda^2} \left(1 + \overline{\gamma' \cos t^+}\right) \Delta V \quad (3.147e)$$

where

$$\overline{\cos t^+} = \theta \cos(t^+ + \Delta t^+) + (1 - \theta) \cos t^+ \quad (3.147f)$$

The energy equation of pulsating flow in the channel (Eq.3.70) is written in the general form of finite volume method (using a control volume is shown in Fig.3.7) as

$$\begin{aligned}
 a_P T_P^+ &= a_N [\theta T_N^+ + (1-\theta) T_N^{+o}] + a_S [\theta T_S^+ + (1-\theta) T_S^{+o}] + \\
 &\quad a_E [\theta u_P^+ T_E^+ + (1-\theta) u_P^{+o} T_E^{+o}] + \\
 &\quad a_W [\theta u_P^+ T_W^+ + (1-\theta) u_P^{+o} T_W^{+o}] + a_P^o T_P^+
 \end{aligned} \tag{3.148}$$

where

$$a_o = \lambda^2 \text{Pr} \frac{\Delta V}{\Delta t^+} \tag{3.149a}$$

$$a_N = \frac{A_n}{\delta y_{PN}^+} \tag{3.149b}$$

$$a_S = \frac{A_s}{\delta y_{SP}^+} \tag{3.149c}$$

$$a_E = \frac{-3}{32} \text{Re}_m \text{Pr} \frac{A_e}{2} \tag{3.149d}$$

$$a_W = \frac{-3}{32} \text{Re}_m \text{Pr} \frac{A_w}{2} \tag{3.149e}$$

$$a_P = a_o + \theta [a_E - a_W] u_P^+ + \theta [a_N + a_S] \tag{3.149f}$$

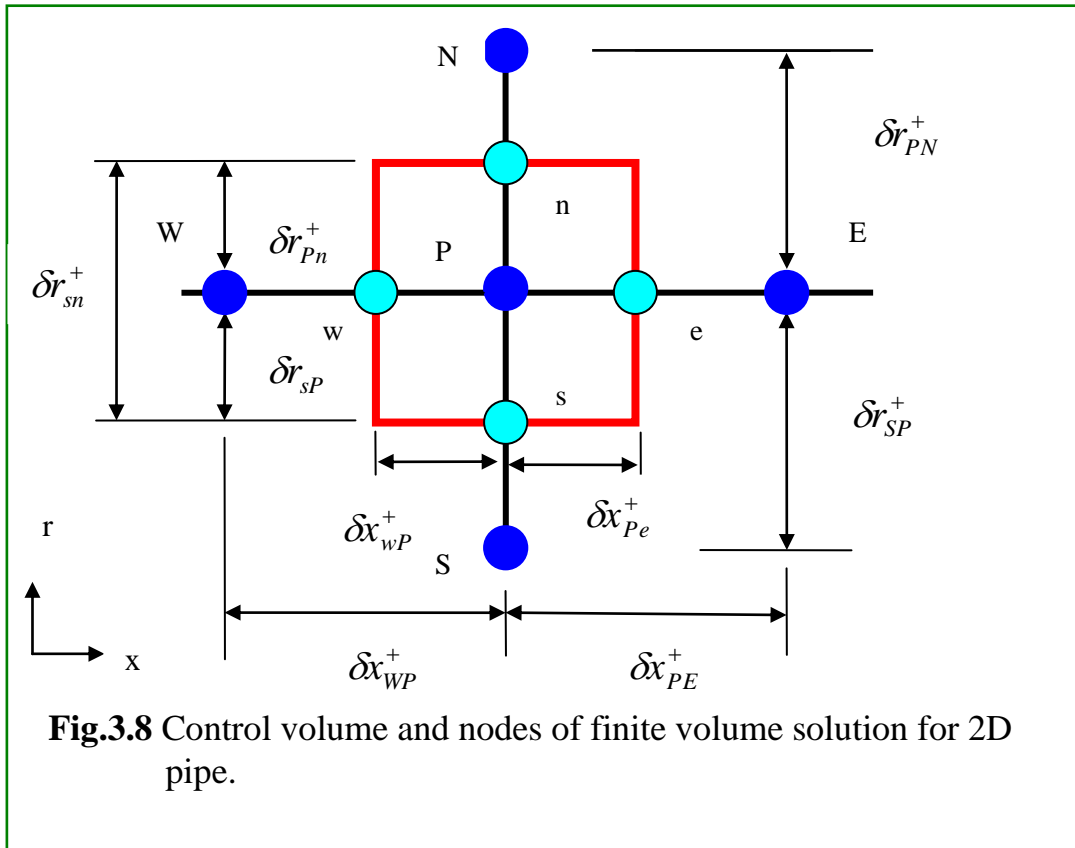
and

$$a_P^o = a_o + (1-\theta)(a_E - a_W) u_P^{+o} - (1-\theta)(a_N + a_S) \tag{3.149g}$$

3.5.4 Numerical Model of Pulsating Flow in the Pipe

Eq.3.94 is rearranged using the finite volume method to obtain the general form (for $r^+ > 0$)

$$a_P u_P^+ = a_N [\theta u_N^+ + (1-\theta)u_N^{+o}] + a_S [\theta u_S^+ + (1-\theta)u_S^{+o}] + a_P^o u_P^+ + b \quad (3.150)$$



where

$$a_o = 4\lambda^2 \Delta V \quad (3.151a)$$

$$a_N = \left[\frac{A_n}{2r_P^+} + \frac{A_n}{\delta r_{PN}^+} \right] \Delta t^+ \quad (3.151b)$$

$$a_S = \left[\frac{-A_s}{2r_P^+} + \frac{A_s}{\delta r_{SP}^+} \right] \Delta t^+ \quad (3.151c)$$

$$a_p = a_o - \frac{\theta}{r_p^+} \left[\frac{A_n - A_s}{2} \right] \Delta t^+ + \theta \left[\frac{A_n}{\delta r_{PN}^+} + \frac{A_s}{\delta r_{SP}^+} \right] \Delta t^+ \quad (3.151d)$$

$$a_p^o = a_o + (1-\theta) \left[\left(\frac{A_n}{2r_p^+} - \frac{A_s}{2r_p^+} \right) \Delta t^+ - \left(\frac{A_n}{\delta r_{PN}^+} + \frac{A_s}{\delta r_{SP}^+} \right) \Delta t^+ \right] \quad (3.151e)$$

and

$$b = 16\Delta V \Delta t^+ \left[1 + \gamma'(\theta \cos(t^+ + \Delta t^+) + (1-\theta) \cos t^+) \right] \quad (3.151f)$$

for $r^+ = 0$

$$a_p u_1^+ = a_N [\theta u_2^+ + (1-\theta) u_2^{+o}] + a_S [\theta u_0^+ + (1-\theta) u_0^{+o}] + a_p^o u_1^+ + b \quad (3.152)$$

where

$$a_o = 4\lambda^2 \Delta V \quad (3.153a)$$

$$a_N = \frac{2A_n}{\delta r_{PN}^+} \Delta t^+ \quad (3.153b)$$

$$a_S = \frac{2A_s}{\delta r_{SP}^+} \Delta t^+ \quad (3.153c)$$

$$a_p = a_o + 2\theta \left[\frac{A_n}{\delta r_{PN}^+} + \frac{A_s}{\delta r_{SP}^+} \right] \Delta t^+ \quad (3.153d)$$

$$a_p^o = a_o - 2(1-\theta) \left(\frac{A_n}{\delta r_{PN}^+} + \frac{A_s}{\delta r_{SP}^+} \right) \Delta t^+ \quad (3.153e)$$

and

$$b = 16 \Delta V \Delta t^+ [1 + \gamma'(\theta \cos(t^+ + \Delta t^+) + (1-\theta) \cos t^+)] \quad (3.153f)$$

The energy equation (Eq.3.10) with control volume and nodes is shown in the Fig.3.8 is formed in the finite volume method for $r^+ = 0$ as

$$\begin{aligned}
 a_P T_P^+ = & a_N \left[\theta T_N^+ + (1-\theta) T_N^{+o} \right] + a_S \left[\theta T_S^+ + (1-\theta) T_S^{+o} \right] + \\
 & a_E \left[\theta u_P^+ T_E^+ + (1-\theta) u_P^{+o} T_E^{+o} \right] \\
 & a_W \left[\theta u_P^+ T_W^+ + (1-\theta) u_P^{+o} T_W^{+o} \right] + a_P^o T_P^+ + b
 \end{aligned} \tag{3.154}$$

where

$$a_o = 4\lambda^2 \text{Pr} \Delta V \tag{3.155a}$$

$$a_N = \left[\frac{A_n}{2r_P^+} + \frac{A_n}{\delta r_{PN}^+} \right] \Delta t^+ \tag{3.155b}$$

$$a_S = \left[\frac{-A_s}{2r_P^+} + \frac{A_s}{\delta r_{SP}^+} \right] \Delta t^+ \tag{3.155c}$$

$$a_W = 2\text{Re}_m \text{Pr} \Delta t^+ \Delta V \tag{3.155d}$$

$$a_E = -2\text{Re}_m \text{Pr} \Delta t^+ \Delta V \tag{3.155e}$$

$$\begin{aligned}
 a_P = & a_o + \theta \left[2\text{Re}_m \text{Pr} u_P^+ \left(\frac{A_e - A_w}{2} \right) \right] \Delta t^+ + \theta \left[\frac{A_n}{\delta r_{PN}^+} + \frac{A_s}{\delta r_{SP}^+} \right] \Delta t^+ \\
 & - \frac{\theta}{r_P^+} \left[\frac{A_n - A_s}{2} \right] \Delta t^+
 \end{aligned} \tag{3.155f}$$

$$\begin{aligned}
a_p^o &= a_o - (1-\theta) \left[2 \text{Re}_m \text{Pr} u_p^{+o} \left(\frac{A_e - A_w}{2} \right) \right] \Delta t^+ - (1-\theta) \left[\frac{A_n}{\delta r_{PN}^+} + \frac{A_s}{\delta r_{SP}^+} \right] \Delta t^+ \\
&\quad + \frac{(1-\theta)}{r_p^+} \left[\frac{A_n - A_s}{2} \right] \Delta t^+ \tag{3.155g}
\end{aligned}$$

and

$$b = 0 \tag{3.155h}$$

for $r^+ = 0$

$$\begin{aligned}
a_p T_1^+ &= a_N \left[\theta T_2^+ + (1-\theta) T_2^{+o} \right] + a_S \left[\theta T_0^+ + (1-\theta) T_0^{+o} \right] + \\
&\quad a_E \left[\theta u_1^+ T_E^+ + (1-\theta) u_1^{+o} T_E^{+o} \right] + \\
&\quad a_W \left[\theta u_1^+ T_W^+ + (1-\theta) u_1^{+o} T_W^{+o} \right] + a_p^o T_1^+ + b \tag{3.156}
\end{aligned}$$

where

$$a_o = 4\lambda^2 \text{Pr} \Delta V \tag{3.157a}$$

$$a_N = \frac{2A_n}{\delta r_{PN}^+} \Delta t^+ \tag{3.157b}$$

$$a_S = \frac{2A_s}{\delta r_{SP}^+} \Delta t^+ \tag{3.157c}$$

$$a_W = 2 \text{Re}_m \text{Pr} \Delta t^+ A_w \tag{3.157d}$$

$$a_E = -2 \text{Re}_m \text{Pr} \Delta t^+ A_e \tag{3.157e}$$

$$a_p = a_o + \theta \left[2 \text{Re}_m \text{Pr} u_1^+ \left(\frac{A_e - A_w}{2} \right) \right] \Delta t^+ + 2\theta \left[\frac{A_n}{\delta r_{PN}^+} + \frac{A_s}{\delta r_{SP}^+} \right] \Delta t^+ \quad (3.157 f)$$

$$a_p^o = a_o - (1 - \theta) 2 \text{Re}_m \text{Pr} u_1^{+o} \left(\frac{A_e - A_w}{2} \right) \Delta t^+ \\ - 2(1 - \theta) \left[\frac{A_n}{\delta r_{PN}^+} + \frac{A_s}{\delta r_{SP}^+} \right] \Delta t^+ \quad (3.157 g)$$

and

$$b = 0 \quad (3.157 h)$$

CHAPTER FOUR

RESULTS AND DISCUSSION

In this chapter the hydrodynamics and heat transfer characteristics due to oscillatory flow is presented. The effects of parameters with various values in the solution of governing equations will be introduced. The results of both types of oscillating flow: reciprocating and pulsating for internal flow inside a channel and a pipe subjected to a constant heat flux will be discussed.

The main parameters characterize the flow and heat transfer are: dimensionless velocity u^+ , dimensionless temperature T^+ , dimensionless bulk temperature T_b^+ , dimensionless center temperature T_c^+ , instantaneous-local Nusselt number Nu_x and time average-local Nusselt number \overline{Nu}_x . The results are presented in three sections:

- 1- Analytical solution of the new model.
- 2- Numerical solution for checking the new model.
- 3- Comparison of the new model with experimental results of other authors.

4.1 Analytical Solution of the New Model

The results of the solution of the new model will be divided into four categories depending on a type of flow and duct shape:

- 1- Analytical results of reciprocating flow and heat transfer in the channel.
- 2- Analytical results of reciprocating flow and heat transfer in the pipe.

- 3- Analytical results of pulsating flow and heat transfer in the channel.
- 4- Analytical results of pulsating flow and heat transfer in the pipe.

4.1.1 Analytical Results of Reciprocating Flow and Heat Transfer in the Channel.

Analytical solution of momentum and energy equations for reciprocating flow inside horizontal channel shows that four parameters have influence on the flow and heat transfer and these are: Womersly number λ , dimensionless amplitude of fluid displacement A_o , Prandtl number Pr and the ratio of distance to hydraulic diameter x/D_h .

The values of λ and A_o are taken not greater than the critical values β_{cri} [7]. To avoid the limit of turbulence intensity region, the values of β_{cri} is taken to be less or equal to 400 as the most of the authors used (table 2.1), and the values of λ and A_o are related to it. The Prandtl number Pr is taken equal to 0.7 (for the air) in the various calculations. The hydraulic diameter for very wide channel (width \gg height) is equal to $4h$, which makes the ratio x/D_h has the values of $0 < x/D_h < 100$. Usually, a large value of x/D_h is used, such as $x/D_h = 10-50$, to avoid the negative value of dimensionless temperature distribution which occurs when the mean value of dimensionless temperature (γx^+) becomes less than the fluctuation value $(\gamma g(y^+)e^{it^+})$. The large values λ and A_o give a similar results (negative values of dimensionless temperature distribution), therefore, in order to keep away from such behavior, the small values of λ and A_o should be taken (Eq.3.24 shows the relation between γ and λ & A_o).

Reciprocating flow require interchange between the inflow and out flow boundaries along the length of pipe or channel during a cycle. It is assumed that the fluid particles during a cycle exiting the flow domain, i.e. the time required for the flow to go along the length equal to the half time of cycle for coming back flow.

Starting from the velocity distribution, Fig.4.1 illustrates the variation of dimensionless velocity u^+ with dimensionless channel height during a half cycle π . The velocity profile is represented at different times (30° between each time used). The figures clarifies that the velocity profile is varied depending on the time at which the velocity is taken for constant controlling parameters ($\lambda=4$, $A_o=15$, $Pr=0.7$ and $x/D_h=20$), therefore at a certain time the u^+ becomes parabolic (unidirection) and in the other time changes specially at the region near the wall. This effect is due to the oscillation of the flow which makes the region near the wall faster than at the core region and this is called Richardson annular effects^[7]. At approximately 130° the flow begins to reverse its direction (the fluid flowing near the wall starts to reverse its direction as much as 30° approximately sooner than the flow reversal in the center of the channel).

In the second half of the cycle, the change of direction of the flow has no influence on the shape or magnitude of u^+ at the same cyclic time ($\theta + \pi$, where θ is the crank angle), but only on the direction of distribution u^+ .

Fig.4.2 shows the distribution of dimensionless temperature T^+ with dimensionless channel height over a half cycle π . The controlling parameters are kept constant as ($\lambda=4$, $A_o=15$, $Pr=0.7$ and $x/D_h=20$). It

is cleared from shape of temperature distribution, that the wall temperature is greater than at the center temperature since the heating is at the wall. The sharp velocity gradient near the wall leads to change in the temperature distribution along the channel height, i.e. the annular effect of velocity gives annular effect in the temperature distribution. It is also clear from the shapes of velocity and temperature distributions that, increasing the velocity causes a decreasing in the temperature (when the velocity is increased, allowing more fluid flow per unit time being passed which makes the value of temperature decreased).

The two Figs. 4.1 & 4.2 show the phase shifting between the velocity and temperature distributions.

Figs.4.3 & 4.4 indicate the influence of Womersly number λ on the dimensionless velocity u^+ profile and dimensionless temperature T^+ profile respectively with dimensionless channel height at the dimensionless time 60° , for ($A_o=15$, $Pr=0.7$ and $x/D_h=30$), where $\lambda=4, 8$ & 12 . For high Womersly number λ of flow, the velocity and temperature distribution is significantly affected by the Richardson's annular effect.

Fig.4.5 & 4.6 present the effects of Womersly number λ and dimensionless amplitude of the fluid displacement A_o on the dimensionless bulk temperature T_b^+ over a one cycle 2π . Fig.4.5 illustrates the influence of increasing Womersly number λ during a one cycle 2π on T_b^+ at constant values of the controlling parameters ($A_o=15$, $Pr=0.7$ and $x/D_h=20$). The values of λ are equal to: 4, 8, and 12. It shows declining in T_b^+ with increasing Womersly number, because of

increasing the velocity of flow due to increase the frequency, which makes the magnitude of temperature is decreased. The effect of dimensionless amplitude of fluid displacement A_o on the dimensionless bulk temperature T_b^+ along one cycle 2π is presented in the Fig.4.6. A_o equal to 10 and 15, while $\lambda=4$, $Pr=0.7$ and $x/D_h=20$. It is illustrated that T_b^+ decreases with increasing A_o , which belong to increase quantity of flow (velocity or volumetric flow rate) with increasing A_o .

The periodical change of the velocity with time for reciprocating flow where the mean value of flow rate equal to zero which requires that the velocity at the certain time reach zero also, makes the value of dimensionless bulk temperature T_b^+ go to infinite at the certain time. This behavior makes a clear discontinuity in the distribution of T_b^+ with time.

Fig.4.7 indicates the variation of instantaneous-local Nusselt number Nu_x with time(one cycle 2π) for different value of Womersly number ($\lambda =4, 8$ and 12), while the other parameters are kept constant ($A_o=15$, $Pr=0.7$ and $x/D_h=20$). The increment of Womersly number (frequency) rise Nu_x , which is attributed to thinner boundary layer and therefore the thermal resistance becomes small. The values of Nu_x go to infinite at the certain time, which is resulting from the value of T_b^+ . It is clearly shown from the figure that the value of Nu_x for reciprocating flow is more than for steady fully developed flow in the channel which equals to $\overline{Nu} = 8.235$ ^[20] by the order of magnitude. This is enhancement making the application of oscillatory flow or

reciprocating flow is very effective means for enhancement of heat transfer and can be used in the wide field of industrial application.

Fig.4.8 illustrates the effect of dimensionless amplitude of fluid displacement A_o ($A_o=10$ and 15 , and $\lambda=4$, $Pr=0.7$ and $x/D_h=20$). On the instantaneous-local Nusselt number Nu_x over a one cycle 2π . It is shown that A_o has no effect on Nu_x , because the varying of A_o means the change of velocity or volumetric flow rate which has no effect on Nu_x for fully developed flow.

Fig.4.9 shows the variation of the dimensionless center temperature T_c^+ at $y^+=0$ over a one cycle 2π for different locations x/D_h ($x/D_h=20, 25$ & 30) while the other parameters are fixed ($\lambda=4$, $A_o=15$ and $Pr=0.7$). It shows that T_c^+ is increased with increasing x/D_h , due to accumulate heat supplied along the channel. It also shows that T_c^+ is varied periodically with time and becomes minimum at the certain time because of varying the velocity with time. Fig.4.10 demonstrates the effect of dimensionless amplitude A_o ($A_o=10, 15$ & 20 , and $\lambda=4$, $Pr=0.7$ and $x/D_h=20$), on T_c^+ with time (one cycle 2π). It refers to decrease T_c^+ with increasing A_o , because of increasing the volumetric flow rate with increasing A_o , which effects on the temperature profile.

Fig.4.11 illustrates the variation of the instantaneous-local Nusselt number Nu_x over a one cycle 2π for different ratio of distance to hydraulic diameter x/D_h ($x^+=10, 20$ & 25) and the other parameters are ($\lambda=4$, $A_o=15$ and $Pr=0.7$). It is seemed from the figure that x/D_h

has no effect on Nu_x , this is return to the fully developed flow along the flow direction.

Finally, the influence of Prandtl number Pr on the time averaged-local Nusselt number \overline{Nu}_x during a one cycle 2π , is presented in the Fig.4.12, for two value of λ ($\lambda=4$ and 8) while the other controlling parameters are kept constant ($A_o=15$ and $x^+=20$). The increment of Prandtl number Pr increases \overline{Nu}_x due to increase the hydrodynamics diffusivity of the fluid or due to increase the specific heat capacity of the fluid ($Pr = \frac{\nu}{\alpha}$). Also, the figure shows the effect of Womersly number λ on the time averaged-local Nusselt number \overline{Nu}_x , which increases with increasing the Womersly number λ .

4.1.2 Analytical Results of Reciprocating Flow and Heat Transfer in the Pipe.

Similarly as in channel flow, the main parameters that influence the reciprocating flow and heat transfer in the pipe that are found in the solution of momentum and energy equations are: Womersly number λ , dimensionless amplitude of fluid displacement A_o , Prandtl number Pr and the ratio of distance to diameter x/D . The parameters ranges used in calculations are:

Womersly number	λ	1 - 12
Dimensionless amplitude of fluid displacement	A_o	5 - 35
Prandtl number	Pr	0.7
The ratio of distance to diameter	x/D	1 - 60

Firstly, the effect of oscillation on the velocity profile will be discussed. Figs.4.13 and 4.14 are drawn for a half cycle π because of similarity between two halves of cycle. Fig.4.13 illustrates the variation of dimensionless velocity u^+ along a half cycle π , with step between each time and other equal to 30° . The values of the controlling parameters are fixed as ($\lambda=8$, $A_o=15$, $Pr=0.7$ and $x/D=30$). It is clear from this figure that (i) The clear effect of oscillation is seemed at the region near the wall.(ii) The particles of fluid in the region near the wall reverse their velocity faster than at the core region.

Fig.4.14 indicates the variation of temporal dimensionless temperature T^+ over a half cycle π with 30° between each time used. The controlling parameters are kept constant ($\lambda=8$, $A_o=15$, $Pr=0.7$ and $x/D=20$). It is clear that for all times the wall temperature is greater than that of other regions because of heating source located at the wall and the low velocity in this region. The effect of reciprocating flow is clearly started at the boundary layer near the wall, while the core region becomes more uniform. The Richardson's annular effect of oscillation has a common effect on both velocity and temperature distribution. These variation in the temperature distribution may be useful in a special applications.

The trends of T^+ profiles in different times are similar, the maximum slope of temperature curves at the wall and zero at the center. The discontinuity in the T^+ at the center point for all curves, because of consequence of the obtained analysis (the denominators of a three terms of Eq.3.52 contain the variable r^+ , which goes to infinite at

$r^+=0$). To overcome this discontinuity, the points just very near the center are taken.

The temperature distribution for the reciprocating flow is different from that for steady laminar fully developed flow, since at the certain time the temperature in the core region is greater than the temperature at the region near the wall. This may be attributed to the cooling effect which is different near the wall than from the core due to the velocity behavior.

Figs.4.15 and 4.16 illustrate the effect of Womersly number λ on the dimensionless velocity and temperature distributions respectively at the time $t^+ = 60^\circ$, for constant parameters A_o, Pr and x^+ ($A_o=15$, $Pr=0.7$ and $x/D=30$). These figures show the annular effect of oscillation with increasing the Womersly number λ . The core region becomes wider than the regions near the wall for both u^+ and T^+ at high Womersly number and the annular effect in the velocity profiles makes the boundary layer thinner.

Fig.4.17 presents the variation of dimensionless bulk temperature T_b^+ over a one cycle 2π , for different values of Womersly number ($\lambda=4, 8$ and 12) while the parameters A_o, Pr and x^+ are fixed ($A_o=15$, $Pr=0.7$ and $x/D=30$). It shows that T_b^+ is decreasing with increasing Womersly number, the reason for that is explained in the section 4.1.1. The effect of dimensionless amplitude of fluid displacement A_o on T_b^+ is shown in the Fig.4.18. The behavior can be explained as: T_b^+ is decreasing with increasing A_o , since the increment of A_o means higher flow rate.

Figs.4.19 and 4.20 show the effect of Womersly number λ and dimensionless amplitude of fluid displacement A_o on the instantaneous-local Nusselt number Nu_x . Fig.4.19 illustrates behavior of three curves of Nu_x for three values of Womersly number ($\lambda=4, 8$ and 12), where other controlling parameters are equal to ($A_o=15, Pr=0.7$ and $x^+=30$). The effect of λ on Nu_x of the pipe is similar to effect of λ on Nu_x in the channel which showed in the Fig.4.7. Its also indicates that Nu_x is doubled with varying λ from 4 to 8 or from 8 to 12. The point of discontinuity in the curves is repeated in Nu_x , because of the previous mentioned reason in the section 4.1.1.

The variation of instantaneous-local Nusselt number Nu_x for two values of dimensionless amplitude A_o that equal to (15 and 25) is represented in the Fig.4.20 . The parameters λ, Pr and x/D are kept constant ($\lambda=4, Pr=0.7$ and $x/D=30$). It shows that the variation A_o has no effect on the Nu_x since the flow is fully developed.

The effect of dimensionless distance x/D on the dimensionless temperature of the center T_c^+ is represented in the Fig.4.21. The values of λ, A_o and Pr are fixed ($\lambda=4, A_o=15$ and $Pr=0.7$) and T_c^+ is drawn for three values of x/D ($x^+=20, 25$ and 30). It shows that T_c^+ is increasing with increasing the distance x^+ , due to accumulative heat or energy with axial distance. Basing on this figure indirectly one can conclude that the periodic effect of oscillation is extending to bulk temperature and center temperature and temperature of all radial points. Its shows at the time $\omega t = 0$, the value of T_c^+ is not a maximum, because

of the phase shifting between the temperature and velocity as well as the pressure gradient of driven flow.

Fig.4.22 shows the variation of dimensionless center temperature T_c^+ with Womersly number ($\lambda=4, 6$ and 8), while the other parameters are kept constant ($A_o=15$, $Pr=0.7$ and $x^+=30$). The figure illustrates that the increment of λ leads to decrease the dimensionless central temperature T_c^+ . The reason of this behavior is similar to that affecting the bulk temperature which is mentioned in the section 4.1.1. Also, the figure indicates phase shifting between the maximum or minimum values of T_c^+ for different values of Womersly number because the phase shifting between the temperature and velocity which is affected by varying Womersly number.

Finally, Fig.4.23 illustrates the variation of time average-local Nusselt number \overline{Nu}_x , with Prandtl number at constant A_o and x/D ($A_o=15$ and $x^+=30$) and two values of λ 4 and 8. This figure shows that \overline{Nu}_x is increasing with increasing Prandtl number which is due to the increment in the hydrodynamics diffusivity of the fluid or specific heat capacity.

4.1.3 Analytical Results of Pulsating Flow and Heat Transfer in the Channel.

The analytical solution of momentum and energy equations with previous simplifications and conditions for pulsating flow in the channel, gives the following effecting parameters with chosen range values used for calculations:

Womersly number	λ	1 - 8
Dimensionless amplitude of pressure gradient	γ'	0 - 0.5
Mean Reynolds number	Re_m	≤ 2300
Prandtl number	Pr	0.7
The ratio of distance to hydraulic diameter	x/D_h	1 - 60

The value of Womersly number λ is varied from 1 to 8 to avoid the transition from the laminar to turbulent flow. The magnitude of γ' is taken to be less than 0.5 to avoid the relaminarization phenomena and reversion of the flow^[27]. There is a relation among the parameters λ, A_o, γ' and Re_m used to detect the criteria of transition from laminar to

turbulent in the pulsating flow defined as $\gamma' = \frac{8 A_o \lambda^4}{3 Re_m}$, where $Re_m \leq 2300$ (see Appendix H). Prandtl number is taken to be constant and equal to 0.7 for air. Reynolds number is calculated for the mean velocity (steady state), and it should be less than the critical value of internal flow $Re_m \leq 2300$.

First, the velocity profile is drawn over a half cycle π . Fig.4.24 shows the variation of dimensionless velocity u^+ with step equal to 60° between each time and other. The parameters $\lambda, \gamma', Re_m, Pr$ and x/D_h are kept constant as ($\lambda = 4, \gamma' = 0.3, Re_m = 1200, Pr = 0.7$ and $x/D_h = 20$). The general trend of profiles of u^+ are parabolic shape, this is because the flow has mean velocity which makes the effects of oscillation is not distinct in the low frequencies.

The distribution of dimensionless temperature over a half cycle π for various values of time starting from 0° crank angle and 60° step, is

illustrated in the Fig.4.25. the controlling parameters are equal to: $\lambda = 4$, $\gamma' = 0.3$, $Re_m = 1200$, $Pr = 0.7$ and $x/D_h = 20$. It indicates that the parabolic profile for temperature distribution due to (i) Symmetric boundary conditions (ii) The velocity profile is parabolic (iii) The flow rate has mean value only.

Effect of Womersly number λ on the dimensionless velocity u^+ and temperature T^+ are shown in the Figs.4.26 & 4.27 respectively. Fig.4.26 illustrates the influence of λ ($\lambda=2, 4$ and 10) on u^+ with constant values of parameters ($\gamma' = 0.3$, $Re_m = 1200$, $Pr = 0.7$ and $x/D_h = 30$). The main effect of λ on the u^+ and T^+ are represented by making the core region more uniform (tip of parabolic) with increasing λ .

Figs.4.28, 4.29 & 4.30 show the variation of temporal dimensionless bulk temperature T_b^+ with the parameters λ , γ' and Re_m respectively. Fig.4.28 illustrates the effect of Womersly number λ on T_b^+ during a one cycle 2π , for three values of λ (4, 8 and 12) and the parameters γ' , Re_m , Pr and x/D_h are kept constant ($\gamma' = 0.3$, $Re_m = 1500$, $Pr = 0.7$ and $x/D_h = 20$). The amplitude of T_b^+ is decreased with increasing λ . This behavior occurs because the variation of velocity with varying λ . The mean value of all profiles are stilled constant value and equal to steady value for laminar fully developed convection.

Fig.4.29 shows the variation of dimensionless bulk temperature T_b^+ over a one cycle 2π for different value of ratio of amplitude to steady pressure gradient γ' ($\gamma' = 0.1, 0.3$ & 0.5), while the other

controlling parameters are remained constant as ($\lambda = 4$, $Re_m = 1200$, $Pr = 0.7$ & $x/D_h = 30$). The amplitude of T_b^+ is increased with increasing γ' . This can be explained as: the increment of γ' means increasing or decreasing the magnitude of pressure gradient (periodically change with time), which leads to large cyclic difference in the thickness of boundary layer which produces from the variation the velocity with varying γ' . The mean value of T_b^+ is remained constant and equal to steady value because Reynolds number is kept constant.

Fig.4.30 illustrates the effect of mean Reynolds number Re_m on the dimensionless bulk temperature T_b^+ during a one cycle 2π , at constant parameters λ , γ' , Pr and x/D_h ($\lambda = 4$, $\gamma' = 0.3$, $Pr = 0.7$ & $x/D_h = 30$). The values of mean Reynolds number are: 1000, 1500 & 2000. The increment of mean Reynolds number makes the mean value of dimensionless bulk temperature T_b^+ to be decreased. This behavior occurs because increasing the velocity with increasing Re_m , which causes decrement in T_b^+ .

Fig.4.31 shows the effect of Womersly number λ on the instantaneous-local Nusselt number Nu_x over a one cycle 2π at constant controlling parameters γ' , Re_m , Pr & x/D_h are ($\gamma' = 0.3$, $Re_m = 1500$, $Pr = 0.7$ & $x/D_h = 20$), while $\lambda = 2, 4$ and 8 . It illustrates that the time average of Nu_x is not affected by the variation frequency of pulsation and it is equal to the value of steady laminar fully developed flow for the channel with width \gg height which equal to $8.235^{[20]}$. The amplitude of Nu_x is decreased with increasing λ . This

behavior occurs because the variation of thickness of boundary layer with varying λ , hence the thermal resistance.

Fig.4.32 shows the effect of ratio of amplitude to steady pressure gradient γ' ($\gamma'=0.1, 0.3$ & 0.5), on the instantaneous-local Nusselt number Nu_x during a one cycle 2π , while the other controlling parameters are kept constant ($\lambda = 4$, $Re_m = 1500$, $Pr = 0.7$ & $x/D_h = 20$). The amplitude of Nu_x is increased with increasing γ' due to increase or decrease the magnitude of pressure gradient (periodically change with time), which leads to large periodically difference in the thickness of boundary layer which produces from the variation the velocity with varying γ' .

Fig.4.33 shows the variation of instantaneous-local Nusselt number Nu_x during a one cycle for different values of Prandtl number ($Pr=0.1, 0.7$ & 10). The other controlling parameters are kept constant ($\lambda = 4$, $\gamma' = 0.3$, $Re_m = 1500$ & $x/D_h = 20$). It is shown that the amplitude of Nu_x is decreased with increasing Prandtl number because of increasing hydrodynamics diffusion or decreasing the specific heat capacity.

Figs.4.34 & 4.35 show the effect of Womersly number λ and the ratio of amplitude to steady pressure gradient γ' on the time-averaged bulk temperature \bar{T}_b^+ , respectively. Fig.4.34 illustrates that the increment of λ has no effect on \bar{T}_b^+ for the values of λ greater than 2, while the percent of enhancement reaches to 4% for values of λ less than 2.

Fig.4.35 illustrates the effect of the ratio of amplitude to steady pressure gradient γ' on the time-averaged bulk temperature \overline{T}_b^+ . It can be noticed that \overline{T}_b^+ is constant with varying γ' . The reason of this behavior may be attributed to the fluctuation of T_b^+ about mean value with varying γ' Fig.4.29.

Figs.4.36 & 4.37 indicate the variation of \overline{Nu}_x with λ and γ' respectively, with kept other parameters constant. Fig.4.36 illustrates the variation of \overline{Nu}_x with Womersly number, which shows the enhancement reaches to only 2% for λ less than 2. Fig.4.37 shows the variation of \overline{Nu}_x with γ' , which illustrates that \overline{Nu}_x is not varying with γ' .

Fig.4.38 shows the variation of instantaneous-local Nusselt number Nu_x during a one cycle for different values of mean Reynolds number ($Re_m = 1000, 1500$ & 2000). The other controlling parameters are kept constant ($\lambda = 4, \gamma' = 0.3, Pr = 0.7$ & $x/D_h = 20$). It indicates that there is no effect for mean Reynolds number on Nu_x , because of the flow is fully developed.

4.1.4 Analytical Results of Pulsating Flow and Heat Transfer in the Pipe.

Both energy equation and momentum equations are solved for pulsating flow in the horizontal pipe to give the velocity and temperature distributions as given in Eqs.3.105 & 3.126 respectively, and the following controlling parameters together with the chosen range values of these parameters are used for calculation:

Womersly number	λ	1 - 8
Dimensionless amplitude of pressure gradient	γ'	0-0.5
Mean Reynolds number	Re_m	≤ 2300
Prandtl number	Pr	0.7
The ratio of distance to diameter	x/D	1 - 60

The values of λ , γ' , Re_m , Pr & x/D that it is used in this section have a similar considerations as in section 4.1.3, but the criteria of transition from laminar to turbulent becomes $\gamma' = \frac{A_o \lambda^4}{4 Re_m}$, where $Re_m \leq 2300$ (see Appendix I).

Figs.4.39 & 4.40 show the distribution of dimensionless velocity u^+ and dimensionless temperature T^+ over a half cycle π with time step equal to 60° between each other. The controlling parameters are equal to: $\lambda = 4$, $\gamma' = 0.3$, $Re_m = 1200$, Pr = 0.7 and $x/D = 40$. The general behavior of these figures are similar to that of the pulsating flow in the channel (section 4.1.3), except the difference in the maximum value at the tip of parabolic profiles, due to the difference in the geometry. These figures show discontinuity in the center of pipe, because of the consequence of the used analysis.

Effect of Womersly number λ on the dimensionless velocity u^+ and temperature T^+ are shown in the Figs.4.41 & 4.42 respectively. Fig.4.41 illustrates the influence of λ ($\lambda=2, 4$ and 8) on u^+ at $\omega t = 60^\circ$ with constant values of parameters ($\gamma' = 0.3$, $Re_m = 1200$, Pr = 0.7 and $x/D_h = 40$). The main effect of λ is represented by making the core region more uniform (tip of parabolic) with increasing λ . Fig.4.42

indicates the influence of λ on the dimensionless temperature profile T^+ at $\omega t = 60^\circ$. It shows that the core region is affected by the pulsating flow at high frequency or λ because the varying of velocity with increasing Womersly number.

Figs.4.43 illustrates the effect of Womersly number λ on the instantaneous dimensionless bulk temperature T_b^+ for constant controlling parameters ($\gamma' = 0.3$, $Re_m = 1000$, $Pr = 0.7$ and $x/D = 30$), where λ equal to 2, 4 and 8. It shows that the amplitudes of T_b^+ are increased with decreasing the Womersly number λ , while the mean value is constant. The reason of this behavior is similarly explained in the section 4.1.3.

The effect of dimensionless amplitude of pressure gradient γ' on the T_b^+ is represented in Fig.4.44. the parameters are equal to ($\lambda = 4$, $Re_m = 1000$, $Pr = 0.7$ and $x/D = 30$), while γ' is taken the values 0.1, 0.3 and 0.5. This figure is similar to Fig.4.29 for pulsating flow in the channel except the difference in the magnitude of T_b^+ because the difference between the parameters of pulsating flow in the channel and pipe.

Fig.4.45 indicates the variation of the instantaneous-local Nusselt number Nu_x with Womersly number $\lambda=2, 4$ & 8 , while the other parameters γ' , Re_m , Pr & x/D are kept constant (where: $\gamma' = 0.3$, $Re_m = 1000$, $Pr = 0.7$ and $x/D = 30$). It shows that the amplitude of Nu_x is decreased with increasing Womersly number, while the mean value remains constant. This is owing to increase the diffusivity with increasing Womersly number which makes the temperature field more

uniform. In general the pulsating of flow has no effect on the mean value of Nu_x , as it is observed in Fig.4.45 the average value of Nu_x is equal to 4.364 as in steady flow in the pipe.

Fig.4.46 shows the variation of instantaneous-local Nusselt number Nu_x during a one cycle for different values of Prandtl number (Pr=0.1, 0.7 & 10). The other controlling parameters are kept constant ($\lambda = 4$, $\gamma' = 0.3$, $Re_m = 1000$ & $x/D = 30$). This figure shows that the amplitude of Nu_x is decreased with increasing Prandtl number.

The effect of dimensionless amplitude of pressure gradient γ' on the instantaneous-local Nusselt number Nu_x is presented in Fig.4.47. the parameters λ , Re_m , Pr & x/D are kept constant ($\lambda = 4$, $Re_m = 1000$ Pr=0.7 & $x/D = 30$). The increment of γ' increase the amplitude of Nu_x , which explains by increasing the pressure gradient with γ' . The mean value of Nu_x is constant and equal to 4.364.

The variation of time-averaged bulk temperature \bar{T}_b^+ with λ and γ' for different values of mean Reynolds number $Re_m = 1000, 1500$ & 2000 , are shown in Figs.4.48 & 4.49 respectively. The parameters λ or γ' , Pr & x/D are fixed ($\lambda = 4$ or $\gamma' = 0.3$, Pr=0.7 & $x/D = 30$). Its show that there is no effect of λ or γ' on \bar{T}_b^+ , while \bar{T}_b^+ is decreased with increasing Reynolds number.

Fig.4.50 shows the influence of Womersly number on the time averaged-local Nusselt number $\overline{Nu_x}$ for different values of mean Reynolds number Re_m with the other parameters are kept constant

($\gamma' = 0.3$, $Pr = 0.7$ & $x/D = 30$). This figure illustrates that both the mean Reynolds number and Womersly number have no effect on \overline{Nu}_x .

Fig.4.51 shows the variation of \overline{Nu}_x with γ' for various values of Re_m and constant λ , Pr & x/D ($\lambda = 4$, $Re_m = 1500$ $Pr = 0.7$ & $x/D = 30$). It is clear from this figure that, there is a decrement in \overline{Nu}_x with increasing γ' , which equal to 0.5%, which is not important from the practical point of view.

4.2 Numerical Solution for Checking the Analytical Model.

The numerical solution based on the finite volume method has the following considerations:

- 1- The solution of the general form of the governing equations is done by iteration method (see Appendix J).
- 2- The weighting parameters θ is taken for explicit method $\theta = 0$.
- 3- The area of the four sides of control volume are equal $A_s = A_n = A_w = A_e$ for 2D or $A_s = A_n$ for 1D.
- 4- The steps of the time chosen is equal to 0.001 second.
- 5- The criteria of convergence for both calculations of velocity and temperature is equal to 1×10^{-4} .
- 6- The small value of dr^+ , dy^+ and dx^+ are taken equal in both sides of point P (i.e. $\delta y_{PN} = \delta y_{SP}$, $\delta r_{PN} = \delta r_{SP}$).

The discussion of the numerical results is divided into four sections depending on the type of flow and duct shape.

4.2.1 Numerical Results of the Reciprocating Flow in the Channel.

Eq.3.5 is solved numerically using the finite volume method to give the general form of F.V.M which is defined in Eq.3.131 with $dy^+ = 0.05$ and the number of nodes equal to 21 at the $\omega t = 0.05$. The controlling parameters are: $\lambda = 4$, $A_o = 15$ $Pr = 0.7$ & $x/D_h = 20$. Fig.4.52 shows the analytical and numerical solution of Eq.3.5, which gives a very good agreement. Fig.4.53 illustrates the analytical and numerical solution of T^+ (solution of Eq.3.13) for controlling parameters as: $\lambda = 4$, $A_o = 15$ $Pr = 0.7$ & $x/D_h = 20$. This figure shows a very good identification between analytical and numerical model. It is shown that in the region near the wall a less agreement is obtained, because of the annular effect or the oscillation flow which is occurred in the region nearest to the wall.

4.2.2 Numerical Results of the Reciprocating Flow in the Pipe.

Eq.3.32 is solved numerically using F.V.M to give a general form of finite volume method as in Eq.3.135. The number of nodes of domain are 21, and the controlling parameters are: $\lambda = 4$, $A_o = 15$ $Pr = 0.7$ & $x/D = 20$ at the time $\omega t = 0.05$. Fig.4.54 illustrates the analytical and numerical solution of u^+ . It indicates that there is a very good agreement between both solutions.

The numerical solution of Eq.3.43 is represented in the Eq.3.141. The solution is based on 21x30 nodes, at the time $\omega t = 0.05$ for parameters as: $\lambda = 4$, $A_o = 15$ $Pr = 0.7$ & $x/D = 20$. Fig.4.55 shows the checking of analytical solution with numerical solution of T^+ , which gives a good identification.

4.2.3 Numerical Results of the Pulsating Flow in the Channel.

The momentum equation (Eq.59) is solved numerically to obtain a general form of finite volume solution Eq.3.146. The domain is divided into 20 node and the parameters used are: $\lambda = 4$, $\gamma' = 0.3$, $Re_m = 1500$, $Pr=0.7$ & $x/D_h = 20$ at the time $\omega t = 0.10$. The comparison between analytical and numerical solution of u^+ are shown in the Fig.4.56 which yields an excellent agreement.

Eq.3.70 is transformed to the general form of finite volume method and expressed by Eq.3.148. The calculation was done using controlling parameters : $\lambda = 4$, $\gamma' = 0.3$, $Re_m = 1500$, $Pr=0.7$ & $x/D_h = 30$ at the time $\omega t = 0.40$. The domain is divided into 20x30 nodes. Fig.4.57 shows the comparison between the analytical and numerical solution of T^+ , which gives a reasonable agreement between them.

4.2.4 Numerical Results of the Pulsating Flow in the Pipe.

The general form of numerical solution of Eq.3.94 is represented in Eq.3.150. The domain has 20 node and the parameters used in the calculation are equal to: $\lambda = 4$, $\gamma' = 0.3$, $Re_m = 1000$, $Pr=0.7$ & $x/D = 30$ at the time $\omega t = 0.05$. Fig.4.58 shows excellent identification between numerical and analytical solution of Eq.3.94.

The temperature distribution T^+ is obtained from numerical solution the general finite volume form given by Eq.3.154. The domain has 20x30 nodes and the parameters used for calculation are equal to: $\lambda = 4$, $\gamma' = 0.3$, $Re_m = 1000$, $Pr=0.7$ & $x/D = 31$ at the time $t^+ = 0.05$.

Fig.4.59 shows the comparison between the analytical and numerical solution of temperature distribution, which gives a good agreement between them.

4.3 Comparison of the New Model with Experimental Results of Other Authors

In order to demonstrate the validity of the present analytical model, a comparison between the experimental work for other authors and the new model is carried out. The main parameters that used in the comparison are: time averaged-local Nusselt number \overline{Nu}_x and space-cycle averaged Nusselt number \overline{Nu} . Because of non identification between the parameters of a new model and the works that is used for comparison, the parameters are simplified.

Heat transfer in reciprocating flow in the channel of the new model is compared with experimental investigation for convective heat transfer in a rectangular duct heated from the below and subjected to a periodic flow, which is investigated by Copper et al. and cited by Zhao and Cheng^[7]. This experimental work was done for turbulent flow and the results were correlated by suitable relation for \overline{Nu} and since no experimental work done for laminar flow therefore the comparison will be made at critical oscillatory parameter β_{cri} only. The parameter that used in the comparison is space-cycle averaged Nusselt number \overline{Nu} which is defined in Eq.2.27. Fig.4.60 shows this comparison between the value of \overline{Nu} obtained from the new model and with the experimental correlation obtained by Copper et al.^[7] for various values of Womersly number. The behavior of the results obtained from both

work have a similar trend, the observed difference between them may be attributed the flow region that used in the experimental correlation (transition and turbulent regions).

Analytical solution of a new model for heat transfer in the reciprocating flow in the pipe is compared also with the study for oscillatory heat transfer in a pipe subjected to a laminar reciprocating flow investigated by Zhao and Cheng^[34]. The values of kinetic Reynolds number is varied from 23 to 464 and A_o is varied from 8.54 to 34.9 and $L/D=44.8$ and the fluid used for comparison is air. Fig.4.61 illustrates this comparison for \overline{Nu} against Womersly number for both the present analytical solution and the experimental correlation defined in the Eq.2.31 which gives a qualitative reasonable agreement. The difference between the two curves may be attributed to that, the correlation of experimental data based on conjugate heat transfer (convection in the fluid and conduction in the tube) in which the temperature at outer wall is used instead of at the inner wall which is equal to fluid temperature, while the present study is made for convection in the fluid only.

The solution of pulsating flow in the channel for the new model is compared using the heat transfer enhancement factor $\frac{\overline{Nu}_p}{\overline{Nu}_s}$ which defined as the ratio between time-averaged Nusselt number for pulsating flow to time-averaged Nusselt number for steady flow which is obtained by Moon et al.^[48]. Fig. 4.62 shows a good agreement between the analytical results and experimental results for fully developed laminar flow, Reynolds number equal to 700, the ratio of amplitude of fluctuate to steady velocity equal to 0.2 and different frequencies (hence

the standard deviation of $\frac{\overline{Nu_p}}{\overline{Nu_s}}$ is 0.061). Also the curve shows the fluctuating of the experimental results about the analytical results of a new model.

The analytical solution of a new model for pulsating flow in the pipe is compared with experimental study for convective heat transfer characteristics of laminar pulsating flow pipe air flow by Habib et al^[45]. The parameter of comparison is the relative mean Nusselt number Nu_r ,

which is defined as $Nu_r = \frac{Nu_{pm}}{Nu_{om}}$, where Nu_{pm} : is the pulsated mean

Nusselt number and Nu_{om} : is the mean Nusselt number without pulsation. The range of mean Reynolds number used are from 780 to 1366, and Stokes number Ω is in the range from 12 to 17.5 where

$\Omega = \frac{D}{2} \sqrt{\frac{\omega}{2\nu}}$. The relative mean Nusselt number defined in Eq.2.34b is

used for comparison. The values used for calculation are $\gamma' = 0.5$, $Pr = 0.7$, $Re_m = 1000$ for various values of λ . Fig.4.63 shows that Nu_r is remained constant and equal to 1 for the present analytical solution of a new model while Nu_r for experimental works of Habib et al. ^[45] is fluctuated about 1 (increased or decreased relative to 1), where the standard deviation of Nu_r is 0.114.

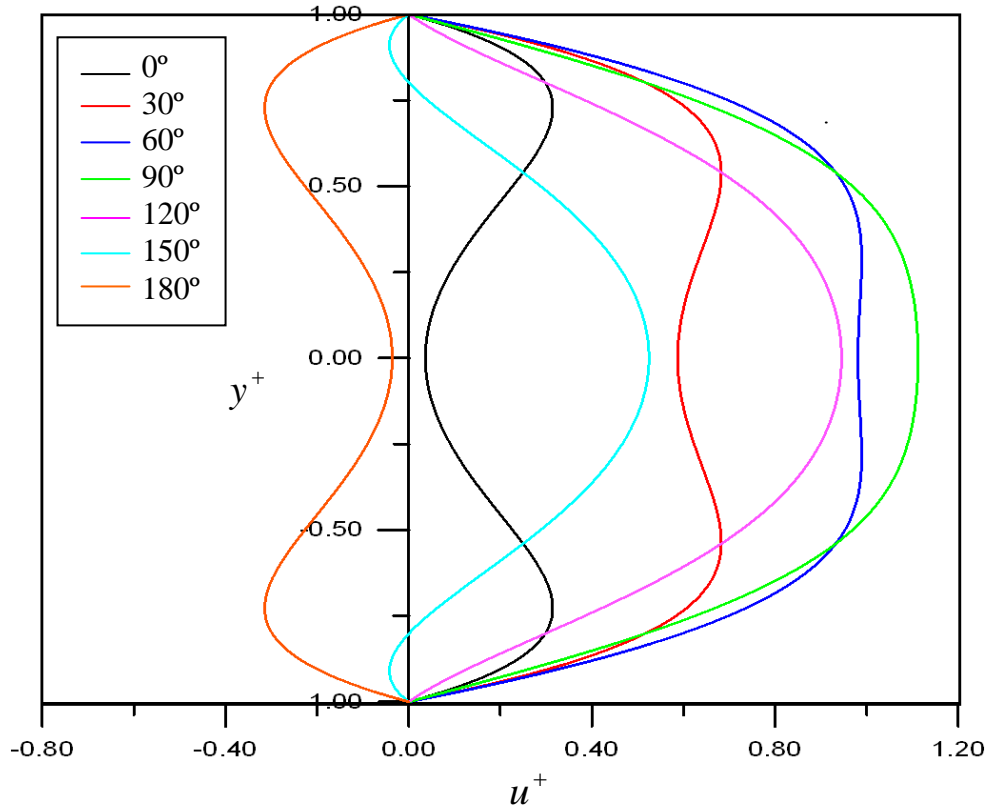


Fig.4.1 The Variation of the dimensionless velocity profile for $\lambda=4$, $A_o=15$, $Pr=0.7$ and $x/D_h=20$. (Reciprocating flow in the channel)

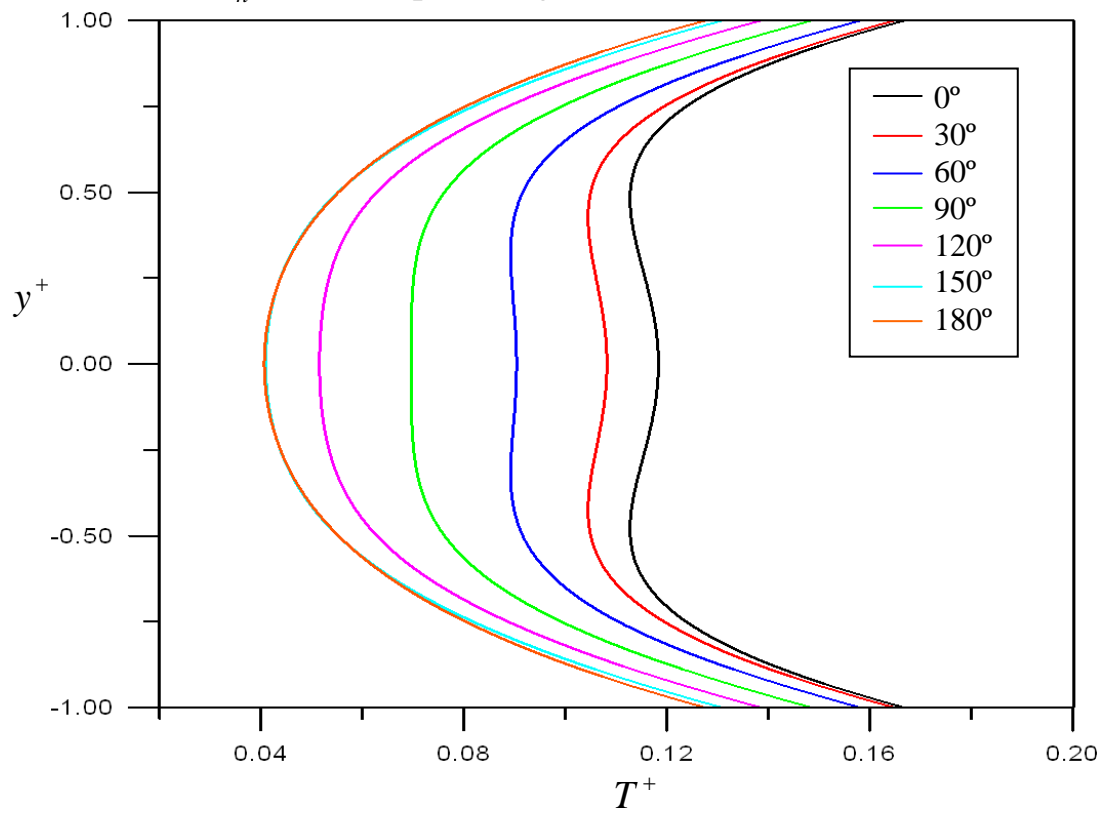


Fig.4.2 The Variation of the dimensionless temperature profile for $\lambda=4$, $A_o=15$, $Pr=0.7$ and $x/D_h=20$. (Reciprocating flow in the channel)

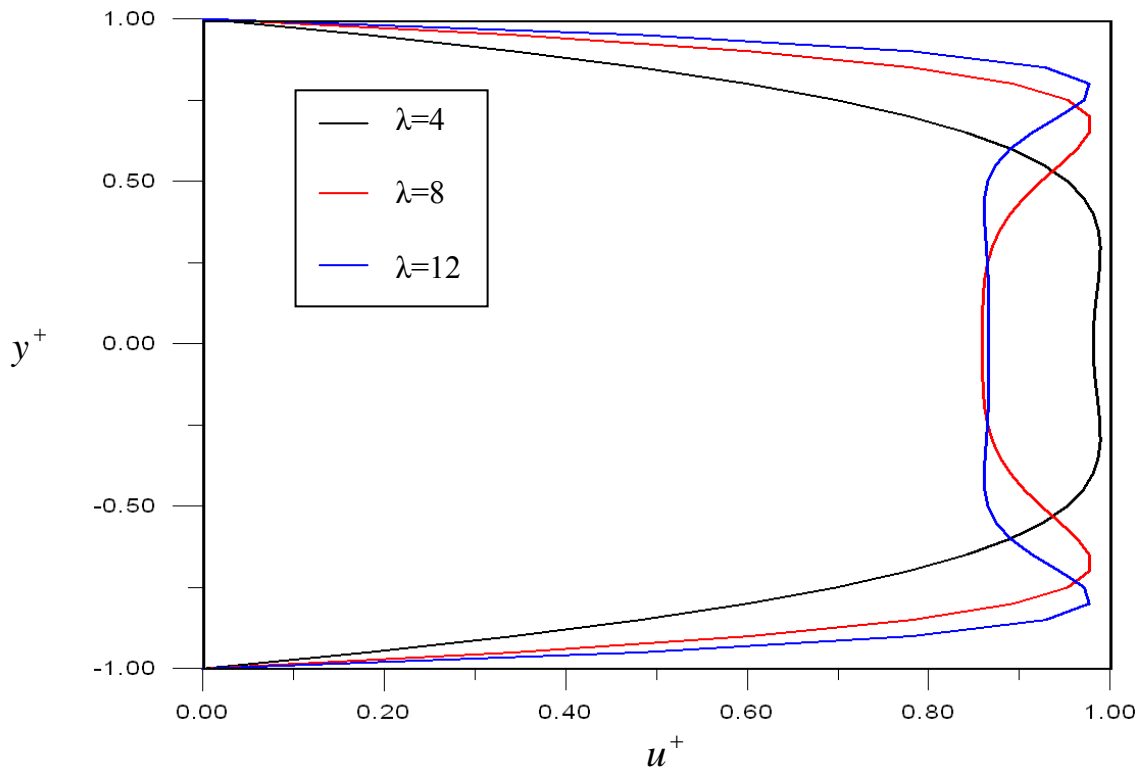


Fig.4.3 The Effect of Womersly number λ on the dimensionless velocity profile at $\omega t=60^\circ$, for $A_o=15$, $Pr=0.7$ and $x/D_h=20$. (Reciprocating flow in the channel)

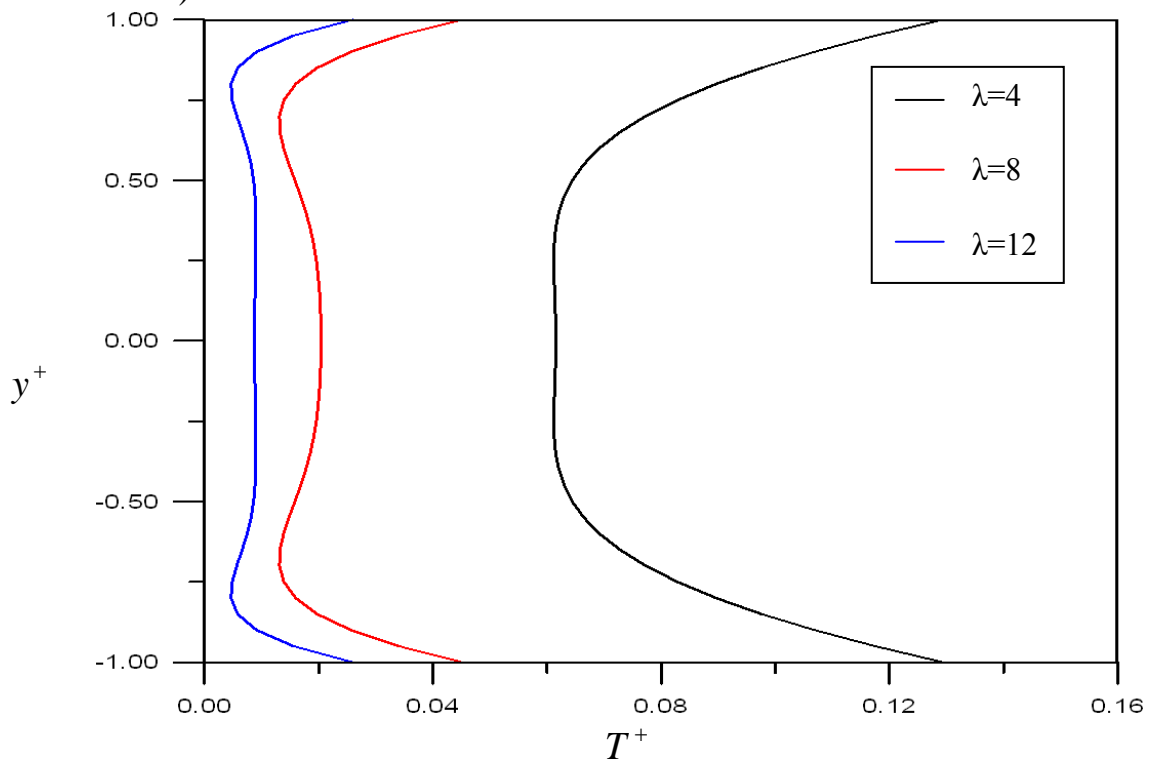


Fig.4.4 The Effect of Womersly number λ on the dimensionless temperature profile at $\omega t=60^\circ$, for $A_o=15$, $Pr=0.7$ and $x/D_h=20$. (Reciprocating flow in the channel)

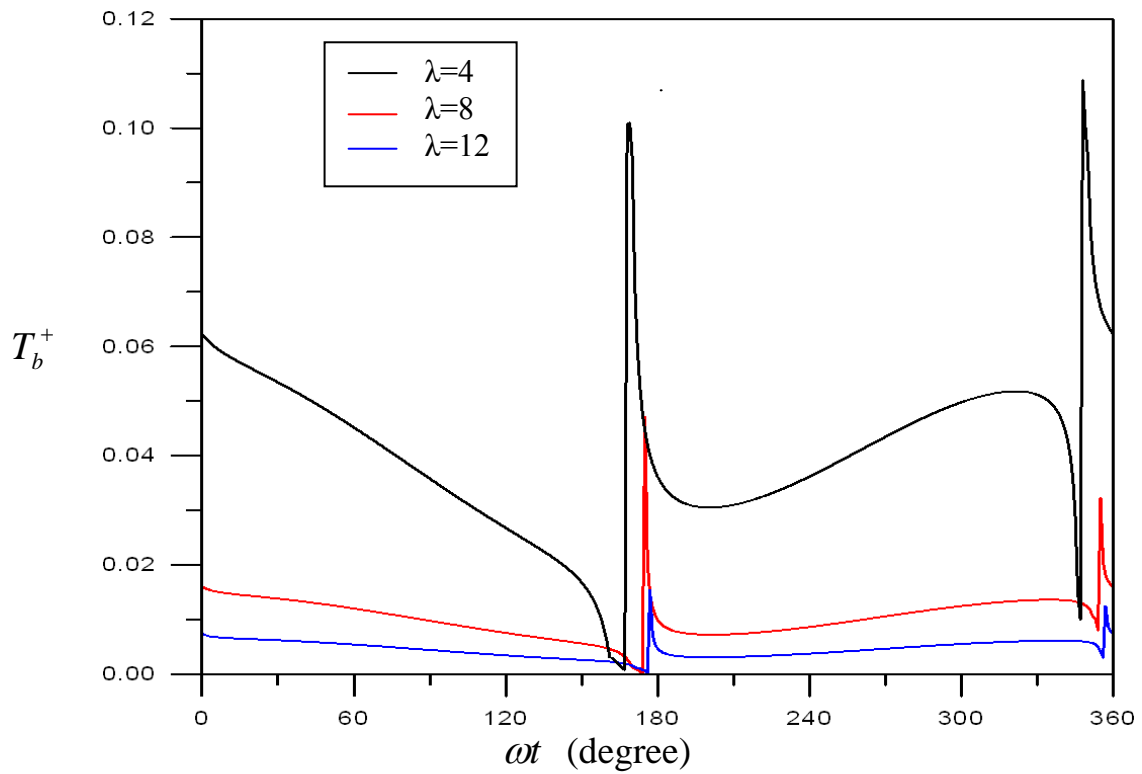


Fig.4.5 The Effect of Womersley number λ on the instantaneous dimensionless bulk temperature at $A_o=15$, $Pr=0.7$ and $x/D_h=20$. (Reciprocating flow in the channel)

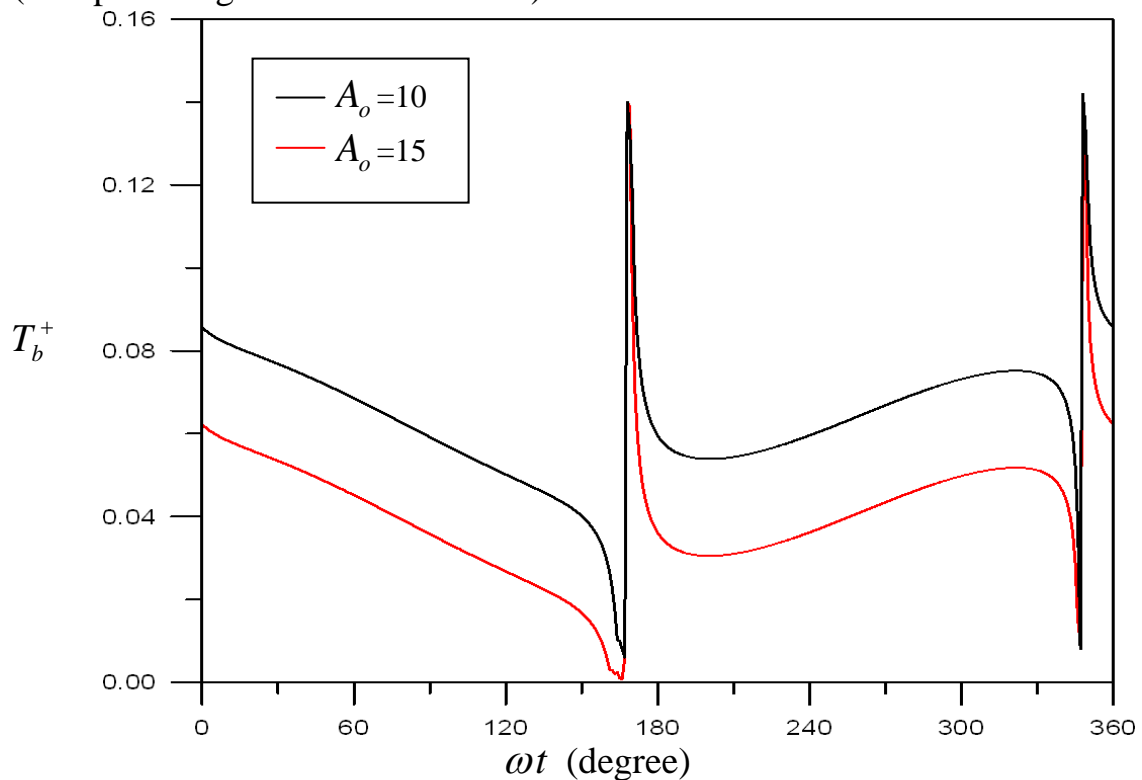


Fig.4.6 The Effect of dimensionless amplitude of fluid displacement on the instantaneous dimensionless bulk temperature at $\lambda=4$, $Pr=0.7$ and $x/D_h=20$. (Reciprocating flow in the channel)

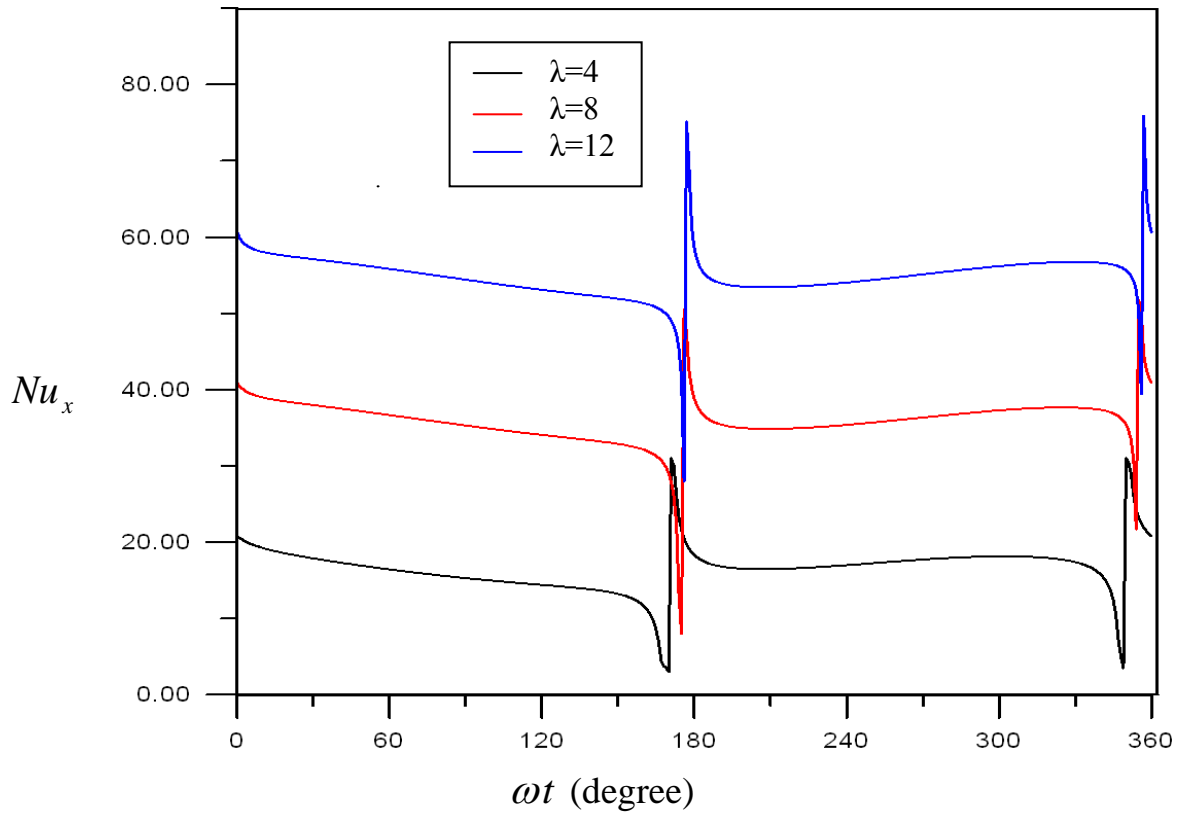


Fig.4.7 The Effect of Womersley number on the instantaneous-local Nusselt number at $A_o=15$, $Pr=0.7$ and $x/D_h=20$. (Reciprocating flow in the channel)

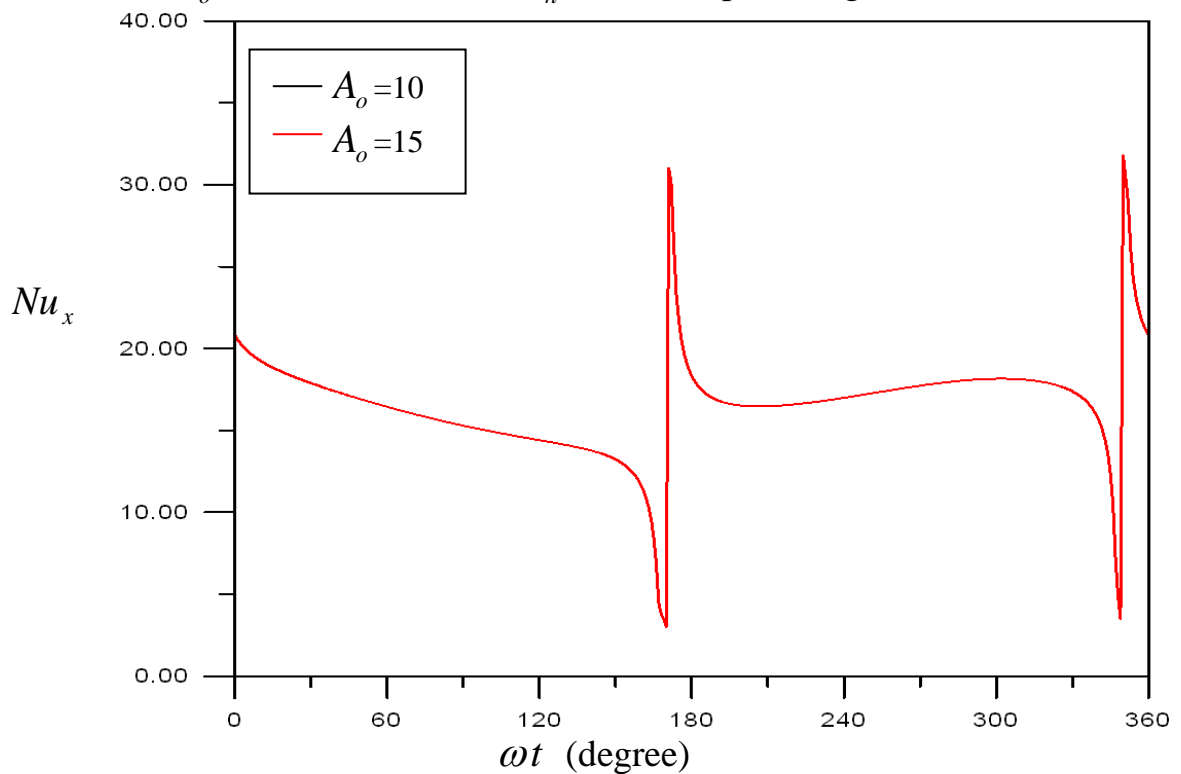


Fig.4.8 The Effect of dimensionless amplitude of fluid displacement on the instantaneous-local Nusselt number at $\lambda=4$, $Pr=0.7$ and $x/D_h=20$. (Reciprocating flow in the channel)

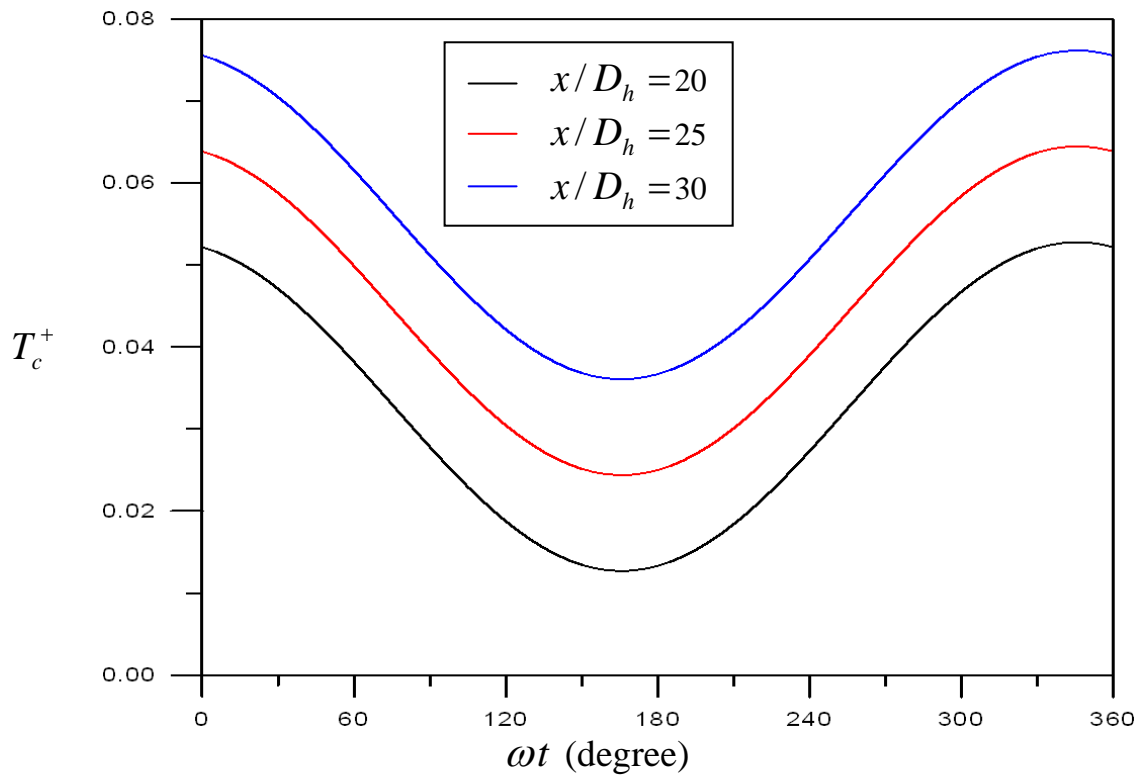


Fig.4.9 The Effect of ratio of the distance to the hydraulic diameter on the instantaneous dimensionless center temperature at $\lambda=4, A_o=15$ and $Pr=0.7$. (Reciprocating flow in the channel)

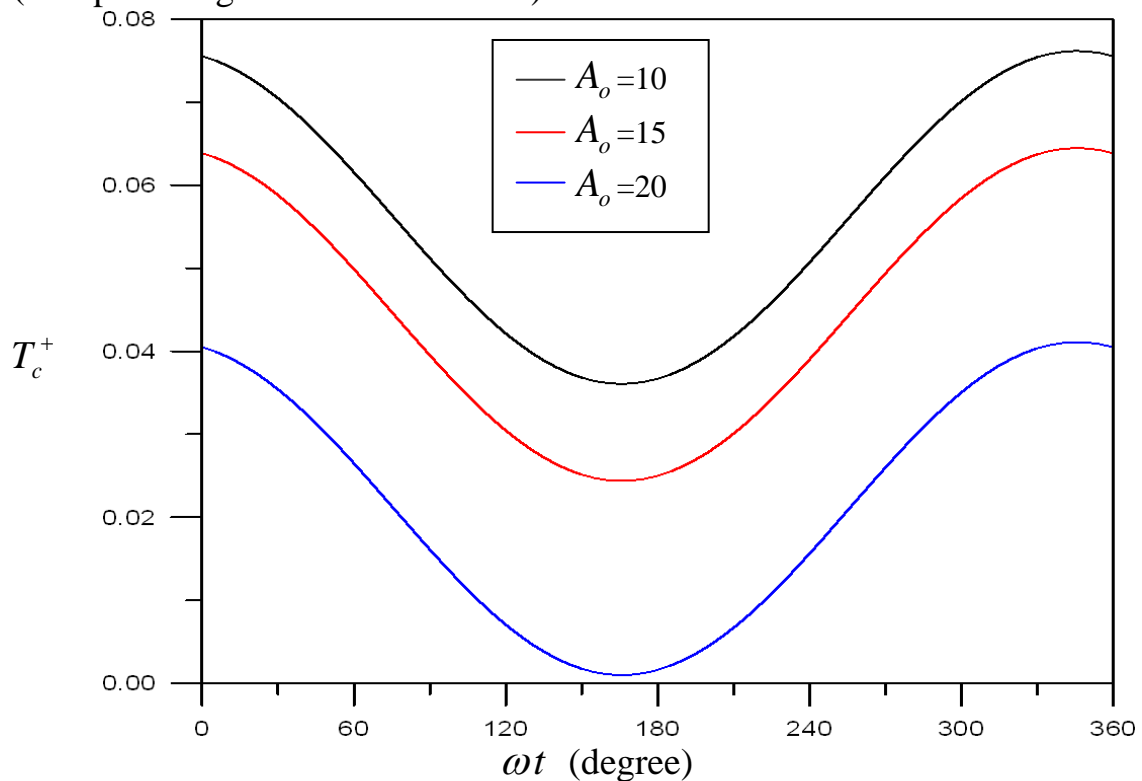


Fig.4.10 The Effect dimensionless amplitude of fluid displacement on the instantaneous dimensionless center temperature at $\lambda=4, Pr=0.7$ and $x/D_h = 20$. (Reciprocating flow in the channel)

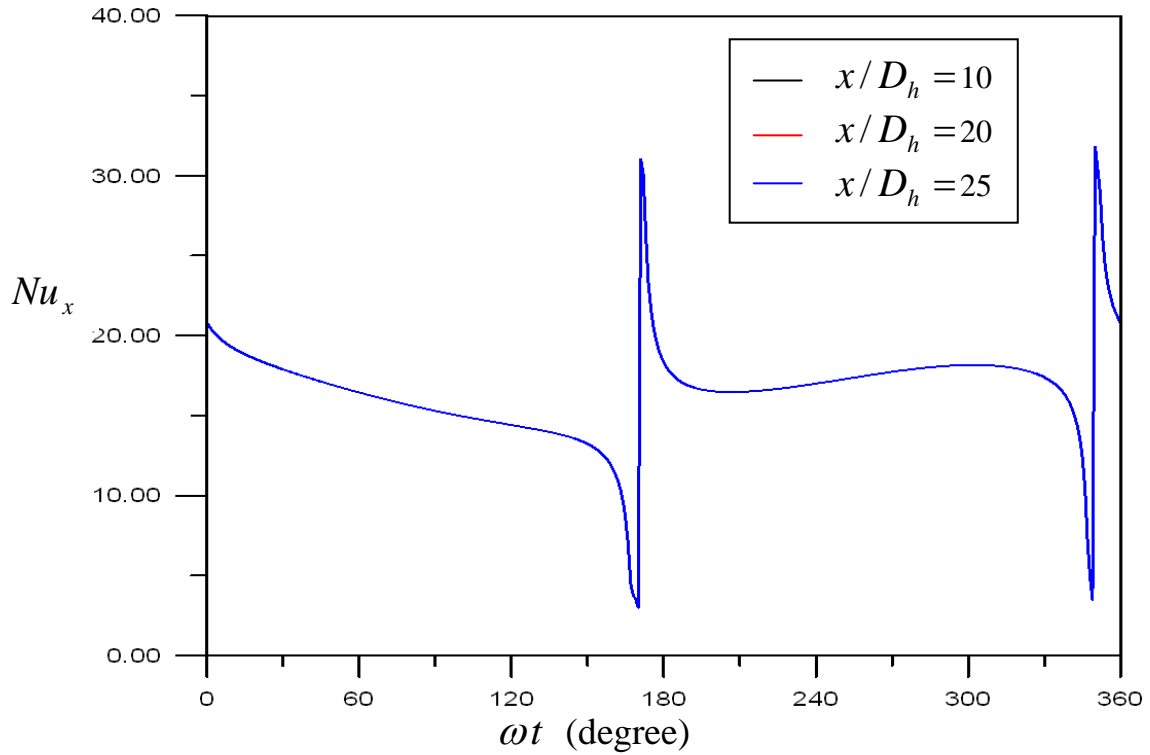


Fig.4.11 The Effect of ratio of the distance to the hydraulic diameter on the instantaneous-local Nusselt number at $\lambda=4$, $A_o=15$ and $Pr=0.7$. (Reciprocating flow in the channel)

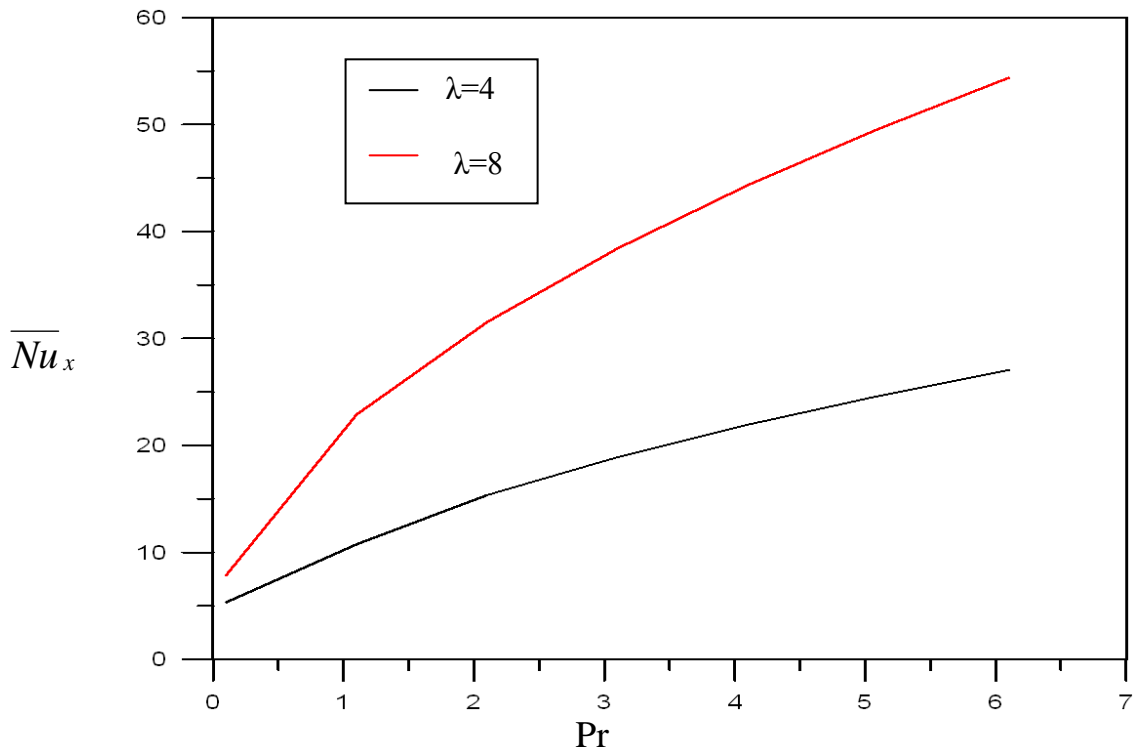


Fig.4.12 The Effect of Prandtl number on the time averaged-local Nusselt number at $\lambda=4$ and 8 , for $A_o=15$ and $x/D_h=20$. (Reciprocating flow in the channel)

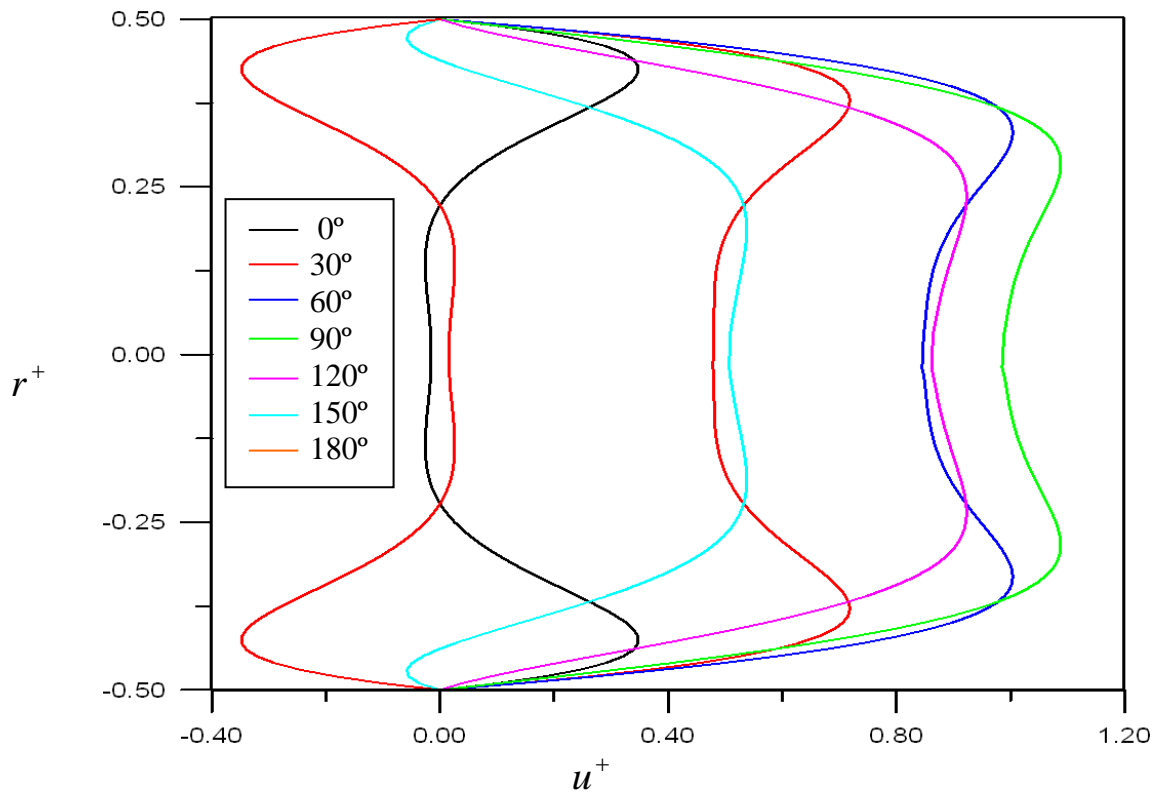


Fig.4.13 The Variation of dimensionless velocity profile for $\lambda=8$, $A_o = 15$, $Pr=0.7$ and $x/D=30$. (Reciprocating flow in the pipe)

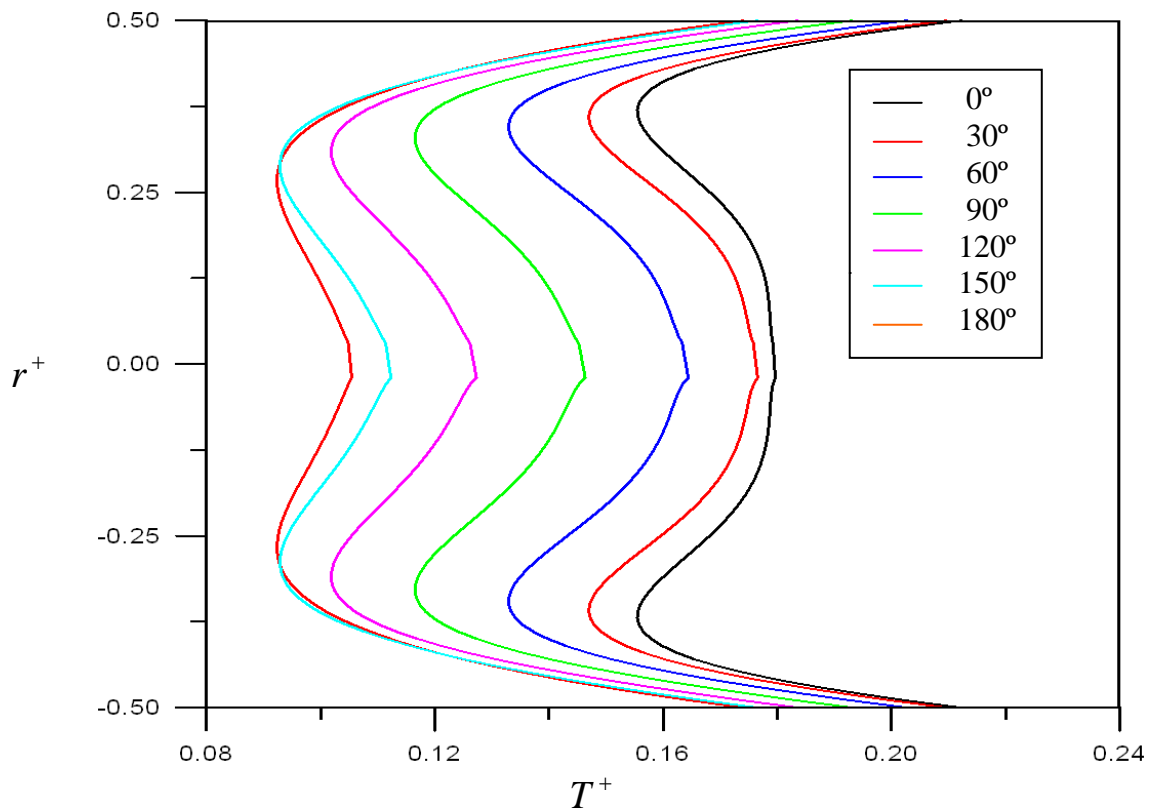


Fig.4.14 The Variation of dimensionless temperature profile for $\lambda=8$, $A_o = 15$, $Pr=0.7$ and $x/D=30$. (Reciprocating flow in the pipe)

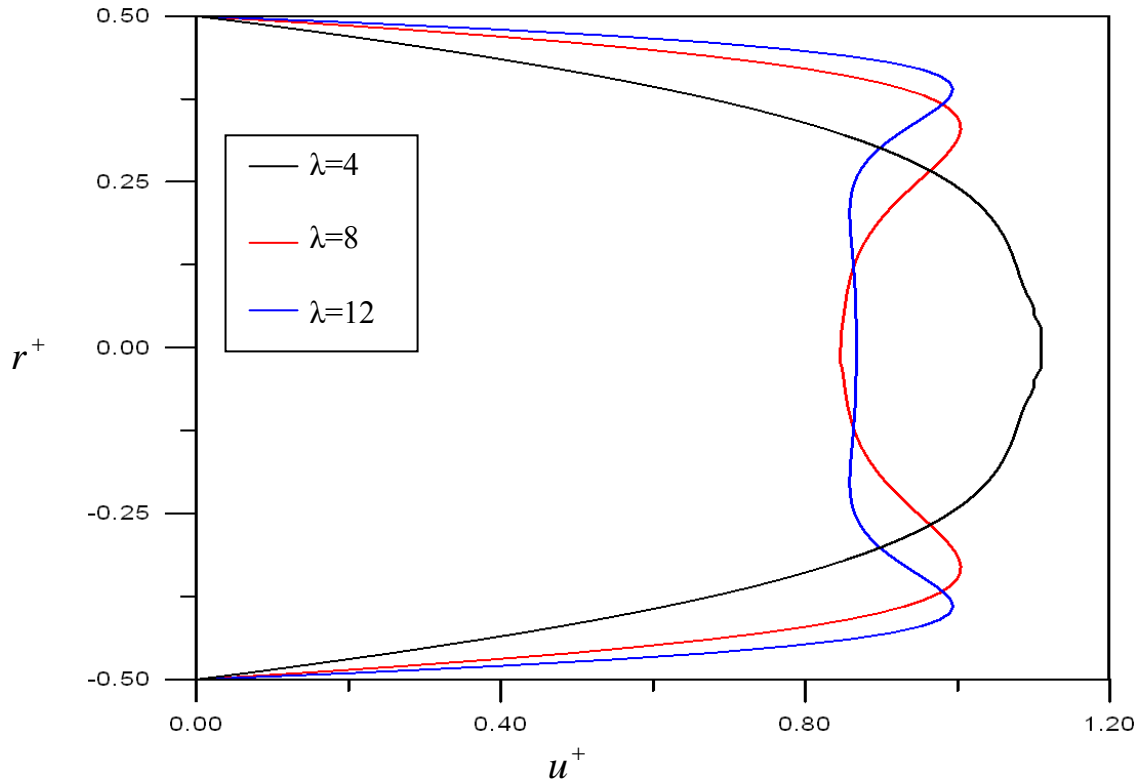


Fig.4.15 The Effect of Womersly number on the dimensionless velocity profile at the time $t^+ = 60^\circ$, for $A_o = 15$, $Pr=0.7$ and $x/D=30$. (Reciprocating flow in the pipe)

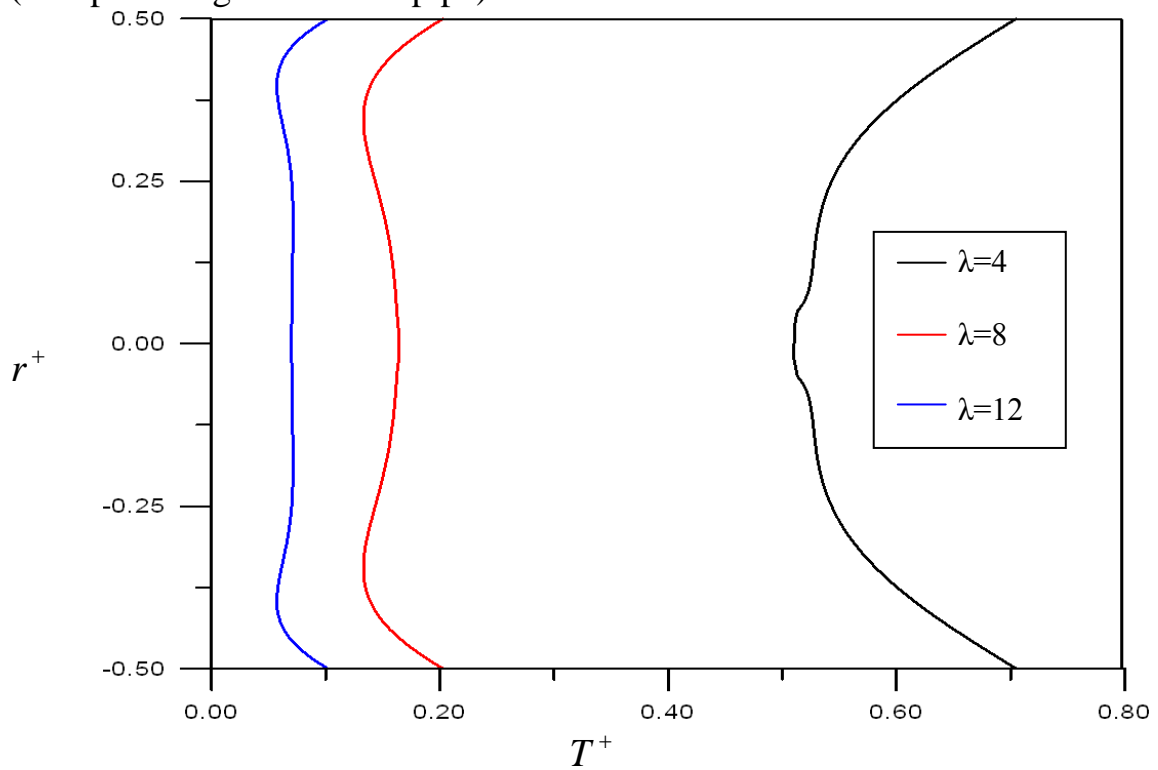


Fig.4.16 The Effect of Womersly number on the dimensionless temperature profile a the time $t^+ = 60^\circ$, for $A_o = 15$, $Pr=0.7$ and $x/D=30$. (Reciprocating flow in the pipe)

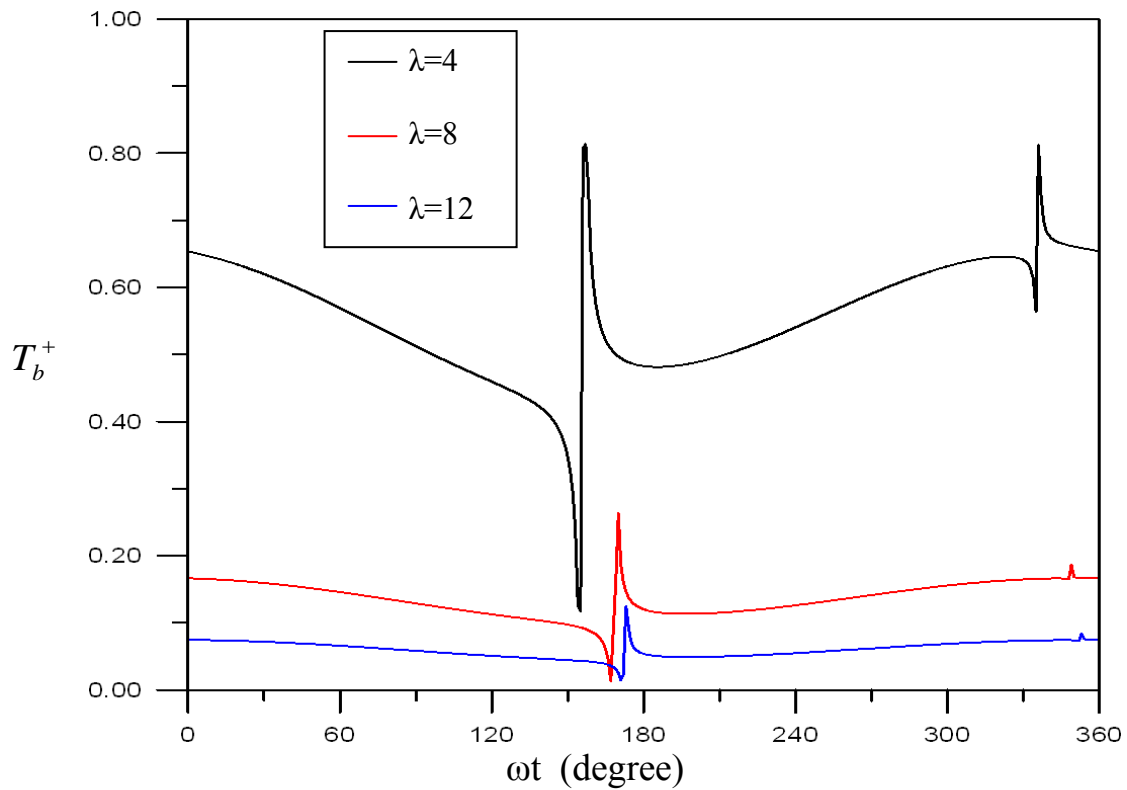


Fig.4.17 The temporal variation of instantaneous bulk temperature for various values of Womersly number at $A_o = 15$, $Pr=0.7$ and $x/D=30$. (Reciprocating flow in the pipe)

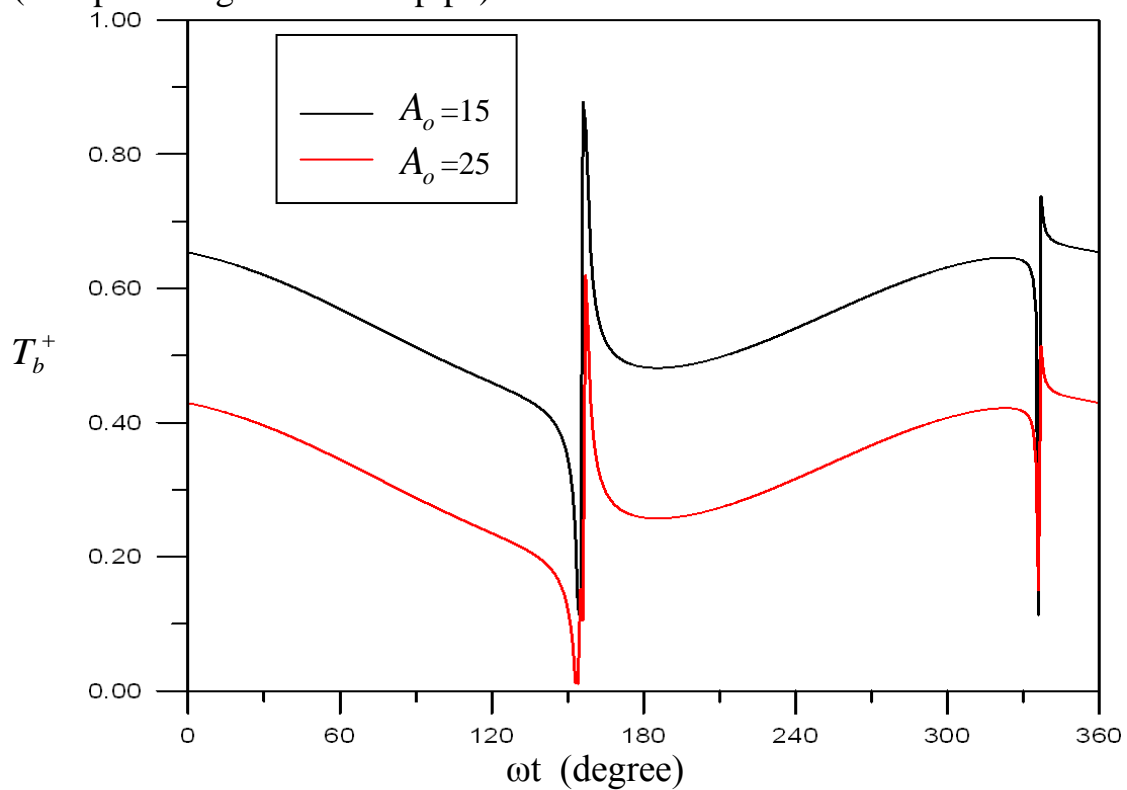


Fig.4.18 The temporal variation of instantaneous bulk temperature for various values of dimensionless amplitude of the fluid displacement at $\lambda=4$, $Pr=0.7$ and $x/D=30$. (Reciprocating flow in the pipe)

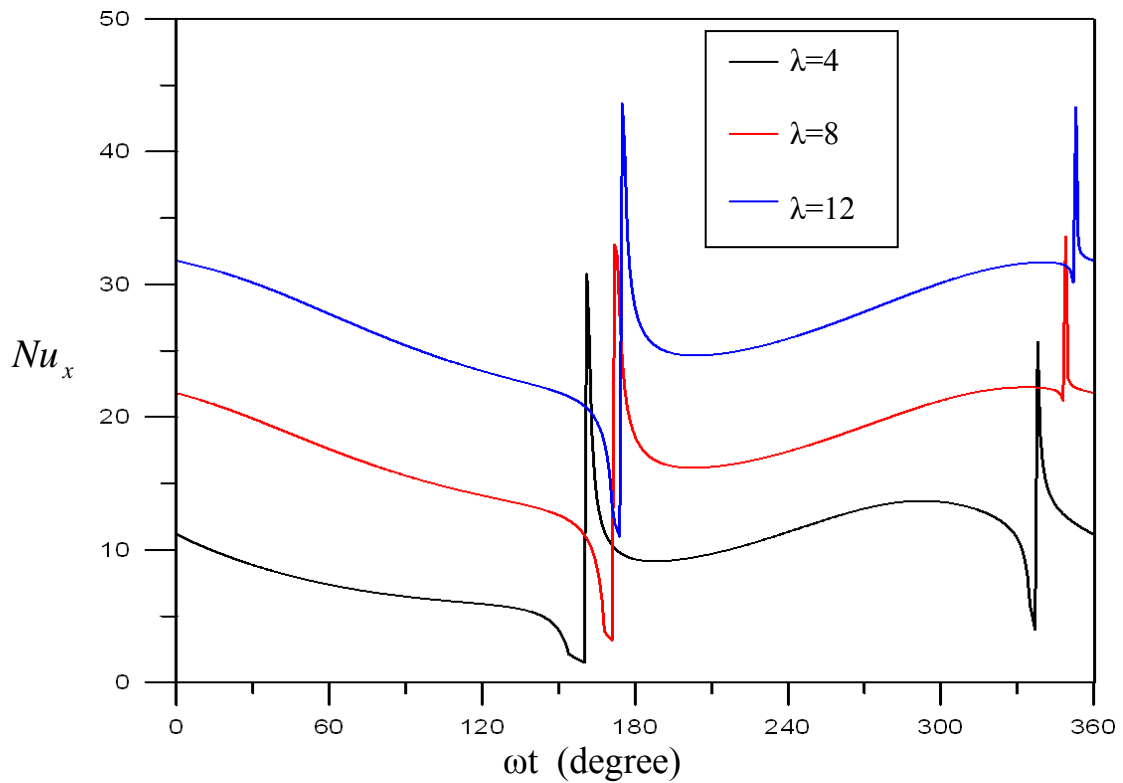


Fig.4.19 The temporal variation of instantaneous–local Nusselt number for various values of Womersly number at $A_o = 15$, $Pr=0.7$ and $x/D=30$. (Reciprocating flow in the pipe)

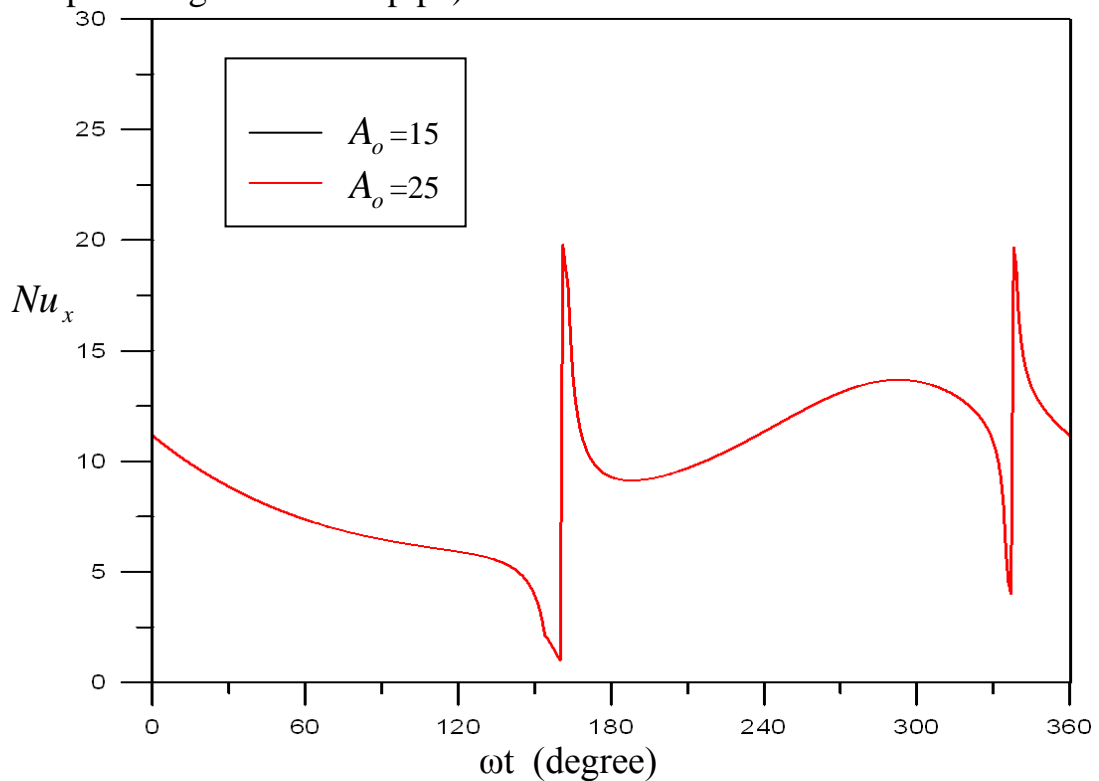


Fig.4.20 The temporal variation of instantaneous-local Nusselt number for various values of dimensionless amplitude of the fluid displacement at $\lambda=4$, $Pr=0.7$ and $x/D=30$. (Reciprocating flow in the pipe)

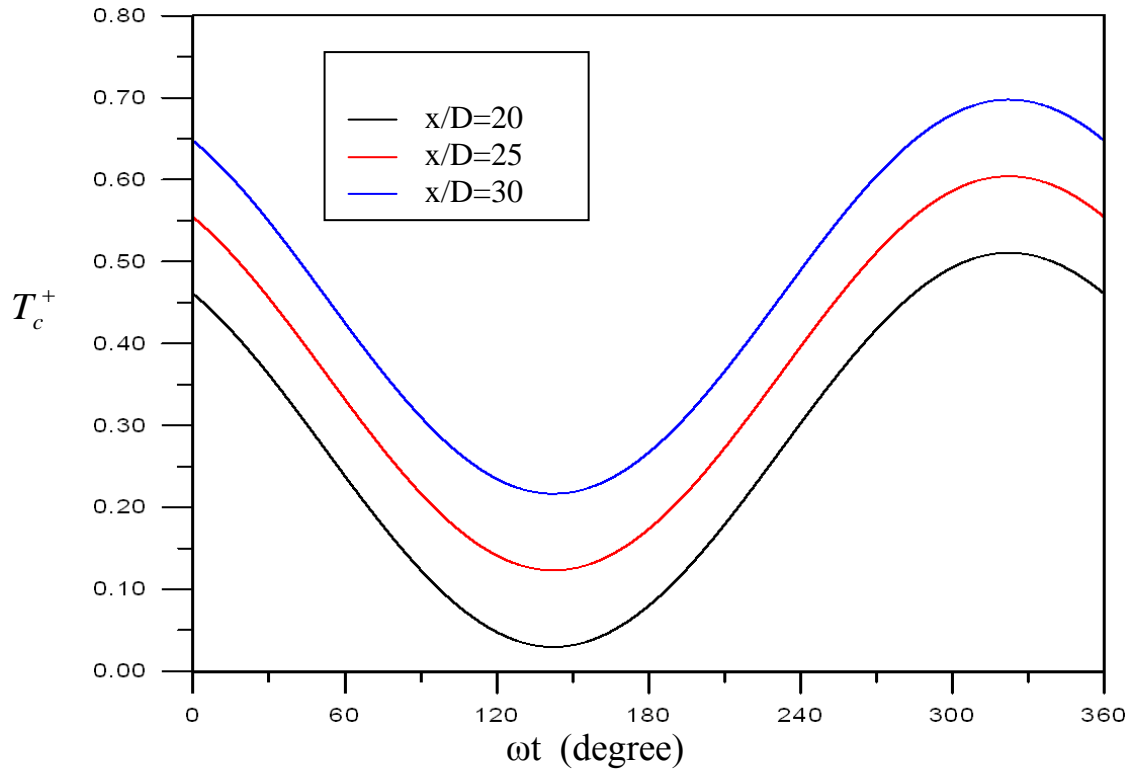


Fig.4.21 The temporal variation of instantaneous center temperature for various values of the ratio of the distance to the diameter at $\lambda=4$, $A_o = 15$ and $Pr=0.7$. (Reciprocating flow in the pipe)

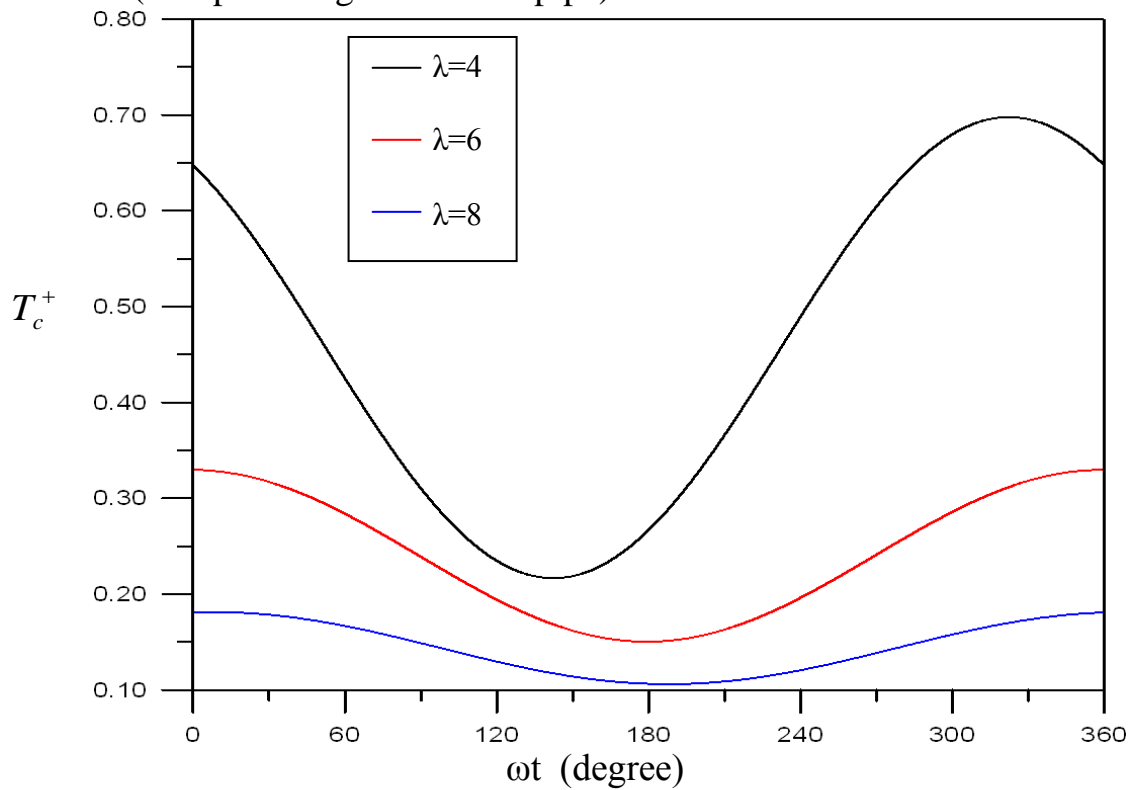


Fig.4.22 The temporal variation of instantaneous center temperature for various values of Womersley number at $A_o = 15$, $Pr=0.7$ and $x/D=30$. (Reciprocating flow in the pipe)

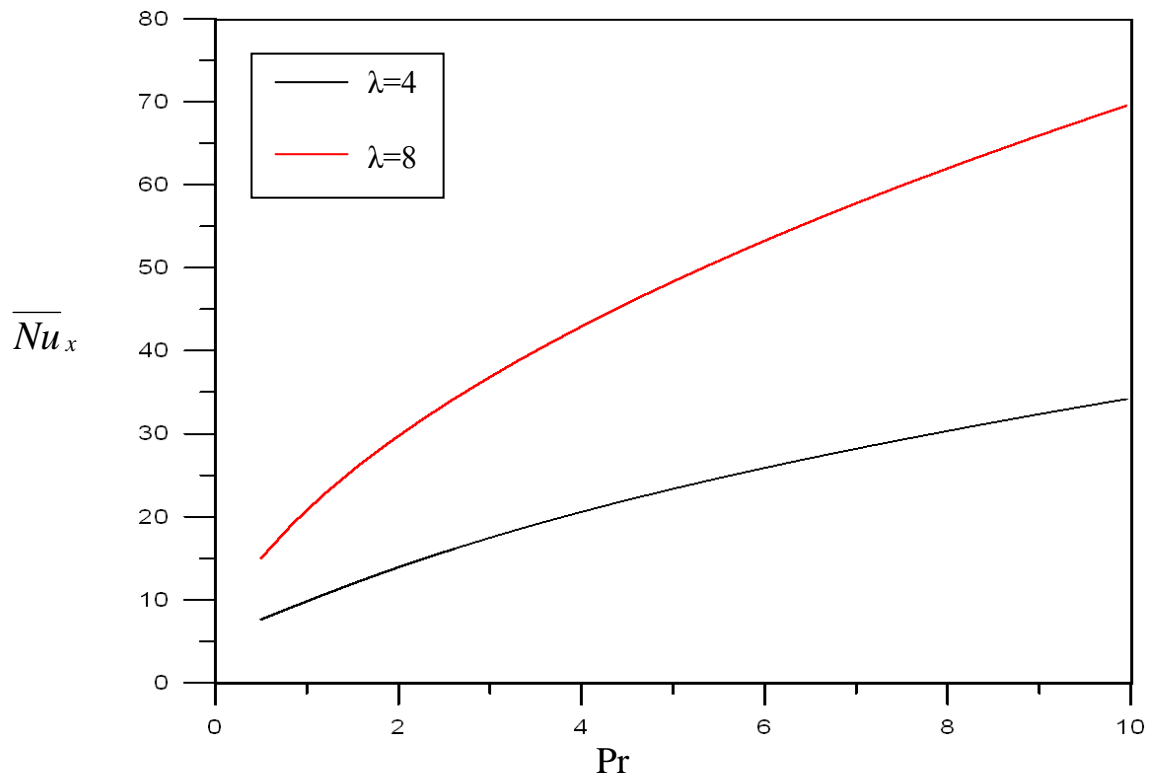


Fig.4.23 Effect of Prandtl number on the time averaged-local Nusselt number for two values of Womersly number at $A_o = 15$ and $x/D=30$. (Reciprocating flow in the pipe)

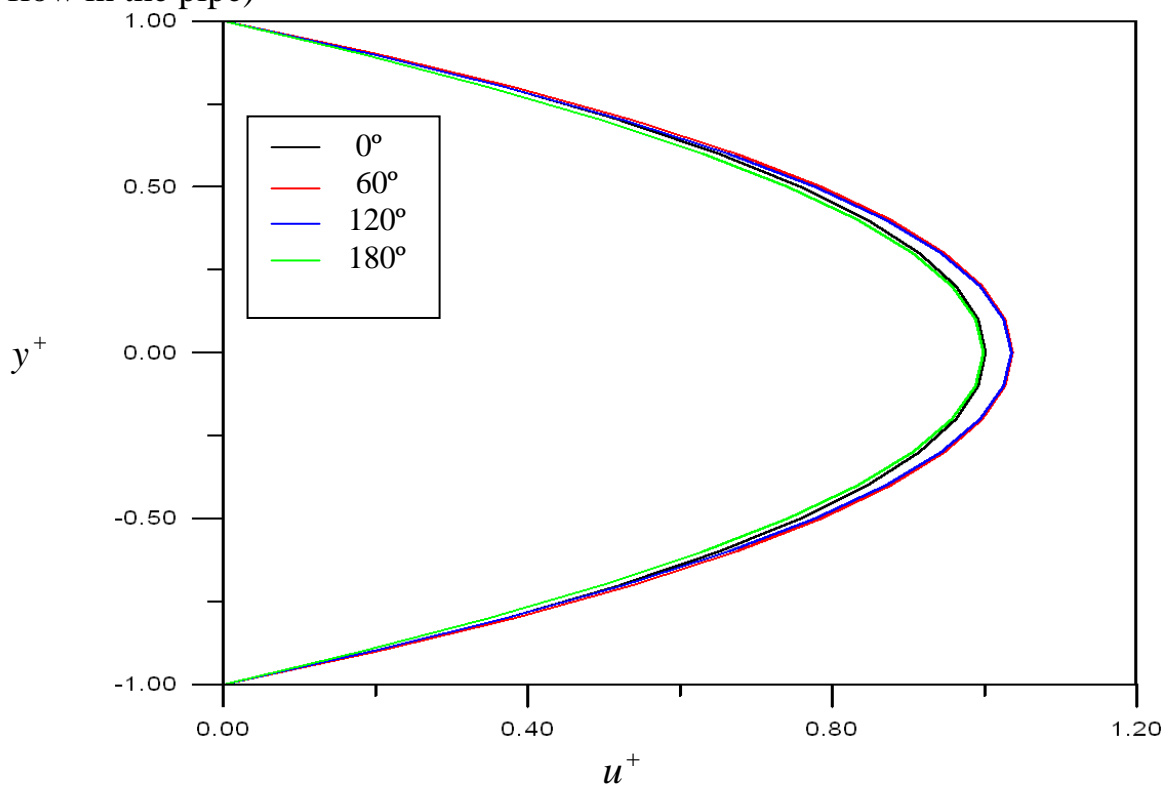


Fig.4.24 The variation of dimensionless velocity profile for $\lambda=4$, $\gamma' = 0.3$, $Re_m = 1200$, $Pr=0.7$ and $x/D_h=20$. (Pulsating flow in the channel)

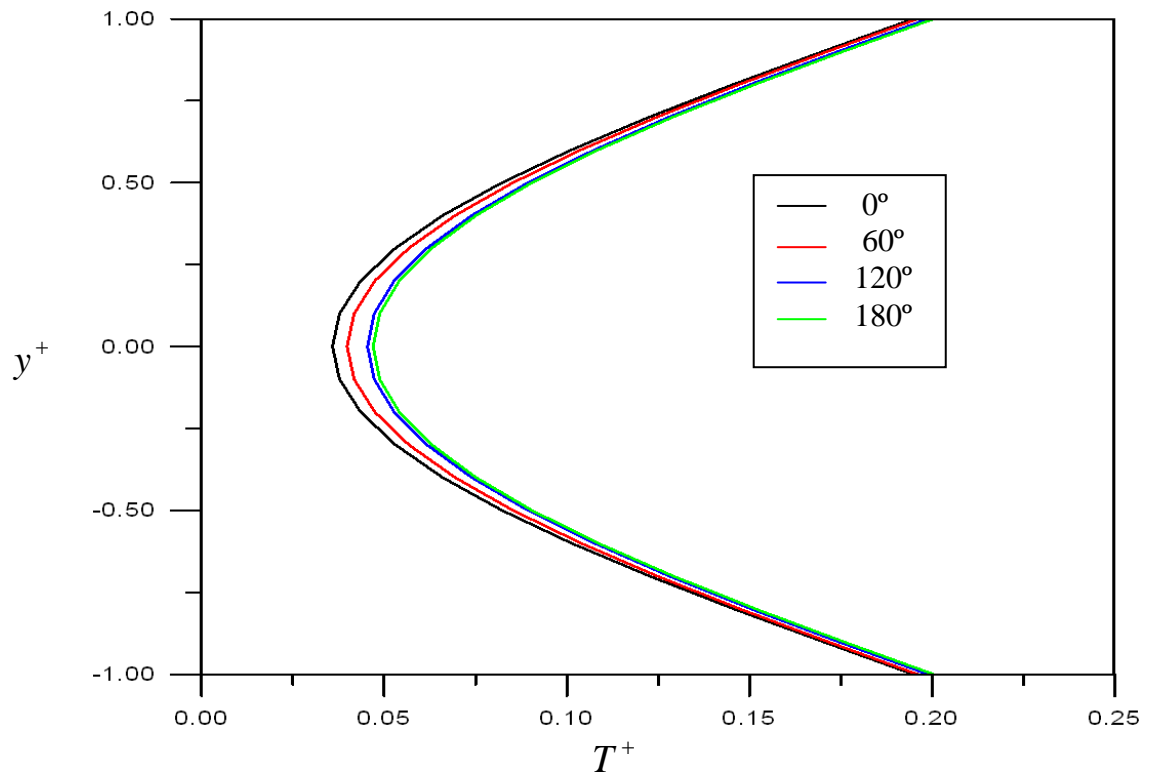


Fig.4.25 The variation of dimensionless temperature profile for $\lambda=4$, $\gamma' = 0.3$, $\text{Re}_m = 1200$, $\text{Pr}=0.7$ and $x/D_h = 20$. (Pulsating flow in the channel)

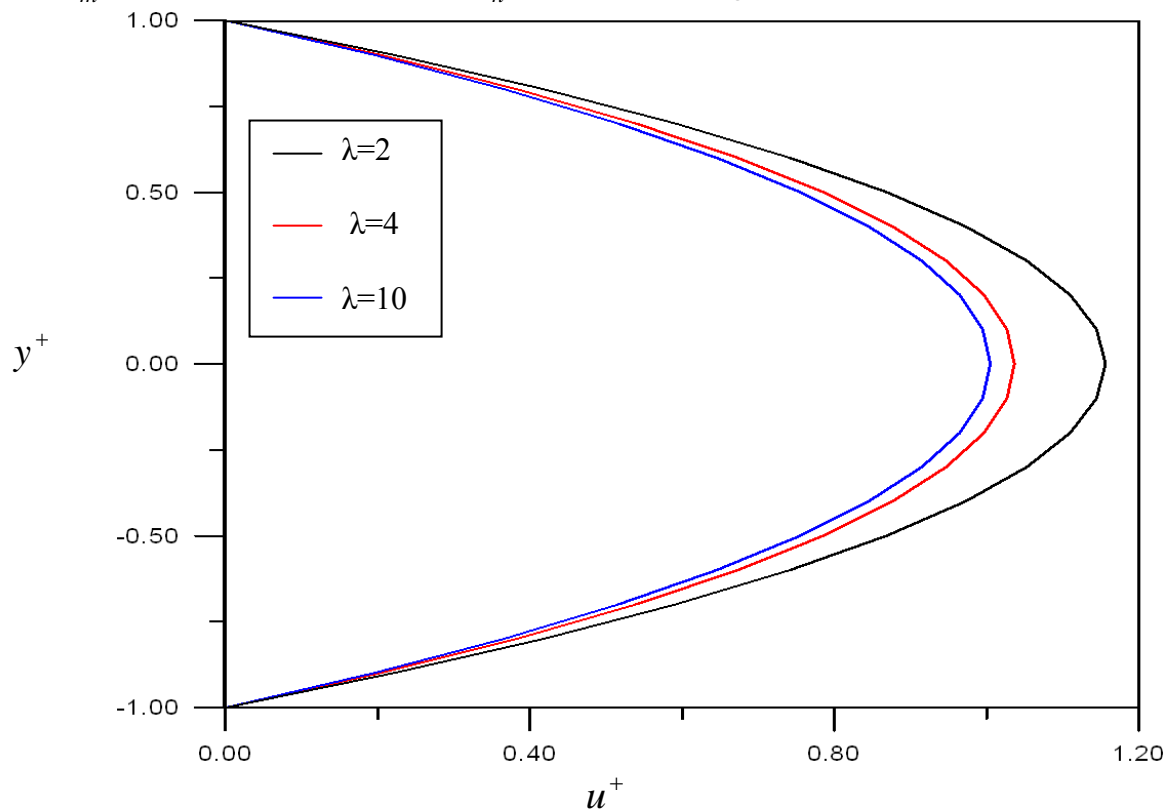


Fig.4.26 Effect of Womersley number on the dimensionless velocity profile at $\omega t = 60^\circ$, for $\gamma' = 0.3$, $\text{Re}_m = 1200$, $\text{Pr}=0.7$ and $x/D_h = 20$. (Pulsating flow in the channel)

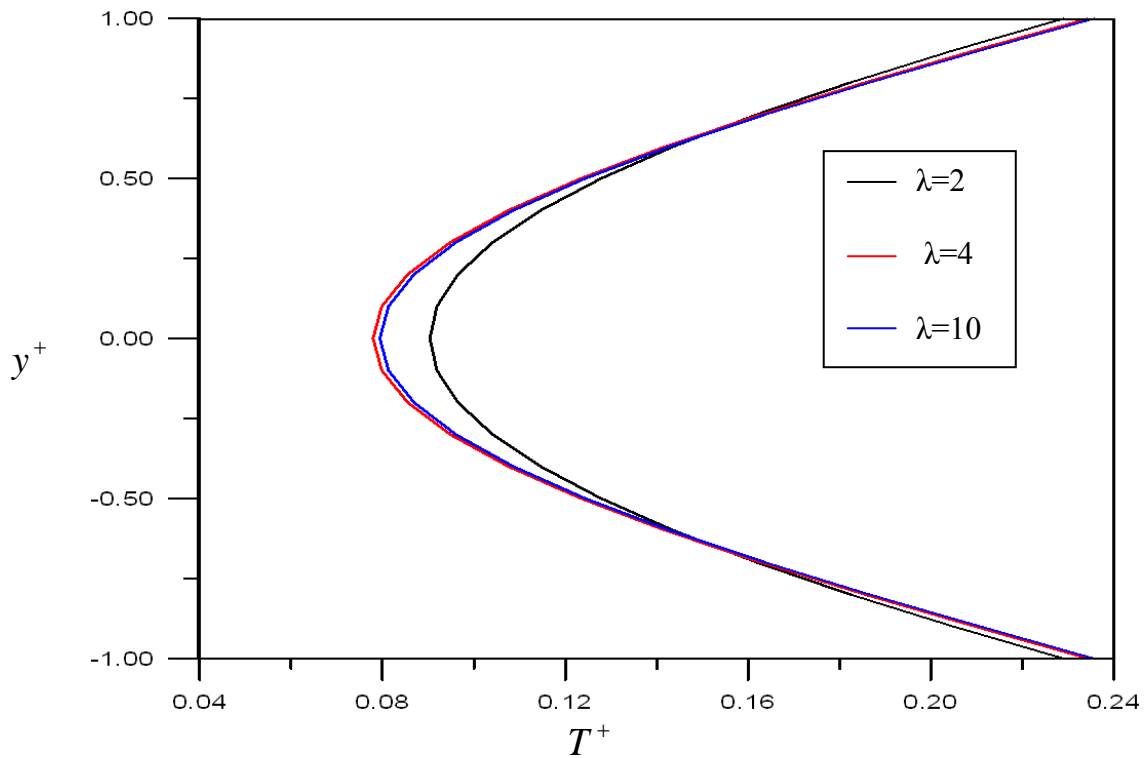


Fig.4.27 Effect of Womersley number on the dimensionless temperature profile at $\omega t = 60^\circ$, for $\gamma' = 0.3$, $Re_m = 1200$, $Pr = 0.7$ and $x/D_h = 20$. (Pulsating flow in the channel)

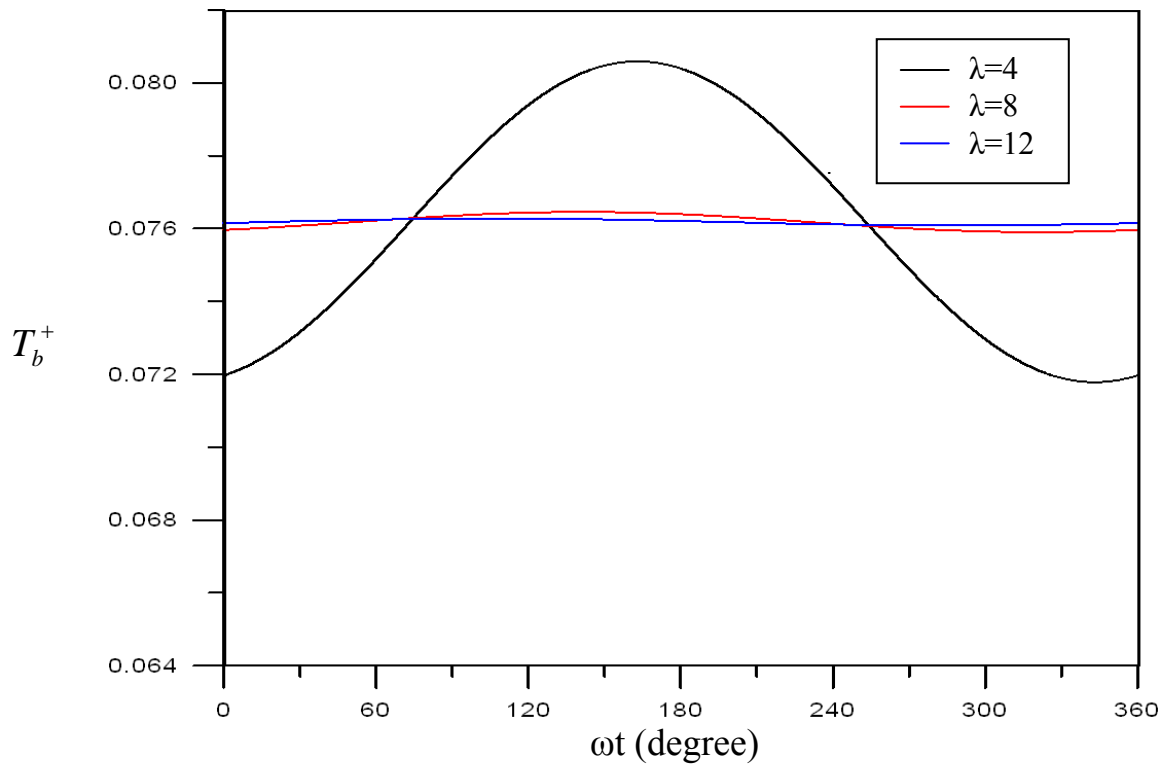


Fig.4.28 Effect of Womersley number on the instantaneous dimensionless bulk temperature at $\gamma' = 0.3$, $Re_m = 1500$, $Pr = 0.7$ and $x/D_h = 20$. (Pulsating flow in the channel)

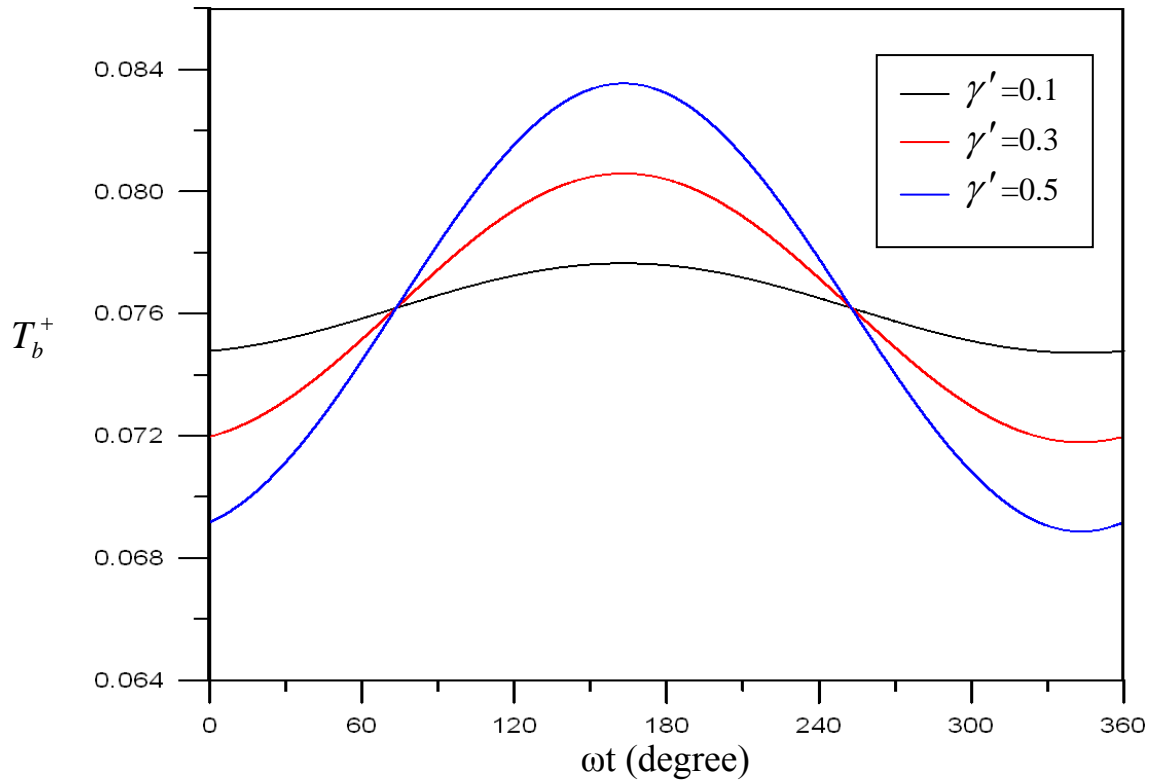


Fig.4.29 Effect of the ratio of the fluctuate to the steady pressure gradient on the instantaneous dimensionless bulk temperature for $\lambda=4$, $Re_m=1500$, $Pr=0.7$ and $x/D_h=20$. (Pulsating flow in the channel)

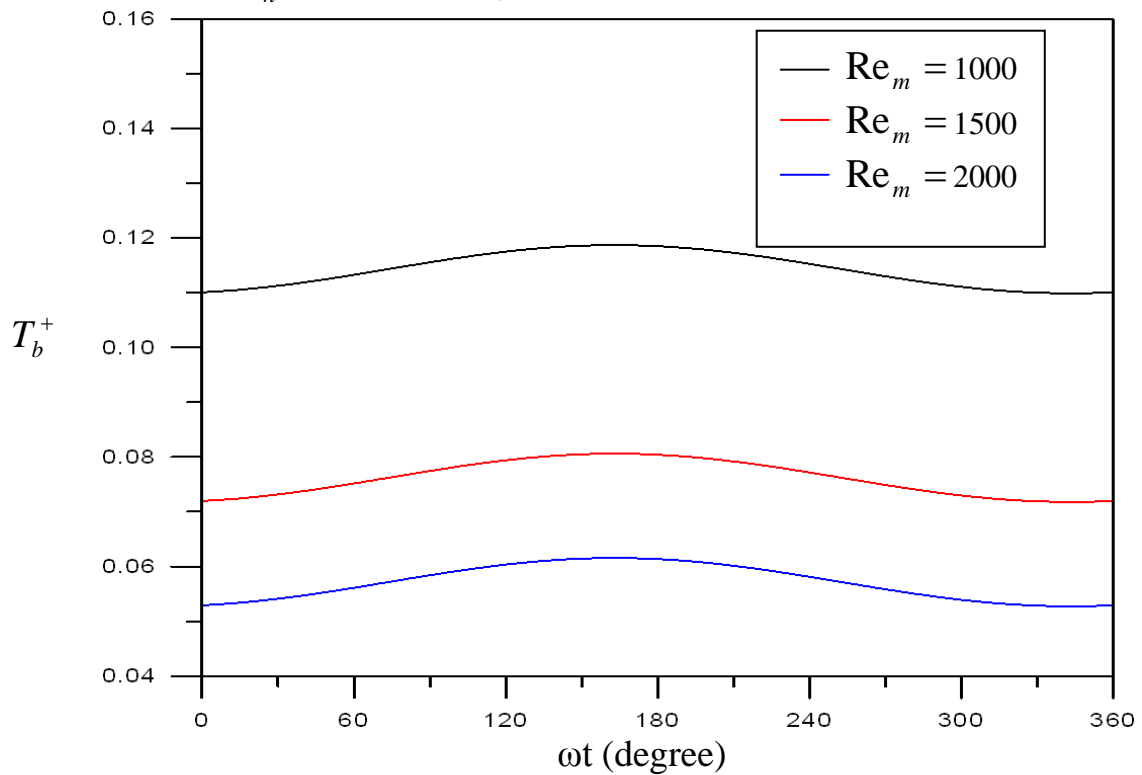


Fig.4.30 Effect of the mean Reynolds number on the instantaneous dimensionless bulk temperature for $\lambda=4$, $\gamma'=0.3$, $Pr=0.7$ and $x/D_h=20$. (Pulsating flow in the channel)

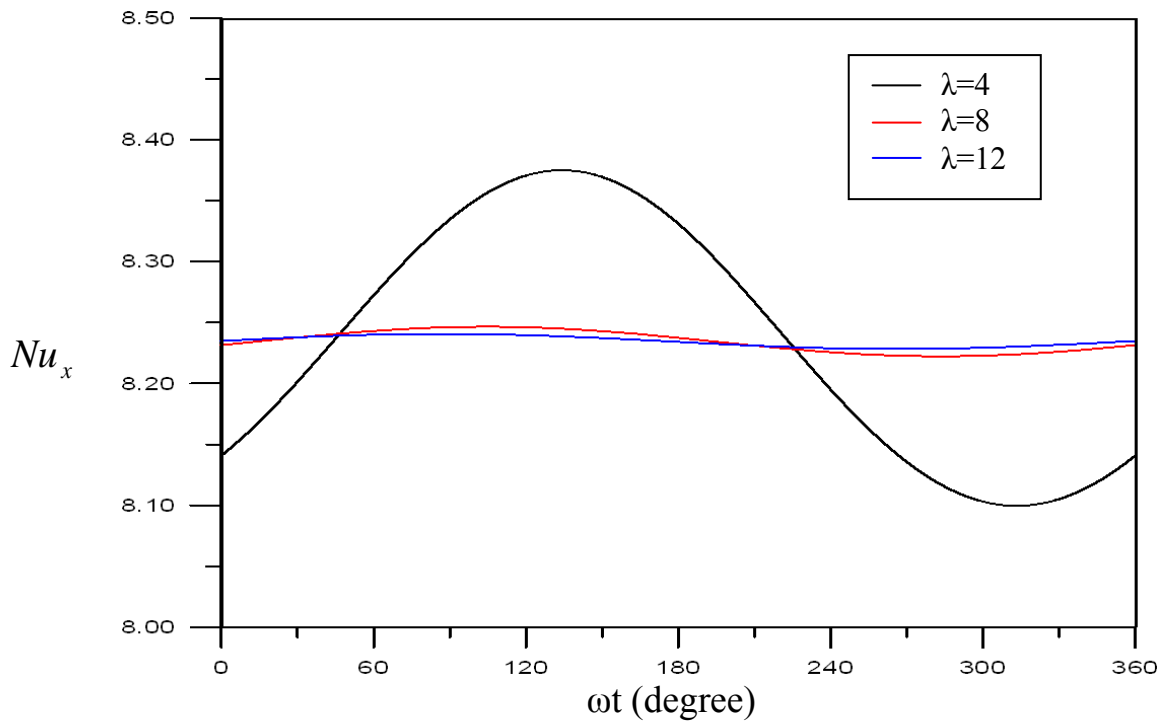


Fig.4.31 Effect of Womersly number on the instantaneous-local Nusselt number for $\gamma' = 0.3$, $Re_m = 1500$, $Pr=0.7$ and $x/D_h=20$. (Pulsating flow in the channel)

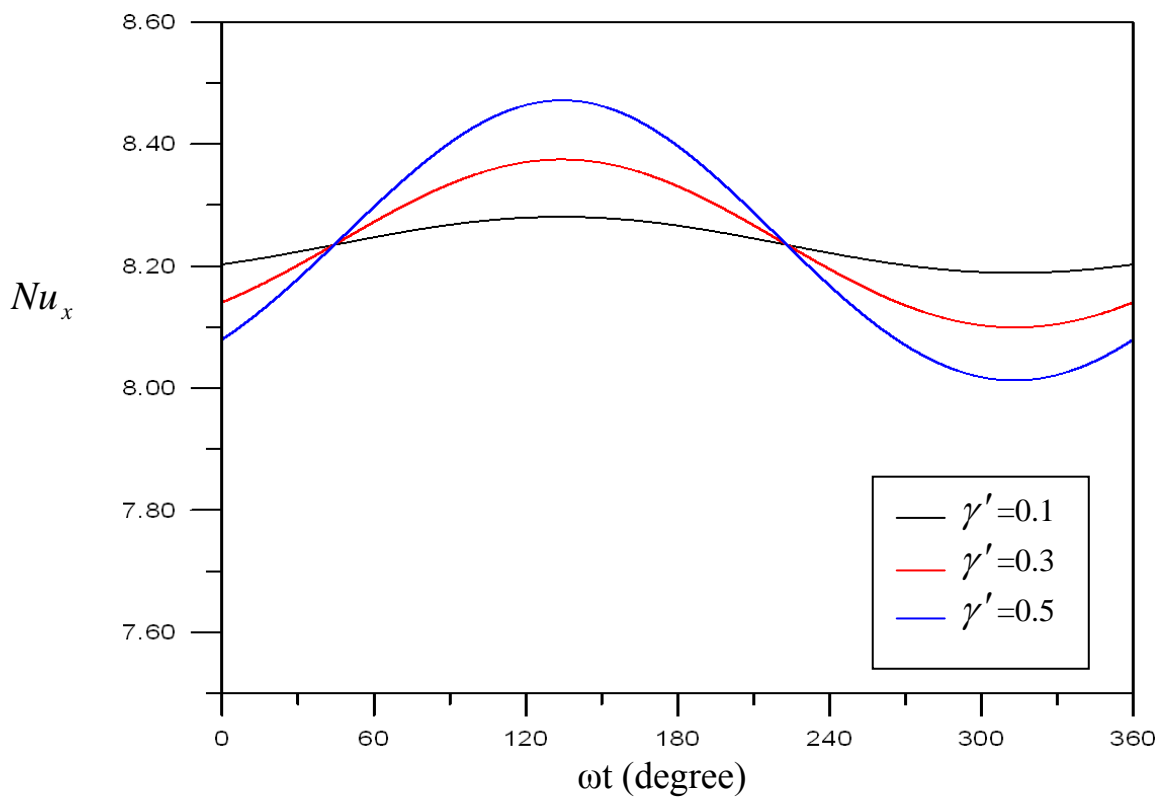


Fig.4.32 Effect of the ratio of the fluctuate to the steady pressure gradient on the instantaneous-local Nusselt number for $\lambda=4$, $Re_m = 1500$, $Pr=0.7$ and $x/D_h=20$. (Pulsating flow in the channel)

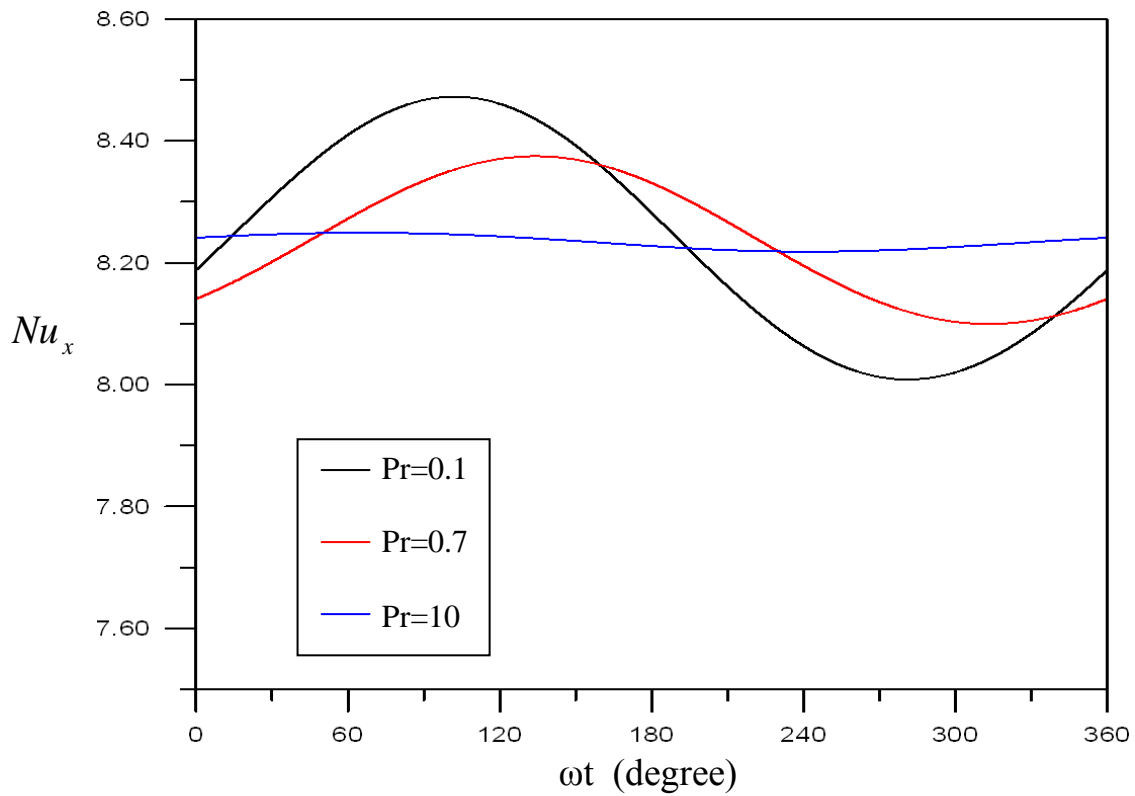


Fig.4.33 Effect of Prandtl number on the instantaneous-local Nusselt number for $\lambda=4$, $\gamma'=0.3$, $Re_m=1500$ and $x/D_h=20$. (Pulsating flow in the channel)

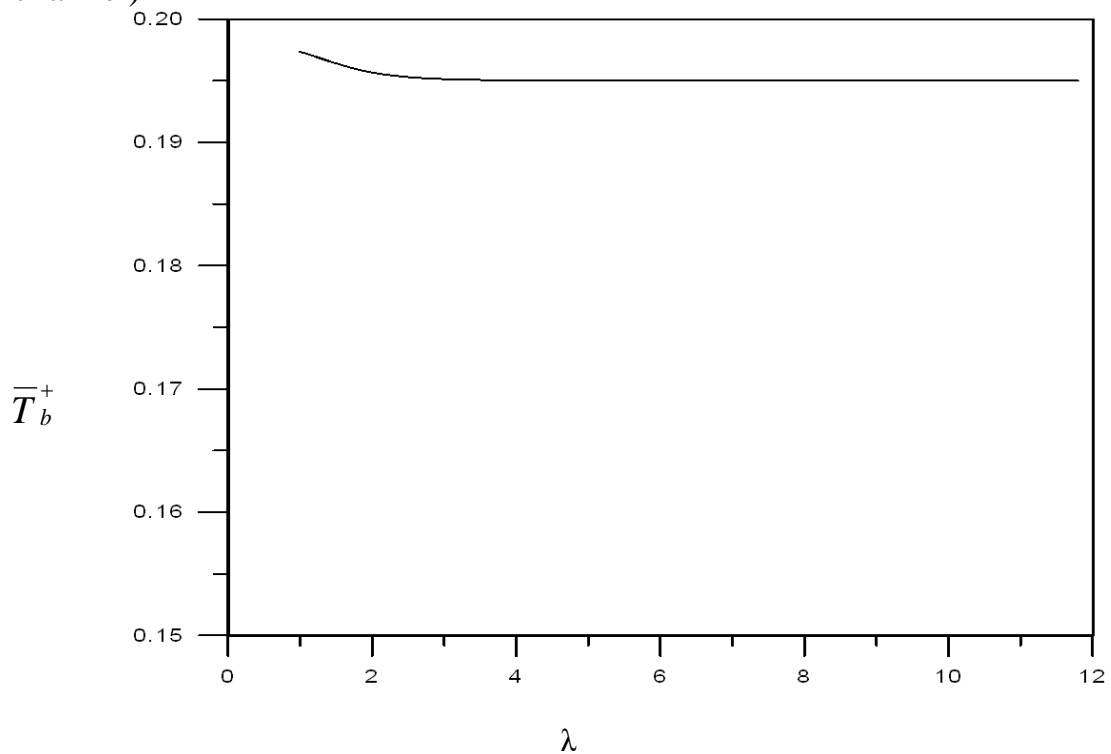


Fig.4.34 Effect of Womersley number on the time-averaged dimensionless bulk temperature for $\gamma'=0.3$, $Re_m=1500$, $Pr=0.7$ and $x/D_h=20$. (Pulsating flow in the channel)

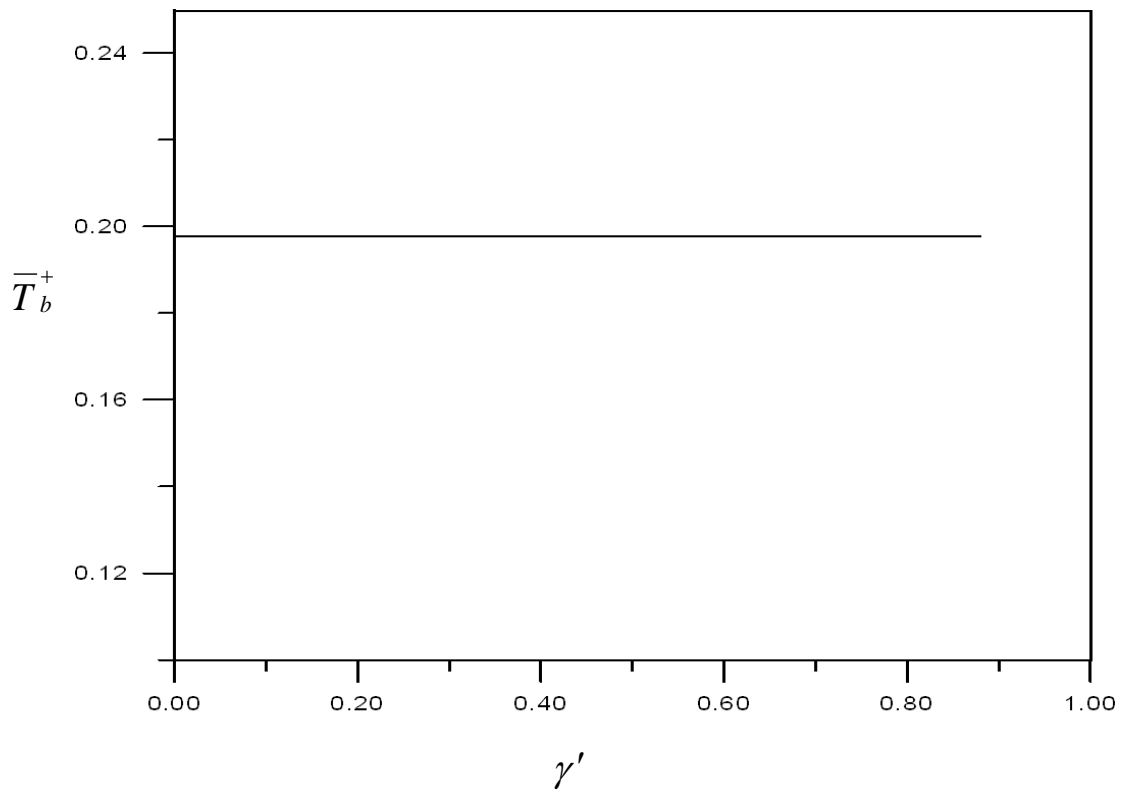


Fig.4.35 Effect of the ratio of the fluctuate to the steady pressure gradient on the time-averaged dimensionless bulk temperature at $\lambda=4$, $Re_m = 1500$, $Pr=0.7$ and $x/D_h=20$. (Pulsating flow in the channel)

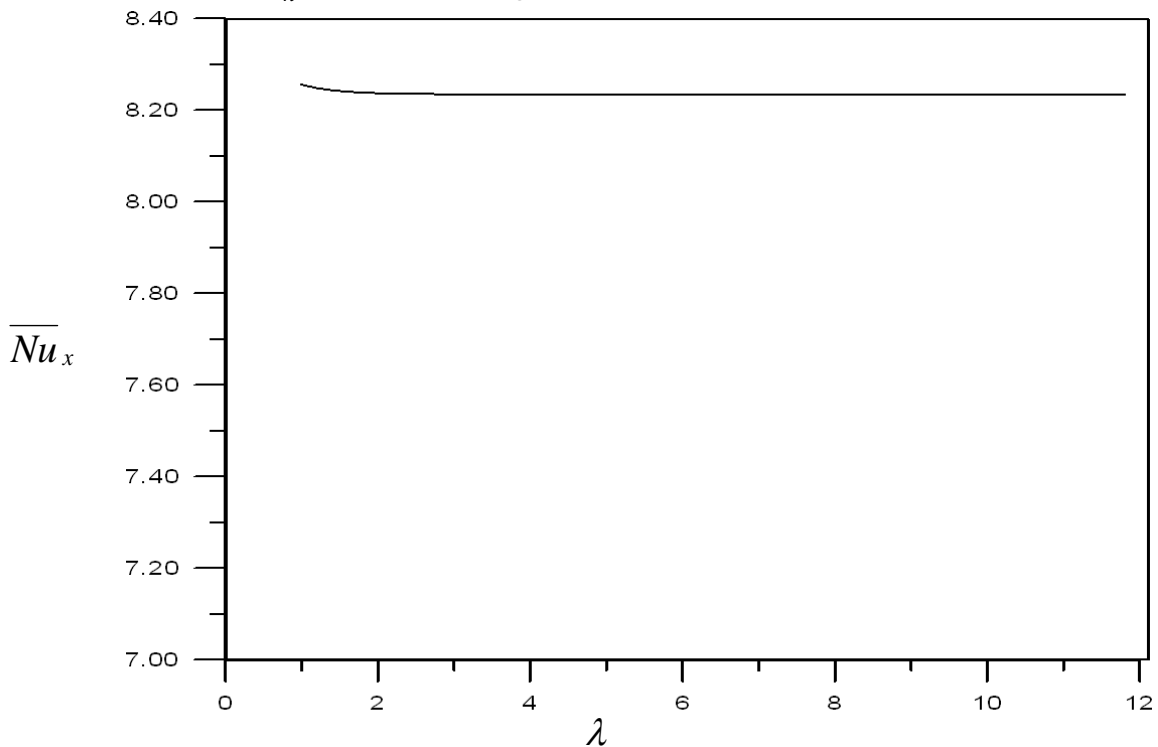


Fig.4.36 Effect of Womersley number on the time averaged-local Nusselt number at $\gamma' = 0.3$, $Re_m = 1500$, $Pr=0.7$ and $x/D_h=20$. (Pulsating flow in the channel)

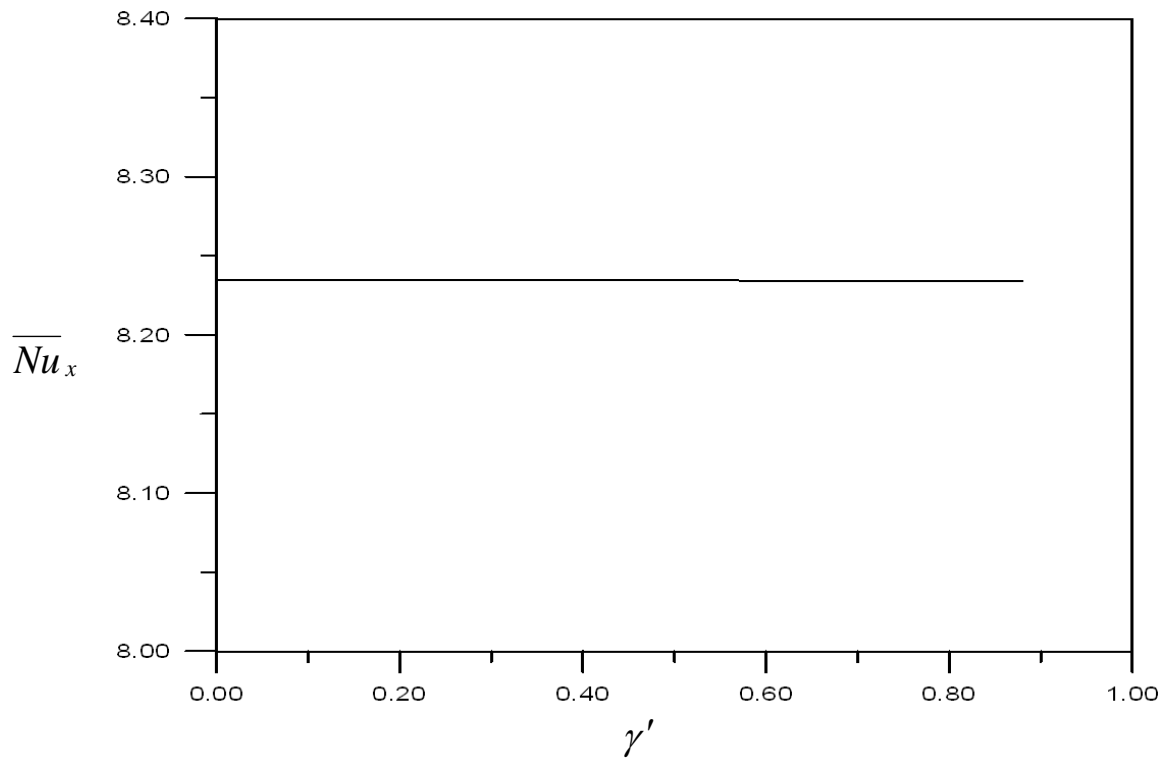


Fig.4.37 Effect of the Ratio of the Fluctuate to the Steady Pressure Gradient on the Time Averaged-Local Nusselt Number at $\lambda=4$, $Re_m = 1500$, $Pr=0.7$ & $x/D_h=20$. (Pulsating flow in the channel)

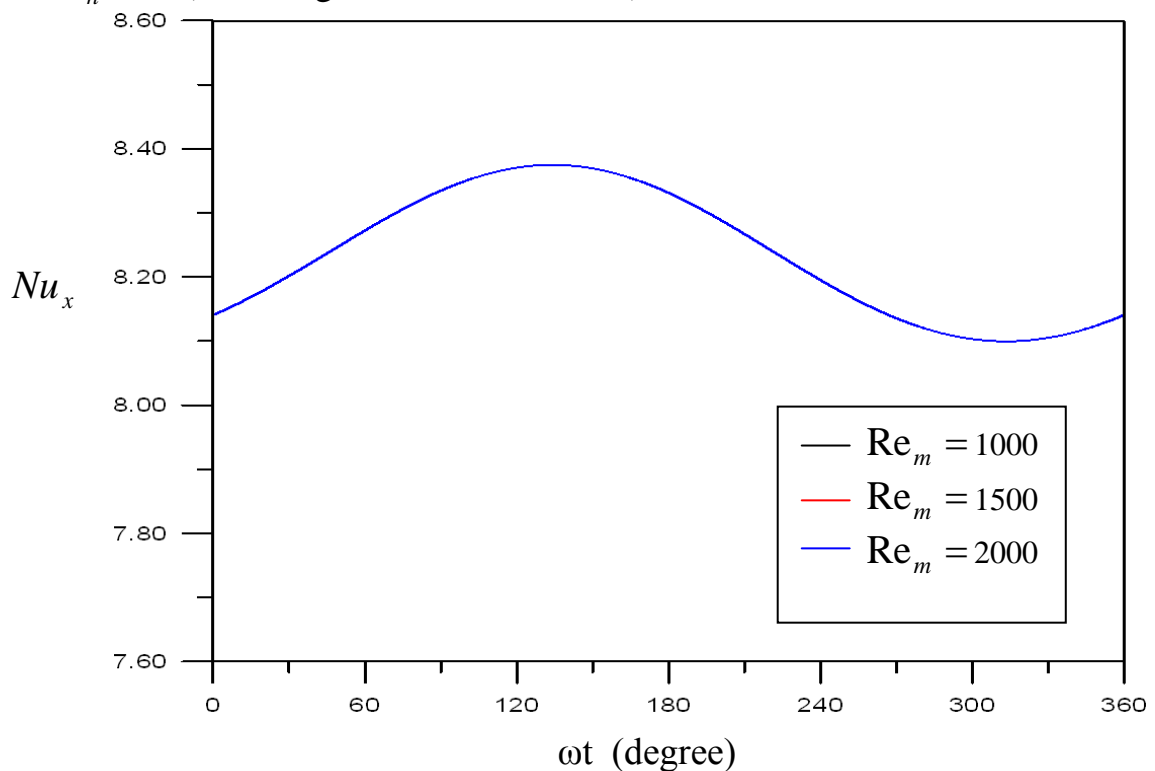


Fig.4.38 Effect of mean Reynolds number on the instantaneous-local Nusselt number at $\lambda=4$, $\gamma' = 0.3$, $Pr=0.7$ and $x/D_h=20$. (Pulsating flow in the channel)

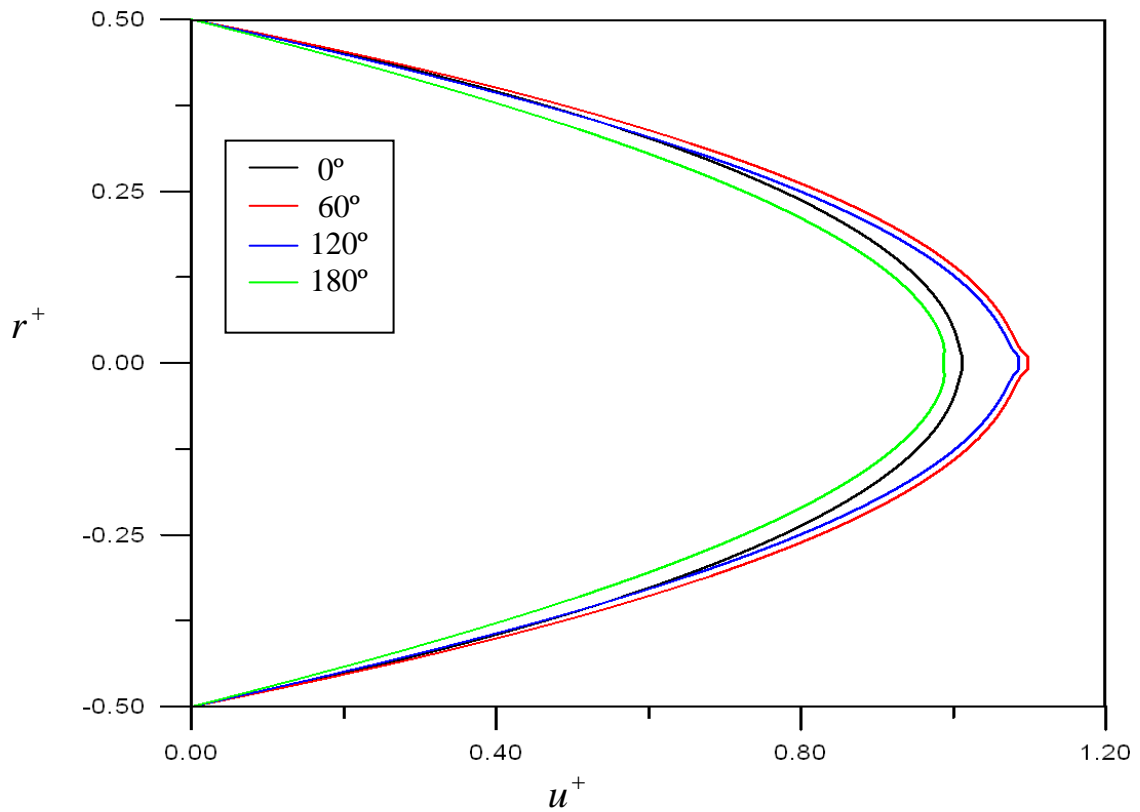


Fig.4.39 The Variation of dimensionless velocity profile for $\lambda=4$, $\gamma' = 0.3$, $Re_m = 1200$, $Pr=0.7$ and $x/D=40$. (Pulsating flow in the pipe)

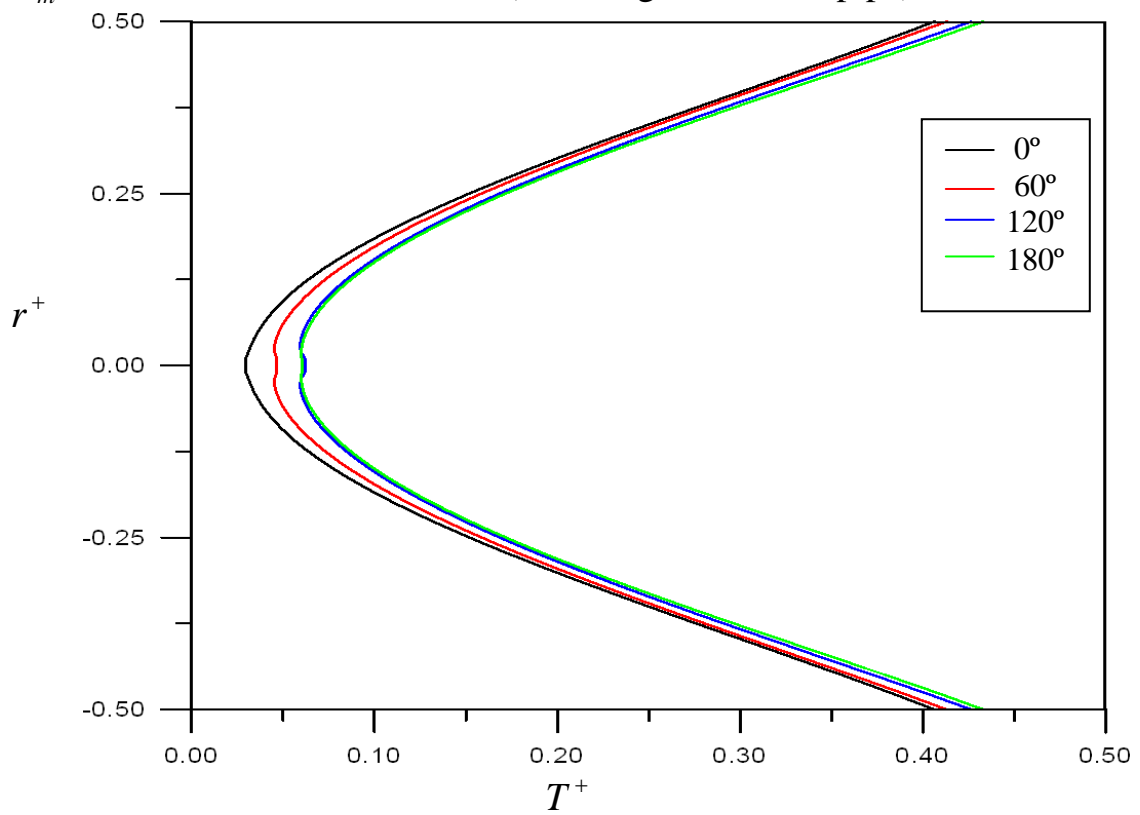


Fig.4.40 The Variation of dimensionless temperature profile for $\lambda=4$, $\gamma' = 0.3$, $Re_m = 1200$, $Pr=0.7$ and $x/D=40$. (Pulsating flow in the pipe)

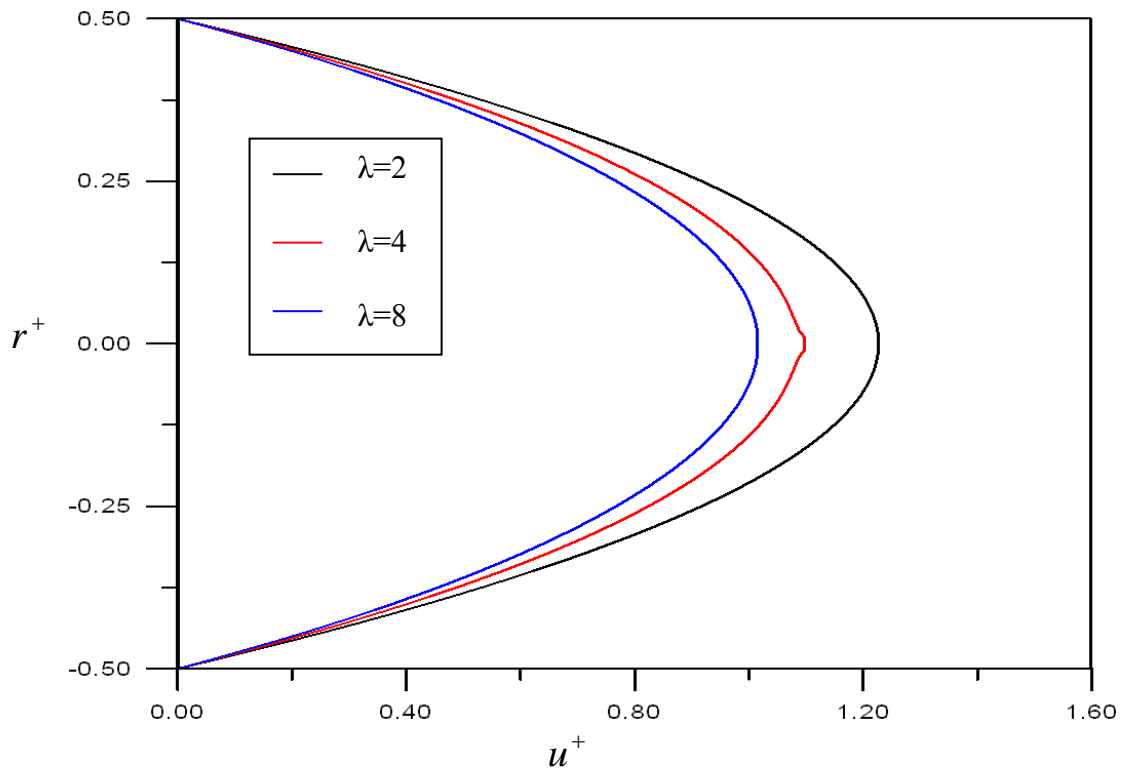


Fig.4.41 Effect of Womersley number on the dimensionless velocity profile at $\omega t = 60^\circ$ for $\gamma' = 0.3$, $Re_m = 1200$, $Pr = 0.7$ and $x/D = 40$. (Pulsating flow in the pipe)

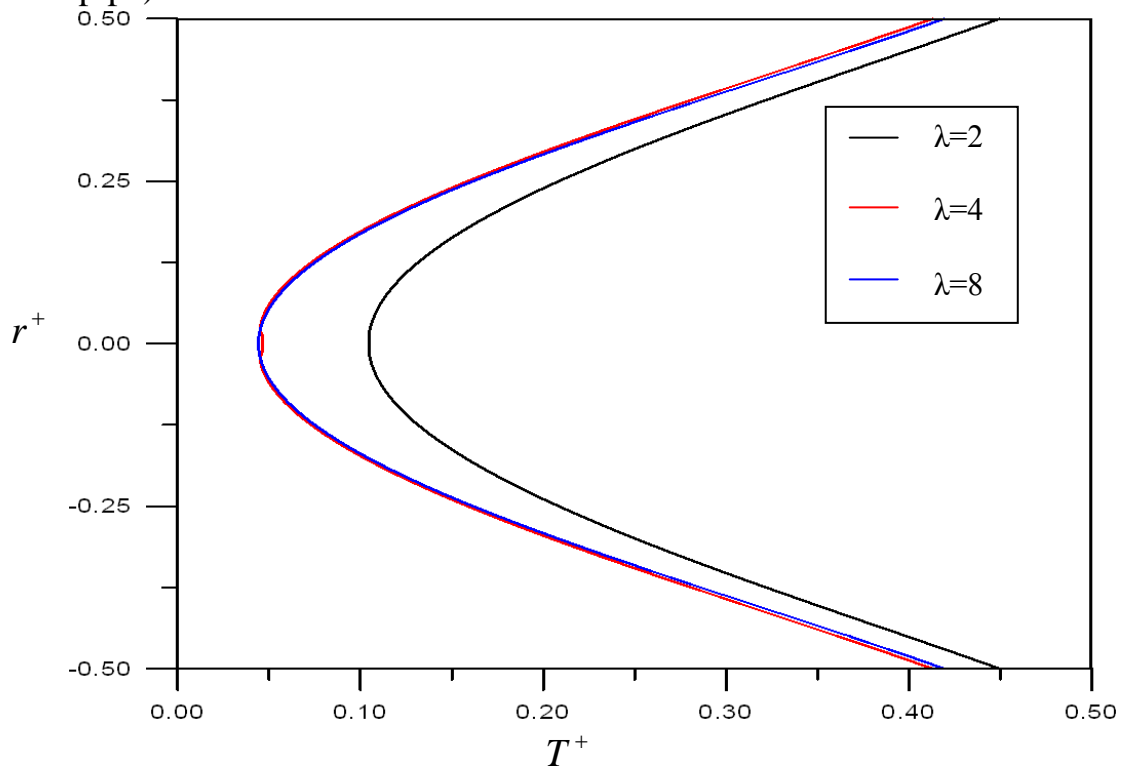


Fig.4.42 Effect of Womersley number on the dimensionless temperature profile at $\omega t = 60^\circ$, for $\gamma' = 0.3$, $Re_m = 1200$, $Pr = 0.7$ and $x/D = 40$. (Pulsating flow in the pipe)

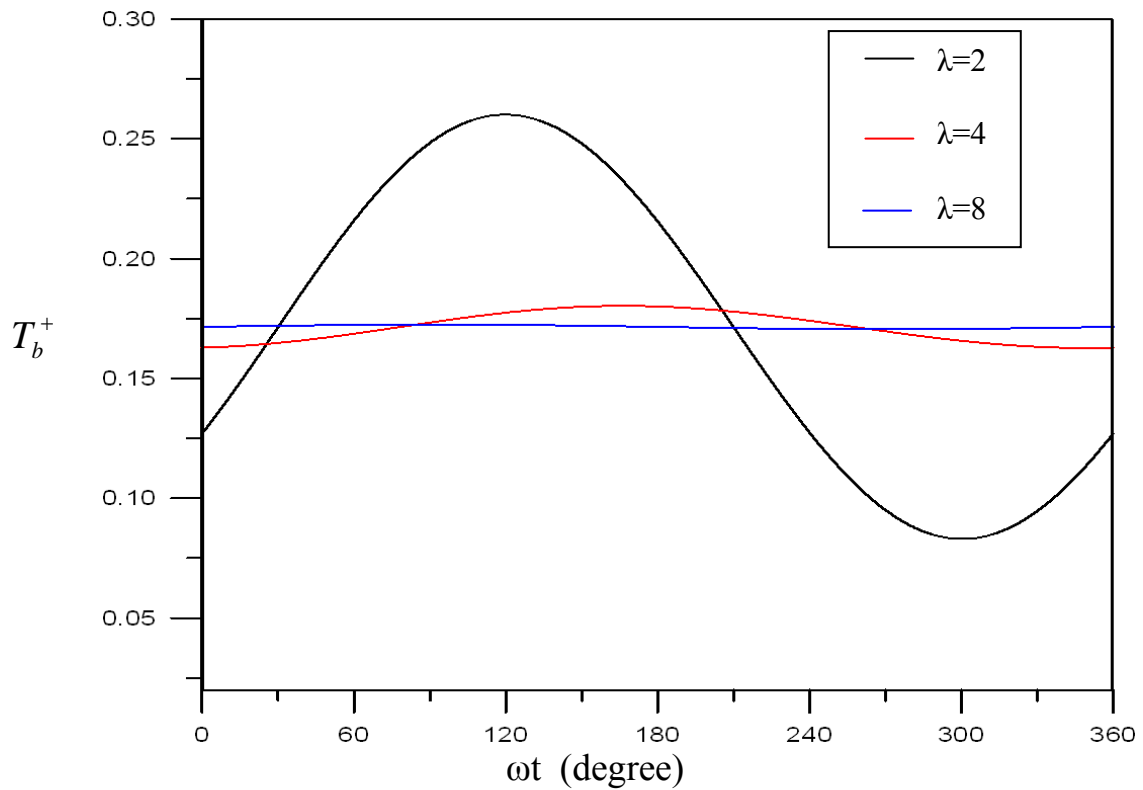


Fig.4.43 Effect of Womersley number on the instantaneous dimensionless bulk temperature at $\gamma' = 0.3$, $Re_m = 1000$, $Pr=0.7$ and $x/D=20$. (Pulsating flow in the pipe)

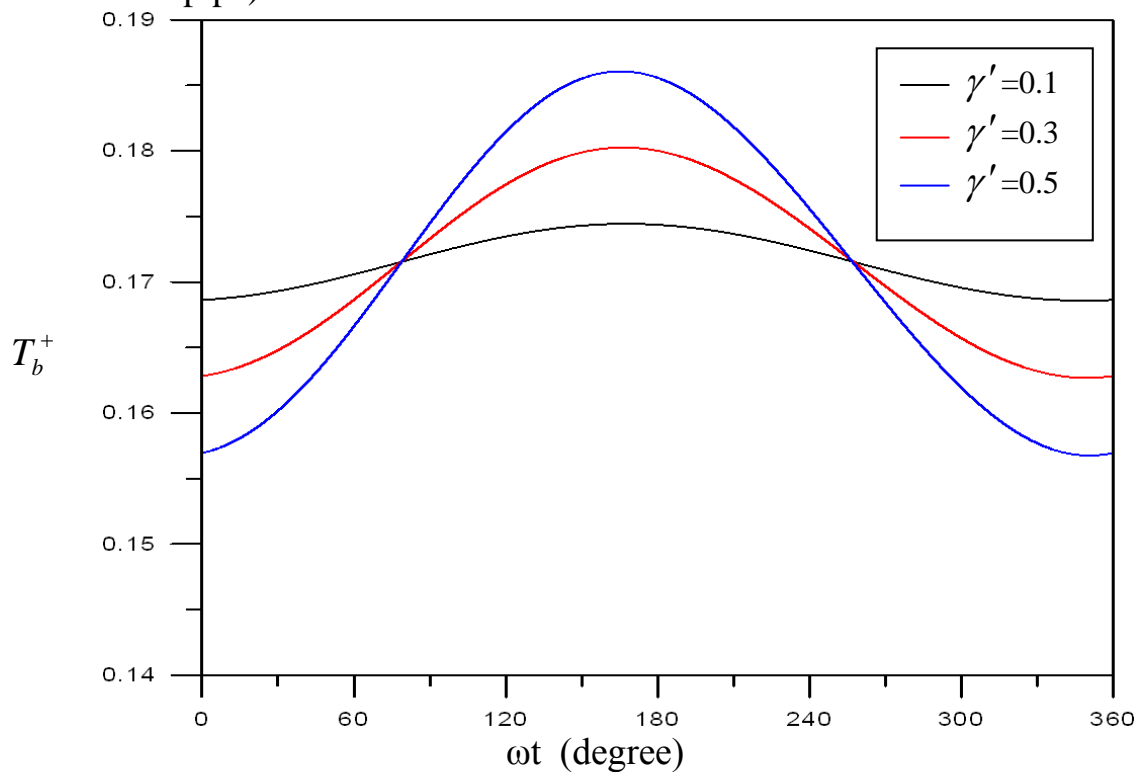


Fig.4.44 Effect of the ratio of the fluctuate to the steady pressure gradient on the instantaneous dimensionless bulk temperature at $\lambda=4$, $Re_m = 1000$, $Pr=0.7$ and $x/D=30$. (Pulsating flow in the pipe)

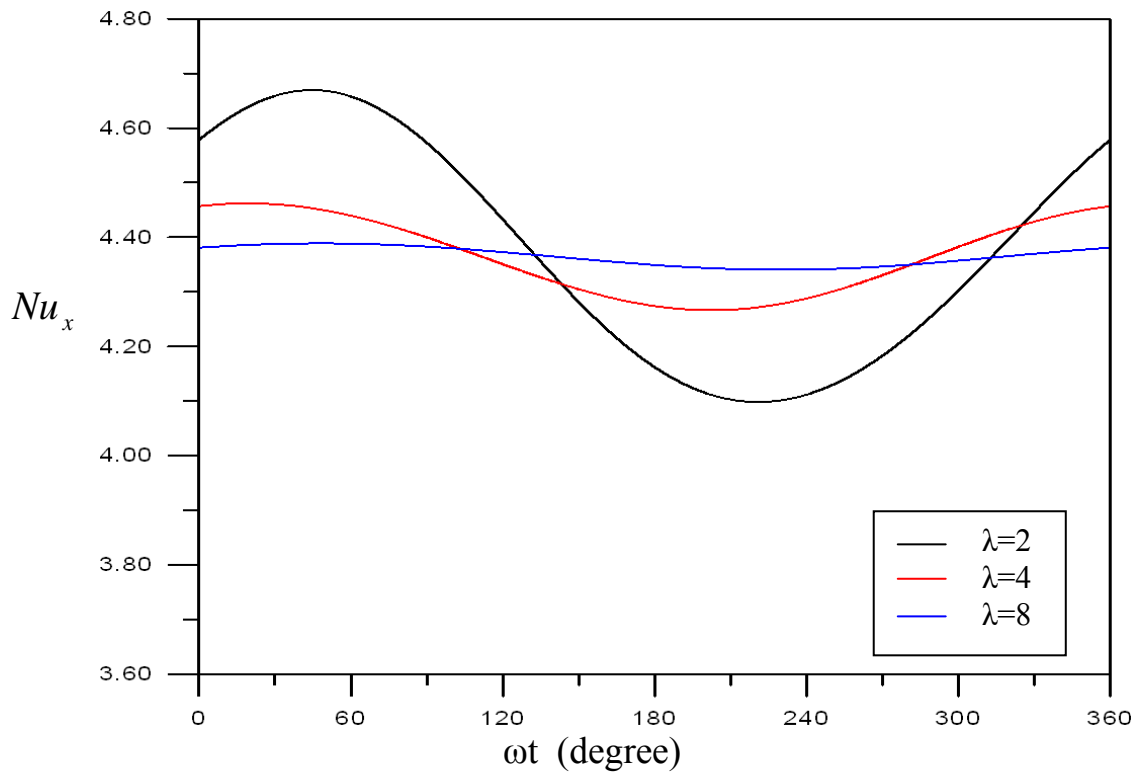


Fig.4.45 Effect of Womersley number on the instantaneous-local Nusselt number at $\gamma' = 0.3$, $Re_m = 1000$, $Pr=0.7$ and $x/D=30$. (Pulsating flow in the pipe)

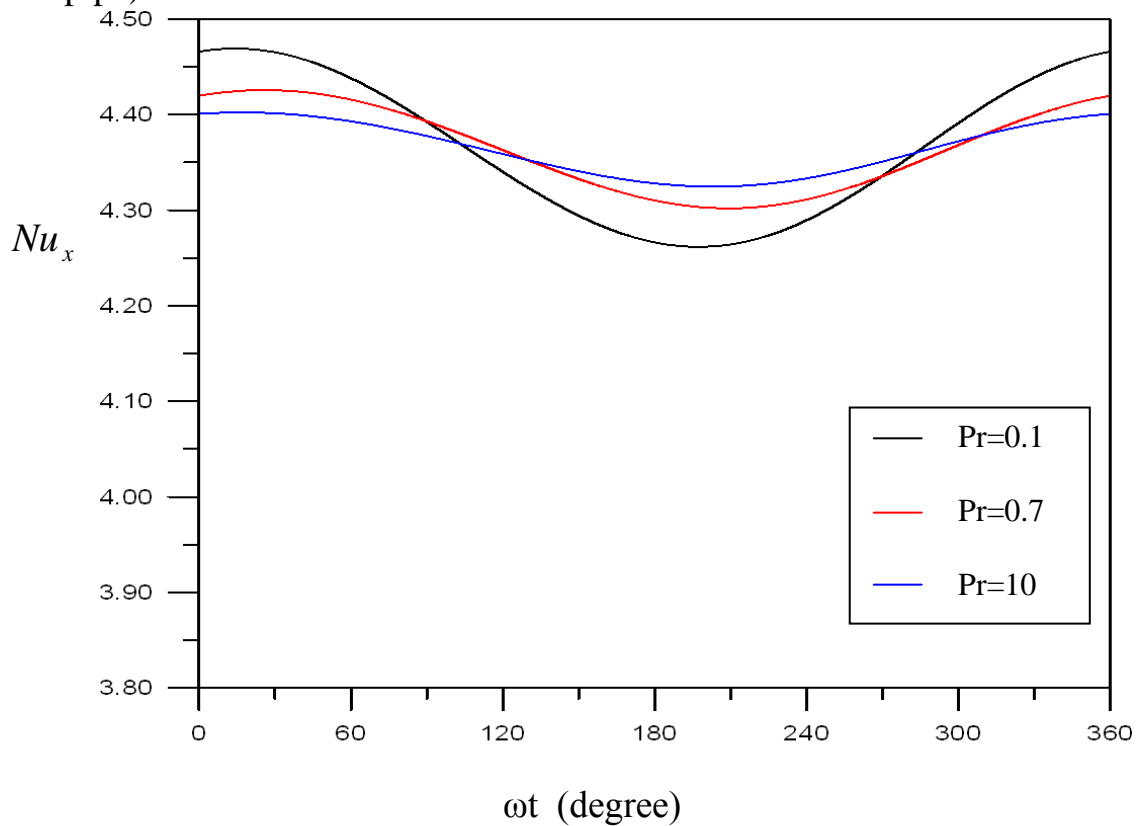


Fig.4.46 Effect of Prandtl number on the instantaneous-local Nusselt number at $\lambda=4$, $\gamma' = 0.3$, $Re_m = 1200$ and $x/D=30$. (Pulsating flow in the pipe)

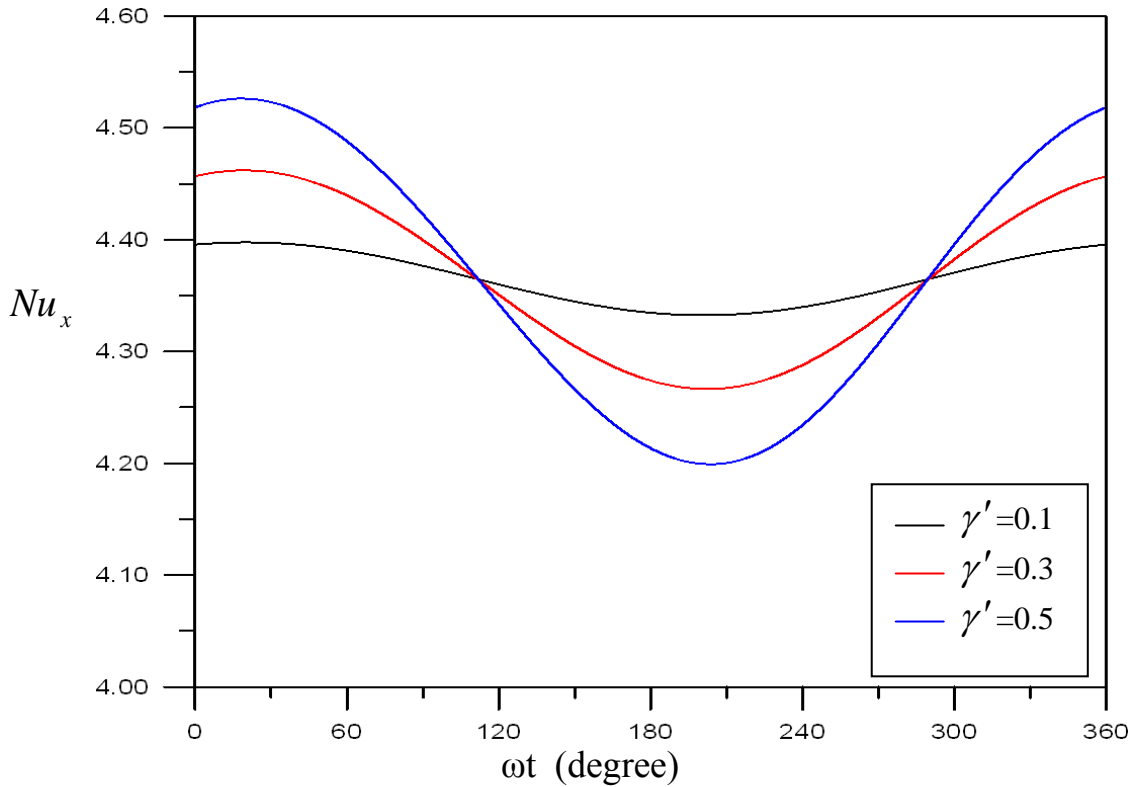


Fig.4.47 Effect of the ratio of the fluctuate to the steady pressure gradient on the instantaneous-local Nusselt number at $\lambda=4$, $Re_m = 1000$, $Pr=0.7$ and $x/D=30$. (Pulsating flow in the pipe)

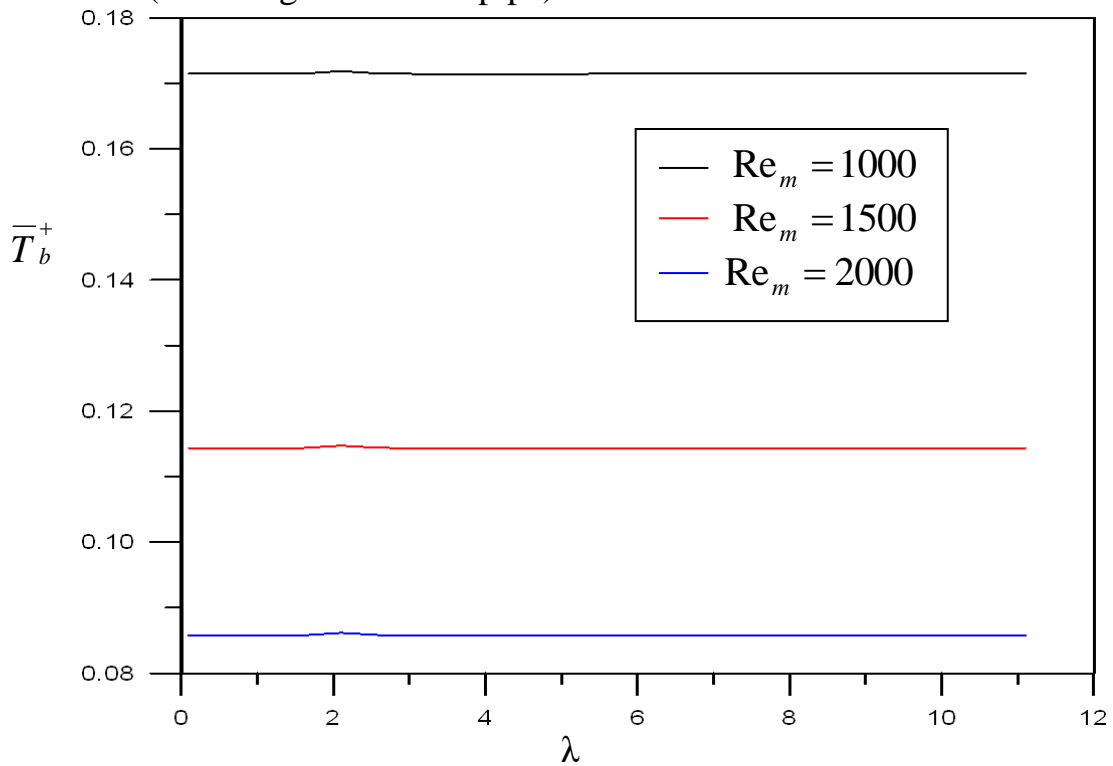


Fig.4.48 The Variation of time-averaged dimensionless bulk temperature with Womersley number for various values of mean Reynolds number at $\gamma' = 0.3$, $Pr=0.7$ and $x/D=30$. (Pulsating flow in the pipe)

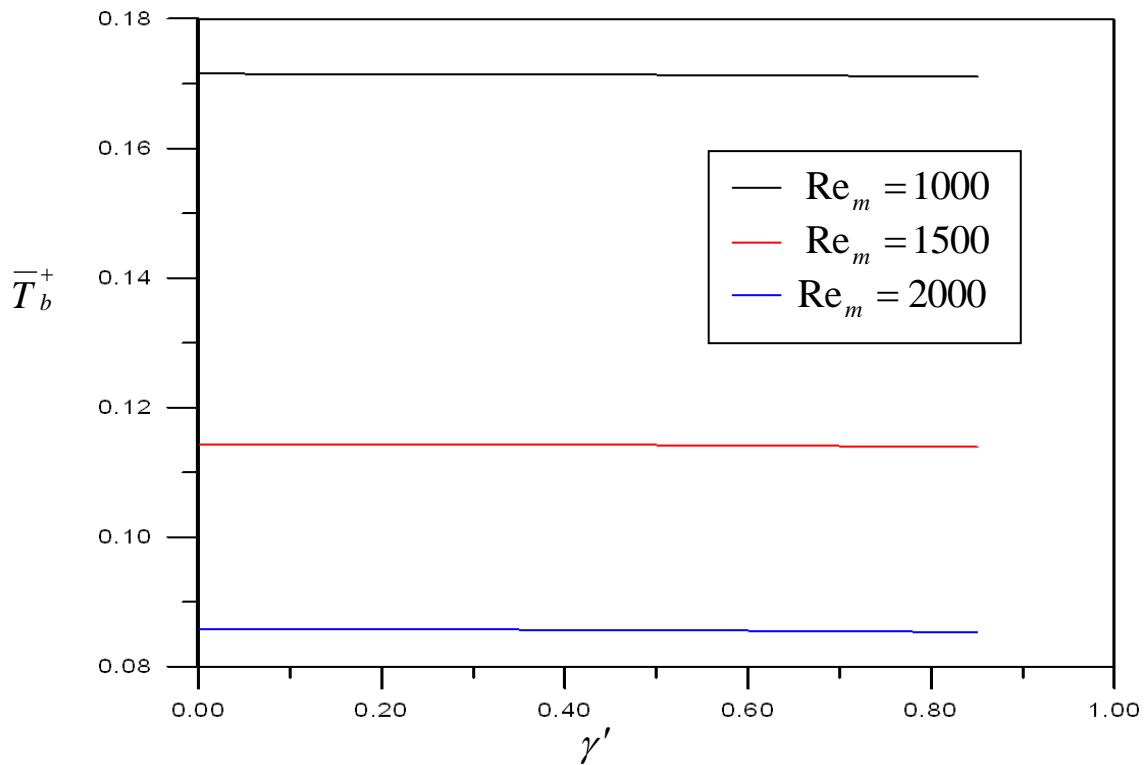


Fig.4.49 The Variation of time-averaged dimensionless bulk temperature with the ratio of the fluctuate to the steady pressure gradient for various values of mean Reynolds number at $\lambda=4$, $Pr=0.7$ and $x/D=30$. (Pulsating flow in the pipe)

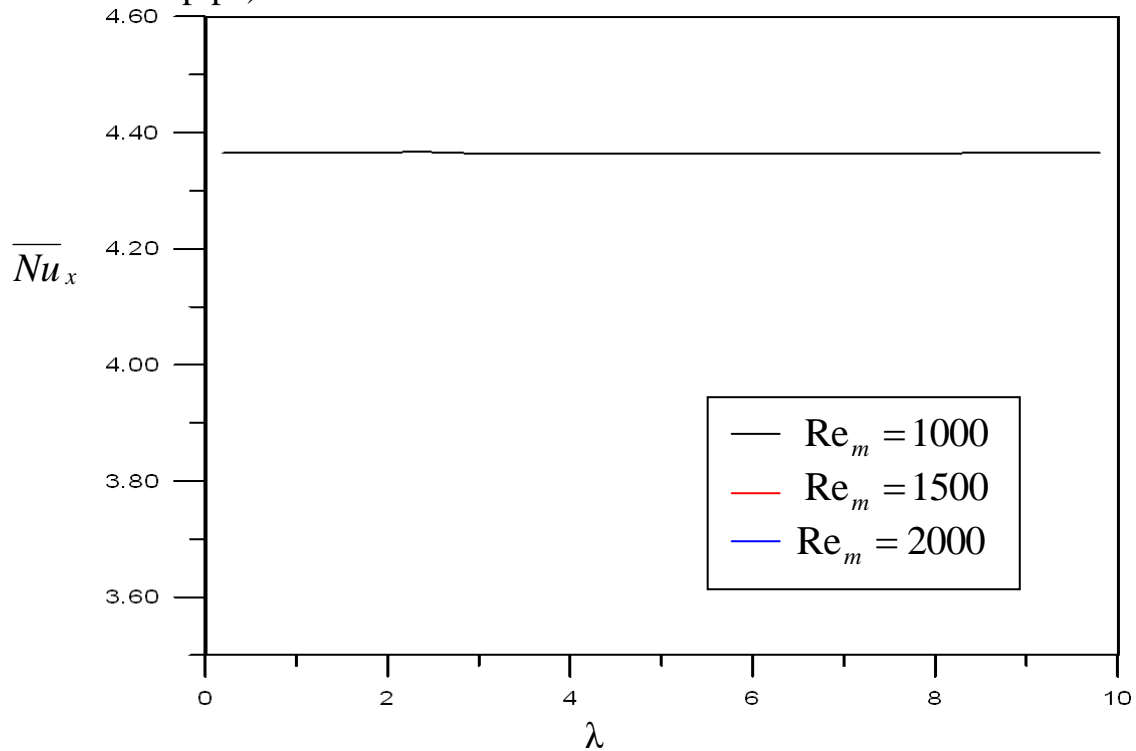


Fig.4.50 The Variation of time averaged-local Nusselt number with Womersly number for various values of mean Reynolds number at $\gamma' = 0.3$, $Pr=0.7$ and $x/D=30$. (Pulsating flow in the pipe)

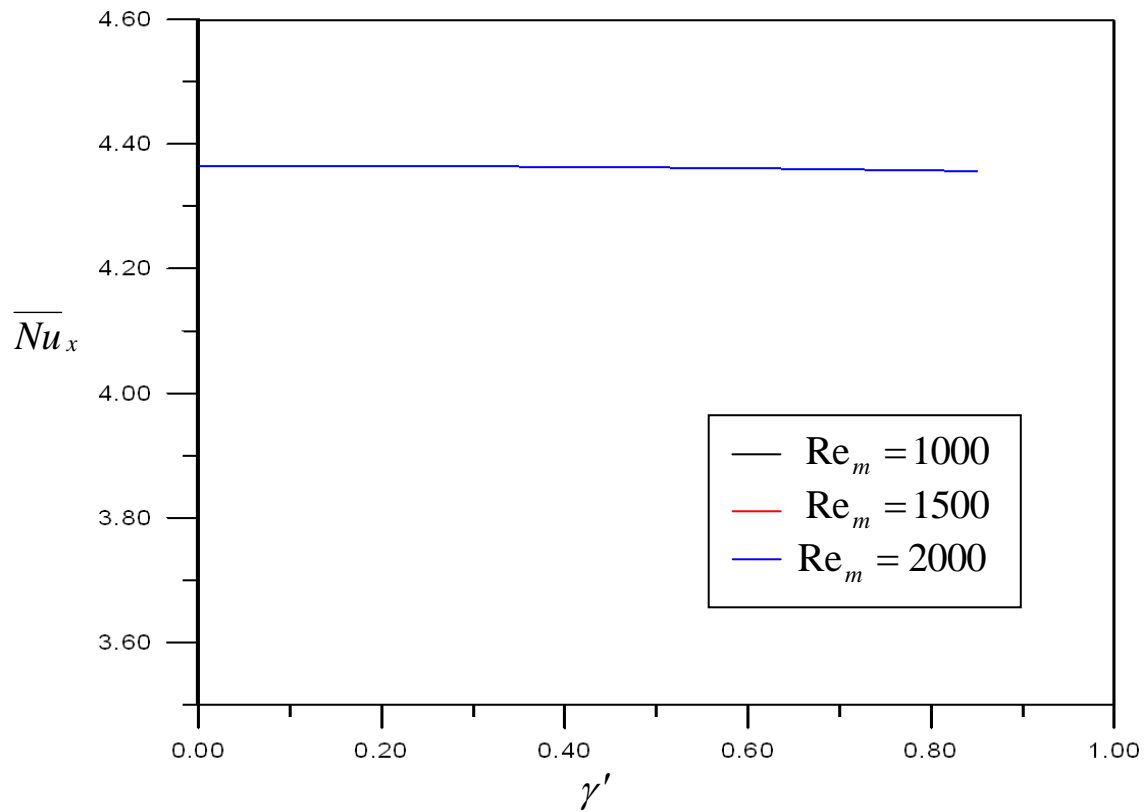


Fig.4.51 The Variation of the time averaged-local Nusselt number with the ratio of the fluctuate to the steady pressure gradient for various values of mean Reynolds number at $\lambda=4$, $Pr=0.7$ and $x/D=30$. (Pulsating flow in the pipe)

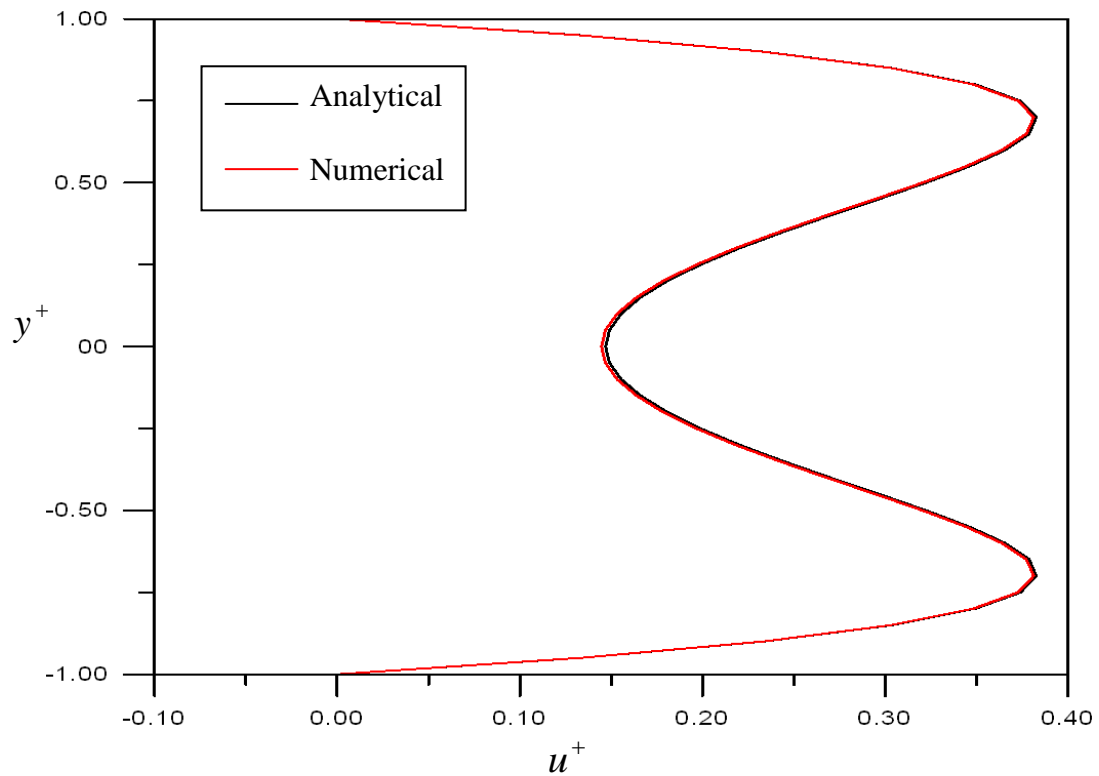


Fig.4.52 Comparison between the velocity profile of analytical and numerical solution of the new model for the reciprocating flow in the channel at $\omega t = 0.05$, $\lambda=4$, $A_o = 15$, $Pr=0.7$ and $x/D_h = 20$.

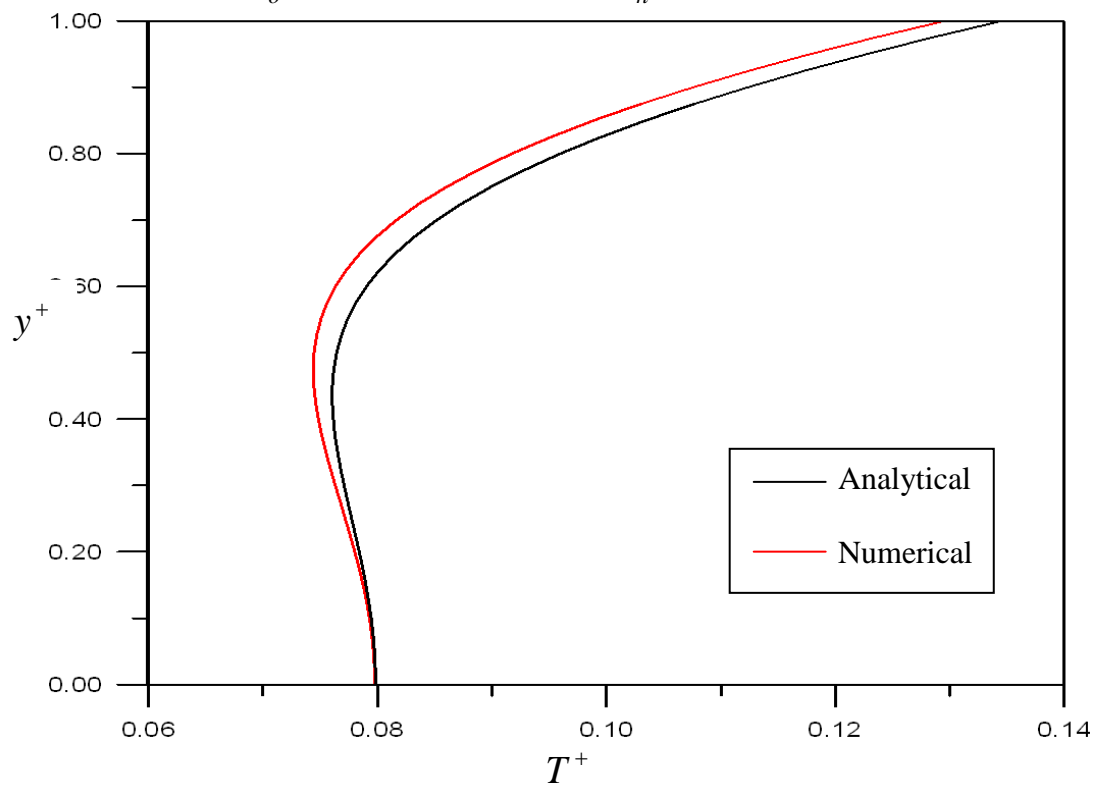


Fig.4.53 Comparison between the temperature profile of analytical and numerical solution of the new model for the reciprocating flow in the channel at $\omega t = 0.05$, $\lambda=4$, $A_o = 15$, $Pr=0.7$ and $x/D_h = 20$.

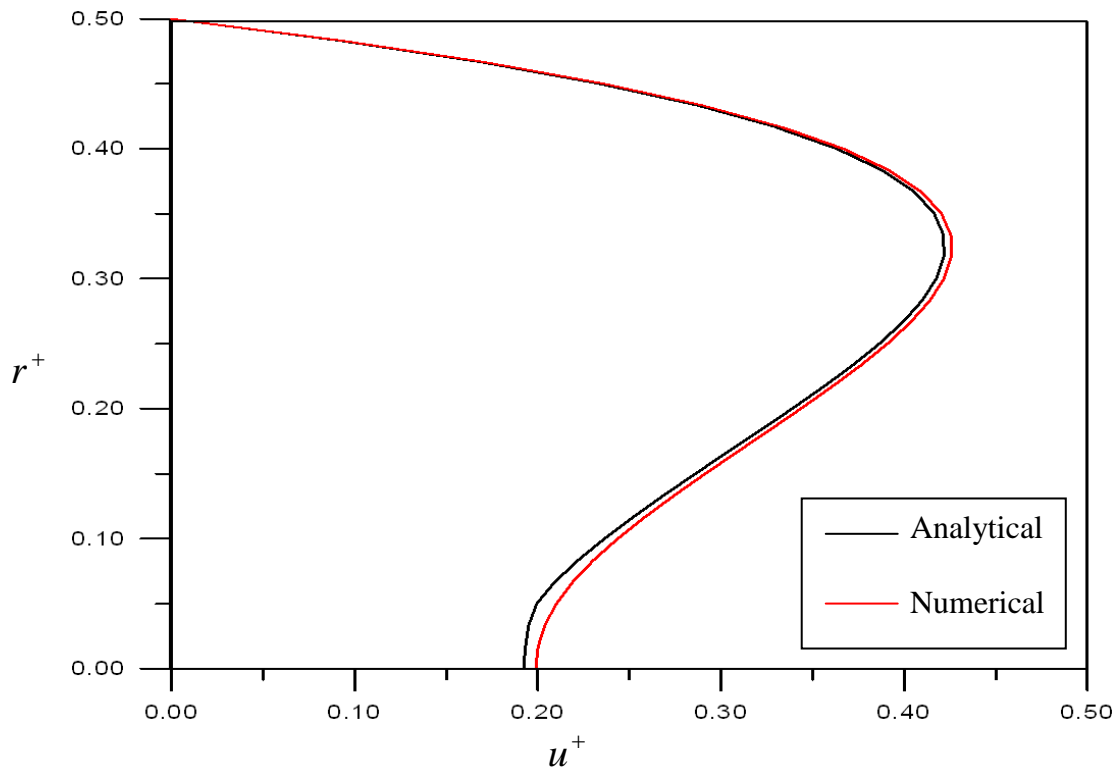


Fig.4.54 Comparison between the velocity profile of analytical and numerical solution of the new model for the reciprocating flow in the pipe at $\omega t = 0.05$, $\lambda=4$, $A_o = 15$, $Pr=0.7$ and $x/D = 20$.

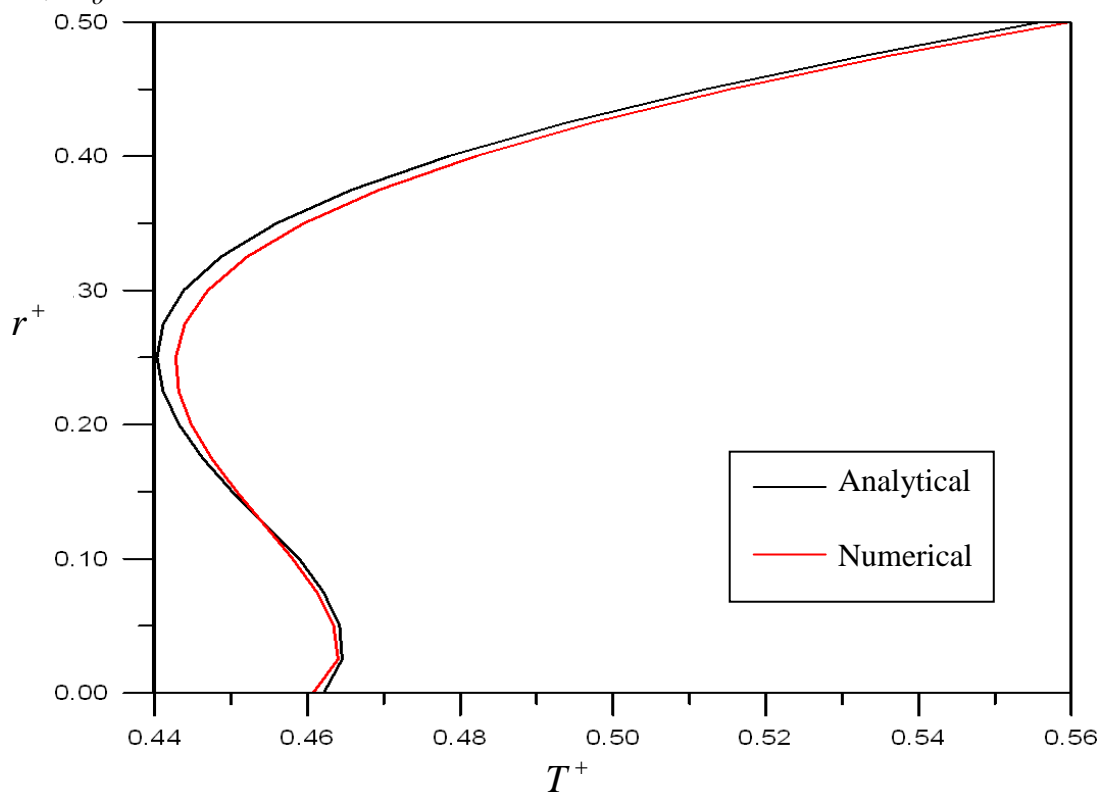


Fig.4.55 Comparison between analytical and numerical solution of the new model for the temperature profile for the reciprocating flow in the pipe at $\omega t = 0.05$, $\lambda=4$, $A_o = 15$, $Pr=0.7$ and $x/D = 20$.

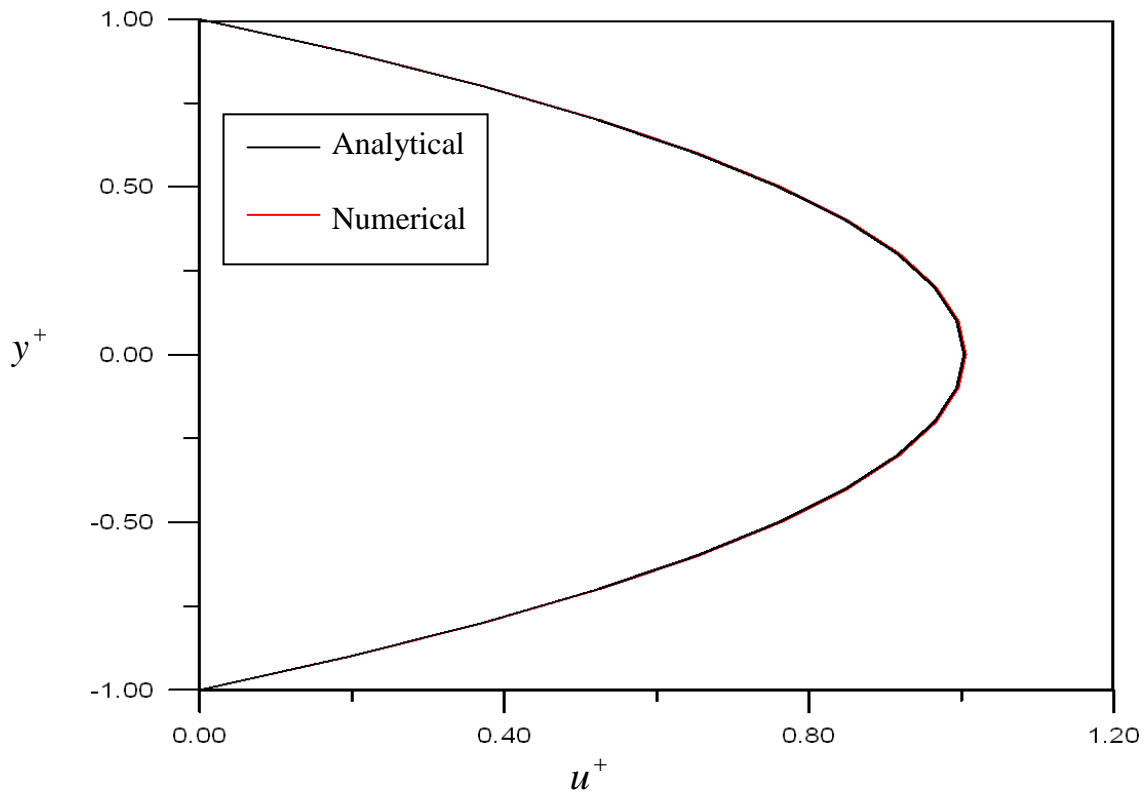


Fig.4.56 Comparison between analytical and numerical solution of the new model of the velocity profile for the pulsating flow in the Channel at $\omega t = 0.1$, $\lambda=4$, $\gamma' = 0.3$, $\text{Re}_m = 1200$, $\text{Pr}=0.7$ & $x/D_h = 20$.

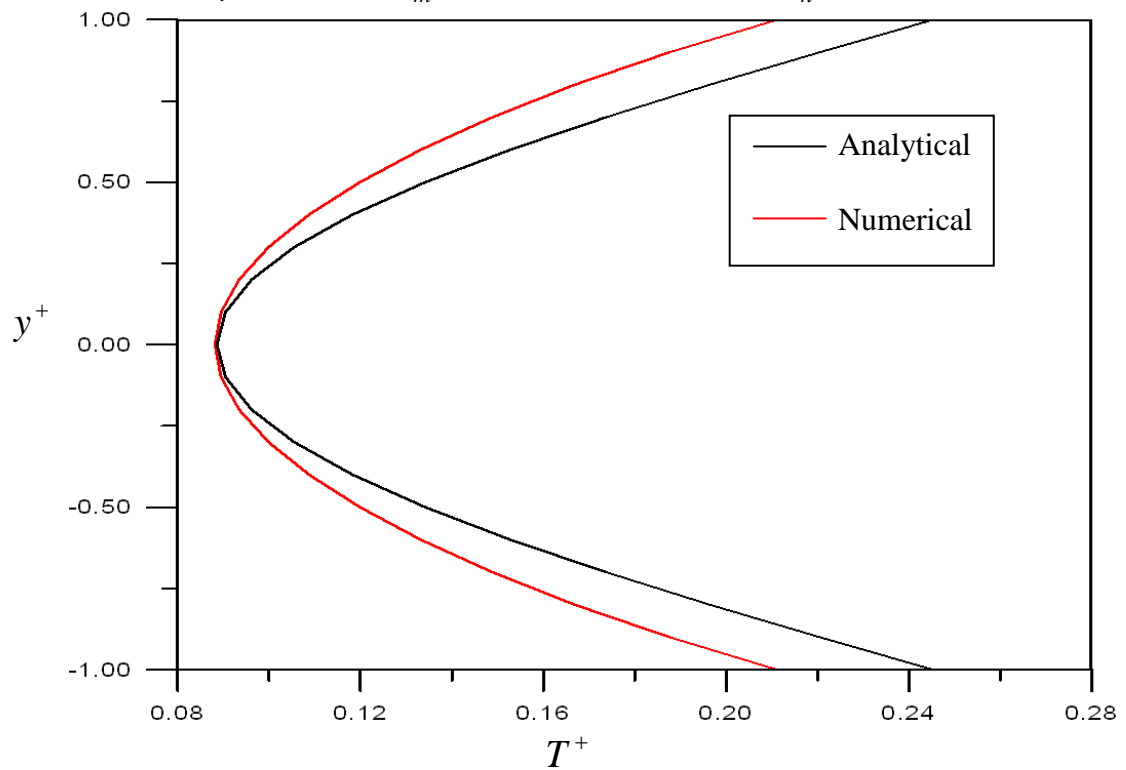


Fig.4.57 Comparison between analytical and numerical solution of the new model of the temperature profile for the pulsating flow in the channel at $\omega t = 0.4$, $\lambda=4$, $\gamma' = 0.3$, $\text{Re}_m = 1500$, $\text{Pr}=0.7$ and $x/D_h = 30$.

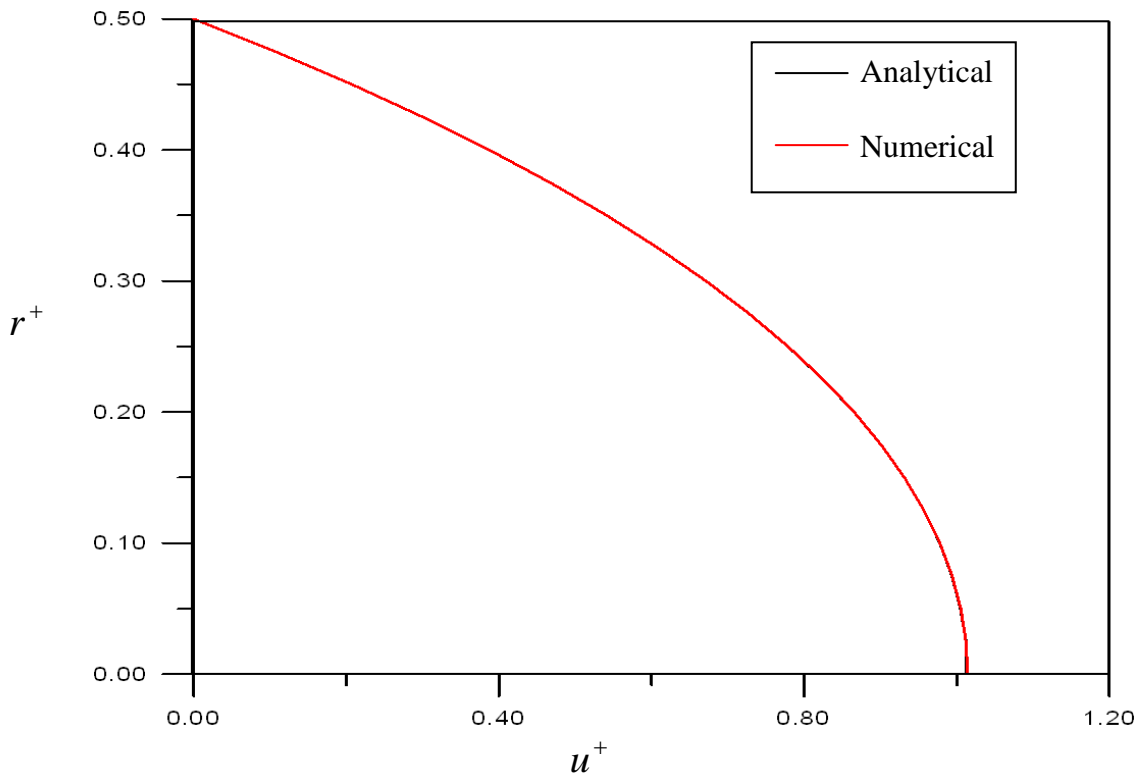


Fig.4.58 Comparison between analytical and numerical solution of the new model for the velocity profile for the pulsating flow in the pipe at $\omega t = 0.05$, $\lambda=4$, $\gamma' = 0.3$, $\text{Re}_m = 1000$, $\text{Pr}=0.7$ and $x/D = 30$.

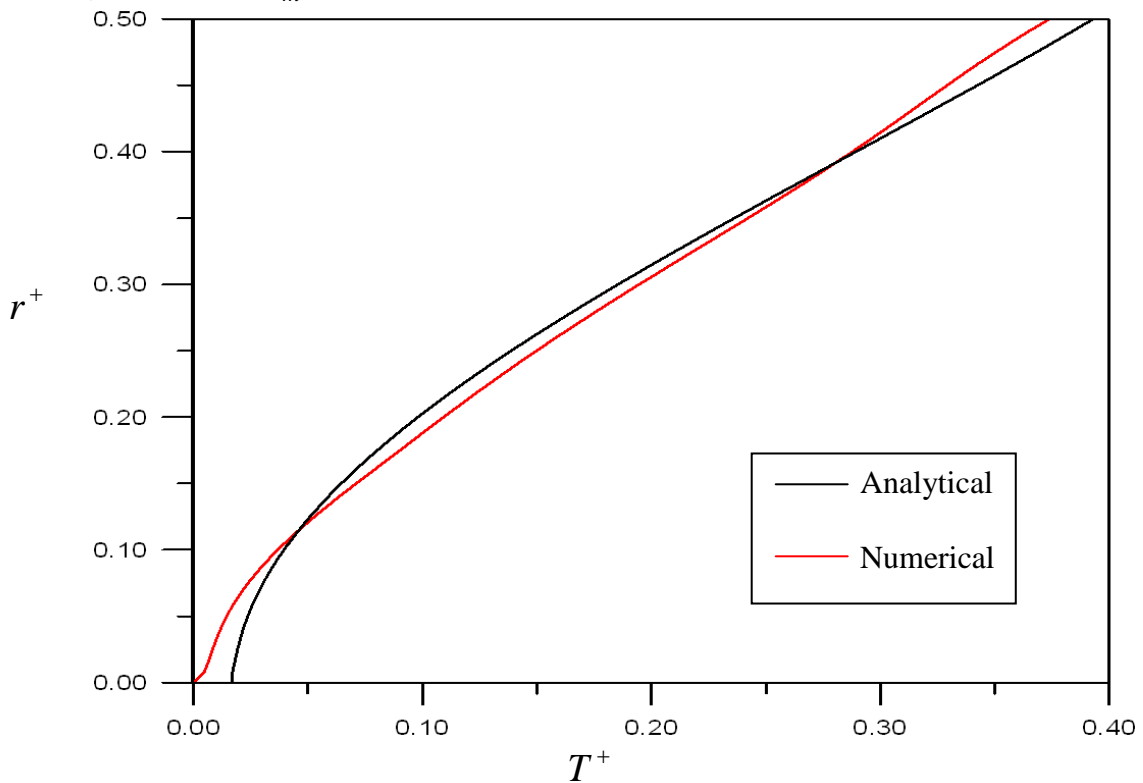


Fig.4.59 Comparison between analytical and numerical solution of the new model for the temperature Profile for the pulsating flow in the pipe at $\omega t = 0.05$, $\lambda=4$, $\gamma' = 0.3$, $\text{Re}_m = 1000$, $\text{Pr}=0.7$ and $x/D = 31$.

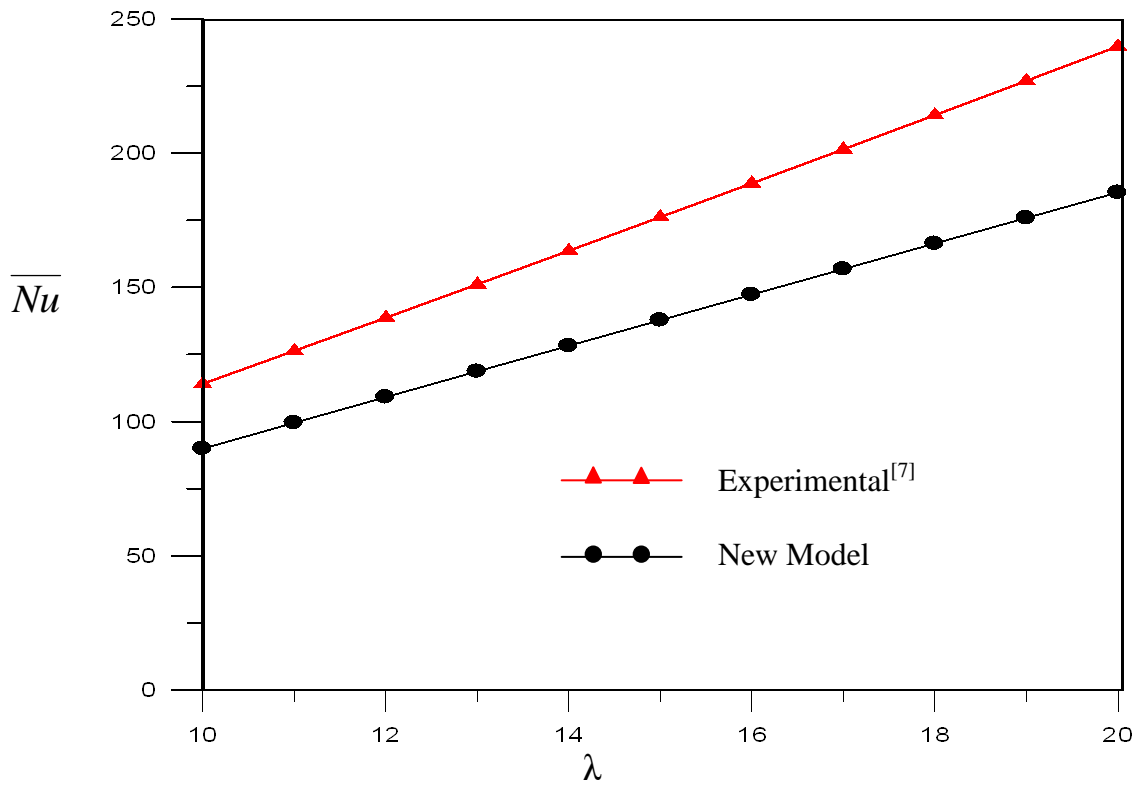


Fig.4.60 Comparison of the space-cycle averaged Nusselt number between present model and the experimental correlation of Copper et al.^[7], for the reciprocating flow in the channel.

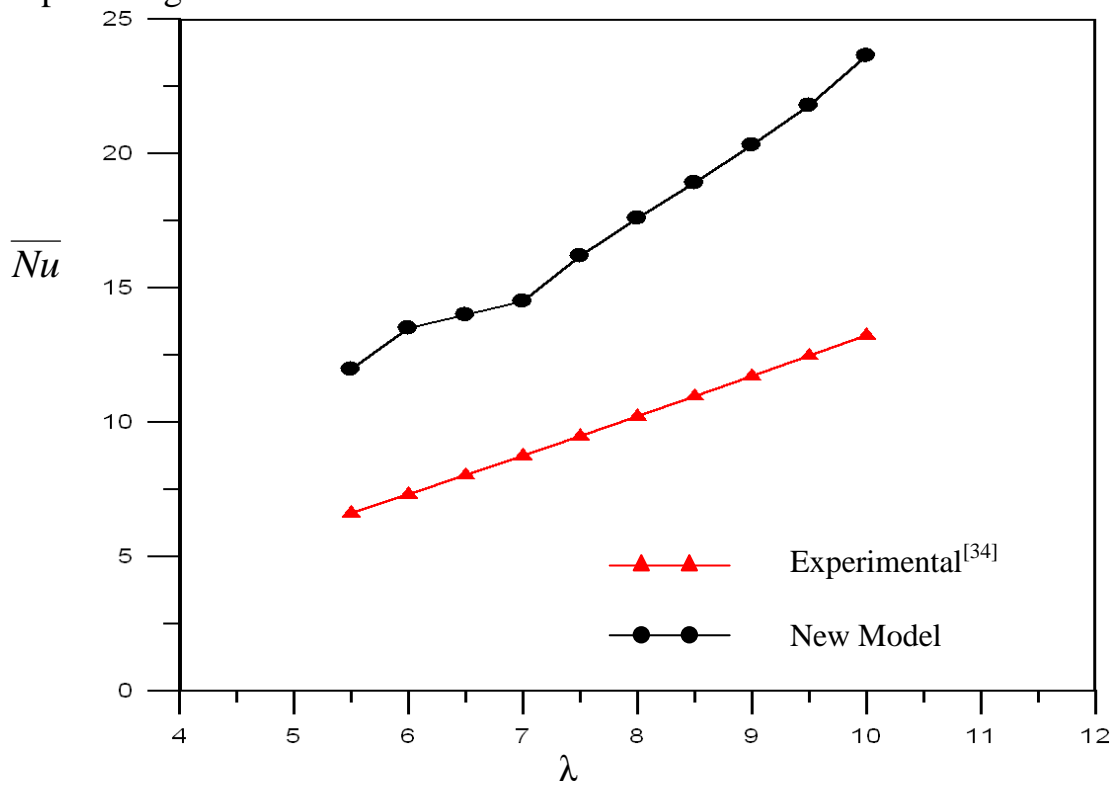


Fig.4.61 Comparison of the space-cycle averaged Nusselt number between the present model and the experimental correlation of Zhao and Cheng^[34], for the reciprocating flow in the pipe.

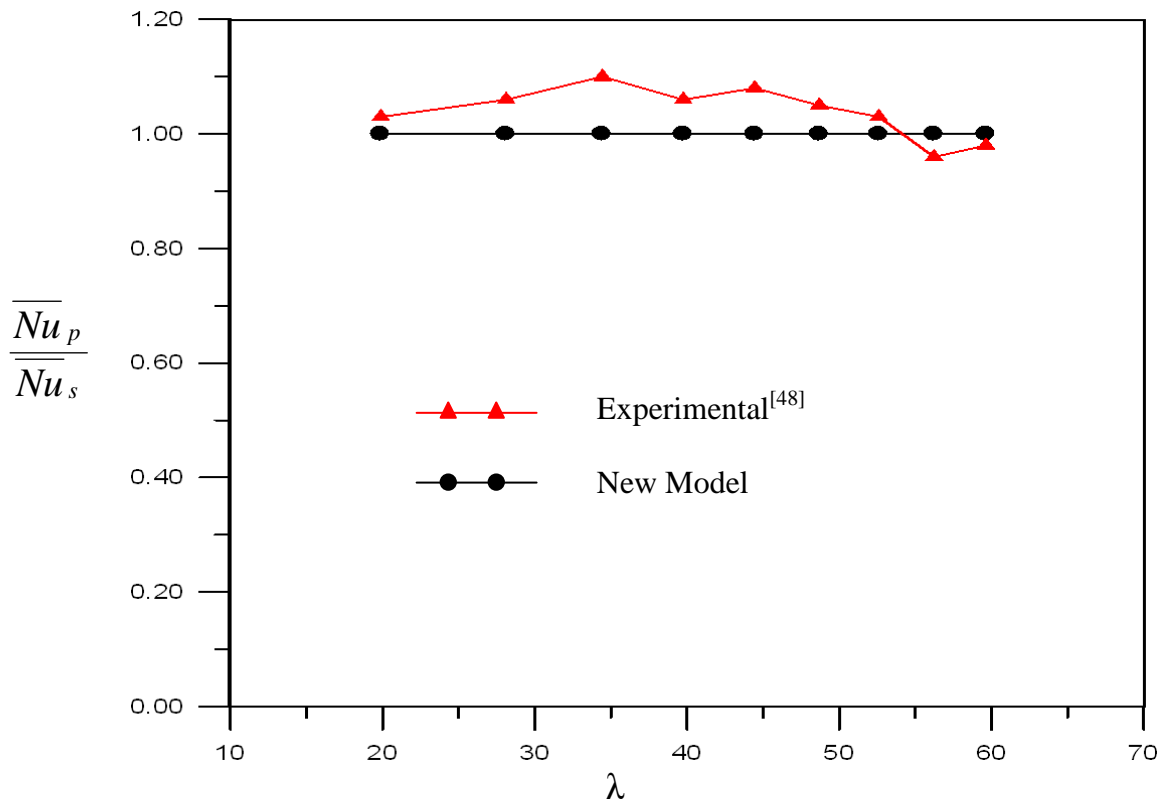


Fig.4.62 Comparison of the ratio of the time-averaged Nusselt number for the pulsating and steady flow in the channel .

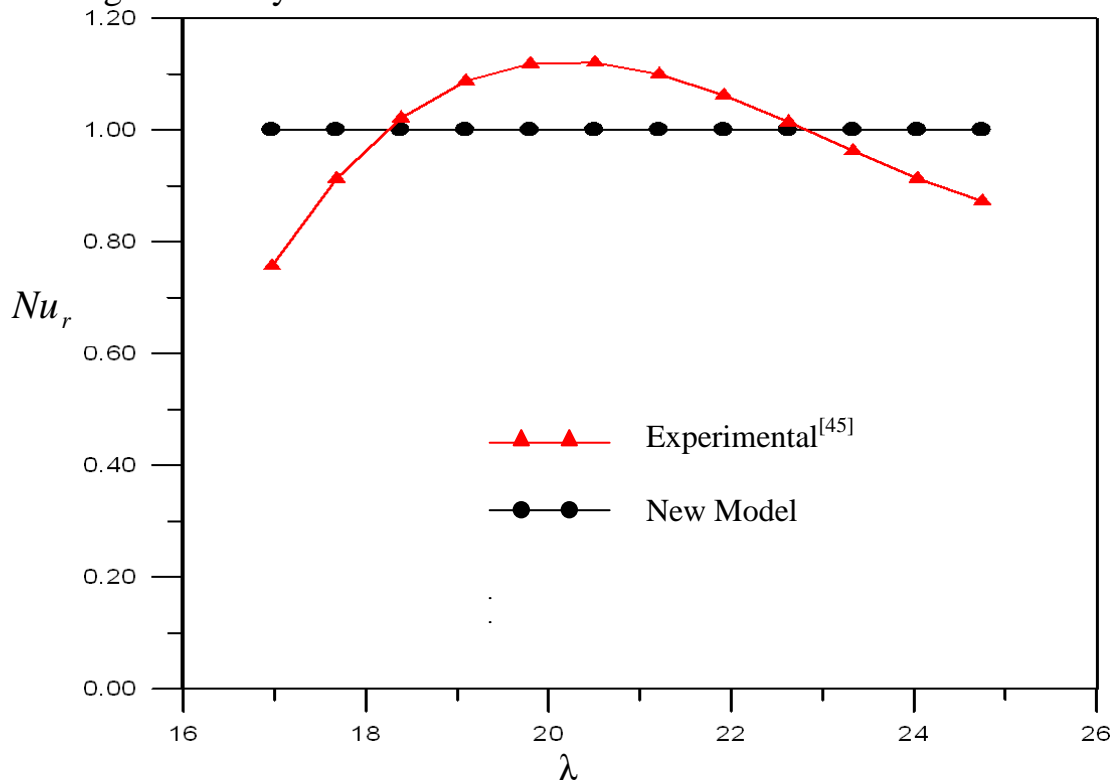


Fig.4.63 Comparison of the present relative mean Nusselt number with the experimental correlation of Habib et al.^[45], for the pulsating flow in the pipe.

CHAPTER FIVE CONCLUSIONS AND RECOMMENDATIONS

5.1 Conclusions

From the present analytical model it can be concluded the following remarks:

1- Analytical modeling for hydrodynamics and heat transfer in the oscillatory flow is possible based on the following considerations: laminar, 2D, incompressible, horizontal channel or pipe, no viscous dissipation $\Phi=0$ and the flow is driven by reciprocating or pulsating pressure gradient.

2- Both reciprocating and pulsating flow is studied and the obtained effecting parameters that control the flow and heat transfer are defined (i)for reciprocating flow as: Womersly number λ , dimensionless amplitude of fluid displacement A_o , Prandtl number Pr and the ratio of distance to hydraulic diameter x/D_h .(ii) for pulsating flow as: Womersly number λ , the ratio of fluctuate to steady pressure gradient γ' , mean Reynolds number Re_m , Prandtl number Pr and the ratio of distance to hydraulic diameter x/D_h .

3- The effect of oscillation on the velocity and temperature profiles is more significant in the reciprocating flow than pulsating flow.

4- The dimensionless bulk or center temperature and the instantaneous-local Nusselt number Nu_x are fluctuated periodically with time for reciprocating flow.

- 5- The instantaneous-local Nusselt number Nu_x and time averaged-local Nusselt number $\overline{Nu_x}$ are clearly increased with increasing Womersly number and Prandtl number in the reciprocating flow.
- 6- The reciprocating flow gives enhancement in the heat transfer rate reaches to order of magnitude for Nu_x or $\overline{Nu_x}$ comparing to steady state at the same considerations.
- 7- The results show that the an imposed flow pulsation causes both the temperature and Nusselt number fluctuate periodically about the solution for steady laminar convection.
- 8- The solution of pulsation flow has been demonstrated strongly that pulsation has no effect on the time average Nusselt number for pulsating convection heat transfer in the channel or the pipe with constant heat flux ($\overline{Nu}=4.364$ for pipe and $\overline{Nu}=8.235$ for channel with width \gg height).

5.2 Recommendations

In extension of the present study it is recommended for future to note the following:

- 1- This study can be developed for turbulent and compressible flow.
- 2- Heat transfer in the micro channels can be studied in the similar manor of the present model.
- 3- Entrance region can be investigated.
- 4- Investigation can be extended to hydrodynamics and heat transfer in oscillating external flow.
- 5- The present study can be accompanied with other devices to enhance heat transfer such as wavy wall or surface.

6- The periodically repeated conditions such as periodic wall temperature or periodic heat flux may be applied for future investigation.

REFERENCES

- [1] **Schlichting H.**, “Boundary- Layer Theory”, 7th Edition, McGraw-Hill, U.S.A., 1979.
- [2] **Hossain M.A., Pop I. and Rees D.A.S.**, “The Effect of Time-Periodic Surface Temperature Oscillations on Free Convection From a Vertical Surface in a Porous Medium”, *Transport in Porous Media*, Vol. 39, pp.119-130, 2000.
- [3] **Bahaidarah H. M.S. and Anand N.K.**, “Numerical Study of Heat and Momentum Transfer in Channels with Wavy Walls”, *Numerical Heat Transfer, Part A*, Vol.47, pp.417-439, 2005.
- [4] **Maikap T.K., Mahaparta T.R., Niyogi P., and Ghosh A.K.**, “Numerical Investigation of Laminar Separated Flow Through a Channel with Symmetric Double Expansion”, *Acta Mechanica*, Vol.179, pp.197-210, 2005.
- [5] **Watson E.J.**, “Diffusion in Oscillatory Pipe Flow”, *J. Fluid Mech.*, Vol.133, pp.233-244, 1983.
- [6] **Kurzweg U.H.**, “Enhanced Heat Conduction in Oscillating Viscous Flows within Parallel-Plate Channels”, *J. Fluid Mech.*, Vol. 156, pp.291-300, 1985.
- [7] **Zhao T.S. & Cheng P.**, “Heat Transfer in Oscillatory Flows”, *Annual Review of Heat Transfer*, Vol. IX, Chapter 7, 1998.
- [8] **Herman C., Kang E.**, “Experimental Visualization of Temperature Field and Study of Heat Transfer Enhancement in Oscillatory Flow in a Grooved Channel”, *Heat and Mass Transfer*, Vol.37, pp.87-99, 2001.

- [9] **Incropera R.P., Dewitt D.P.**, “Fundamentals of Heat and Mass Transfer”, 2nd Edition, John Wiley & Sons, 1985.
- [10] **Evans N. A.**, “Heat Transfer Through the Unsteady Laminar Boundary Layer on a Semi-Infinite Flat Plate, Part I: Theoretical Considerations”, *Int. J. Heat Mass Transfer*, Vol.16, pp.555-565, 1973.
- [11] **Peattie R. A.**, “Heat Transfer in Laminar Oscillatory Flow in Cylindrical and Conical Tube”, *Int. J. Heat Mass Transfer*, Vol.32, No.5, pp.923-934, 1989.
- [12] **Aziz A. and Lunardini V.J.**, “Analytical and Numerical Modeling of Steady Periodic Heat Transfer in Extended Surfaces”, *Computational Mechanics*, Vol.14, pp.387-410, 1994.
- [13] **Robertson M. B., Köhler U., Hoskins P. R. and Marshall I.**, “Flow in Elliptical Vessels Calculated for a Physiological Waveform”, *J. Vasc. Res.*, Vol.38, pp.73-82, 2000.
- [14] **Al-Slaman K.Y.Y.**, “Analysis of Direct Contact Condensation on Subcooled Wavy Falling Liquid Film”, Thesis Submitted to the Engineering College-University of Basrah, Basrah, Iraq, 2002.
- [15] **Wan Q. and Kuznetsov A.V.**, “Theoretical Analysis of Oscillating an Streaming Fields Between Two Parallel Beams and Numerical Investigation of the Cooling Efficiency”, *Proceeding of ASME Summer Heat Transfer Conference*, Nevada, USA, pp.1-12, 2003.
- [16] **Khaled A.-R.A. and Vafai K.**, “Analysis of Flow and Heat Transfer Inside Oscillatory Squeezed Thin Films Subject to a Varying Clearance”, *Int. J. Heat Mass Transfer*, Vol.46, pp.631-641, 2003.
- [17] **Khaled A.-R.A. and Vafai K.**, “The Effect of the Slip

Condition on Stokes and Couette Flows Due to an Oscillating Wall: Exact Solution”, Int. J. of Non-Linear Mechanics, Vol.39, pp.795 -809, 2004.

- [18] **Zhao T. & Cheng P.**,” A Numerical Solution of Laminar Forced Convection in a Heated Pipe Subjected to a Reciprocating Flow”, Int. J. Heat Mass Transfer. Vol.38, No.16, pp.3011-3022, 1995.
- [19] **Zhao T.S. and Cheng P.**, “The Friction Coefficient of a Fully Developed Laminar Reciprocating Flow in a Circular Pipe”, Int. J. Heat and Fluid Flow, Vol.17, No.2, p.p.167-172, 1996.
- [20] **Burmeister L. C.**, “Convective Heat Transfer”,1st Edition, John Wiley& Sons, 1983.
- [21] **Yakhot A., Arad M., and Ben-Dor G.**, “Numerical Investigation a of Laminar Pulsating Flow in a Rectangular Duct”, Int. J. Numer. Meth. Fluids, Vol.29, pp.935-950, 1999.
- [22] **Karagöz İ.**, ”Similarity Solution of the Oscillatory Pressure Driven Fully Developed Flow in a Channel”, Uludağ Üniversitesi Mühendislik- Mimarlık Fakültesi Dergisi, Cilt7, Sayı 1, 2002.
- [23] **Sert C. and Beskok A.**,” Oscillatory Flow Forced Convection in Micro Heat Spreaders”, Numerical Heat Transfer, Part A, Vol.42, pp.685-705, 2002.
- [24] **Sert C. and Beskok A.**, “Numerical Simulation of Reciprocating Flow Forced convection in Two-Dimensional Channels”, ASME J. Heat Transfer, Vol.125, pp.403-412, 2003.
- [25] **Cosgrove J.A., Buick J.M., Tonge S.J., Munro C.G., Great C.A. and Campbell D.M.**, “Application of the Lattice Boltzman Method to Transition in Oscillatory Channel Flow”, J. Phys. A: Math. Gen., Vol.36, pp.2609-2620, 2003.

- [26] **Von Kerczek C. H.**, “The Instability of Oscillatory Plane Poiseuille Flow”, *J. Fluid Mech.*, Vol.116, pp.91-114, 1982.
- [27] **Shemer L., Wygnanski I. and Kit E.**, “Pulsating Flow in Pipe”, *J. Fluid Mech.*, Vol.153, pp.313-337, 1985.
- [28] **Valencia A. and Hinojosa L.**, “Numerical Solutions of Pulsating Flow and Heat Transfer Characteristics in a Channel with a Backward-Facing Step”, *Heat and Mass Transfer*, Vol.32, pp.143-148, 1997.
- [29] **Ju Y. L., Wong C. and Zhou Y.**, “Numerical Simulation and Experimental Verification of the Oscillating Flow in Pulse Tube Refrigerator”, *Cryogenics*, Vol.38, No.2, pp.169-176, 1998.
- [30] **Ju Y., Jiang Y. and Zhou Y.**, “Experimental Study of the Oscillating Flow Characteristics for a Regenerator in a Pulse Tube Cryocooler”, *Cryogenics*, Vol.38, pp.649-656, 1998.
- [31] **José G., Carlos S., Eduardo B. and Joaquin F.**, “Unsteady Flow Structure on a Centrifugal Pump: Experimental and Numerical Approaches”, *Proceedings of the US-European Fluids Engineering Summer Conference*, Montreal, Canada, 2002.
- [32] **Yakhot A. and Grinberg L.**, “Phase Shift Ellipses for Pulsating Flows”, *Physics of Fluids*, Vol.15, No.7, pp.2081-2083, 2003.
- [33] **Baranyi L.**, “Computation of Unsteady Momentum and Heat Transfer from a Fixed Circular Cylinder in Laminar Flow”, *J. of Computational and Applied Mechanics*, Vol.4, No.1, pp.13-25, 2003.
- [34] **Zhao T. & Cheng P.**, “Oscillatory Heat Transfer in a Pipe Subjected to a Laminar Reciprocating Flow”, *ASME J. Heat Transfer*, Vol.118, p.p.592-598, 1996.

- [35] **Joshi C.H., Kamm R.D., Drazen J.M. and Stutsky A.S.**, “An Experimental Study of Gas Exchange in Laminar Oscillatory Flow”, *J. Fluid Mech.*, Vol.133, pp.245-254, 1983.
- [36] **Kurzweg U.H.**, “Enhanced Heat Conduction in Fluids Subjected to Sinusoidal Oscillations”, *J. Heat Transfer*, Vol. 107, pp.459-462, 1985.
- [37] **Kaviany M.**, “Performance of a Heat Exchanger Based on Enhanced Heat Diffusion in Fluids by Oscillation: Analysis”, *J. Heat Transfer*, Vol.112, pp.49-55, 1990.
- [38] **Kaviany M and Rekker M.**, “Performance of a Heat Exchanger Based on Enhanced Heat Diffusion in Fluids by Oscillation: Experiment”, *J. Heat Transfer*, Vol.112, pp.56-62, 1990.
- [39] **Khaled A.-R.A. and Vafai K.**, “Flow and Heat Transfer Inside Thin Films Supported by Soft Seals in the Presence of Internal and External Pressure Pulsations”, *Int. J. Heat and Mass Transfer*, Vol.42, pp.5107-5115, 2002.
- [40] **Karagoz I.**, “Variation of Momentum and Thermal Boundary Layers for Oscillatory Flows in a Channel”, *Int. Comm. Heat Mass Transfer*, Vol.28, No.3, pp.379-388, 2001.
- [41] **Chang S.W.**, “Forced Heat Convection in a Reciprocating Duct Fitted with 45 Degree Crossed Ribs”, *Int. J. Therm. Sci.*, Vol.41, pp.229-240, 2002.
- [42] **Habib M.A., Said S.A.M., Al-Farayedhi A.A., Al-Dini S.A., Asghar A. and Gbadebo S.A.**, “Heat Transfer Characteristics of Pulsated Turbulent Pipe Flow”, *Heat and Mass Transfer*, Vol.34, pp.413-421, 1999.

- [43] **Herman C. and Kang E.**, “Experimental Visualization of Temperature Fields and Study of Heat Transfer Enhancement in Oscillatory in a Grooved Channel”, Heat and Mass Transfer, Vol.37, pp.87-99, 2001.
- [44]] **Valencia A., Martin J.S. and Gormaz R.**, “Numerical Study of the Unsteady Flow and Heat Transfer in Channels with Periodically Mounted Square Bars”, Heat and Mass Transfer, Vol.37, pp.265-270, 2001.
- [45] **Habib M.A., Attya A.M., Eid A.I. and Aly A.Z.**, “Convective Heat Transfer Characteristics of Laminar Pulsating Pipe Air Flow”, Heat and Mass Transfer, Vol.38, pp.221-232, 2002.
- [46] **Bouhadji A. and Djilali N.**, “Forcing of Unsteady Separated Flow and Convective Heat Transfer via Bulk Upstream Oscillations”, Int. J. Heat and Fluid Flow, Vol.24, pp.77-90, 2003.
- [47] **Yu J.-C., Li Z.-X. and Zhao T.S.**, “An Analytical Study of Pulsating Laminar Heat Convection in a Circular Tube with Constant Heat Flux”, Int. J. of Heat and Mass Transfer, Vol.47, pp.5297-5301, 2004.
- [48] **Moon J.W., Kim S.Y. and Cho H.H.**, “Frequency-Dependent Heat Transfer Enhancement from Rectangular Heated Block Array in a Pulsating Channel Flow”, Int. J. Heat and Mass Transfer, Vol.48, pp.4904-4913, 2005.
- [49] **Zohir A.E., Habib M.A., Attya A.M. and Eid A.I.**, “An Experimental Investigation of Heat Transfer to Pulsating Pipe Air Flow with Different Amplitudes”, Heat Mass Transfer, Vol.42 No.7, 2006.

- [50] **Spiegel M.R.**, “Schaum’s Outline of Theory and Problems of Advanced Mathematics for Engineering and Scientists”, 1st Edition, McGraw-Hill, U.S.A., 1971.
- [51] **Versteeg H.K. and Malalasekera W.**, “An Introduction Computational Fluid Dynamics: The Finite Volume Method”, Longman Group, England, 1995.
- [52] **Hornbeck R.W.**, “Numerical Marching Techniques for Fluid Flows with Heat Transfer”, NASA SP-297, Washington, 1973.

APPENDICES

Appendix A

The functions that find in the Eq.3.20 are defined as

$$E_1 = E U + F W \quad (A.1)$$

$$F_1 = F U - E W \quad (A.2)$$

$$U_2 = U^2 + W^2 \quad (A.3)$$

$$Y_1 = Y C + Z D \quad (A.4)$$

$$Z_1 = Z C - Y D \quad (A.5)$$

$$C_3 = C^2 + D^2 \quad (A.6)$$

$$Q_1 = Q C + P D \quad (A.7)$$

$$P_1 = P C - Q D \quad (A.8)$$

and

$$E = \cosh(\sqrt{\text{Pr}/2} \lambda y^+) \cos(\sqrt{\text{Pr}/2} \lambda y^+) \quad (A.9)$$

$$F = \sinh(\sqrt{\text{Pr}/2} \lambda y^+) \sin(\sqrt{\text{Pr}/2} \lambda y^+) \quad (A.10)$$

$$U = \sinh(\sqrt{\text{Pr}/2} \lambda) \sin(\sqrt{\text{Pr}/2} \lambda) \quad (A.11)$$

$$W = \cosh(\sqrt{\text{Pr}/2} \lambda) \cos(\sqrt{\text{Pr}/2} \lambda) \quad (A.12)$$

$$Q = \cosh(\lambda/\sqrt{2} y^+) \cos(\lambda/\sqrt{2} y^+) \quad (A.13)$$

$$P = \sinh(\lambda/\sqrt{2} y^+) \sin(\lambda/\sqrt{2} y^+) \quad (A.14)$$

$$C = \cosh(\lambda/\sqrt{2}) \cos(\lambda/\sqrt{2}) \quad (A.15)$$

$$D = \sinh(\lambda/\sqrt{2}) \sin(\lambda/\sqrt{2}) \quad (A.16)$$

$$Y = \sinh(\lambda/\sqrt{2}) \cos(\lambda/\sqrt{2}) \quad (A.17)$$

$$Z = \cosh(\lambda/\sqrt{2}) \sin(\lambda/\sqrt{2}) \quad (A.18)$$

Appendix B

The general form of Bessel function with complex variable $(i^{3/2})$ is ^[50]

$$J_n(i^{3/2} 2r^+ \lambda) = Ber_n(2r^+ \lambda) + i Bei_n(2r^+ \lambda) \quad (B.1)$$

where

J_n : Bessel function of order n.

n: the order of Bessel function.

and

$$Ber_n(x) = \sum_{k=0}^{\infty} \frac{(x/2)^{2k+n}}{k! \Gamma(n+k+1)} \cos\left(\frac{3n+2k}{4}\right)\pi \quad (B.2)$$

$$Bei_n(x) = \sum_{k=0}^{\infty} \frac{(x/2)^{2k+n}}{k! \Gamma(n+k+1)} \sin\left(\frac{3n+2k}{4}\right)\pi \quad (B.3)$$

and

Γ : is Gama function defined as

$$\Gamma = \int_0^{\infty} e^{-x} x^{n-1} dx \quad (B.4)$$

$$\Gamma(n+1) = n! \quad , n=1,2,3, \quad (B.5)$$

for n=0 (zero order)

$$Ber_0(x) = \sum_{k=0}^{\infty} \frac{(-1)^k (x)^{4k}}{2^{4k} [(2k)!]^2} = 1 - \frac{x^4}{2^2 4^2} + \frac{x^8}{2^2 4^2 6^2 8^2} + \dots \quad (B.6)$$

$$Bei_0(x) = \sum_{k=0}^{\infty} \frac{(-1)^k (x)^{4k+2}}{2^{4k+2} [(2k+1)!]^2} = \frac{x^2}{2^2} - \frac{x^6}{2^2 4^2 6^2} + \dots \quad (B.7)$$

Appendix C

The complex functions in the Eq.3.50 are simplified as

$$J_0\left(2i^{3/2}\lambda\sqrt{\text{Pr}r^+}\right) = \text{Ber}_0(2\lambda\sqrt{\text{Pr}r^+}) + i\text{Bei}_0(2\lambda\sqrt{\text{Pr}r^+}) = BR_1 + iBI_1 \quad (\text{C.1})$$

$$J_1\left(i^{3/2}\lambda\sqrt{\text{Pr}}\right) = \text{Ber}_1(\lambda\sqrt{\text{Pr}}) + i\text{Bei}_1(\lambda\sqrt{\text{Pr}}) = BR_2 + iBI_2 \quad (\text{C.2})$$

$$J_1\left(i^{3/2}\lambda\right) = \text{Ber}_1(\lambda) + i\text{Bei}_1(\lambda) = BR_3 + iBI_3 \quad (\text{C.3})$$

$$J_0\left(i^{3/2}\lambda\right) = \text{Ber}_0(\lambda) + i\text{Bei}_0(\lambda) = BR_4 + iBI_4 \quad (\text{C.4})$$

$$J_0\left(2i^{3/2}\lambda r^+\right) = \text{Ber}_0(2\lambda r^+) + i\text{Bei}_0(2\lambda r^+) = BR_5 + iBI_5 \quad (\text{C.5})$$

and the function RE_1 , IM_1 , RE_2 , IM_2 , RE_3 , and IM_3 in Eq.3.51 are

$$RE_1 = \frac{BR_1 BR_2 + BI_1 BI_2}{BR_2^2 + BI_2^2} \quad (\text{C.6})$$

$$IM_1 = \frac{-BR_1 BI_2 + BI_1 BR_2}{BR_2^2 + BI_2^2} \quad (\text{C.7})$$

$$RE_2 = \frac{BR_3 BR_4 + BI_3 BI_4}{BR_4^2 + BI_4^2} \quad (\text{C.8})$$

$$IM_2 = \frac{-BR_3 BI_4 + BI_3 BR_4}{BR_4^2 + BI_4^2} \quad (\text{C.9})$$

$$RE_3 = \frac{BR_5 BR_4 + BI_5 BI_4}{BR_4^2 + BI_4^2} \quad (\text{C.10})$$

$$IM_3 = \frac{-BR_5 BI_4 + BI_5 BR_4}{BR_4^2 + BI_4^2} \quad (\text{C.11})$$

Appendix D

The complex Bessel function in Eq.3.50 are simplified using asymptotic Bessel function for complex variable Eq.3.38 as below

$$\frac{J_0(2i^{3/2}\lambda\sqrt{\text{Pr}r^+})}{J_1(i^{3/2}\lambda\sqrt{\text{Pr}})} = \frac{\sqrt{\frac{2}{\pi}} e^{i\frac{2(1-i)}{\sqrt{2}}\lambda\sqrt{\text{Pr}r^+}} (i2i^{3/2}\lambda\sqrt{\text{Pr}r^+})^{-1/2} (i)^0}{\sqrt{\frac{2}{\pi}} e^{i\frac{(1-i)}{\sqrt{2}}\lambda\sqrt{\text{Pr}}} (ii^{3/2}\lambda\sqrt{\text{Pr}})^{-1/2} (i)^{-1}} \quad (D.1)$$

$$\frac{J_0(2i^{3/2}\lambda\sqrt{\text{Pr}r^+})}{J_1(i^{3/2}\lambda\sqrt{\text{Pr}})} = \frac{1}{\sqrt{2r^+}} e^{i\frac{(1-i)}{\sqrt{2}}\lambda\sqrt{\text{Pr}}(2r^+-1)} \cdot i \quad (D.2)$$

$$\frac{J_0(2i^{3/2}\lambda\sqrt{\text{Pr}r^+})}{J_1(i^{3/2}\lambda\sqrt{\text{Pr}})} = \frac{1}{\sqrt{2r^+}} e^{\frac{(1+i)}{\sqrt{2}}\lambda\sqrt{\text{Pr}}(2r^+-1)} \cdot i \quad (D.3)$$

$$\frac{J_0(2i^{3/2}\lambda\sqrt{\text{Pr}r^+})}{J_1(i^{3/2}\lambda\sqrt{\text{Pr}})} = \frac{i}{\sqrt{2r^+}} e^{\sqrt{\frac{\text{Pr}}{2}}\lambda(2r^+-1)} e^{i\sqrt{\frac{\text{Pr}}{2}}\lambda(2r^+-1)} \quad (D.4)$$

$$\frac{J_0(2i^{3/2}\lambda\sqrt{\text{Pr}r^+})}{J_1(i^{3/2}\lambda\sqrt{\text{Pr}})} = \frac{i}{\sqrt{2r^+}} e^{\sqrt{\frac{\text{Pr}}{2}}\lambda(2r^+-1)} \left[\begin{array}{l} \cos(\sqrt{\text{Pr}/2}\lambda(2r^+-1)) + i \\ \sin(\sqrt{\text{Pr}/2}\lambda(2r^+-1)) \end{array} \right] \quad (D.5)$$

and

$$\frac{J_1(i^{3/2}\lambda)}{J_0(i^{3/2}\lambda)} = \frac{\sqrt{\frac{2}{\pi}} e^{ii^{3/2}\lambda} (ii^{3/2}\lambda)^{-1/2} (i)^{-1}}{\sqrt{\frac{2}{\pi}} e^{i\frac{(1-i)}{\sqrt{2}}\lambda} (ii^{3/2}\lambda)^{-1/2} (i)^0} = \frac{1}{i} = -i \quad (D.6)$$

and

$$\frac{J_0(2i^{3/2}\lambda r^+)}{J_0(i^{3/2}\lambda)} = \frac{\sqrt{\frac{2}{\pi}} e^{i2i^{3/2}\lambda r^+} (i2i^{3/2}\lambda r^+)^{-1/2} (i)^0}{\sqrt{\frac{2}{\pi}} e^{i\frac{(1-i)\lambda}{\sqrt{2}}} (ii^{3/2}\lambda)^{-1/2} (i)^0} \quad (D.7)$$

$$\frac{J_0(2i^{3/2}\lambda r^+)}{J_0(i^{3/2}\lambda)} = \frac{1}{\sqrt{2r^+}} e^{i\frac{(1-i)\lambda}{\sqrt{2}}\lambda(2r^+-1)} \quad (D.8)$$

$$\frac{J_0(2i^{3/2}\lambda r^+)}{J_0(i^{3/2}\lambda)} = \frac{1}{\sqrt{2r^+}} e^{\frac{(1+i)\lambda}{\sqrt{2}}\lambda(2r^+-1)} \quad (D.9)$$

The Eqs.E.5, E.6 and E.9 are substituted in Eq.3.50 to obtain Eq.3.52.

Appendix E

For steady flow the solution of momentum equation in x-direction gives the velocity distribution as

$$u^+ = 1 - y^{+2} \quad (E.1)$$

where

$$u^+ = \frac{u}{u_{\max}}, \quad u_{\max} = \frac{P_o h^2 / \nu}{2}$$

the average velocity defined as

$$u_m = \frac{Q}{\text{area}} = \frac{\int u dA}{\int dA} \quad (E.2)$$

by substituting Eq.E.1 obtain

$$u_m = u_{\max} \int_0^1 (1 - y^{+2}) dy^+ = \frac{2}{3} u_{\max} \quad (E.3)$$

then

$$u_m = \frac{2}{3} u_{\max} \quad (E.4)$$

Appendix F

The function which defined in Eq.3.88 are

$$E_1 = E U + F W \quad (F.1)$$

$$F_1 = F U - E W \quad (F.2)$$

$$U_2 = U^2 + W^2 \quad (F.3)$$

$$Y_1 = Y C + Z D \quad (F.4)$$

$$Z_1 = Z C - Y D \quad (F.5)$$

$$C_2 = C^2 + D^2 \quad (F.6)$$

$$Q_1 = Q C + P D \quad (F.7)$$

$$P_1 = P C - Q D \quad (F.8)$$

and

$$E = \cosh(\sqrt{\text{Pr}/2} \lambda y^+) \cos(\sqrt{\text{Pr}/2} \lambda y^+) \quad (F.9)$$

$$F = \sinh(\sqrt{\text{Pr}/2} \lambda y^+) \sin(\sqrt{\text{Pr}/2} \lambda y^+) \quad (F.10)$$

$$U = \sinh(\sqrt{\text{Pr}/2} \lambda) \cos(\sqrt{\text{Pr}/2} \lambda) \quad (F.11)$$

$$W = \cosh(\sqrt{\text{Pr}/2} \lambda) \sin(\sqrt{\text{Pr}/2} \lambda) \quad (F.12)$$

$$Q = \cosh(\lambda/\sqrt{2} y^+) \cos(\lambda/\sqrt{2} y^+) \quad (F.13)$$

$$P = \sinh(\lambda/\sqrt{2} y^+) \sin(\lambda/\sqrt{2} y^+) \quad (F.14)$$

$$C = \cosh(\lambda/\sqrt{2}) \cos(\lambda/\sqrt{2}) \quad (F.15)$$

$$D = \sinh(\lambda/\sqrt{2}) \sin(\lambda/\sqrt{2}) \quad (F.16)$$

$$Y = \sinh(\lambda/\sqrt{2}) \cos(\lambda/\sqrt{2}) \quad (F.17)$$

$$Z = \cosh(\lambda/\sqrt{2}) \sin(\lambda/\sqrt{2}) \quad (F.18)$$

Appendix G

The complex Bessel function of Eq.3.102 are simplified as

$$\frac{J_0(2i^{3/2}\lambda r^+)}{J_0(i^{3/2}\lambda)} = \frac{\sqrt{\frac{2}{\pi}} e^{i2i^{3/2}\lambda r^+} (i2i^{3/2}\lambda r^+)^{-1/2} (i)^0}{\sqrt{\frac{2}{\pi}} e^{ii^{3/2}\lambda} (ii^{3/2}\lambda)^{-1/2} (i)^0} \quad (G.1)$$

$$\frac{J_0(2i^{3/2}\lambda r^+)}{J_0(i^{3/2}\lambda)} = \frac{1}{\sqrt{2r^+}} e^{ii^{3/2}\lambda(2r^+-1)} \quad (G.2)$$

Completed the simplifications of Eq.3.102 gives

$$u_t^+ = \frac{4i\gamma'}{\lambda^2} \left[\frac{1}{\sqrt{2r^+}} e^{ii^{3/2}\lambda(2r^+-1)} - 1 \right] e^{it^+} \quad (G.3)$$

The value of $i^{3/2} = \frac{1-i}{\sqrt{2}}$, then

$$u_t^+ = \frac{4i\gamma'}{\lambda^2} \left[\frac{1}{\sqrt{2r^+}} e^{\frac{1+i}{\sqrt{2}}\lambda(2r^+-1)} - 1 \right] e^{it^+} \quad (G.4)$$

or

$$u_t^+ = \frac{4i\gamma'}{\lambda^2} \left[\frac{1}{\sqrt{2r^+}} e^{\lambda/\sqrt{2}(2r^+-1)} e^{i\lambda/\sqrt{2}(2r^+-1)} e^{it^+} - e^{it^+} \right] \quad (G.5)$$

The real part of u_t^+ Eq.G.5 gives

$$u_t^+ = \frac{4\gamma'}{\lambda^2} \left[\sin t^+ - \frac{1}{\sqrt{2r^+}} e^{\lambda/\sqrt{2}(2r^+-1)} \sin(t^+ + \lambda/\sqrt{2}(2r^+-1)) \right] \quad (G.6)$$

Appendix H

Momentum equation of steady flow in the horizontal channel is

$$\nu \frac{\partial^2 u}{\partial y^2} = -\frac{1}{\rho} \frac{\partial p}{\partial x} = P_o \quad (H.1)$$

with boundary conditions

$$1. \quad u = 0 \quad \text{at} \quad y = \pm h \quad (H.2)$$

$$2. \quad \frac{\partial u}{\partial y} = 0 \quad \text{at} \quad y = 0 \quad (H.3)$$

where h: half height of the channel.

Integrating Eq.H.1 with boundary conditions Eqs.H.2 and H.3 obtain

$$u = u_{s,\max} \left((y/h)^2 - 1 \right) \quad (H.4)$$

where

$$u_{s,\max} = \frac{P_o h^2}{2\nu}$$

The ratio of amplitude to steady pressure gradient is defined as

$$\gamma' = \frac{P_t}{P_o} = \frac{u_{t,\max} \cdot \omega}{3u_m \nu / h^2} = \frac{8 A_o \lambda^4}{3 \text{Re}_m} \quad (H.5)$$

where

$$P_t = u_{t,\max} \cdot \omega$$

$$u_m = \frac{2}{3} u_{s,\max} \quad (\text{Appendix E})$$

and

$$u_{t,\max} = \frac{X_{\max} \cdot \omega}{2}$$

Appendix I

Momentum equation of steady flow in the horizontal pipe is

$$\nu \frac{1}{r} \frac{\partial}{\partial r} \left(r \frac{\partial u}{\partial r} \right) = -\frac{1}{\rho} \frac{\partial p}{\partial x} = P_o \quad (I.1)$$

with boundary conditions

$$1. \quad u = 0 \quad \text{at} \quad r = D/2 \quad (I.2)$$

$$2. \quad \frac{\partial u}{\partial r} = 0 \quad \text{at} \quad r = 0 \quad (I.3)$$

Integrating Eq.I.1 with boundary conditions Eqs.I.2 and I.3 obtain

$$u = u_{s,\max} \left(4(r/D)^2 - 1 \right) \quad (I.4)$$

where

$$u_{s,\max} = \frac{P_o D^2}{32\nu}$$

The ratio of amplitude to steady pressure gradient is defined as

$$\gamma' = \frac{P_t}{P_o} = \frac{u_{t,\max} \cdot \omega}{32u_m \nu / D^2} = \frac{A_o \lambda^4}{4\text{Re}_m} \quad (I.5)$$

where

$$P_t = u_{t,\max} \cdot \omega$$

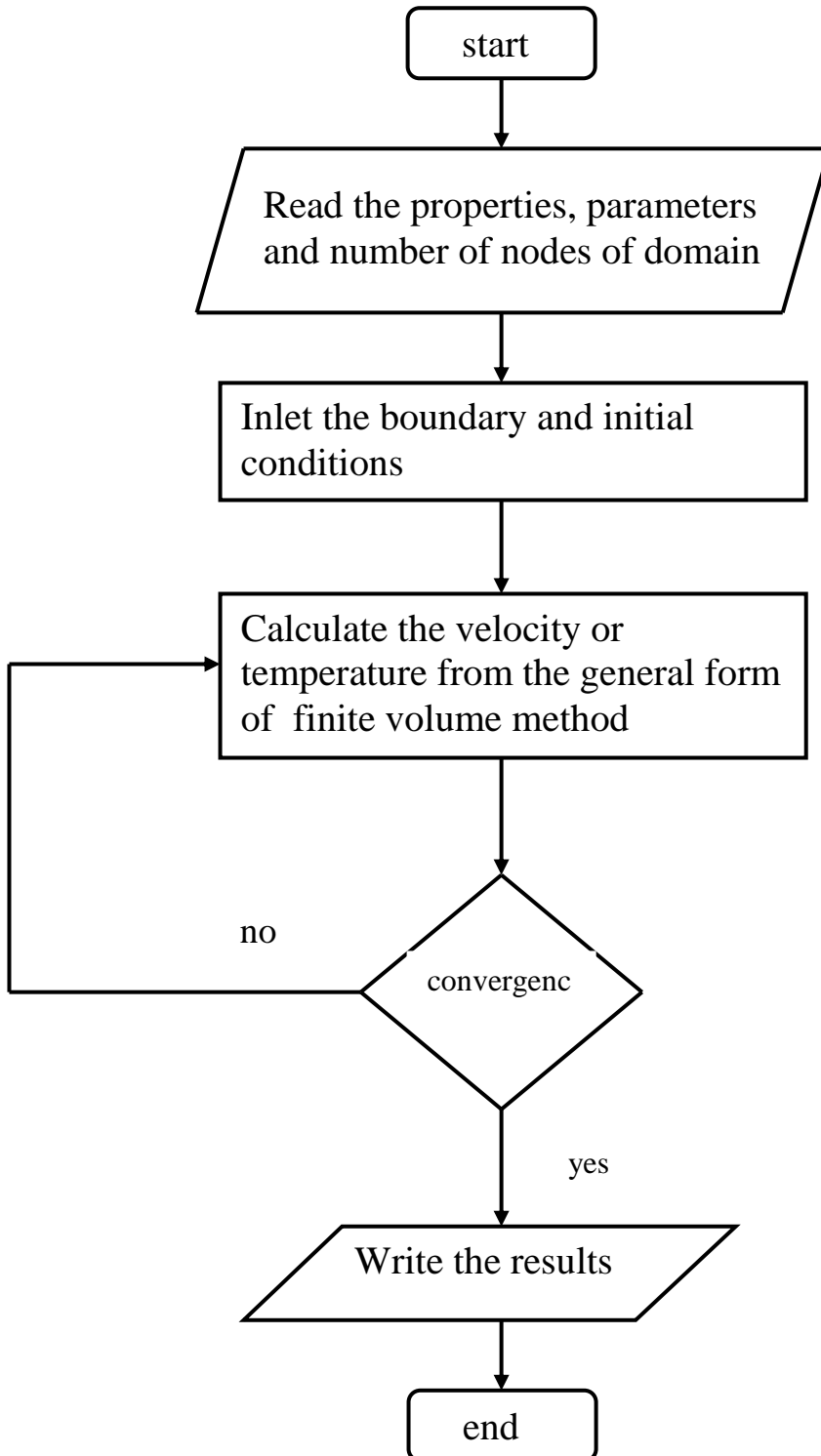
$$u_m = \frac{1}{2} u_{s,\max} \quad [9]$$

and

$$u_{t,\max} = \frac{X_{\max} \cdot \omega}{2}$$

Appendix J

A simple flow chart of iteration method for numerical solution using the finite volume method.



المخلص

تمت دراسة هيدروديناميكية وانتقال الحرارة في جريان ترددي وآخر نبضي تام التشكيل، طباقى، غير انضغاطي، التشتت اللزج في قناة أو أنبوب أفقي معرض لفيض حراري ثابت. تم تطوير نموذج نظري جديد من الحل التحليلي لمعادلات الزخم والطاقة للجريان الترددي والنبضي في قناة و أنبوب باستخدام حلول التحولات المتماثلة. وكانت المتغيرات الرئيسية المؤثرة على الجريان الترددي هي: عدد ومورسلي، السعة اللابعديّة لإزاحة المائع، عدد برندتل و النسبة بين المسافة إلى القطر الهيدروليكي، بينما المتغيرات المؤثرة على الجريان النبضي هي: عدد ومورسلي، عدد رينولدز لمعدل السرعة، نسبة سعة إلى معدل انحدار الضغط، عدد برندتل و النسبة بين المسافة إلى القطر الهيدروليكي.

أن النتائج التي تم الحصول عليها من الجريان الترددي بينت بأن توزيع السرعة و درجة الحرارة يتأثر بالتذبذب وتأثير رجردسون الحلقي حيث يظهر في توزيع السرعة ودرجة الحرارة. أن عدد نسلت اللحظي-الموقعي يتغير دوريا مع الزمن و يتحسن بمقدار مرتبة عددية مع زيادة رقم ومورسلي أو تردد الجريان. أظافة إلى ذلك فإن نتائج الجريان النبضي بينت بأن الجريان النبضي يسبب تكرار في درجة الحرارة وعدد نسلت حول حل الجريان الطباقى المستقر. وأن المعدل الزمني لعدد نسلت الموقعي يبقى ثابت ويساوي ٨,٢٣٥ للقناة و ٤,٣٦٤ للأنبوب مع تغير كل العوامل المؤثرة.

النتائج وُجدت متطابقة بنسبة جيد جدا مع التي تم الحصول عليها عدديا باستخدام طريقة الحجم المحددة. المقارنات بين النتائج العملية لباحثين آخرين و النموذج التحليلي الجديد أعطت تطابق معقولا.

دراسة تحليلية لتحسين انتقال الحرارة
نتيجة جريان داخلي متذبذب
عند ثبوت الفيض الحراري

رسالة مقدمة إلى
كلية الهندسة - جامعة البصرة
كجزء من متطلبات درجة الدكتوراه فلسفة في
الهندسة الميكانيكية

من قبل
أحمد كاظم محمد الشرع
(ماجستير هندسة ميكانيكية)

كانون الأول-٢٠٠٦
ذي الحجة-١٤٢٧